THE SYNTHESIS OF GLYCODENDRIMERS AND THEIR APPLICATIONS IN CARBOHYDRATE-PROTEIN INTERACTIONS AND CATALYSIS

by

Joel Ryan Morgan

A dissertation submitted in partial fulfillment
of the requirements for the degree

of

Doctor of Philosophy

in

Chemistry

MONTANA STATE UNIVERSITY
Bozeman, Montana

July 2006

APPROVAL

of a dissertation submitted by

Joel Ryan Morgan

This dissertation has been read by each member of the dissertation committee and has been found to be satisfactory regarding content, English usage, format, citations, bibliographic style, and consistency, and is ready for submission to the Division of Graduate Education.

Dr. Mary J. Cloninger

Approved for the Department of Chemistry and Biochemistry

Dr. David J. Singel

Approved for the Division of Graduate Education

Dr. Joseph J. Fedock

STATEMENT OF PERMISSION TO USE

In presenting this dissertation in partial fulfillment of the requirements for a doctoral degree at Montana State University, I agree that the Library shall make it available to borrowers under rules of the Library. I further agree that copying of this dissertation is allowable only for scholarly purposes, consistent with "fair use" as prescribed in the U.S. Copyright Law. Requests for extensive copying or reproduction of this dissertation should be referred to ProQuest Information and Learning, 300 North Zeeb Road, Ann Arbor, Michigan 48106, to whom I have granted "the exclusive right to reproduce and distribute my dissertation in and from microform along with the non-exclusive right to reproduce and distribute my abstract in any format in whole or in part."

Joel R. Morgan

July, 2006

To Mom and Dad

Linda and Ray Morgan

ACKNOWLEDGEMENTS

First, I would like to thank my advisor, Mary Cloninger, for your guidance, for funding me, and for your irrepressible enthusiasm. Thanks to the Cloninger research group, past members and present, for your support and teaching. Also, without the kind help of the Douglas and Singel research groups this work would have been much more difficult, if not impossible. Thanks to my friends from Oregon, Tim and Todd, for recruiting me to Montana State University, and for your constant friendship.

TABLE OF CONTENTS

TABLE OF CONTENTS CONTINUED

LIST OF TABLES

LIST OF FIGURES

LIST OF FIGURES CONTINUED

Figure Page

LIST OF FIGURES CONTINUED

Figure Page

LIST OF FIGURES CONTINUED

Figure Page

LIST OF FIGURES CONTINUED

Figure Page

LIST OF FIGURES CONTINUED

Figure Page

LIST OF SCHEMES

LIST OF SCHEMES CONTINUED

Scheme Page

LIST OF SCHEMES CONTINUED

Scheme Page

ABSTRACT

Glycodendrimers were synthesized for studies in carbohydrate-protein interactions, and from these studies we gained insight into the mechanism of some carbohydrate-protein interactions. First, the synthesis of tris-mannose cluster functionalized glycodendrimers of different sizes using a 'click chemistry' approach is described. The macromolecules were characterized using ^{1}H and ^{13}C NMR and MALDI-TOF MS. Next, a heterogeneous dendrimer functionalization strategy to control the presentation of the carbohydrate clusters around the dendrimer periphery is reported. N-acetyl galactosamine and phenyl azide heterogeneously functionalized PAMAM dendrimers were synthesized and used as macromonomers in a 'click chemistry' polymerization reaction. The dendritic polymer was designed as a lipid raft microdomain mimic. Next, the synthesis dimannose functionalized PAMAM dendrimers for evaluation of binding with Cyanovirin N, an HIV inactivating protein is described. These glycodendrimers and others were evaluated in protein binding experiments using transmission electron microscopy, precipitation assays, isothermal titration microcalorimetry, and a hemagglutination inhibition assay. This work represents advancements in the synthesis of glycodendrimers with new carbohydrate architectures. Also, the results of the protein binding studies afforded insight into the mechanism of carbohydrate-protein interactions.

Poly(polyoxometalate) metallodendrimers were synthesized and characterized using ^{31}P NMR, transmission electron microscopy and MALDI-TOF MS. Polyoxometalates and poly(polyoxometalate) dendrimers were analyzed as oxidation catalysts.

CHAPTER 1

BACKGROUND AND RATIONALE

Cell Surface Carbohydrates

Carbohydrates in living systems come in varying forms spanning glycoproteins, glycolipids, polysaccharides, and monosaccharides. Glycoproteins are particularly significant since glycosylation of proteins is a common post-translational modification. Glycoproteins and glycolipids contain the majority of carbohydrates in cells.[1]

Oligosaccharides bound to proteins are classified into N-glycans and O-glycans. N-glycans all have a common pentasaccharide core Manα1-6(Manα1-3)Manβ1-4GlcNAcβ1-4GlcNAc (Figure 1.1) bound to an asparagine amino acid residue on a protein. Variations on this core alter branching, extend the oligomer, and alter the sugar types present. The modifications on the core are performed by a number of glycosidases and glycotransferases.[1] Unlike the DNA and proteins, linear biopolymers, the potential for structural variation of cell surface glycans is due to the branching ability of oligosaccharides that results in multiantennary structures. Connections can occur at three or four specific oxygen atoms on the carbohydrate, and the glycosidic linkage can occur in α or β anomeric geometry. Therefore, many more possible polysaccharides combinations could exist than either DNA or proteins. Consider that four different sugars can theoretically form 35560 different possible tetrasaccharides, while four amino acids can form 24 tetrapeptides.[2] However, in reality the total number of glycans is limited by

the number of different glycosidases and glycotransferases, themselves products of the genome. O-type glycans are bound to the protein by serine, threonine, or hydroxylysine. O-glycans are commonly called mucin-type because they are predominantly found in mucus membranes in the intestinal and respiratory systems. The study of the structure and function of glycans is highly complex field, and is often referred to as the next major frontier in biochemistry.[3, 4] Unfortunately, glycans remain difficult to characterize, and require involved synthesis performed chemically or chemoenzymatically.

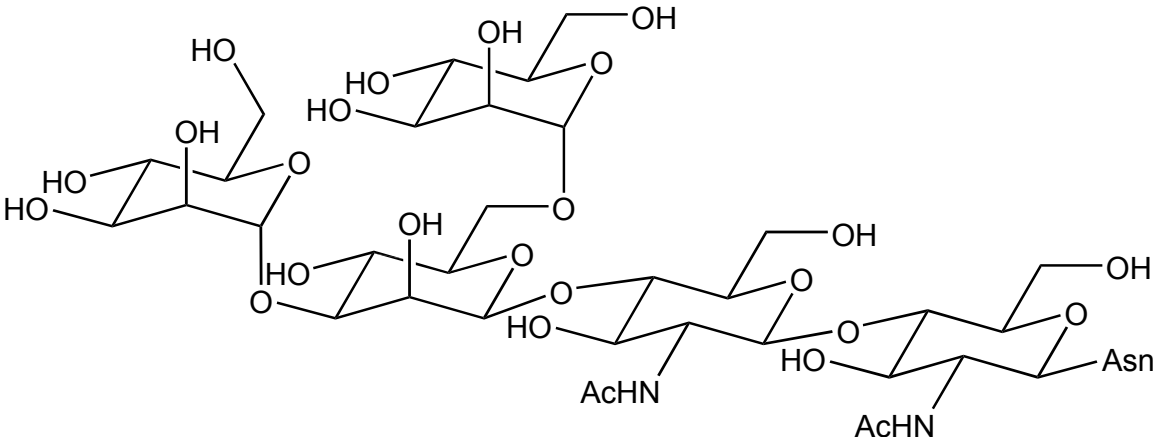

Figure 1.1 The biantennary core of N-linked glycans Manα1-6(Manα1-3)Manβ1-4GlcNAcβ1-4GlcNAc linked to a protein by an asparagine amino acid side chain.

Glycans are specific to cell, tissue, and species type in living systems. Sugar moieties on lipids and proteins are constructed stepwise in the endoplasmic reticulum and Golgi apparatus, and therefore are dependent on the specific cellular environment.[1, 4] Many different glycoproteins and glycolipids exist on the cell surface. Multiple glycans can be present on a single protein, and often these glycans vary in branching and type of

carbohydrates at the termini. Different cells can therefore express very different oligosaccharides with unique presentations depending on cell type and even cell age.

Cell surface carbohydrates are significant in a variety of biological processes such as fertilization, cell adhesion, tissue formation, antigen/antibody interactions, cancer metastasis, inflammatory response, and infection of bacteria or viruses.[3] A primary function in many of these cases is a carbohydrate's role in adhesion to carbohydrate recognition domains on proteins. Early work performed by Ashwell *et. al.* demonstrated the adhesion function of glycoproteins very well.[5, 6] Their experiments showed that certain radiolabeled plasma glycoproteins bearing glycans with terminal sialic acid (N-acetyl neuraminic acid) residues survive in the plasma with a half-life of 56 hours, enzymatic cleavage of these terminal carbohydrates using a neuraminidase enzyme exposed terminal galactose residues on the non-reducing end of the glycans and the glycoproteins disappeared from the plasma in minutes (Figure 1.2). Further enzymatic modification of the galactose residues with galactose oxidase, oxidizing the terminal C-6 alcohol, resulted in a reversal to longer protein survival times. The research also verified that the galactose terminated glycoproteins accumulated in the liver through binding to galactose specific binding proteins.

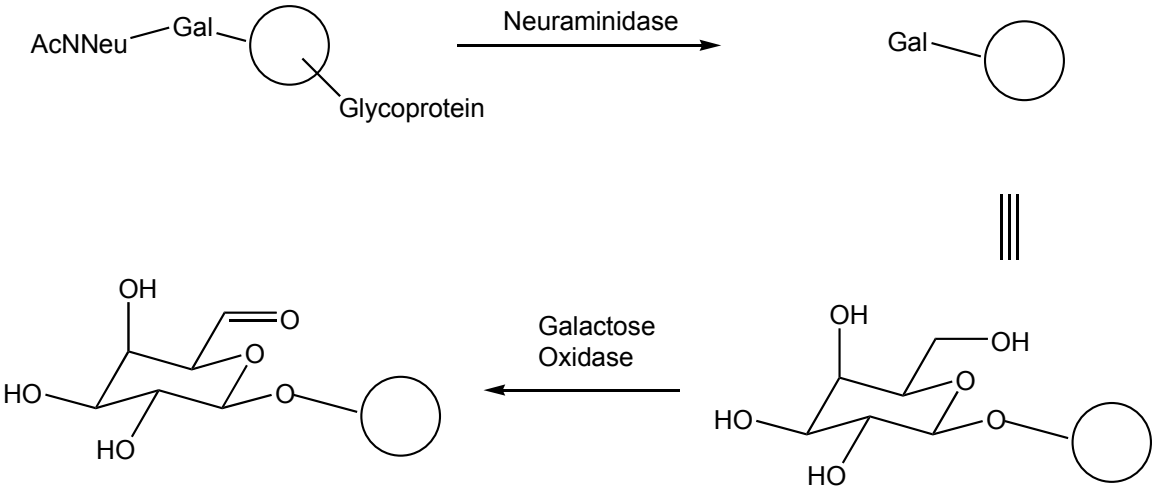

Figure 1.2 Asiaceruloplasmin, a glycoprotein, is cleared from plasma if the galactose residues on the glycans are exposed. Oxidation of the primary alcohol on galactose to an aldehyde restores the half-life of the glycoprotein in plasma.

Since the discovery of surface carbohydrates as major components in cellular recognition, scientists have learned how these adhesion processes contribute to some vital biological processes. For example, when endothelial cells (cells that line the interior of blood vessels) are near a site of inflammation, cytokines are released that trigger the expression of E- and P- Selectins on the cell surface (Figure 1.3). Neutrophils (a type of leukocyte or white blood cell) in the fast flowing blood stream have glycoproteins displaying sialyl Lewis^x (Figure 1.4), a tetrasaccharide which binds to E- and P-Selectins. The carbohydrate-Selectin interactions slow the neutrophil into close contact. In addition endothelial cell surface sialyl Lewis^x can interact with L-Selectin on the neutrophil surface. The contact between the endothelial cell and the neutrophil then leads to vascular extravasation and response to the inflammatory stimulus.[1]

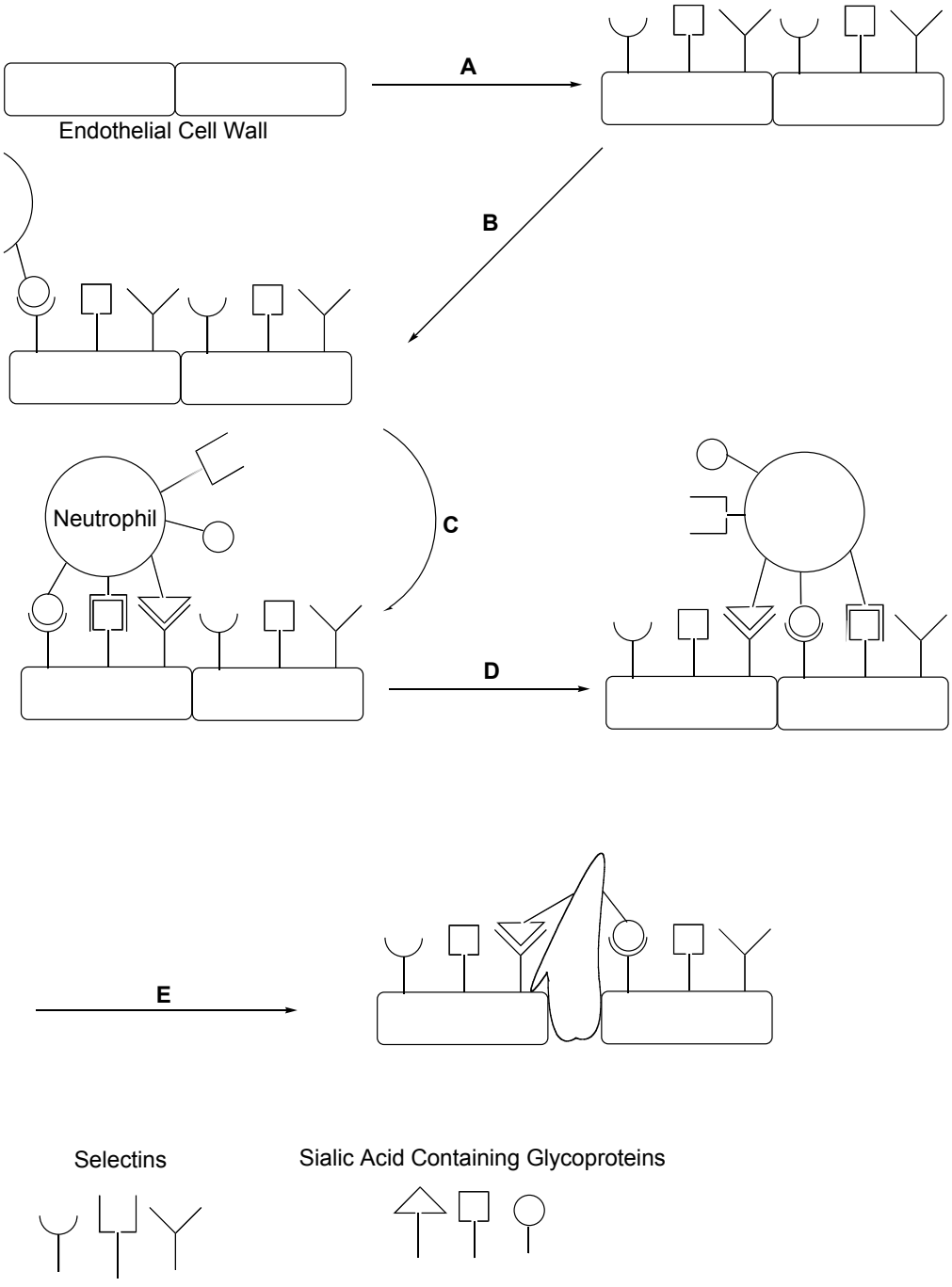

Figure 1.3 Selectin mediated inflammation response. A) Selectins are exposed on the cell surface; B) then a neutrophil attaches to the endothelial cell; C) and the neutrophil rolls along the surface; D) into a static position; E) then extravasation occurs.

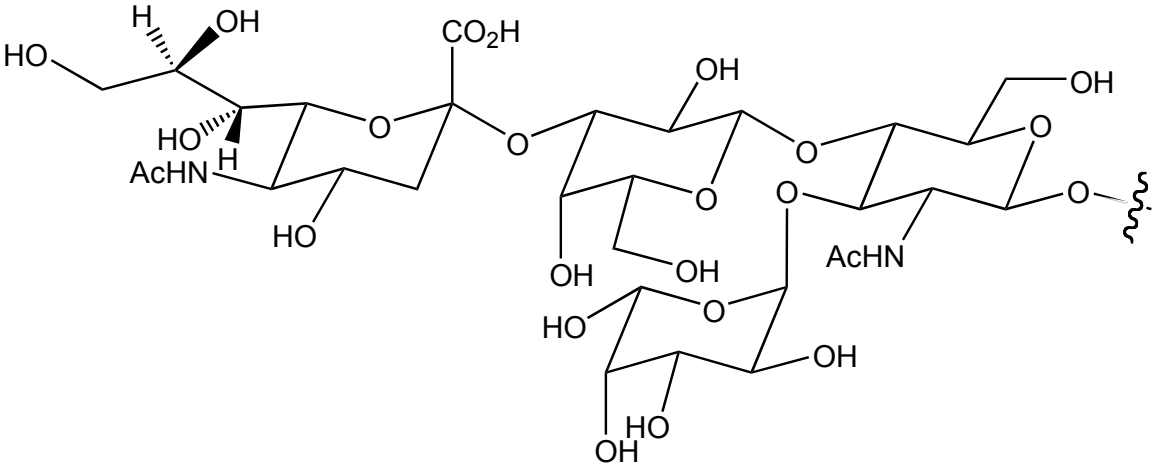

Figure 1.4 Sialyl Lewis^X tetrasaccharide.

An important function of mucin type glycoproteins, aside from acting as a barrier between body fluid proteases (and other enzymes) and epithelial cells, is that mucin glycoproteins can adhere to pathogens, leading to excretion pathways, and so preventing infection. Although some mucin type glycoproteins inhibit pathogen infection, other cell surface carbohydrates may facilitate infection.[1] One of the earliest and most widely studied examples in glycobiology is the carbohydrate-mediated adhesion of influenza virus to bronchial epithelial cells.[7]

Tumor cells have been shown to contain altered expression patterns of cell surface carbohydrates, when compared to normal cells.[2, 8] This is true for glycolipids where their accumulation and complexity is altered, and glycoproteins where glycans become more abundant and more heavily glycosylated. Some carbohydrates, such as sialic acid, are more abundant in tumor cells, and the distribution of the carbohydrates on the cell surface impacts the metastatic properties of the cell as well.

Understanding the adhesion between carbohydrates and carbohydrate binding proteins in biological systems is a difficult task due to the complexity of carbohydrate structure and function. There are many possible N- and O- glycans, and these can be attached to any number of possible protein side chains. However difficult the problem may be, an understanding of adhesive properties of cell surface carbohydrates will lead to better understanding of biochemical processes, with particular regard to bacterial and viral infection, and cancer, due to their respective importance in human death and disease.

Studies directed at understanding cell surface carbohydrate adhesion processes, including the studies described herein, have two goals: to gain insight into how carbohydrate-protein interactions occur and to develop potential therapeutics for combating disease.

Lectins

The protein receptors for cell surface carbohydrate ligands include lectins. Broadly defined 'lectins' are carbohydrate-binding proteins that are not generated from the immune system (such as antibodies) and have no enzymatic activity (such as glycotransferases and glycosidases).[9] The first lectins were recognized over 100 years ago when a lectin from the castor bean (*Ricinus Comununis*) was observed to agglutinate (form cross-linked aggregates of) red blood cells. As more compounds with similar properties were discovered they formed the class of molecules called the haemagglutinins. It was later discovered that some haemagglutinins could recognize only blood cells from specific blood types in the ABO blood group system, as each displays

unique cell surface glycans. The name, lectin, was derived from the Latin root for selection, *lectio*. More recently, certain toxins and monomeric carbohydrate binding proteins that are unable to agglutinate red blood cells have been included into the class based on structural and functional similarities. While many scientists loosely agree on the definition above, to date no strict definition for lectins has been universally accepted.[10-12]

Lectins exist in nearly all organisms, although they have little homology as a group, vary in size, and even contain very different carbohydrate recognition domains. Lectins are often easy to isolate in pure form by affinity chromatography. A simple classification divides lectins into plant and animal varieties, while a more functional division is based on the sugars that bind to them. In the latter case there are four types, each followed with an example lectin: mannose/glucose specific (Concanavalin A, from the jack bean *Canavalia ensiformis*), N-acetylglucosamine specific (from the potato, *Solanum tuberosum*), N-acetylgalactosamine/galactose specific (from the peanut, *Arachis hypogea*), and fucose specific (from the common gorse, *Ulex europaeus L*).[9]

In many laboratories the biological function of a lectin is less important than how the lectin can be used in a meaningful experiment in vitro. In these cases plant lectins are chosen because they can be isolated in large quantities easily with affinity chromatography. Given that animal cell surfaces change over the lifespan of the cell and also change upon disease states such as cancer, simple plant lectins are used to probe these biological events. Perhaps the widest use of lectins has been in the field of immunology, as lectins can mimic, interfere with, and be used to study antibodies and antigens.

The most commonly used plant lectin is Concanavalin A, or Con A, isolated from the jackbean, and commercially available.[11, 13] This mannose and glucose specific lectin is a homotetramer at biological pH, with a carbohydrate-binding site on each monomer (Figure 1.5). The monomer of Con A contains 137 amino acids and has a molecular weight of 26,500 g/mol. Several crystal structures of Con A have been reported with and without bound carbohydrates. Concanavalin A requires Ca^{2+} and Mn^{2+} to facilitate carbohydrate binding.

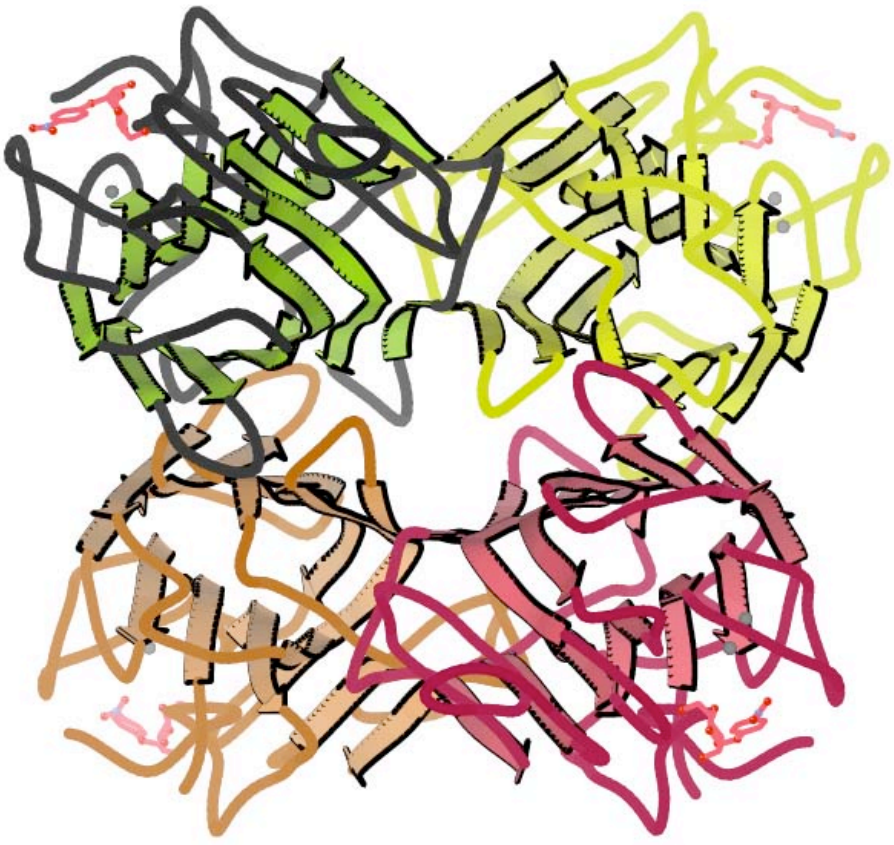

Figure 1.5 Concanavalin A, a tetrameric lectin shown with four bound 4'-nitrophenyl-α-D-glucose ligands.[14]

Plant lectins, such as Con A, are usually chosen for an experiment based on their carbohydrate specificity. These lectins are useful in experiments designed to gain insight into the molecular basis for protein carbohydrate interactions. To gain an understanding of human biological interactions, or to develop potential therapeutics it is necessary to choose a lectin significant to the problem being studied. For this reason Cyanovirin N is another very important protein. Cyanovirin N was originally isolated from blue-green algae. This is an HIV-inactivating protein, weighing 11 kDa, that interferes with viral entry by binding gp120, a heavily glycosylated HIV envelope protein with 24 N-linked oligosaccharides (Figure 1.6).[15-20] Cyanovirin N is specific for the manα1-2man disaccharide on the non-reducing termini of the N-linked glycans on gp120.[20]

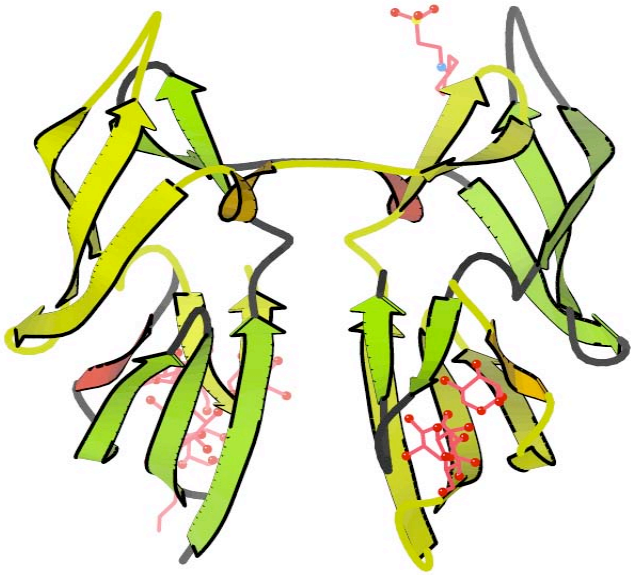

Figure 1.6 Cyanovirin N, a dimeric HIV inhibiting protein with two bound hexasaccharides, and a single bound 2-(cyclohexylamino)ethanesulfonic acid (from the buffer solution.[16]

The galectins, galactose and N-acetylgalactosamine selective animal lectins, such as galectin-3, may have major roles in cancer metastasis.[21, 22] Galectin-3 in normal cells regulates cell growth, adhesion, and death.[23] This lectin is a 31 kDa monomer (with a 14 kDa carbohydrate recognition domain) that oligomerizes either at high concentrations or through binding to carbohydrate arrays (Figure 1.7).

Figure 1.7 Human Galectin-3 carbohydrate recognition domain with bound N-acetyl lactosamine.[24]

Lectins vary in size, structure, and even in the makeup of the carbohydrate recognition domain. A uniform characteristic among lectins is that they bind reversibly and non-covalently with carbohydrates at shallow, solvent exposed binding pockets. A striking feature in this binding event is the relative weakness of the affinity with monosaccharide, with $K_a = 10^3 - 10^4$ M^{-1}.[25] Alone this interaction wouldn't be very

biologically significant, however lectins elevate their affinity and specificity through multivalent interactions.

Multivalency

Binding in systems both biological and chemical can become stronger through multivalent effects.[7, 25-27] When one or both binding partners have multiple receptor-ligand sites of attachment, a greater binding affinity may be observed, greater even than the sum of individual binding events. In chemistry, such an effect is quite common, for example, in metal ion chelation with organic binding ligands.

In biology many processes benefit from, or require, multi-point attachment between a ligand and receptor. All antibodies have multiple equivalent points of attachment. In the antibody-mediated uptake of bacteria into a macrophage, multivalency permits stability and specificity while triggering the events leading to subsequent action. Likewise, relevant carbohydrate-protein interactions involve: lectins with multiple carbohydrate recognition domains, glycans with multiple terminal saccharides by virtue of the multiantennary structures, glycoproteins with multiple glycans, or cell surfaces with multiple copies of glycoproteins and glycolipids. Multivalency, particularly in chemical biology, manifests itself in a number of binding modes (Figure 1.8): monovalent, clustered, multivalent, and aggregation.

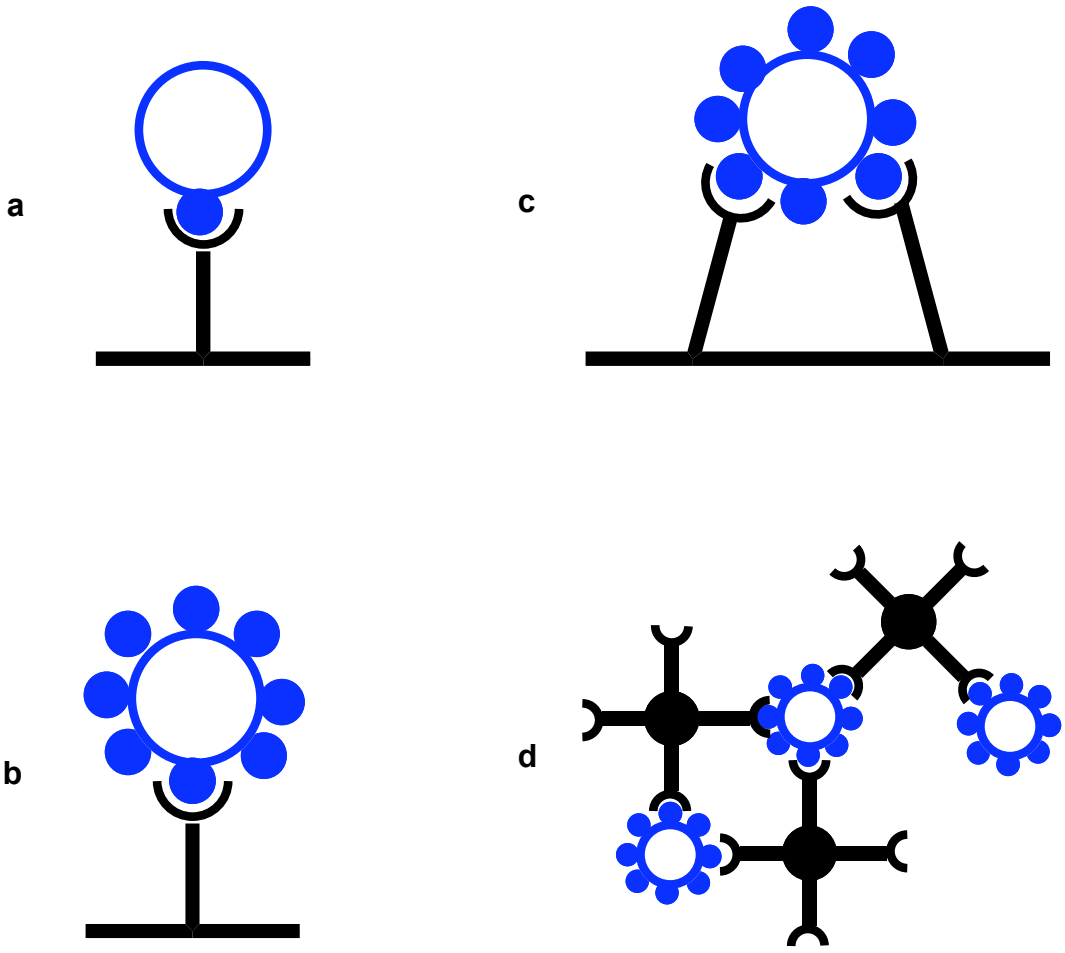

Figure 1.8 Modes of carbohydrate-protein interactions a) monovalent; b) cluster effects; c) multivalent; and d) aggregation.

The simplest mode of interaction is monovalent (Figure 1.8a), where one receptor binds to one ligand. The strength of this interaction is generally weak in carbohydrate-protein interactions. An increase in affinity may be observed when the local concentration of a ligand on one binding partner is increased (Figure 1.8b). The presence of multiple binding epitopes effectively reduces the disassociation rate of the ligand. An increase in affinity for sugars to lectins is commonly called the "glycoside cluster effect",[27, 28] although most literature on synthetic multivalent ligands doesn't differentiate

between the different possible modes of binding when using the phrase. The cluster effect can be derived from a statistical advantage by having an increased local concentration.[29] Also, if the ligand has an appropriate conformation, secondary interactions between ligands outside the primary binding site with the receptor may also enhance the affinity between the binding partners. In some cases affinity can be extraordinarily increased by the presence of a minor binding pocket.

When two or more binding ligands on the same molecule bind with two or more receptors on the same molecule multi-point, or multivalent, attachment can occur (Figure 1.8c). An increase in binding avidity results from a combination of enthalpic and entropic effects. Recent reports propose thermodynamic models for multivalent interactions, although they usually apply only to specific systems and focus on one particular mode of binding.[7, 27, 30-33] Consider a bivalent ligand binding with a bivalent receptor (Figure 1.9) where the thermodynamics rely on both enthalpic and entropic contributions. In simple terms, the advantage from multivalency arises from the fact that the entropic cost for a bivalent interaction is less than the cost for two monovalent interactions because the second binding event is intramolecular. If the bivalent interaction imposes structural stress on one of the partners, as might be the case with a rigid linker, the enthalpic cost might prohibit multivalent binding (Figure 1.9b), as it is unlikely a rigid linker could be constructed with perfect complementarity (Figure 1.9a). If the linker is too flexible, as in a poly(ethylene glycol) chain, the conformational entropy cost prohibits multivalency (Figure 1.9d). So interestingly, enthalpy and entropy effects are somewhat compensating for one another. In real systems enhanced avidity between binding partners involved in protein-carbohydrate interactions utilizes

clustering, multivalency (multipoint attachment), and aggregative effects, and to date detailed theoretical models remain complex and specific to certain binding parameters. However, the thermodynamic arguments must be considered heavily in designing synthetic multivalent ligands.[30]

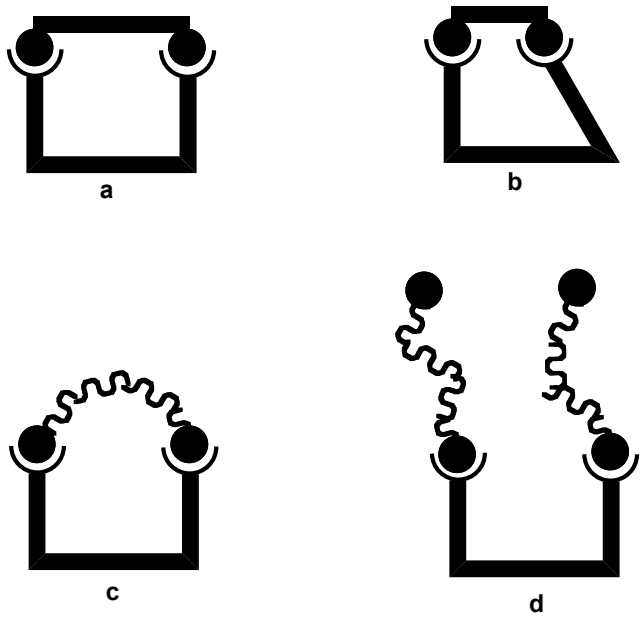

Figure 1.9 Bivalent interactions between a receptor and a) a complementary rigid ligand (unlikely); b) a rigid ligand leading to a conformational change; c) a flexible ligand; or d) two flexible ligands.

Yet another mode of multivalency is aggregation, where cross-linked ligand receptor aggregates are formed (Figure 1.8d).[27] The driving force for this type of interaction may be due to solubility driven equilibrium. Aggregation can occur with small ligands that can't span multiple receptor binding sites, or it can also occur with ligands able to bind multiple receptor sites. Even without precipitation, the formation of soluble aggregates can lead to a binding enhancement.[34]

An important result from theoretical work on multivalency concerns cooperativity. In many biological processes involving monovalent ligands with polyvalent receptors cooperativity is important, and well defined. Cooperativity is involved in oxygen binding to hemoglobin, for example. Though when the ligand is polyvalent as well, the standards for measuring positive cooperativity, non-cooperativity, or negative cooperativity (Hill and Scatchard plots) fail because intramolecular forces are involved.[7, 33] So while the enhancements in binding affinity from multivalency are similar to cooperativity, neither the nomenclature nor thermodynamics are appropriate for intramolecular binding models.

Multivalency is how nature compensates for, and takes advantage of, weak interactions, such as between a lectin and a carbohydrate.[7] The net effect of the different possible modes leads to tight binding, which is necessary for some biological events to develop. Beyond this advantage, multivalency in biological systems allows for increased specificity so connections are modulated by altering the types of sugars displayed on the cell surface, their presentation, and the spacing between them. These interactions are then difficult to inhibit, and to study as well, partially due to the large contact area of the interaction. This is likely how nature prevents unwanted competing interactions with the myriad of small molecules in biology as well. As in the case described earlier where lymphocytes attach to endothelial cells by the interaction between glycoproteins containing sialyl Lewis^x and the selectins, the multiple weak interactions are likely more resistant to cleavage from the shear force of blood flow. Large multivalent contacts enable large conformational changes (on the cellular level) to occur through relatively simple ligand-receptor interactions.

Multivalency is important in protein-carbohydrate interactions and likely many other interactions of biopolymers as well. The challenge for chemists in studying protein-carbohydrate interactions and in designing therapeutics based on these principles becomes a problem of understanding the fundamentals of multivalency.

Different Modes of Interaction in Physiological Carbohydrate-Protein Interactions

The infection of a cell by influenza virus relies on multivalent binding between the cell surface and the virus. The hemagglutinin lectin is a trimer, with three carbohydrate recognition domains selective for sialic acid.[7, 35] This lectin is densely packed on the surface of the influenza virus (600-1200 per virus particle, 2-4 per 100 nm^2). Sialic acid residues occur on many cell surface glycoproteins and glycolipids thus the density is also relatively large (50-200 molecules per $100nm^2$). A large area, multipoint (multivalent, Figure 1.8c), attachment between the virus and the cell is necessary for infection to occur, as the interaction between surface poly-sialic acids and hemagglutinin trimer alone is not sufficient for infection.

Programmed cell death relies on aggregative binding effects. Apoptosis of immature thymocytes occurs in the presence of Galectin-1, a dimeric animal lectin.[36, 37] Galectin-1 binds with CD45 (red dye labeled) and CD43 (green dye labeled) glycoproteins on the cell surface. Upon binding galectin-1, CD45 and CD43 redistribute into discrete localized domains, as observed using microscopy with dye labeled glycoproteins. Under normal conditions the CD45 and CD43 are dispersed on the cell surface (Figure 1.10), yet galectin-1 forms patches by an extended homogeneous cross-linked complex (Figure 1.8d). The segregation of the glycoproteins is involved in cell

death. Mature thymocytes, not susceptible to galectin-1 mediated cell death, did not show similar segregation of CD45 and CD43 into localized domains. This results from altered glycosylation patterns of the glycoproteins on mature cells. The two carbohydrate recognition domains on the galectin-1 dimer are on opposite faces of the molecule, and so galectin-1 is apt to cross-linking for favorable multivalent enhancements.

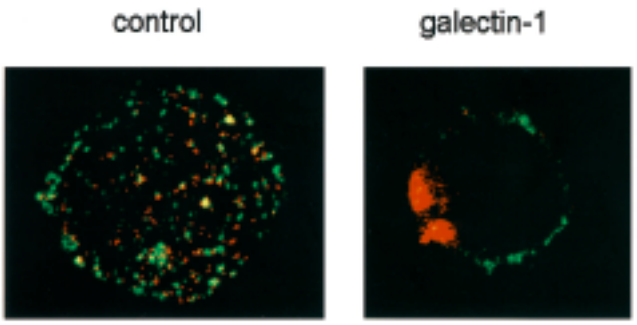

Figure 1.10 Dye labeled glycoproteins CD45 (red) and CD43 (green) form localized domains in the presence of Galectin-1, leading to apoptosis, or programmed cell death. (Image from reference 37).

These two examples show different modes of binding in physiological events. In many cases, however, it is far less clear whether aggregation, multivalency, clusters effects, or a combination of these is occurring in carbohydrate-protein interactions.

Synthetic Multivalent Ligands

To study the fundamentals of protein carbohydrate interactions and develop potential therapeutics, the design of synthetic multivalent ligands for protein receptors has been a major effort by many scientists.[30] A large number of synthetic multivalent ligands have been constructed using large linear and branched polymers,[38-41] micelles,[42]

dendrimers,[43-45] nanoparticles,[46] and smaller to medium ligands with cores such as cyclodextrins,[47-49] sugars,[50] macrocycles,[34] and other small cores.[30] In each case it is appropriate to consider the application for the synthetic compound, consider the determinants for affinity, and then choose the best scaffold for sugar display.

The most effective body of compounds yet created for multivalent binding is the glycopolymers. Carbohydrates have been conjugated with DNA or peptide biopolymers and these have the advantage of a well-defined structure.[51-53] However the programs designed to probe issues involving multivalency mostly take advantage of synthetic water-soluble linear polymers.[54] Polysialic acid copolymers of polyacrylamide (Figure 1.11) bind to hemagglutinin 10 to 100 times more actively than monomeric sialic acid, from work demonstrated by the Whitesides group.[7,54] The same polymers could inhibit influenza binding 10^6 to 10^8 times better than the monomer, because of the many copies of hemagglutinin lectin on the virus exterior. The Kiessling group has also pioneered multivalent glycopolymers using ring opening metathesis polymerization (Figure 1.12).[55-57] In some of these cases, fewer carbohydrate residues on the polymer resulted in an increased activity due to less steric hindrance between the polymer and lectin.

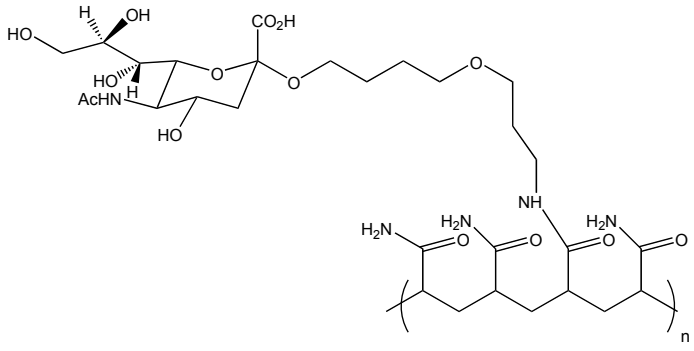

Figure 1.11 Polyacrylamide containing sialic acid residues used to inhibit hemagglutinin lectin on the influenza virus.

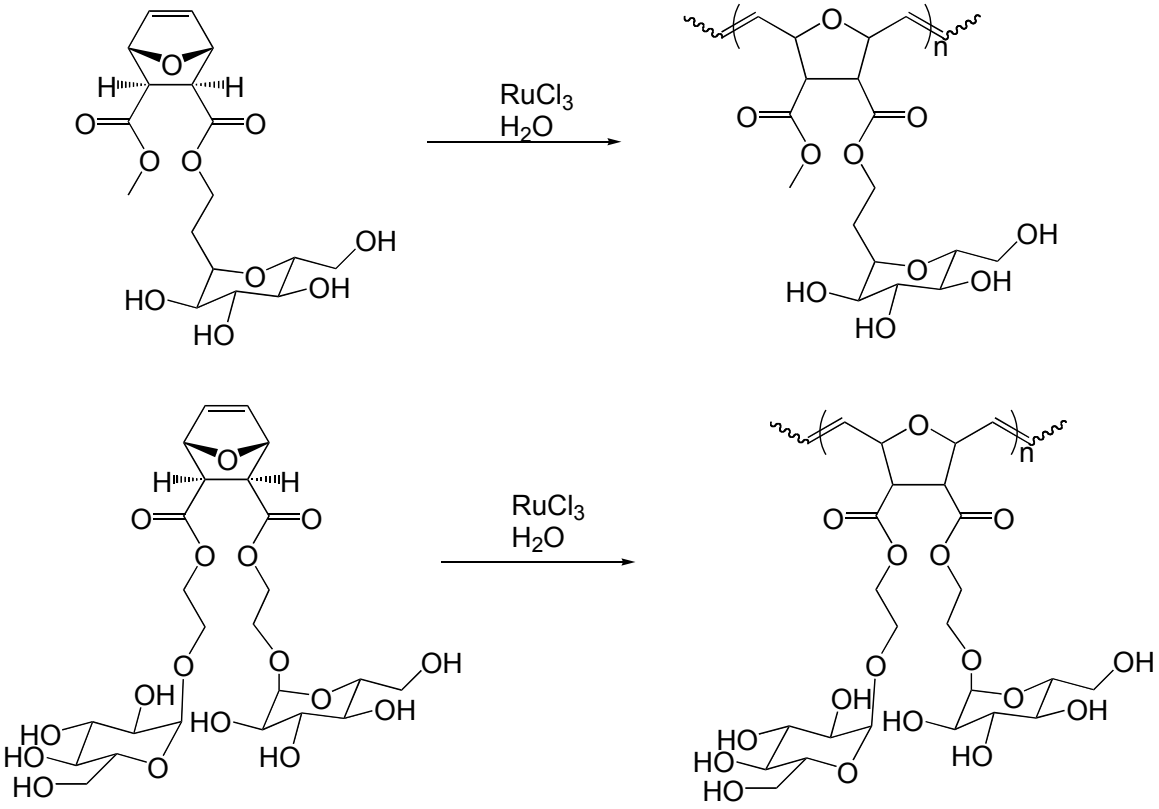

Figure 1.12 Glycopolymers by ring opening metathesis polymerization: polymers from (top) monosaccharide monomers are more active than from (bottom) disaccharide monomers.

Stoddart *et. al.* developed pseudopolyrotaxanes for studies in binding with galectin-1 (Figure 1.13).[58] The "beads-on-a-string" compounds offer mobility of the pendant saccharides along the polymer backbone to spin around the axis or move up and down the axis. The mobility of the saccharides is proposed to mimic the mobility of cell surface glycolipids and glycoproteins (as was observed in the example with galectin-1 in cell apoptosis). The lactose functionalized pseudopolyrotaxane bound galectin-1 better than similar polymers with covalently linked lactose. As thermodynamics dictates, flexibility is important in good synthetic multivalent ligands. This was verified in work by Kobayashi *et. al.* where rigid glycosylated poly(phenylisocyanide)s bound effectively

only as well as the corresponding carbohydrate monomers, yet flexible glyco-poly(acryloylaminophenyl) compounds displayed multivalent enhancements in lectin binding assays.[59]

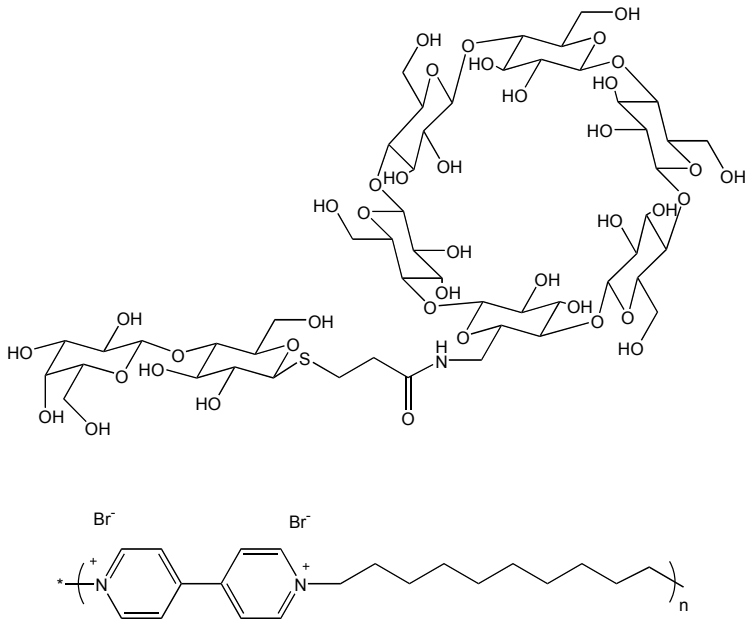

Figure 1.13 Rotaxanes developed by Stoddart as a flexible synthetic multivalent ligand. The polymer and saccharide mono-functionalized cyclodextrin self-assemble over 4 days into a "beads-on-string" complex.

Glycopolymers have very large multivalent enhancements, yet the low degree of synthetic control often results in polymers without a well-defined structure, particularly on the level of sugar presentation, making a molecular understanding of multivalency difficult when the size, structure, topology, and valency of the polymer are not precisely known.

Smaller ligands with two to ten carbohydrate moieties are very common in studies of multivalent interactions. While large frameworks serve to better understand large-

scale multivalent effects, smaller multivalent ligands are more useful as possible therapeutics. A large body of work has been produced with carbohydrate functionalized cylcodextrans and calixarenes so host-guest chemistry and multivalency can be used for specific drug delivery.[47, 48]

Lee and coworkers first presented the phrase "glycoside cluster effect" in 1983 to describe the enhanced affinity of mono-, di-, and trisaccharide clusters of galactose in binding studies with the hepatic Gal/GalNAc Lectin.[28] In some cases with small synthetic multivalent ligands, often when affinity enhancements are very large, secondary binding effects are responsible. Proximity effects also play a role, and aggregation is another probable mode of binding. Two smaller ligands, both structurally similar to glycans, bear further mention due to their significance to our work.

Carbohydrate presentation has become very important for synthetic multivalent ligands, as it is a large determinant of its affinity for a receptor. The Stoddart research group presented an effort to understand the best architecture for sialic acid binding proteins by synthesizing a number of different small saccharides (Figure 1.14).[60] In this case valency was not a factor in measurements of inhibitor potency (using an Enzyme Linked Lectin Assay, or ELLA). The tetravalent molecule, (Figure 1.14a), was the least effective binder, relative to the monovalent saccharide (Figure 1.14d), possibly a reflection of steric interactions that inhibit binding. The bivalent β-linked compound (Figure 1.14b) was the next most followed by the most effective binding ligand bivalent α-linked compound (Figure 1.14c), the difference between the two arising from the nature of the interior branches of the molecules effectively increasing the spatial relationship between the binders. This work indicates that the specific presentation of the

carbohydrates, the distance between the binding epitopes, represents a compromise between steric factors and proximity effects.

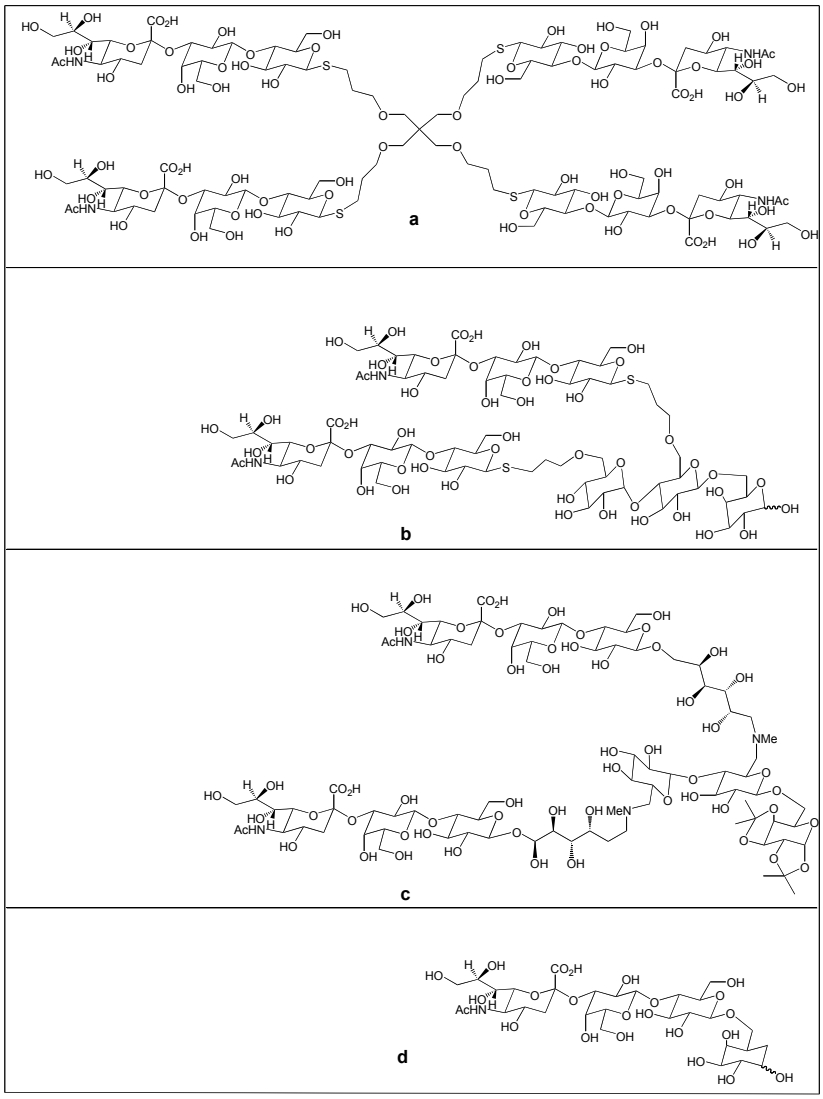

Figure 1.14 Small a) tetravalent; b) bivalent on the same face; c) bivalent on opposite faces; and d) monovalent sialosides for studies with a sialic acid binding protein.

The Danishefsky group recently synthesized N-glycans as synthetic antigens[61] to mimic the glycosylation of gp120 (Figure 1.15), an HIV envelope glycoprotein

responsible for binding with T-cells. The high degree of gp120 glycosylation is thought to shield the protein backbone from antibody recognition. An antibody, 2G12, found in long-term HIV survivors, recognizes the gp120 glycans, and gp120 glycan mimics could be used as antigens for broad immune response, or at least binding studies will provide insights into the real requirements for gp120 antigens. The glycopeptides synthesized by Danishefsky *et. al*. included high mannose glycans or hybrid glycans including mannose and lactose termini. The surface plasmon resonance (SPR) binding studies with the 2G12 antibody revealed two important features. First, the glycopeptides formed dimers by a sulfide cross-link about the cysteine amino acid of the peptide. These dimers were responsible for the observed 2G12 binding. Monomers formed under reducing conditions didn't display significant binding, suggesting multivalency, beyond that available from a single triantennary glycan, is required in gp120 mimics. Another important observation from this work is the hybrid glycans didn't produce significant binding with 2G12 even in dimeric form indicating high mannose type glycans are also required. While the SPR binding studies didn't indicate the precise nature of the binding event, they concluded that a conformational adjustment was required for the binding of the second glycan of the dimer. This conforms to the thermodynamic models for multivalency discussed earlier.

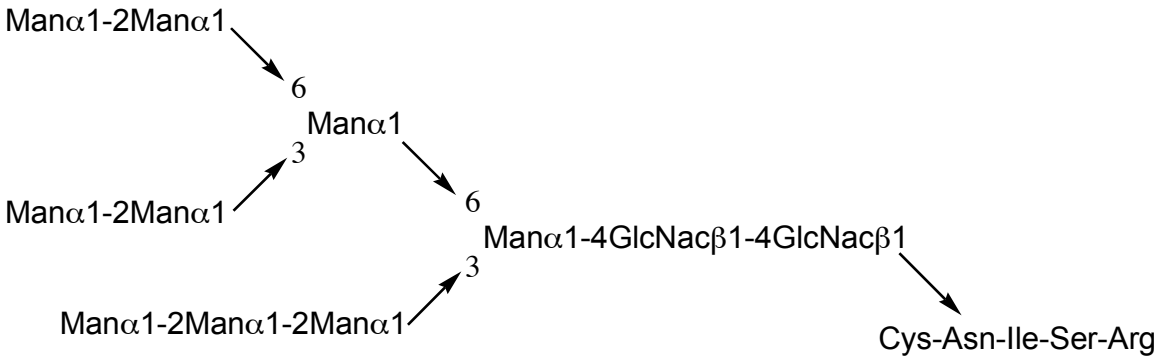

Figure 1.15 High mannose glycan used as a gp120 mimic.

Carbohydrate Architecture

Controlling the architecture of synthetic multivalent ligands is essential for an understanding of carbohydrate-protein interactions. As shown in the work by Stoddart, adjustments in sugar spacing and presentation can have a large impact on affinity. An elegant example of spacing sugars in a deliberate fashion on a polymer comes from the Kiick research group.[53, 62] First helical protein polymers with a specific amino acid sequence $(AAAQAAQAQAAAEAAAQAAQAQ)_6$ were made. The glutamic acid (E) side chains were then chemically modified with β-D-galactosyl amine. The use of a specific sequence of amino acids allows for unprecedented control of carbohydrate spacing along a polymer chain.

Another level of controlling the architecture of carbohydrates on a macromolecular level is through the formation of carbohydrate clusters. The discovery of the glycoside cluster effect, by Lee and coworkers, was based on a tris-galactose cluster (Figure 1.16).[28, 63] The difference in affinity for the mono-galactose, bis-galactose, and tris-galactose analogs was 1 to 1000 to 1 million respectively. The

products of the synthesis of these compounds were separated by size exclusion chromatography.

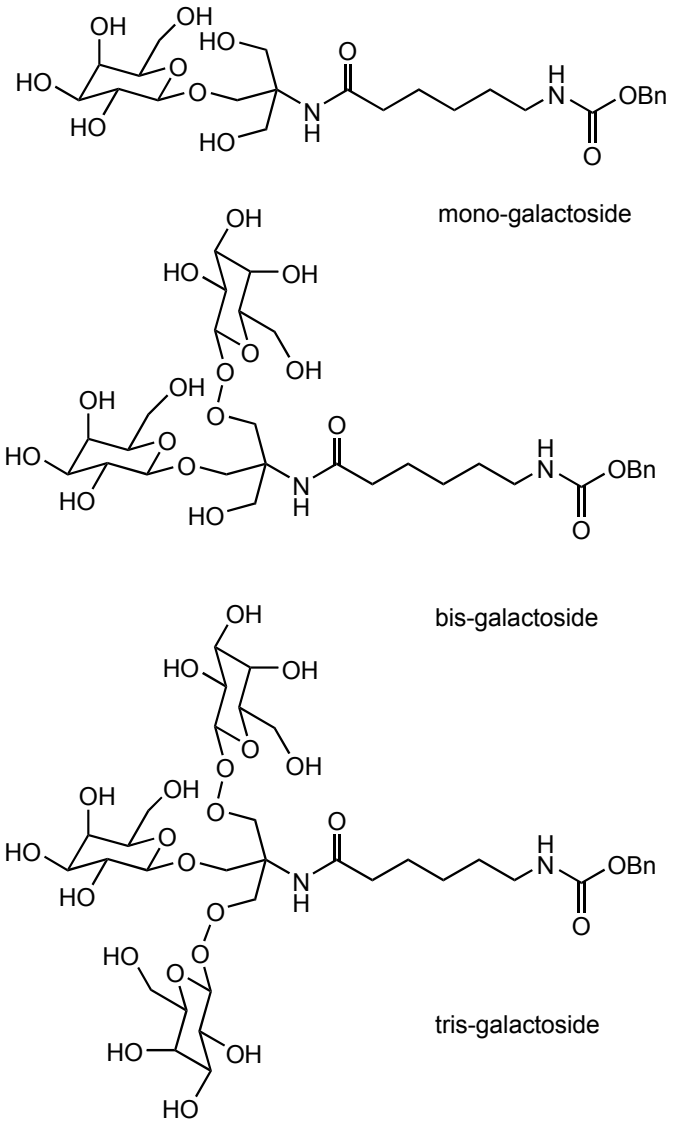

Figure 1.16 Mono-, bis-, and tris-galactosides from made by Lee and coworkers to observe the glycoside cluster effect.

Another example of a tris-carbohydrate cluster comes from Lindhorst *et. al.* where a tris-mannoside was made from glycosylation of a triol (Figure 1.17).[64] A similar

tris-mannoside was made by Grindley *et.al.* with a glycosylation strategy, followed by coupling to a tris-core to form a nonavalent glycodendrimer.[65]

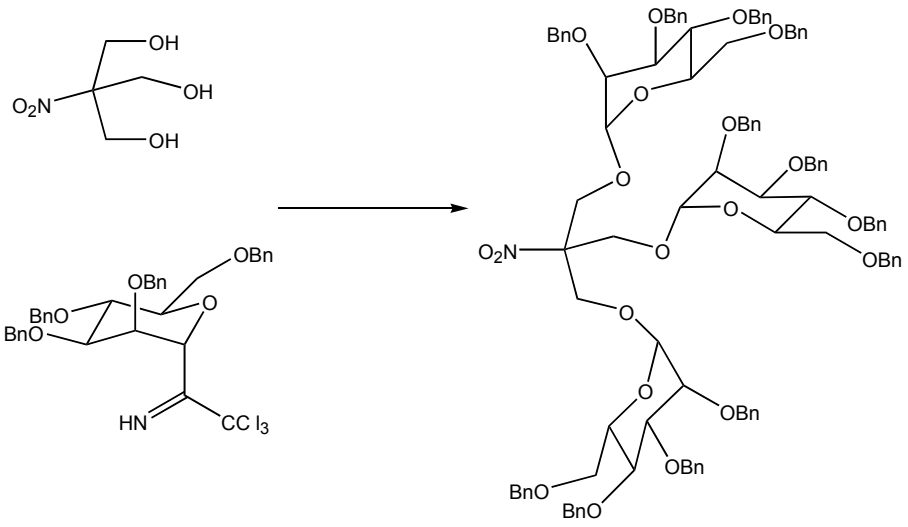

Figure 1.17 A tris-mannoside cluster developed by Lindhorst and coworkers.

One key component from these reports is that sugar clustering and sugar spacing each play a major role in the affinity of synthetic multivalent ligands. Clusters of carbohydrates contribute to the affinity through glycoside cluster effects, although high densities of sugars on a polymer can have negative impacts on the affinity of the ligand for a lectin. In this report we propose that tris-sugar clusters, spatially distributed on a dendrimer for optimal interaction with multiple lectin carbohydrate recognition domains, are valuable targets for studying carbohydrate-protein interactions.

Dendrimers

Dendrimers are synthetic macromolecules consisting of branches growing out from a single core (Figure 1.18a).[66-69] In the simplest case dendrimers are made divergently. A core molecule is selected, to this core AB_2 type monomers are added iteratively (Figure 1.18b). Each iteration accounts for a new dendrimer generation. A generation 1.0 might have six end groups, and after one more iteration, it becomes a generation 2.0 dendrimer with twelve end groups (Figure 1.18c). Convergent dendrimer synthesis allows for even more control over the synthesis, as the branches are made first then added to the core in the last synthetic step. Dendrimers alone have enormous potential in many applications including materials, therapeutics, and catalysis (Chapter 6). Attributes such as commercial availability for (some) different sized well defined macromolecules, and ease of surface, core, or interior- functionalization has generated interest for dendrimer applications across many avenues of science.

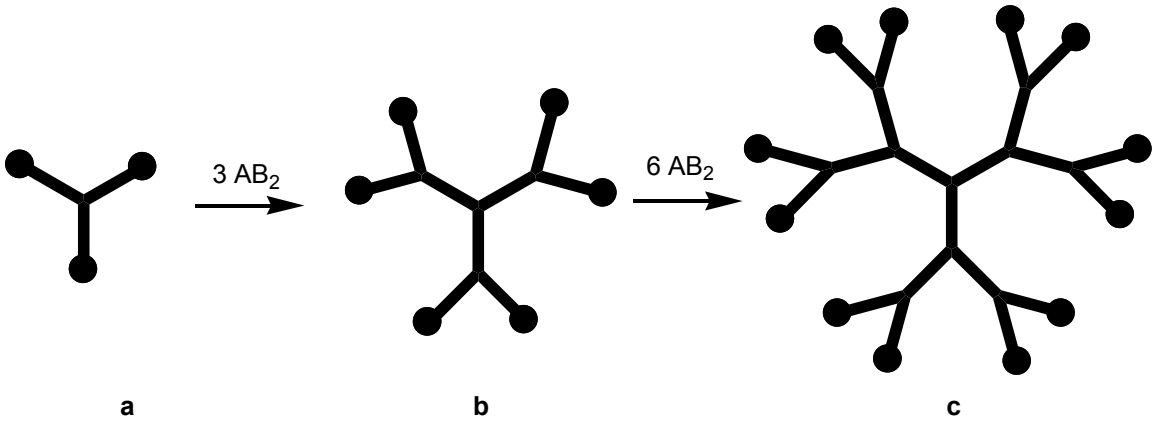

Figure 1.18 A diagram of dendrimer synthesis from the a) core; b) generation 1; and c) generation 2.

Surface functionalized dendrimers are highly appropriate scaffolds for synthetic multivalent ligands. By virtue of their structure they present carbohydrates as multiantennary ligands that mimics glycans and glycoproteins, which linear polymers and oligosaccharides fail to do. In addition the size of glycodendrimers can be easily varied according to dendrimer generation. This allows the same technology to be used in large-scale model studies and smaller-scale systems more appropriate for therapeutics. The relative medium size of dendrimers bridges the larger bodies of synthetic multivalent ligands of big multivalent polymers and small clusters. Dendrimers can be as well defined as small multivalent ligands, unlike the more heterogeneous populations of polymers. Yet dendrimers are large enough to span multiple lectin carbohydrate recognition domains, and also the sugar presentation can be changed with relative ease.

Poly(amidoamine), or PAMAM, dendrimers are particularly advantageous macromolecules. Ethylene diamine undergoes a Michael addition with four equivalents of methylmethacrylate (Scheme 1.1).[70] In this step the number of terminal groups doubles. Next four equivalents of ethylene diamine are coupled by peptide bond formation, and this returns primary amine functionality to the surface of what is now a generation 0.0 PAMAM dendrimer. These two iterations are repeated for each generation. Ester terminated dendrimers of this type may be converted to a carboxylic acid to form a half generation dendrimer, i.e. a generation 0.5 PAMAM. Both amine-terminated and carboxylic acid-terminated PAMAM dendrimers are commercially available.

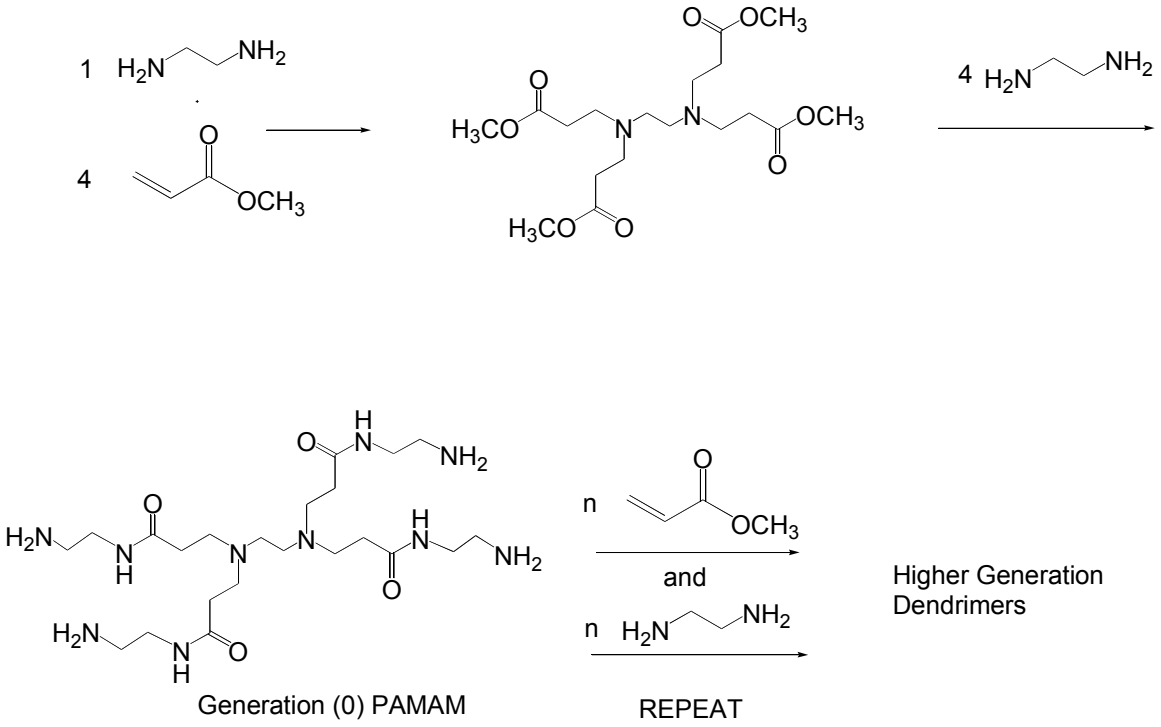

Scheme 1.1 Synthesis of PAMAM dendrimers.

PAMAM dendrimers are three dimensionally relatively well defined (Figure 1.19) with the larger dendrimers roughly spherical. The interior chains impart a large degree of flexibility to PAMAM dendrimers as well, which is important for multivalent binding scaffolds. The model of the G(5) PAMAM dendrimer in Figure 1.19 is meant to represent an idealized dendrimer structure, emphasizing the void volume on the dendrimer interior. PAMAM dendrimers in solution are very dynamic molecules able to encapsulate solvent guest molecules, or accommodate folding of the exterior branches.

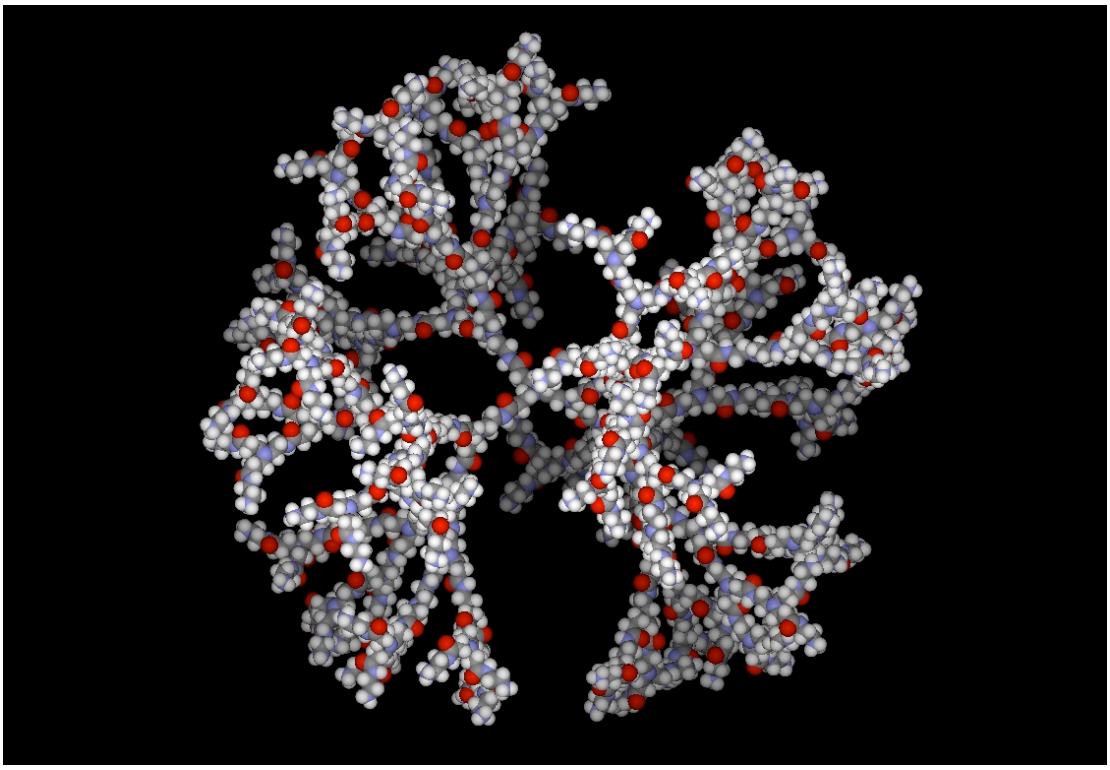

Figure 1.19 CPK model of a Generation 5 PAMAM dendrimer (Configuration file from Dr. James Baker, University of Michigan)

Early Work

Previously in our labs mannose functionalized dendrimers (Figure 1.20) were synthesized and used in conjugation with Con A in studies on protein carbohydrate interactions.[71, 72] It is noteworthy that fewer sugars were actually appended to the dendrimer surface than theoretically possible, which was due to in part to imperfections in the PAMAM dendrimer starting material and also due to steric hindrance at the dendrimer surface.

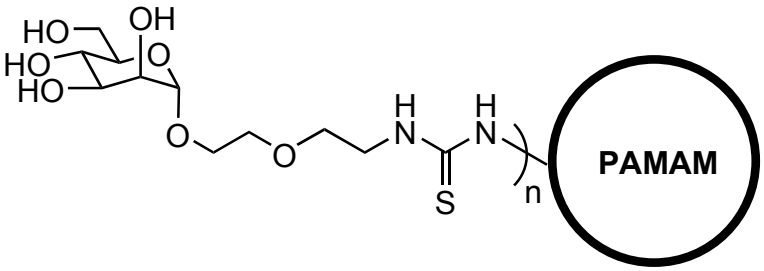

Figure 1.20 Mannose-functionalized PAMAM dendrimer.

Mannose functionalized PAMAM dendrimer generation 1 to generation 6, or G(1) to G(6), were compared with methyl mannose in a hemagglutination inhibition assay (Table 1.1).

Generation	Theoretical Number of Sugars	Actual Number of Sugars	Activity Relative to Methyl Mannose
1	8	8	1 ± 0.1
2	16	16	1.5 ± 0.1
3	32	29	21 ± 5
4	64	55	275 ± 90
5	128	95	510 ± 295
6	256	172	660 ± 230

Table 1.1 Mannose functionalized PAMAM dendrimer loading and activity.

The binding activity of the dendrimers was enhanced through multivalency relative to monomeric methyl-α-D-mannose (Table 1.1). The small dendrimers, generations 1 and 2, bind to Con A with activity as comparable to that of methyl-α-D-mannose. Generation 3, while too small to span the 65 Å separating the carbohydrate

recognition domains of the lectin, contains terminal mannose molecules spaced appropriately for proximity enhanced binding, and this is observed from the order of magnitude increase in activity in the hemagglutination inhibition assay. This increase in activity is valency corrected on a per mannose basis, so if the enhancement were simply additive from having a greater number of carbohydrates per molecule, the relative activity would be the same, valency corrected. EPR studies indicate that the generation 4 mannose functionalized dendrimer is able to span the distance between the Con A carbohydrate recognition domains, and the observed activity in the assay is more than 2 orders of magnitude greater than methyl-α-D-mannose.[73, 74] Generations 5 and 6 each demonstrate incremental increases caused by increased ability to engage in multivalent effects by becoming larger.

In the cases of the larger dendrimers, both proximity and multiple attachment sites could be responsible for the increased, valency corrected, activity. The relative activity of the multivalent dendrimers was increased when fewer sugars were appended to the dendrimer by heterogeneously functionalizing the dendrimers with both carbohydrates and spacer molecules (Figure 1.21). Dendrimers with varying degrees of sugar loading were examined in a hemagglutination inhibition assay.[73] Interestingly, a loading of about 50% (corresponding to an area per mannose around 550 $Å^2$ for each of the larger dendrimers) resulted in maximum activity. That dendrimers with 50% sugar and 50% spacers were more active than dendrimers fully loaded with sugars was an effect likely caused by steric congestion at the dendrimer surface.

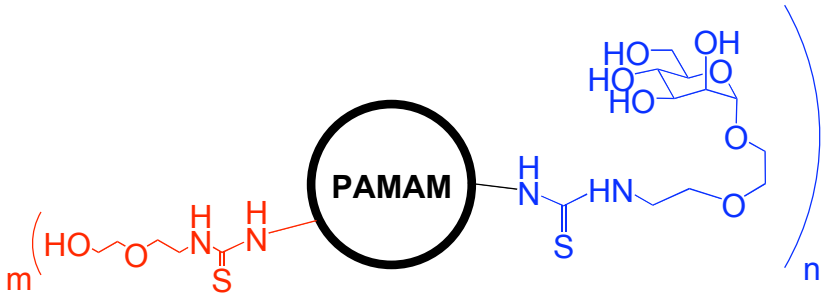

Figure 1.21 A mannose and ethoxyethanol heterogeneously functionalized PAMAM dendrimer.

Summary

Cell surface carbohydrates are complex biomolecules active in important and complex biological processes. Synthetic multivalent ligands can be used to elucidate the underlying mode of interactions between cell surface carbohydrates and protein receptors involved in both beneficial and negative biological pathways. As such, the two main goals in the studies described have been to analyze binding between proteins and synthetic multivalent ligands, and to use the knowledge and materials obtained for potential therapeutic uses. This report presents a number of experiments with these aims.

Organization

The first project described is the synthesis of heterogeneous mannose cluster functionalized dendrimers for binding studies with Con A for the purpose of evaluating the relative contributions of proximity effects and multivalency. The clusters acted to bind with proximity enhancements, and a heterogeneous functionalization strategy allowed for controlled cluster spacing. Although the addition of clusters is random, forcing the sugars into close proximity added another level of synthetic control to the

dendrimer functionalization. Comparisons of the affinities of cluster functionalized dendrimers and randomly functionalized dendrimers could provide a quantitative analysis of proximity effects in multivalency. An alternate purpose in this project was the evaluation of click chemistry methods for glycodendrimer synthesis.

Next, the synthesis of N-acetyl galactosamine, and phenyl azide, heterogeneous PAMAM dendrimers allowed for the synthesis of glycodendrimer-polymers, made to mimic lipid raft binding domains, again taking advantage of click chemistry.

Another project described is the synthesis of multivalent glycodendrimers, as gp120 mimics, for binding studies with Cyanovirin N. Dendrimers were functionalized with Manα1-2Man disaccharide from the corresponding isothiocyanate.

The next project discussed is the evaluation of the mannose functionalized PAMAM dendrimers introduced above (Figure 1.20), as well as evaluation of the new glycodendrimers presented in this report, in protein binding experiments. A number of techniques were used including precipitation assays, hemagglutination inhibition assays, isothermal titration microcalorimetry, and transmission electron microscopy. Through collaboration with Dr. Angela Gronenborn the National Institutes of Health (now at the University of Pittsburgh), binding studies with the manα1-2man functionalized dendrimers and Cyanovirin N were performed.

The final segment of the research described in this report is the synthesis of poly(polyoxometalate) cluster functionalized dendrimers and evaluation of these metallodendrimers and polyoxometalates as organic oxidation catalysts. A thorough introduction to polyoxometalates accompanies Chapter 6.

CHAPTER 2

TRIS-MANNOSE CLUSTER FUNCTIONALIZED DENDRIMERS

Introduction

The hypothesis for the work described in this section is that a dendrimer optimally suited for binding with lectins would contain clusters of carbohydrates in close proximity that would effectively increase the local concentration of sugars around the lectin carbohydrate recognition domain. Also these sugar clusters would be positioned around the dendrimer periphery appropriately to minimize negative steric interactions between the binding partners in the space between carbohydrate recognition domains.

One way to achieve this result would be to tether dendrimer end-groups together. However, dendrimers are dynamic molecules and once the end-groups are un-tethered, a random distribution of end-groups again occurs.[75] To form a more permanent arrangement, one cluster can be bound to a single dendrimer end-group. Isothiocyanates can be readily appended to PAMAM surface primary amines. The sugar clusters reported here, bearing an isothiocyanate functional group, were synthesized using 'click chemistry'.

K. Barry Sharpless, referring to near perfect carbon-heteroatom bond forming reactions, coined the phrase 'click chemistry'.[76, 77]. A click chemistry reaction should be bioorthogonal, have no by-products, be quantitative, efficient, and compatible with other functional groups on the combining molecules. In each case the addition occurs between

two high-energy functional groups with a very narrow range of reactivity, such that the reaction is energetically downhill and selective. Click chemistry reactions are performed in water, using water as a co-solvent or heterogeneously on water.[78, 79] Among the reasons for this is because water has a relatively high heat capacity and click reactions are endothermic by definition.

Some examples of click chemistry reactions are nucleophilic opening of strained rings, hetero diels-alder reactions, the formation of hydrazones or oximes, and a copper (I) catalyzed Huisgen dipolar cycloaddition reaction between an azide and an alkyne (Scheme 2.1).

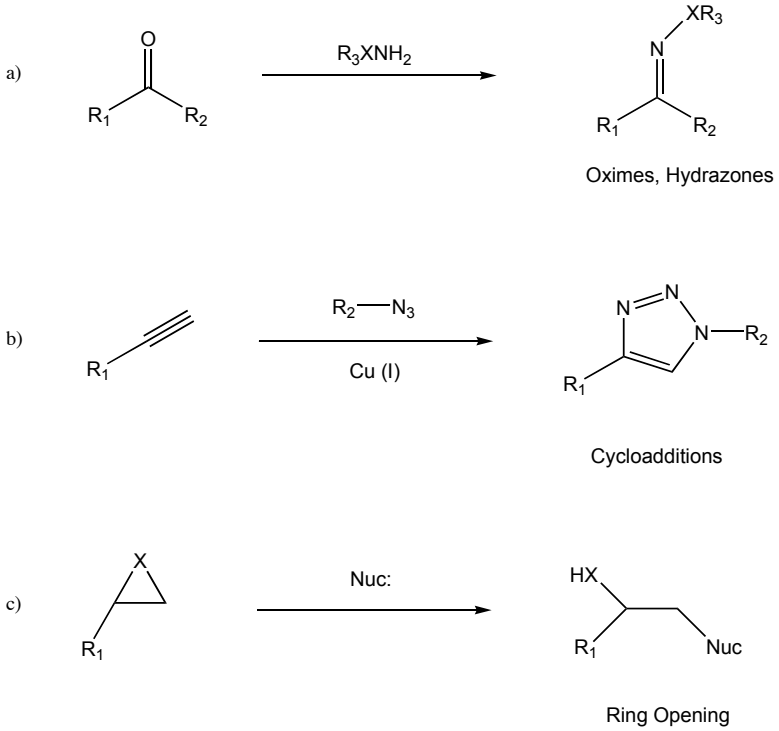

Scheme 2.1 Examples of click chemistry: a) condensation reactions with carbonyls b) some cycloadditions c) nucleophilic opening of strained rings.

For the purpose of making new carbohydrate architectures, click chemistry allows for large, perfect, molecules to be made relatively quickly, without purification, in quantitative yield, and without disruption of other existing functionality, such as an isothiocyanate. The reaction selected for the synthesis of carbohydrate clusters was the 1,3 dipolar cycloaddition of an azide and an alkyne.

The Huisgen cycloaddition can be performed under thermodynamic conditions, although this results in a mixture of 1,4 and 1,5 disubstituted 1,2,3-triazoles (Figure 2.1).[80] In the presence of catalytic Cu(I) the reaction is regioselective and is under kinetic control. This form of the reaction was reported around the same time by two different research groups,[81, 82] and has since been used in a large number of syntheses.[83-87]

Figure 2.1 A) a 1,4 disubstituted 1,2,3-triazole and B) a 1,5 disubstituted 1,2,3-triazole.

Synthesis of a tris-Mannose Cluster

The synthesis of a tris-mannose cluster began with 2-amino-2-hydroxymethyl, 1,3-propanediol as a starting molecule. This starting point was advantageous as it contains three equivalent branches for a carbohydrate linkage. The amino-alcohol, more commonly known as 'TRIS', or tris(hydroxymethyl)aminomethane, is readily available in large quantity because it is a component in a common buffer, TRIS buffer.

First the amine group was protected as the *t*-butyloxycarbamate **1**.[88] This protecting group is easily cleaved in acid, and is stable to the basic conditions required for the next step. The triol was deprotonated with sodium hydride, followed by the addition of four equivalents of propargyl bromide at -50 °C, in DMF, which formed product **2** with 45 % overall yield (Scheme 2.2).

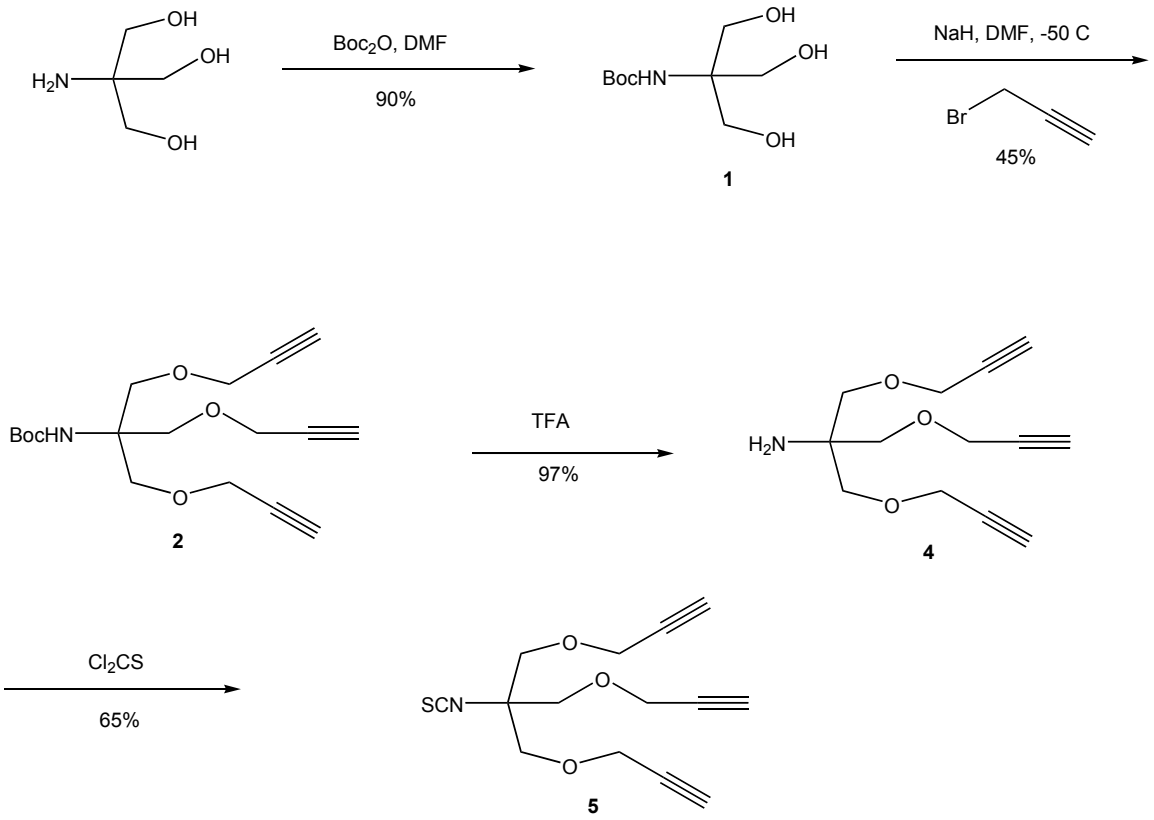

Scheme 2.2 Synthesis of tris(propargyloxymethyl)isothiocyanatomethane (**5**).

Propargylations were also attempted using different bases, temperatures, solvents, and inert atmosphere based on selected propargylations in recent literature reports.[89-91] Propargyl benzene sulfonate (**3)** was synthesized according the conditions reported by

Reppe,[92] and this was used as an alternative to propargyl bromide,[93] though this failed to yield the desired tris-propargyl ether. Ultimately, the conditions shown for the reaction were accepted.

Next the amine was deprotected using trifluoroacetic acid in dichloromethane to form **4**, followed by the conversion of the amine to an isothiocyanate **5** using thiophosgene. The tris-propargyl ether **5** could then be used as the alkyne component for copper mediated addition of three equivalents of an azido-functionalized mannose.

The sugar was prepared first by penta-acetylation of α-D-mannose, followed by the selective removal of the anomeric protecting group using hydrazine acetate followed by activation of the anomeric position by the formation of a trichloroacetimidate **8** (Scheme 2.3).[94]

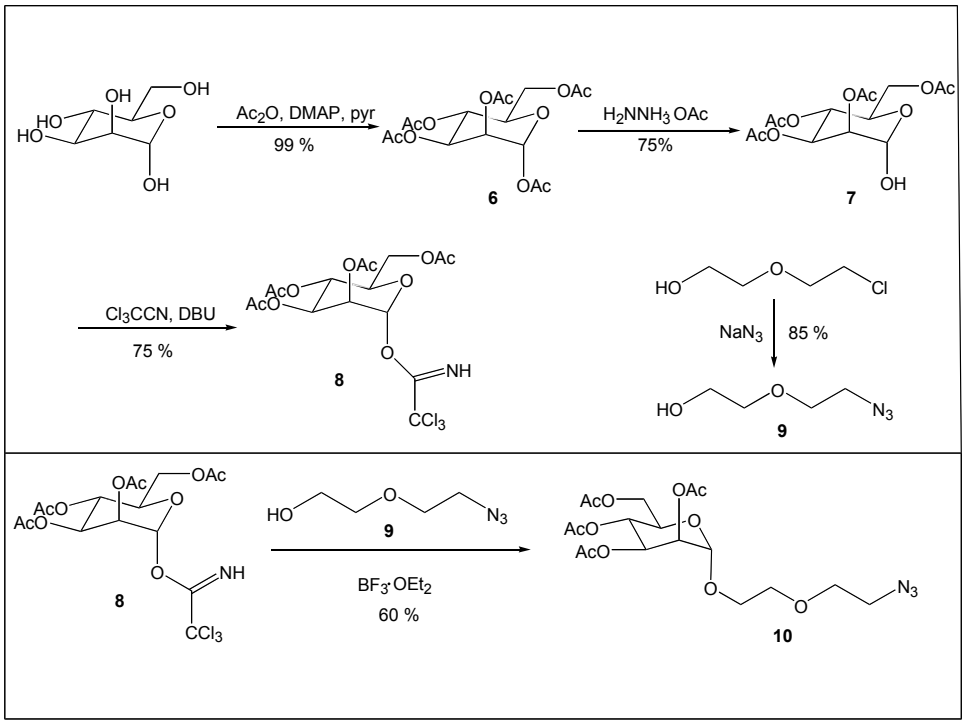

Scheme 2.3 The synthesis of 1-*O*-(5-azido-3-oxapentyl)-2,3,4,6-tetra-*O*-acetyl-α-D-mannopyranoside (**10**).

The 2-2-(azidoethoxy)ethanol linker **9** was made from simple substitution of the corresponding chloride with sodium azide in DMF at 80 °C over two days. The lewis acid mediated coupling of the azido-alcohol **9** to the activated sugar **8** was performed using boron trifluoride etherate as the Lewis acid, giving azido-mannose **10**. This coupling procedure was appealing because the product had the desired α configuration, due in part to the anomeric effect, and also largely due to neighboring group participation from the acetyl protected alcohol on the number 2 carbon of the sugar pyran ring.

The click chemistry cycloaddition reaction was initially performed in a 1:1 mixture of *tert*-butanol and water.[81] The tris-propargyl ether **5** and four equivalents of azide **10** were combined in the solvent mixture followed by a catalytic amount of copper sulfate, 10 mol % per alkyne, or 30 mol % overall (Scheme 2.4).

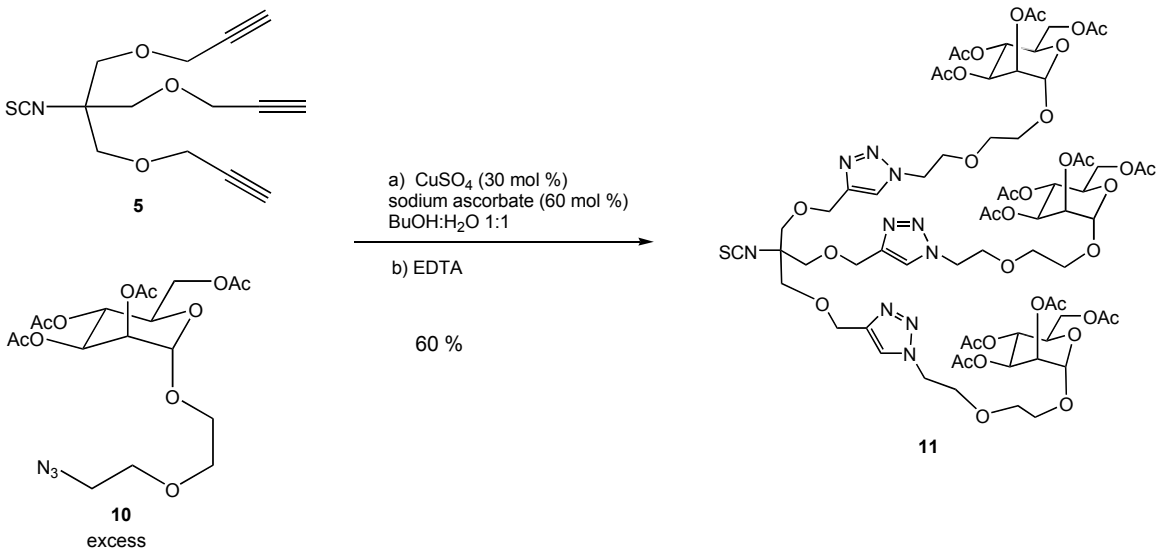

Scheme 2.4 The synthesis of tris-mannose cluster **11**.

Instead of using a copper (I) salt, which is more susceptible to degradation over time, a copper (II) salt was added and reduced to copper (I) in situ using sodium ascorbate. A small excess of azide was used in this case because under these conditions the reaction wasn't perfect, and a bis-functionalized mannose cluster was observed in addition to tris-mannose cluster **11**. Chromatography using silica gel failed to adequately separate the products, although TLC could be used to visualize the consumption of the starting materials in the reaction, a process taking one to two days.

In their development of this dipolar cycloaddition reaction, the scientists at Scripps Research Institute made an interesting discovery. If the reaction was used to synthesize tris-1,2,3-triazoles (Figure 2.2), an autocatalytic effect was observed.[95, 96]

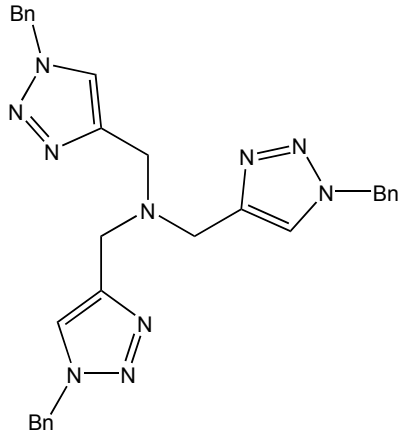

Figure 2.2 The Cu(I) stabilizing ligand tris-(benzyltriazolylmethyl)amine.

Tris-triazoles are good ligands for copper (I) stabilization, binding tightly enough to protect the ion from oxidation or disproportionation, yet loosely enough to not inhibit the catalytic activity of the metal. In general tris-triazoles have not been reported as

ligands for transition metal catalysts, a fact the authors attribute to the previous lack of a facile synthesis of the compounds.[95] The use of tris-triazole stabilizing ligands is of particular interest in bioconjugation chemistry where high concentrations of copper ions can be detrimental to certain biomolecules.

For the purposes of the work described here, it was uncertain whether autocatalysis was observed, yet any bound copper ions needed to be removed prior to characterization and subsequent synthetic steps. In order to accomplish this, the product was stirred with the sodium salt of ethylenediamine tetra acetic acid (EDTA), which has a high affinity for copper (II) $K_{eq} = 8.0 \times 10^{18}$, and for copper (I) $K_{eq} = 3.2 \times 10^{8}$.[97]

To efficiently scavenge the excess azide upon completion of the cluster forming click chemistry reaction, a hexynoate solid phase resin was made from Wang resin, polystyrene cross-linked with divinylbenzene, with benzyl alcohol groups at approximately 0.1mmol/g. Hexynoic acid was added to the resin using a diisopropyl carbodiimide coupling procedure previously reported in the literature (Scheme 2.5) giving alkyne-functionalized resin **12**.[98] The alkyne could then be hydrolyzed with 20% trifluoroacetic acid in dichloromethane. Higher acid concentrations led to higher levels of impurity in the product, and lower acid concentrations failed to cleave the alkyne. In addition the reaction was performed in plastic centrifuge tubes without stir bars to avoid contamination. The cleavage occurred with shaking, turning the resin pink, and after filtration and solvent evaporation, hexynoic acid was measured indicating an average of 0.6 mmol alkyne / g resin.

The resin was then used as a possible azide scavenger after formation of the tris-mannose cluster by click chemistry, however an excess of azide was still present in the

product after the resin was filtered from the reaction solution. To test the effectiveness of the dipolar cycloaddition on the solid phase resin a simple test was performed combining resin **12** with the simple azide **9** in the presence of copper (I) (Scheme 2.6). After cleavage with trifluoroacetic acid the only observed product was hexynoic acid indicating no triazole was likely formed on the resin, thus it's use as a scavenger was limited.

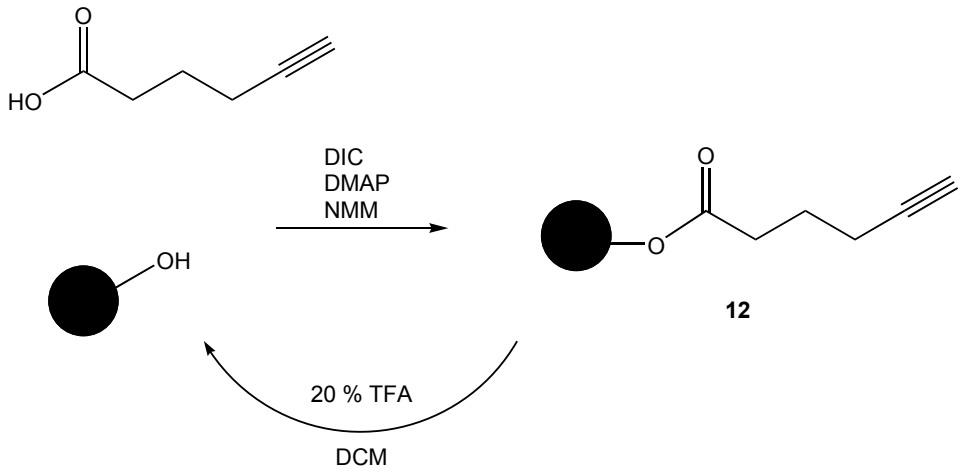

Scheme 2.5 Hexynoate resin synthesis and cleavage.

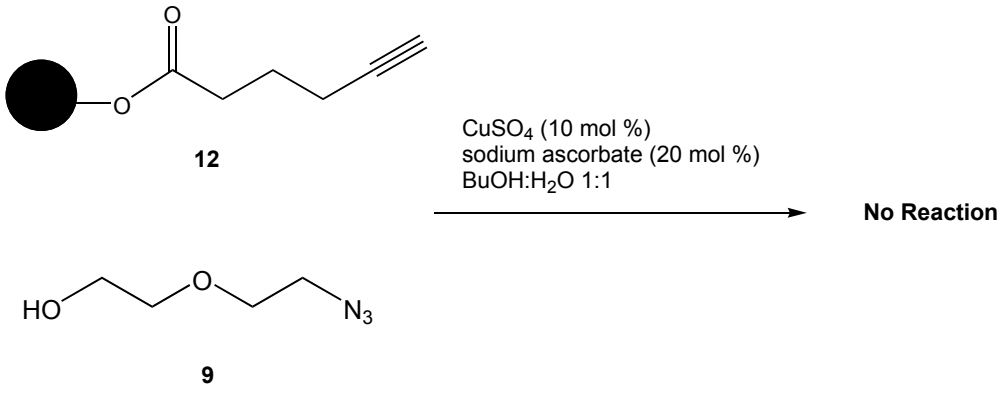

Scheme 2.6 No dipolar cycloaddition occurs with the hexynoate resin under normal conditions.

The relatively large size of the click chemistry products inspired attempts at purification by size exclusion chromatography. Most size exclusion resins are developed for use with water, and fail for organic compounds in organic solvents. As such a Sephedex G-50 gel failed to purify cluster **11**. However, lipophilic Sephedex was ideal for purification in organic solvents and was used to very effectively separate the bis-mannose, the tris-mannose, and any starting materials in dimethylformamide (the water soluble catalysts were extracted from the products in chloroform).

The need for purification obviated an important attribute of click chemistry. Although the conditions used to form the 1,2,3-triazoles were the most common from similar reactions reported in the literature, other methods for the copper catalyzed Huisgen dipolar cycloaddition have been used.[83, 99-101] Combinations of solvent, reductant, and temperature were tested to optimize the reaction (Figure 2.3).

55 °C sodium acorbate *t*-butanol:water	55 °C copper wire *t*-butanol:water	
25 °C sodium acorbate THF:water	25 °C copper wire THF:water	55 °C sodium acorbate THF:water
25 °C sodium acorbate DMSO:water	55 °C sodium acorbate DMSO:water	25 °C copper wire DMSO:water

Figure 2.3 A grid representing combinations of dipolar cycloaddition conditions applied in the synthesis of cluster **11**.

Sterically hindered azides or alkynes may require elevated temperatures; so one set of click chemistry reactions to form **11** was performed at 55 °C and another at room temperature (25 °C). Another reducing agent to convert copper (II) into copper (I) is copper metal itself. One set of click reactions was done with sodium ascorbate and another with copper wire. Finally the solvent system was altered using 1:1 mixtures of dimethyl sulfoxide and water, and tetrahydrofuran and water in addition to *t*-butanol and water. Each combination of these variables led to at least some product formation after two days. The products were extracted with chloroform, washed, and analyzed by ^{1}H NMR. The best combination resulted from the use of a tetrahydrofuran:water solvent system at room temperature using sodium ascorbate as the reducing agent. Using these conditions the formation of the tris-mannose cluster **11** could be done with simple workup, without byproducts, and with no purification in quantitative yield (Scheme 2.7).

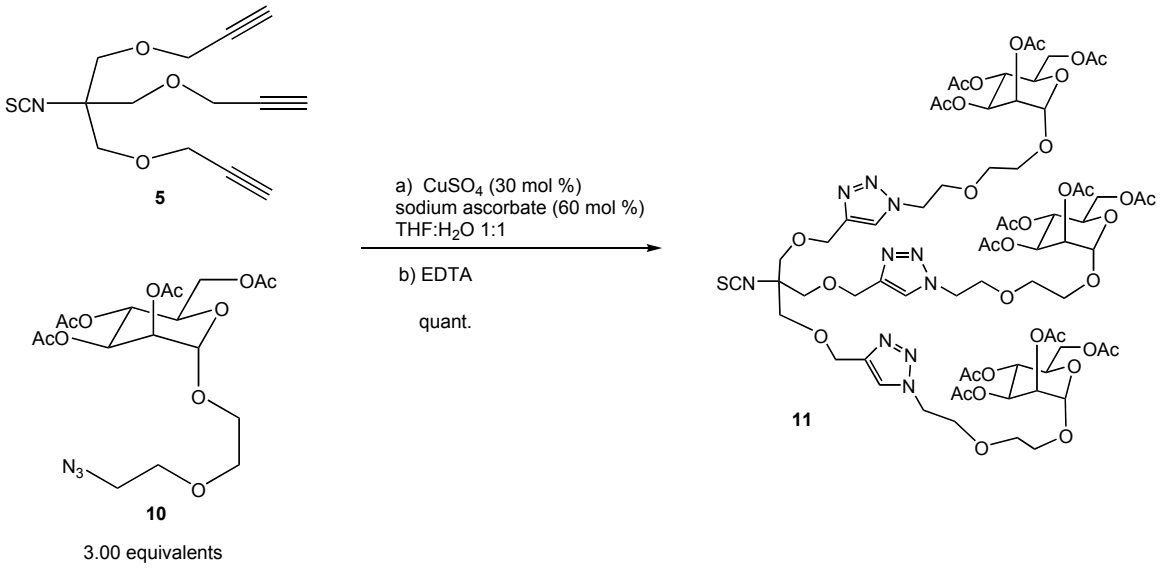

Scheme 2.7 Improved synthesis of tris-mannose cluster **11**.

Two similar products were formed using the early dipolar cycloaddition conditions (Scheme 2.8). The *t*-butyloxycarbamate **2** was converted into an amine-protected form of a tris-mannose cluster **13**. This compound was used for a heteronuclear multiple-quantum coherence (HMQC) experiment to determine NMR assignments, and **13** could also later be used as a reference in protein binding experiments.

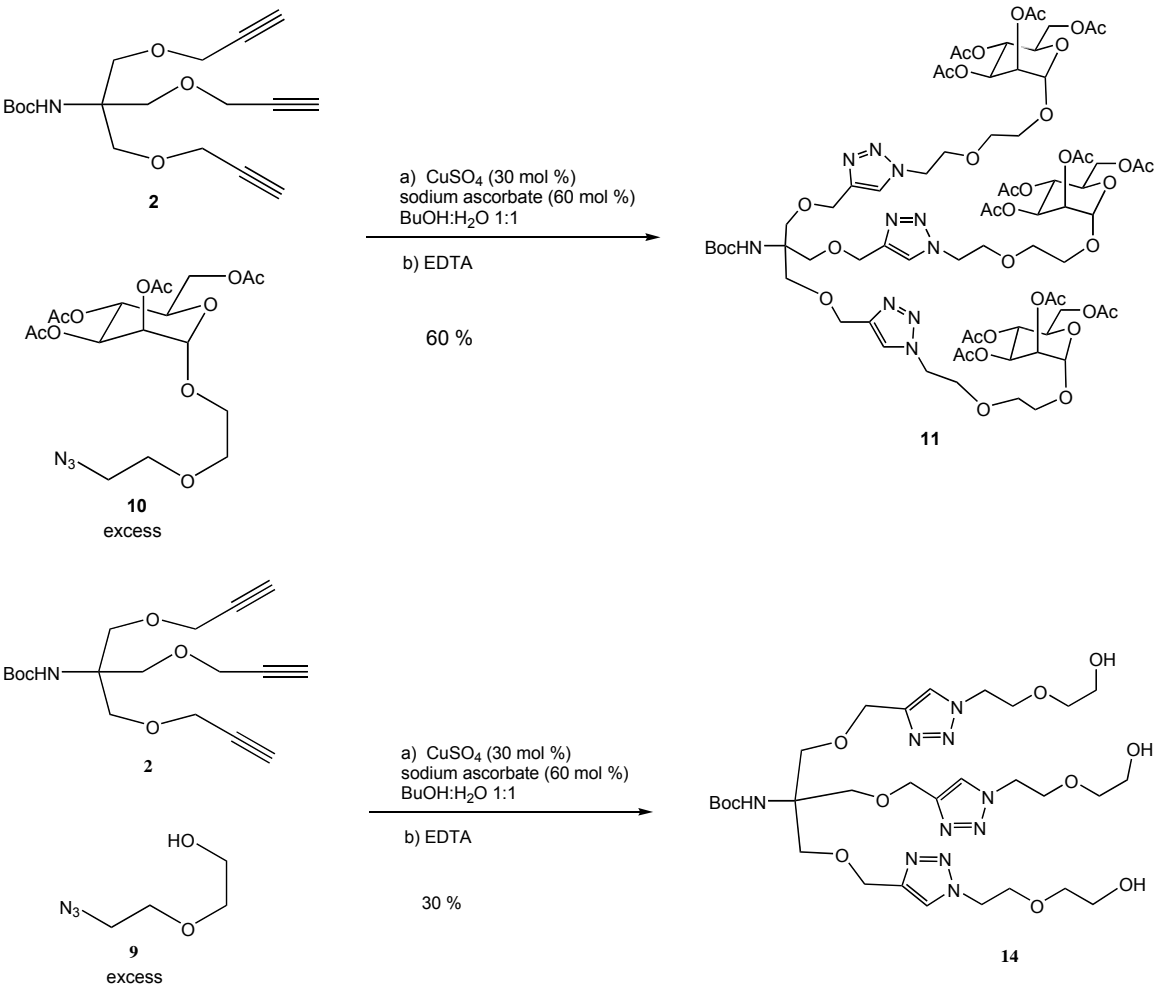

Scheme 2.8 Synthesis of the mannose cluster **13** (top) and ethoxyethanol cluster **14** (bottom).

Compound **2** and azide **9** were also coupled with a dipolar cycloaddition, and this model compound **14** was used in NMR experiments to observe nuclear Overhauser enhancements used to determine the triazole regiochemistry (Figure 2.4). Excitation at the aromatic proton (7.8 ppm) resulted in signal enhancements for two sets of protons; from the neighboring methylene of the TRIS derivative (4.58 ppm), which would occur in the case of either regioisomer, and from the triplet of the methylene closest to the aromatic ring from the ethoxyethanol (4.52 ppm), which can only arise from the 1,4 disubstituted triazole. The equal magnitude of the enhancement indicates this is the predominant regioisomer as predicted for this reaction. The reciprocal enhancement, exciting at each methylene signal, confirms this relationship.

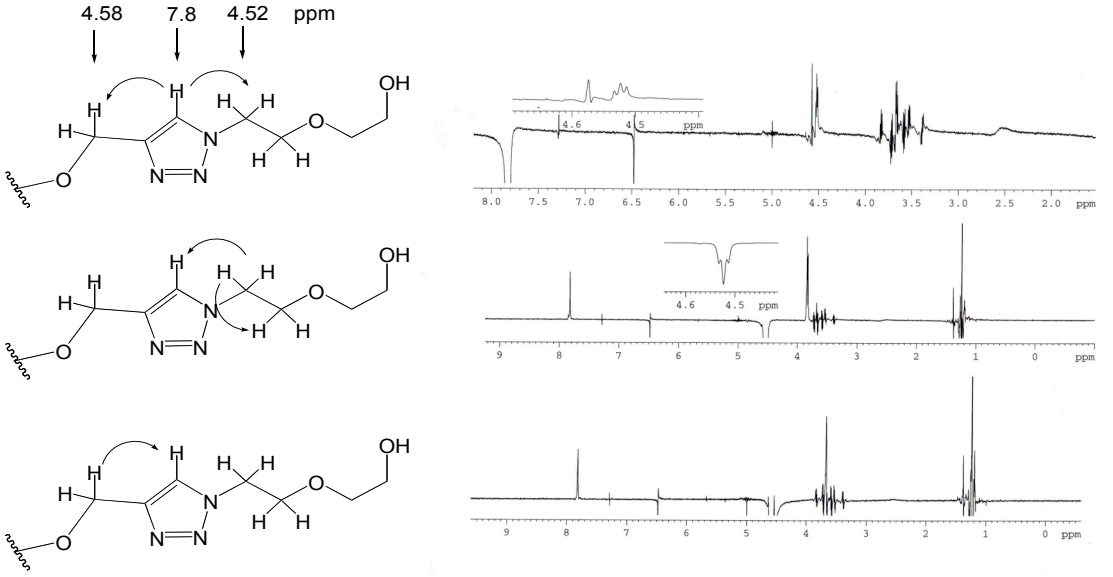

Figure 2.4 Nuclear Overhauser effect NMR experiment with compound **14**. Excitation at the aromatic signal enhances both the ethoxyethanol methylene triplet (4.52 ppm) and TRIS methylene singlet (4.57 ppm) indicating proximity to both (top). Excitation at the triplet ehances the signal at the neighboring methylene and the aromatic proton (middle) and excitation at the singlet results in similar enhancement at the aromatic proton (bottom).

Synthesis of Cluster Functionalized PAMAM Dendrimers

The synthesis of cluster-functionalized dendrimers **15-19** with isothiocyanate **11** and PAMAM dendrimers is shown in Scheme 2.9. An excess of isothiocyanate was used to saturate the PAMAM dendrimer surface with tris-mannose clusters. The reaction between an isothiocyanate and a primary amine formed a thiourea covalent linkage between the components. Product purification was first attempted by dialysis against dimethyl sulfoxide using a regenerated cellulose membrane with a molecular weight cutoff (MWCO) of 3500 Da. This failed to separate **15-19** from the cluster **11**, a surprising result because **11** has a molecular weight of only 1662 g/mol. If a membrane with a MWCO of 10,000 Da was used instead the dendrimers retained inside the membrane were pure. One conclusion from exhaustive dialysis experiments with glycodendrimers in organic solvents is that the reported membrane cutoff is not reliable, and the appropriate membrane is best determined experimentally.

The acetyl protecting groups on the mannose compounds were not required for dendrimer functionalization, however they were retained during this step for their diagnostic NMR signals and for macromolecular characterization by mass spectrometry. Deacetylation of **15-19** was done using Zemplén conditions (sodium methoxide in methanol and water)[45, 102] resulting in the dendrimers **20-24**, which were purified by dialysis again, this time in Millipore water with MWCO 1000 Da membranes.

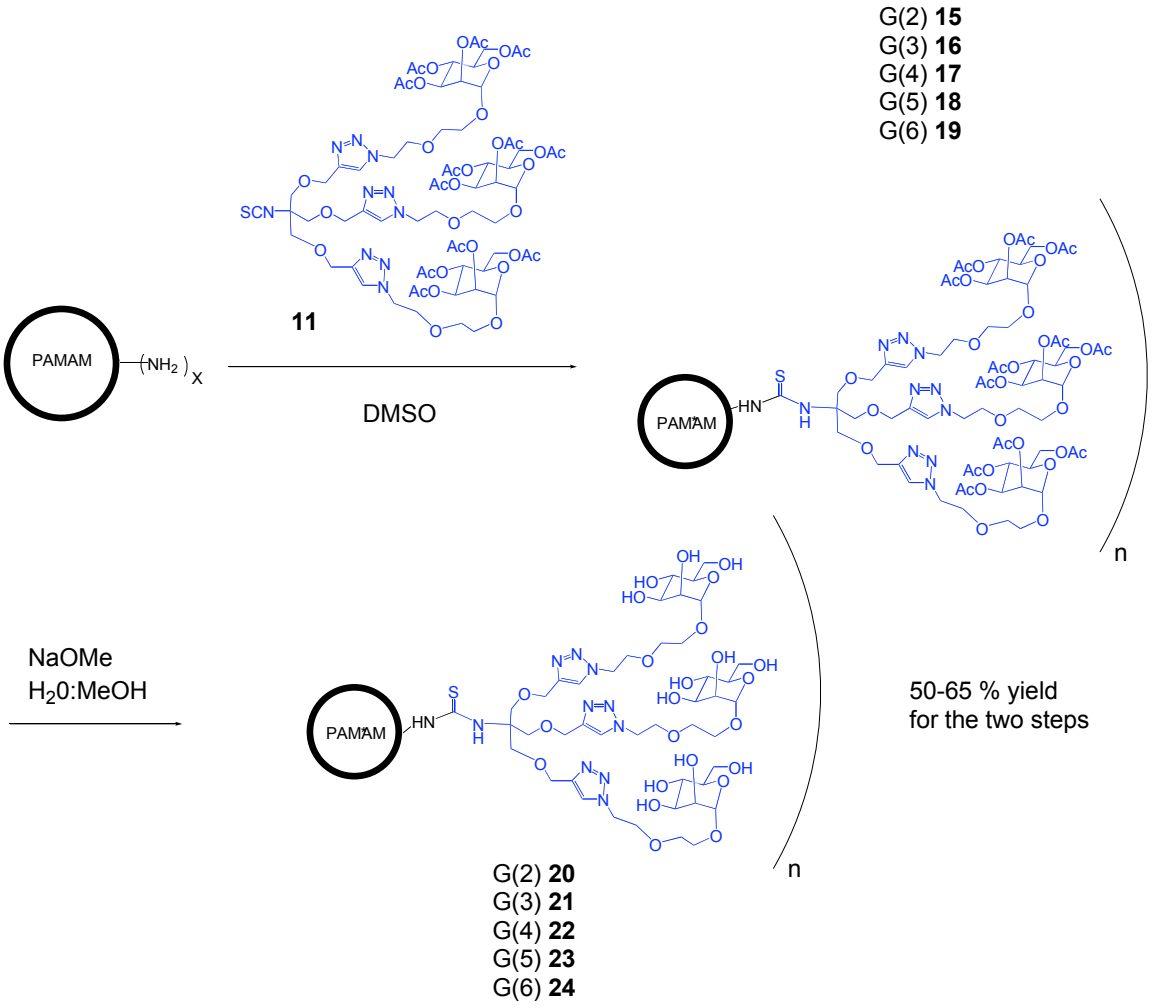

Scheme 2.9 Synthesis of tris-mannose cluster functionalized PAMAM dendrimers **20-24**.

Recent work from our group with other glycodendrimers has shown the presence of aromatic groups on the linker can have a negative impact on water solubility of the final product, which is requisite for protein binding studies.[71] Fortunately the triazole-linked dendrimer displayed no such insolubility, as even the large dendrimers saturated with clusters were readily dissolved and purified in water.

Prior to deacetylation the dendrimers encapsulated a certain quantity of solvent, and if dried on vacuum too long it reduced the solubility of the dendrimers. This can lead

to error in calculating the correct yield for this type of macromolecule, though the calculated yields are generally less than 110% (see the experimental section at the end of this chapter). The deacetylated dendrimers can be dried fully, however, and the final product mass determined accurately. In these dendrimers the two steps are accomplished in approximately 50% to 65% yield. The product loss from these reactions is mostly due to the dialysis purification, as can be observed by evaporating the solvent and analyzing the material that diffused through the membrane.

Characterization by NMR

The ^{1}H NMR (500 MHz) spectrum of the mannose cluster **11** in d_6-DMSO is shown in Figure 2.5. The peak at 8.0 ppm corresponds to the triazole proton, the peaks at 5.0, 4.5, and 3.9 to 4.2 ppm result from the protons on the sugar ring, the peak at 4.5 ppm is from the linker protons adjacent to the triazole ring. These two signals were separate in $CDCl_3$, however they overlap in d_6-DMSO. From 3.4 to 3.8 ppm represents the remaining linker protons, and from 1.8 to 2.1 ppm the signals correspond to the protons on the acetyl protecting groups.

The spectra from acetyl-protected mannose cluster functionalized G(2) dendrimer **15** and deacetylated G(2) dendrimer **20** are shown in Figure 2.6 for comparison. The sharp signal of the singular triazole proton is still observed farthest downfield, however, broad peaks from the dendrimer amide protons, and thiourea protons overlap the signal forming a multiplet. A very small broad peak at 6.8 arises from the very hindered thiourea proton of the TRIS linker. Interestingly, the signals from the methylenes adjacent to the triazole ring (4.45 and 4.49 ppm) differentiate upon tethering with the

dendrimer. The smaller broadened peaks between 2.1 and 3.4 ppm correspond to dendrimer protons. The difference between Figure 2.6a (acetylated) and 2.6b (deacetylated) is significant. The deprotection leads to a high degree of broadening of the signals from sugar and linker protons, and the four distinct acetyl signals are removed.

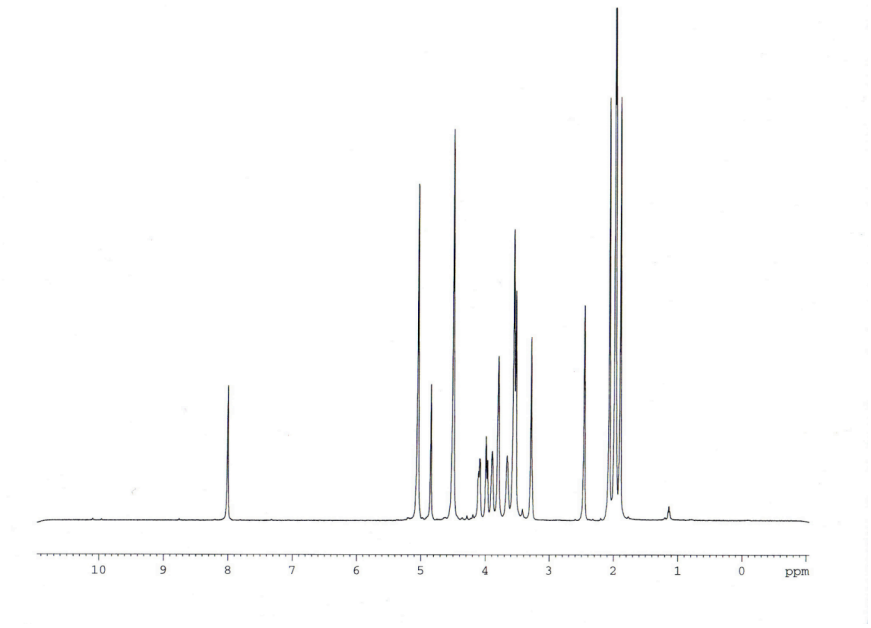

Figure 2.5 ^{1}H NMR spectrum (500 MHz) of **11** in d_6-DMSO.

The ^{1}H NMR (500 MHz) spectrum of acetyl-protected mannose cluster functionalized dendrimer **19** in d_6-DMSO is shown in Figure 2.7 for further comparison. The dendrimer in Figure 2.6 is a G(2), and in Figure 2.7 is a G(6). The increased molecule size has the consequence of broadening the signals in each region of the spectrum, though the line broadening is more severe with the protons further into the molecular interior because of increased T_2 relaxation rates from the sterically congested environment. The ^{13}C NMR (125 MHz) of compounds **11**, **20**, and **24** are shown in Figure 2.8.

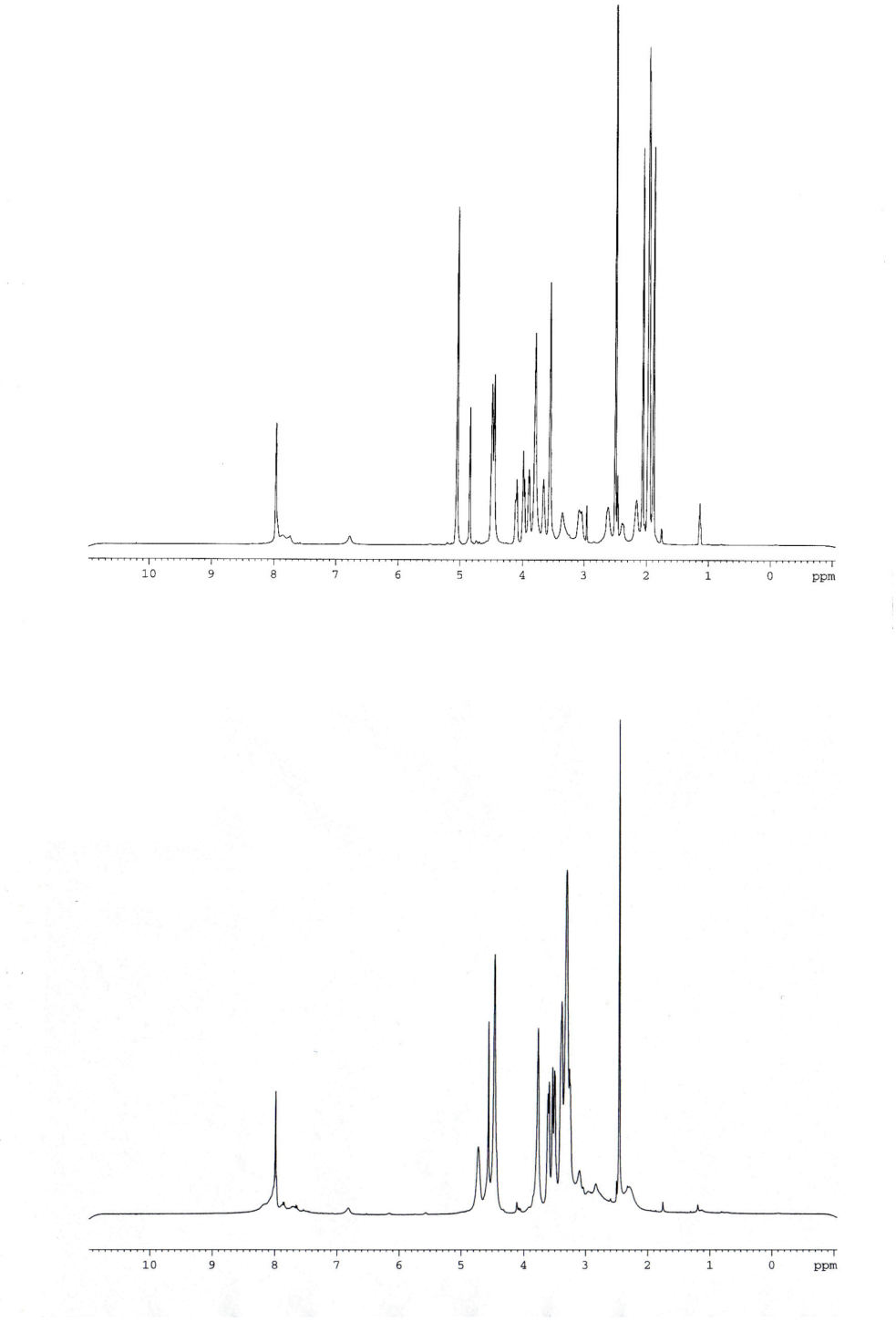

Figure 2.6 ^{1}H NMR spectra (500 MHz) of **15** (top) and **20** (bottom) in d_6-DMSO.

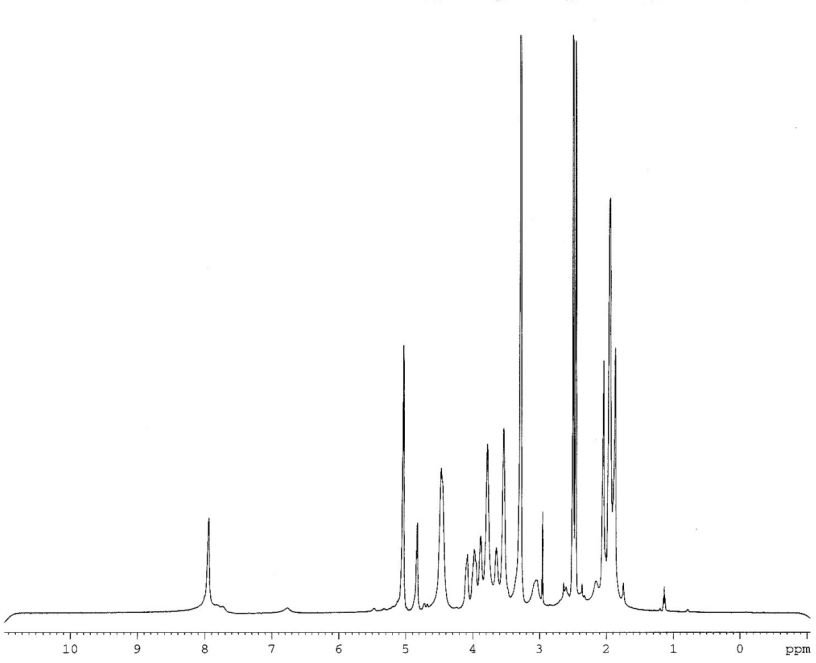

Figure 2.7 ^{1}H NMR spectrum (500 MHz) of **19** in d_6-DMSO.

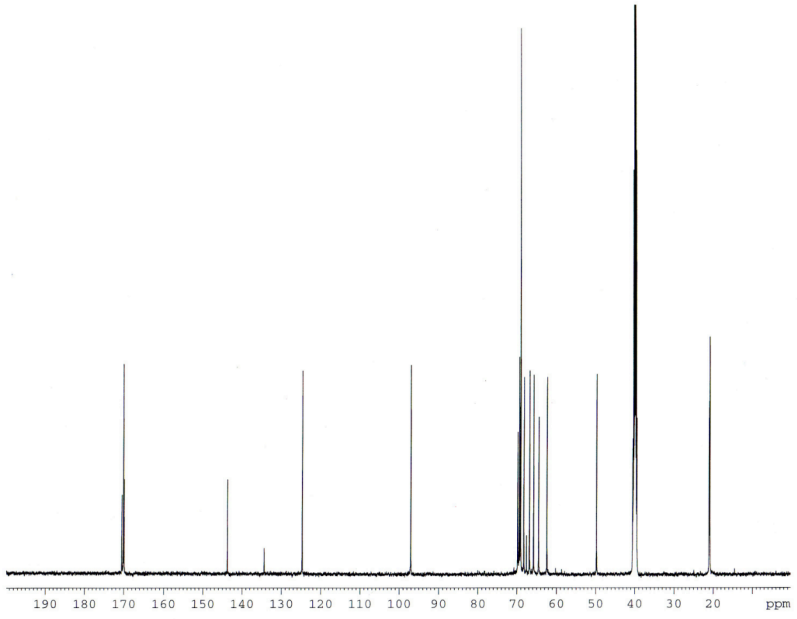

Figure 2.8 The ^{13}C NMR spectrum (125 MHz) of **11** in d_6-DMSO.

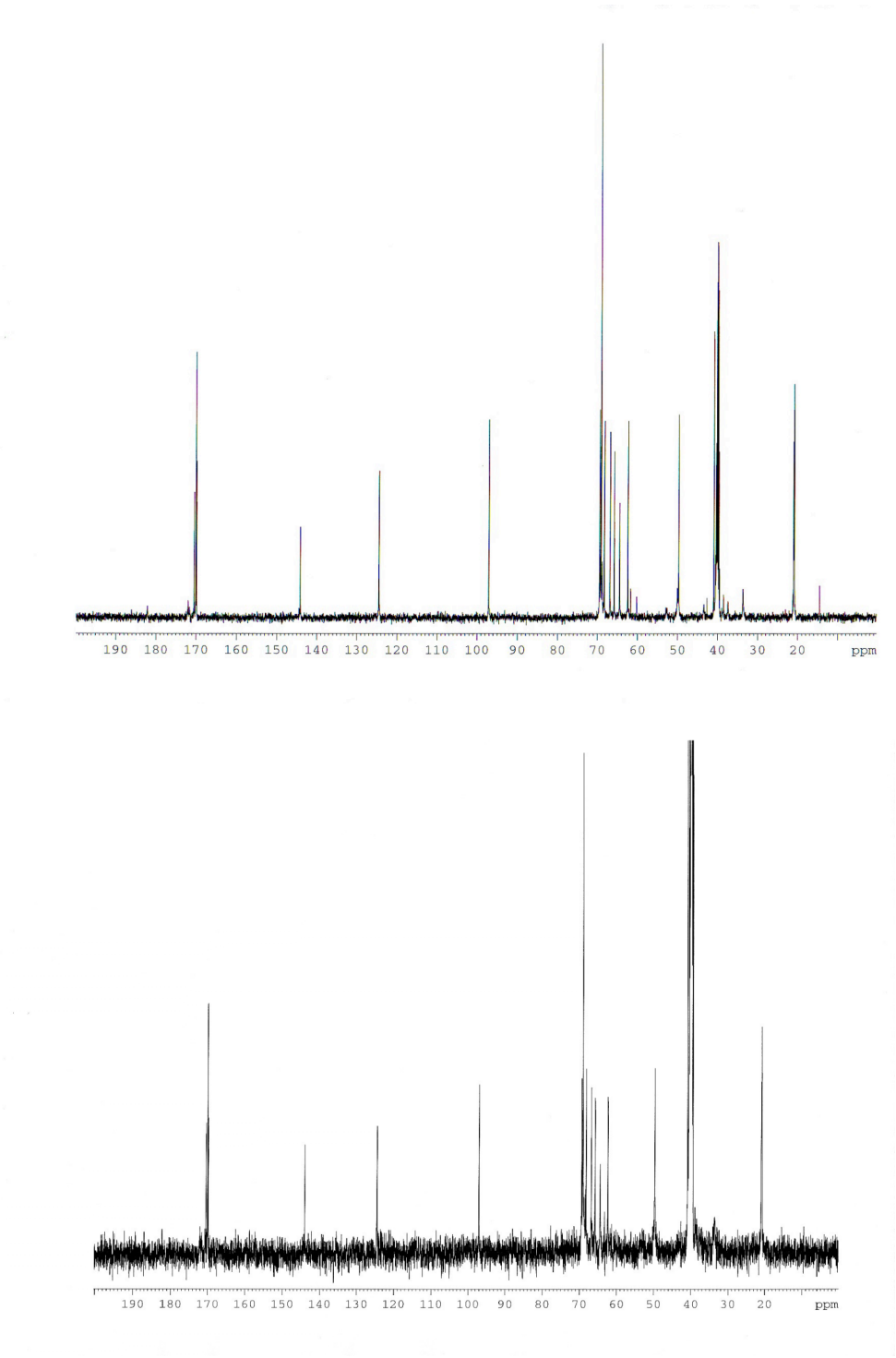

Figure 2.8 continued: ^{13}C NMR spectrum (125 MHz) of **20** (top) and **24** (bottom) in d_6-DMSO.

Characterization by MALDI-TOF MS

Matrix assisted laser desorption ionization time of flight mass spectrometry (MALDI-TOF MS) is a powerful technique for the measurement of the molecular weight of glycodendrimers. The MALDI-TOF spectra for compounds **15-24** are given in Figure 2.9.

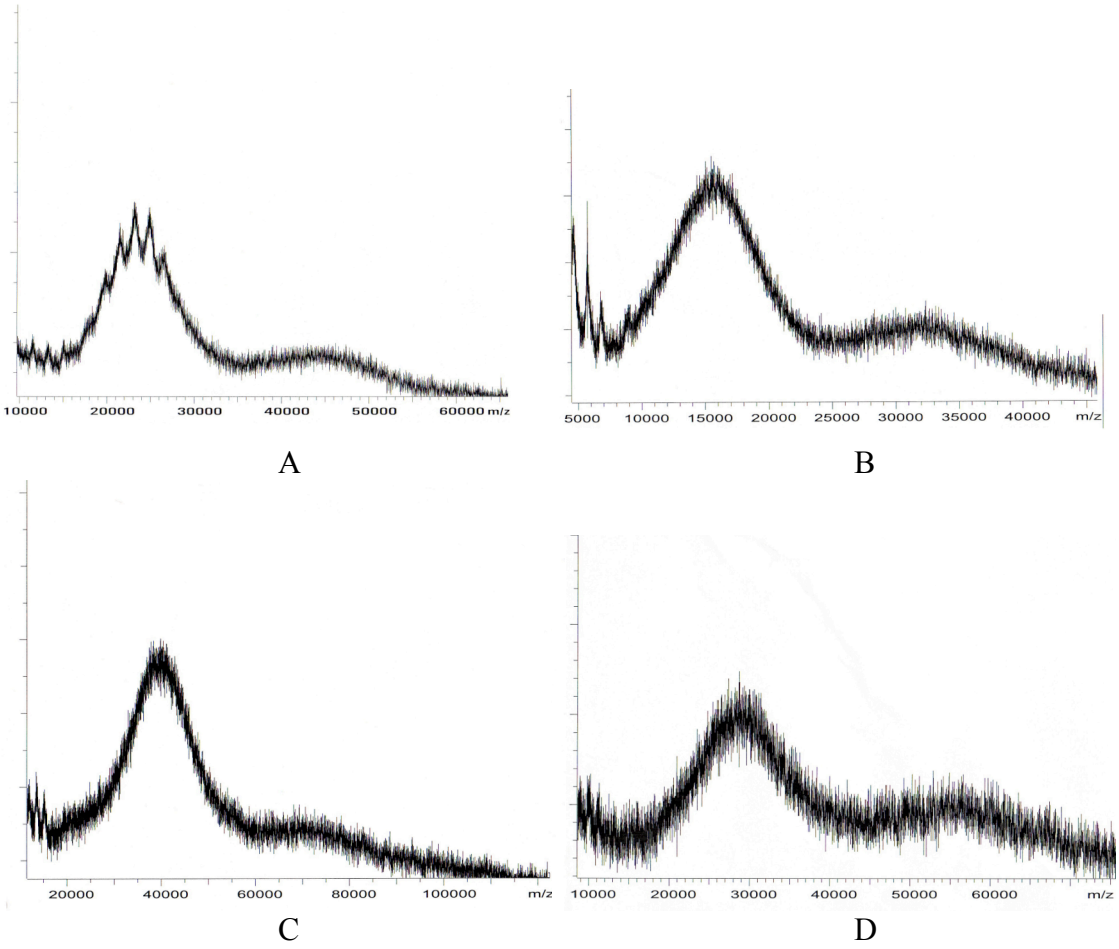

Figure 2.9 MALDI-TOF spectra of A) acetylated G(2) **15**; B) deacetylated G(2) **20**; C) acetylated G(3) **16**; and D) deacetylated G(3) **21.**

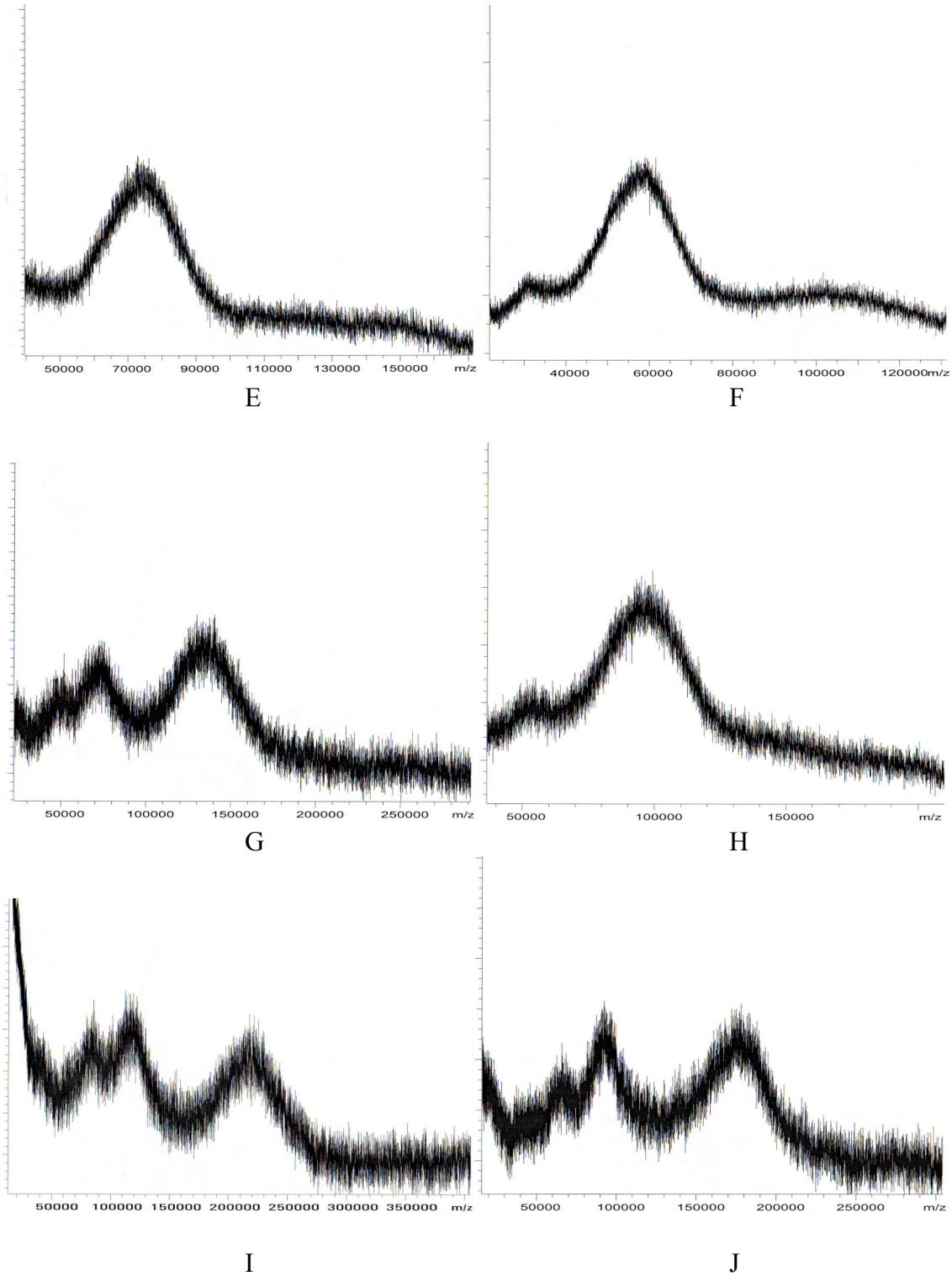

Figure 2.9 continued: MALDI-TOF spectra of E) acetylated G(4) **17**; F) deacetylated G(4) **22**; G) acetylated G(5) **18**; H) deacetylated G(5) **23**; I) acetylated G(6) **19**; and J) deacetylated G(6) **24**.

Notably the peaks are broad. This is due to imperfections in the synthesis of commercially available starting material leading to a heterogeneous population of compounds (Scheme 2.10).[103] The most prevalent problem comes from incomplete addition of one of the dendrimer branches, although intramolecular reactions between branches can occur as well. The number and magnitude of the imperfections increase greatly with dendrimer size. This affects the number of amines on the dendrimer periphery, which is less than theoretical (Table 1.1).

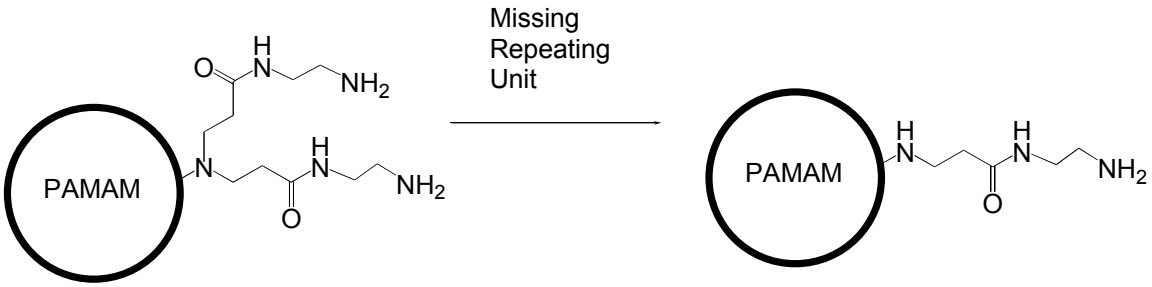

Scheme 2.10 Imperfections in the synthesis of PAMAM dendrimers.

Because a heterogeneous population of molecules was present in the dendrimer samples, the molecular weight is reported as a weighted average with each molecule contributing to the average (M_W) in proportion to the square of its mass.[104] In this report we use M_W rather than the number average molecular weight (M_N), because it more accurately reflects the whole population of macromolecules (Figure 2.10). There was a small degree of uncertainty in measuring M_W because of the shape of the spectrum. Two separate measurements of the same compound can result in slightly different calculated

M_W's. To address this, each sample was analyzed on three separate experiments, and the calculated M_W's were averaged.

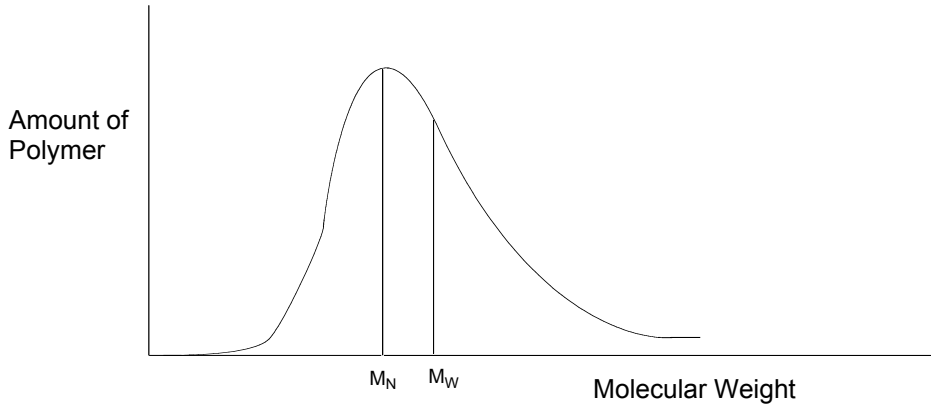

Figure 2.10 Example molecular weight distribution of a polymer.

The number of sugars per dendrimer was calculated from the changes in M_W during functionalization and deacetylation. The MALDI-TOF MS data for dendrimers **15-24** are shown in Table 2.1. First, the number of clusters appended to the dendrimer is less than the number of available terminal amines, even considering the imperfections in the starting material. Presumably this is because the dendrimers here are tethered to a steric maximum number of clusters that can fit around the periphery of the roughly spherical PAMAMs. Despite this steric limit, the actual number of sugars on each PAMAM generation is about double what was possible with single mannose functionalization (Chapter 1).[72] The additional triazole linker effectively adds another generation to the dendrimer by increasing its size and total number of carbohydrates to the degree that would be expected for a PAMAM generation N+1.

PAMAM Generation	Weight Average Molecular Weight Acetylated (g/mol)	Weight Average Molecular Weight Deacetylated (g/mol)	# tris-mannose Clusters	# Mannose
2	24000 (**15**)	17200 (**20**)	13	39
3	44000 (**16**)	30000 (**21**)	23	69
4	78000 (**17**)	59000 (**22**)	39	117
5	137000 (**18**)	101000 (**23**)	68	204
6	223000(**19**)	169000 (**24**)	103	309

Table 2.1 Mass spectrometry data for compounds **15**-**24**.

Heterogeneously Cluster Functionalized PAMAM Dendrimers: Spacer Compounds

Dendrimers with multiple and different surface groups, heterogeneously functionalized dendrimers (Figure 2.11), comprise a class of macromolecules with interesting and varied applications. A review on this topic, written in our labs, explores many aspects of this field.[105] Specifically dendrimers with varied surface groups have been in used in recent research as amphiphiles, as donor/acceptor combinations in photochemistry, or in biological applications. The additional degree of complexity of these compounds requires an extra level of synthetic control beyond other dendrimers. Convergent synthetic routes are common in the synthesis of diblock or bifunctional termini dendrimers (Figure 2.11 a and b respectively). In our labs stoichiometric control is used to make partially functionalized and random bifunctional dendrimers (Figure 2.11c and d respectively). This mechanism is used to control surface carbohydrate density. Alternatively clusters can be added to a partially functionalized dendrimer to make cluster bifunctional dendrimers (Figure 2.11e).

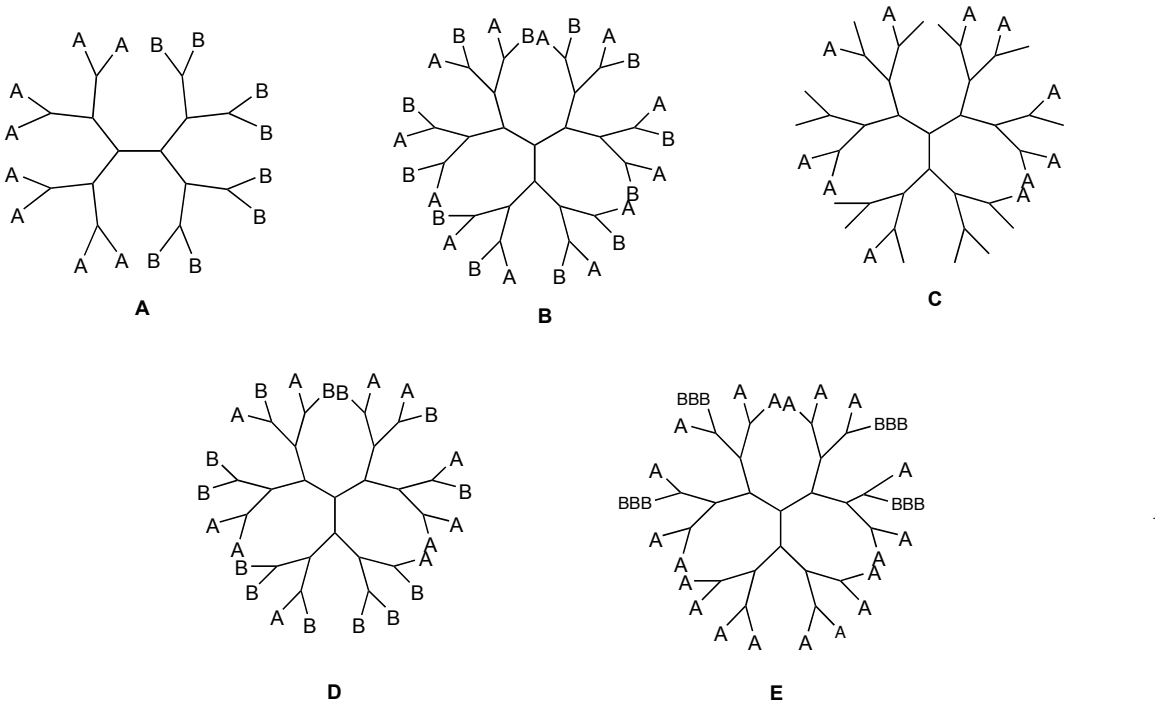

Figure 2.11 Possible forms of heterogeneously functionalized dendrimers including A) diblock, B) bifunctional terminus, C) partially functional, and D) random bifunctional and E) clustered bifunctional.

In light of the expanded size of the tris-mannose cluster versus the single mannose isothiocyanates, we explored the synthesis of a tether that matched the length of the linker used. A tetraethylene glycol type spacer is approximately as big as the linker used for the mannose cluster (Figure 2.12).

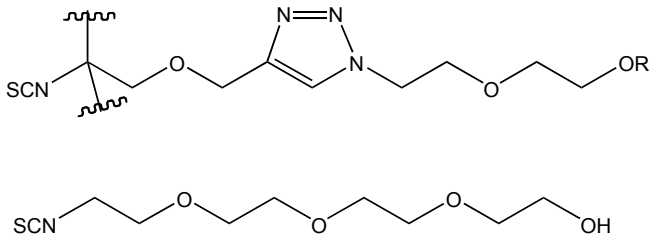

Figure 2.12 The linker length between the mannose and the dendrimer (top) is approximately the same size as a tetraethylene glycol derivative (bottom).

This spacer was synthesized starting from tetraethylene glycol. The first transformation was a silver (I) oxide mediated monotosylation (Scheme 2.11).[106] The silver (I) oxide was made fresh from silver nitrate and sodium hydroxide,[107] and was then added to the diol followed by toluenesulfonyl chloride. A mixture of mono- (**25)** and di-tosyl products resulted and could be separated, with difficulty, by column chromatography. Heating in the presence of sodium azide in dimethyl formamide displaced the tosyl group, and produced the desired azido-alcohol **26** in good yield.[108] The Staudinger reduction of the azide produced the desired amine product, though the triphenylphospine oxide byproduct proved difficult to remove. A simpler approach to the amine **27** was reduction under hydrogen in the presence of palladium/carbon that cleanly gave **27** as a clear oil. Conversion to the corresponding isothiocyanate using thiophosgene and triethylamine was attempted next, and analysis of the crude product mixture indicated product **28** formation. Purification of this long chain molecule proved difficult. In our hands column chromatography failed to cleanly provide the product. Kugelrohr distillation turned the yellow oil into a clear oil, though ^{1}H NMR indicated the product still contained a a small amount of impurities.

For the first attempt at heterogeneously mannose cluster functionalized dendrimers, we opted to use a shorter spacer. The spacer compounds are necessary to effectively block the remaining amine groups that would likely participate in nonspecific interactions with a protein. Also the spacer groups fill in the area between the clusters, without taking up too much interstitial space between the clusters. Toward this aim the

isothiocyanato alcohol **29** was made as previous described (Scheme 2.12),[72] again from the corresponding amine with thiophosgene and triethyl amine. Kugelrohr distillation of this product provided **29** cleanly as a clear oil.

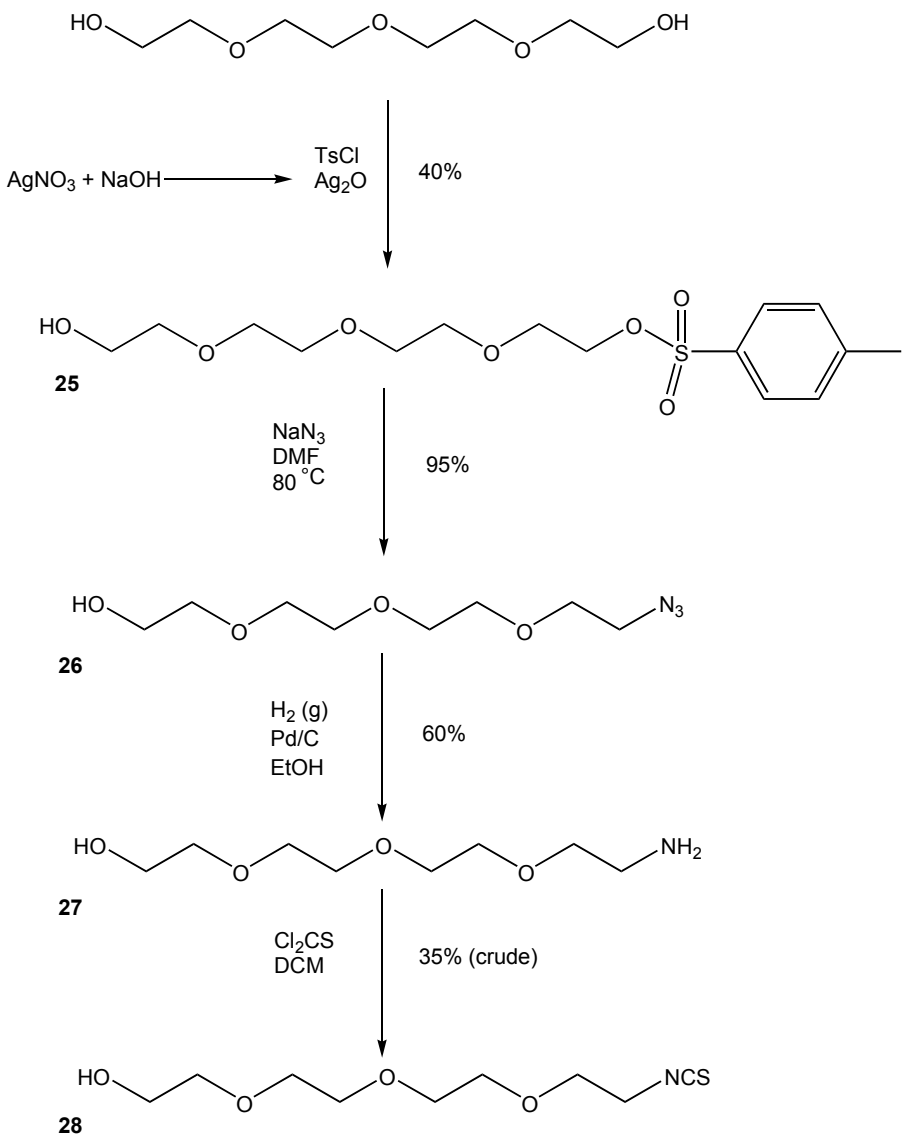

Scheme 2.11 Synthesis of 11-isothiocyanato-3,6,9-trioxaundecan-1-ol **28**.

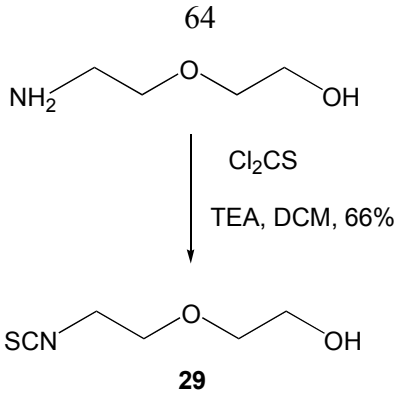

Scheme 2.12 Synthesis of 2-(2-isothiocyanatoethoxy)ethanol (**29**).[72]

Heterogeneously Cluster Functionalized PAMAM Dendrimers: Macromolecules

PAMAM dendrimers G(2) through G(6) were each partially functionalized with spacer **29** (Scheme 2.13) by reacting for two days, forming a thiourea bond, and so appending the spacer onto the dendrimer surface: G(2) **30a-g**, G(3) **31a-g**, G(4) **32a-g**, G(5) **33a-g**, and G(6) **34a-f**.

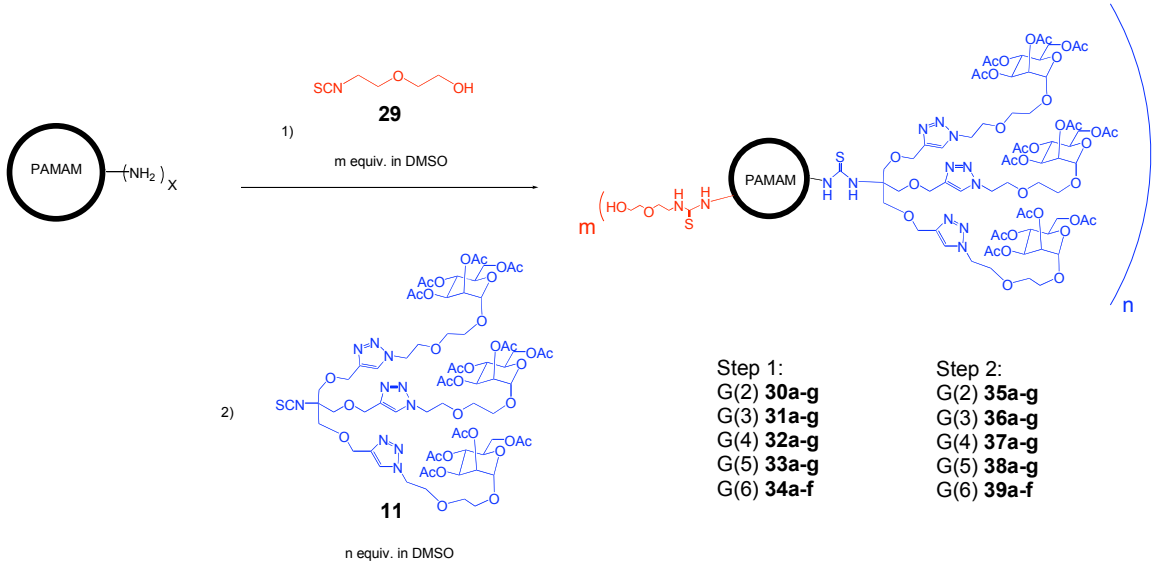

Scheme 2.13 Synthesis of heterogeneously functionalized tris-mannose cluster and ethoxyethanol PAMAM dendrimers **30-39**.

Within each generation, a series of different carbohydrate densities were prepared, roughly corresponding to 75, 50, 25, 15, 10, and 5 % loading of the number of surface primary amines available (with corresponding spacer loadings of 25, 50, 75, 85, 90, and 95 %). With regard to the sterically maximum allowed number of clusters, the percentages vary, and so the loadings are simply reported as the number of sugar clusters per dendrimer. Also, in each series, a dendrimer was functionalized with only **29** and no mannose clusters, and these compounds are used as controls in the protein binding studies because they have no specificity for the lectin carbohydrate recognition domains.

After the formation of the partially functionalized PAMAM dendrimers **30-34** a small aliquot (corresponding to approximately 1% of the solution) was taken for MALDI-TOF analysis. Next a small excess of the tris-mannose cluster **11** was added to saturate the remaining amines. It should be noted that with smaller isothiocyanates the order of addition of the two components could be reversed without consequence. The isothiocyanate functionality on **11** is hindered and the molecule is relatively large, so a 1.2 to 1.5-mole excess was required for the second addition to ensure proper loading within two days.

The macromolecules were purified by dialysis in dimethyl sulfoxide with a regenerated cellulose membrane MWCO 10,000 Da. After extensive dialysis some of the lower molecular weight glycodendrimers were still mixed with excess tris-mannose clusters. Fortunately, this mixture could be easily recognized due to a small change in the chemical shift of the acetyl protons in the NMR spectrum between mannose on dendrimer and free mannose cluster. In cases where dialysis was insufficient, even when

solvents other than dimethyl sulfoxide were used, another method for purification proved useful.

Polymer bound ethylene diamine (Figure 2.13) was commercially available as polystryrene, divinylbenzene cross-linked, beads. When the product mixture solution was stirred with the polymer beads the excess isothiocyanate was successfully scavenged by the polymer, which was simply filtered from the product solution. After purification by dialysis, or a combination including dialysis and solid phase scavengers, functionalized PAMAM dendrimers G(2) **35a-g**, G(3) **36a-g**, G(4) **37a-g**, G(5) **38a-g**, and G(6) **39a-f** were obtained in an average yield of 81%.

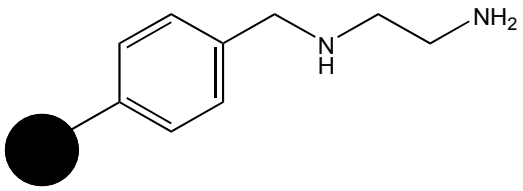

Figure 2.13 Polymer bound ethylene diamine.

The macromolecules were deprotected exactly as described earlier, using Zemplén conditions and purified by dialysis (MWCO 1000 Da) against Millipore water, followed by lyophilization to remove the water and yield the deprotected heterogeneously tris-mannose cluster functionalized dendrimers G(2) **40a-g**, G(3) **41a-g**, G(4) **42a-g**, G(5) **43a-g**, and G(6) **44a-f** (Scheme 2.14).

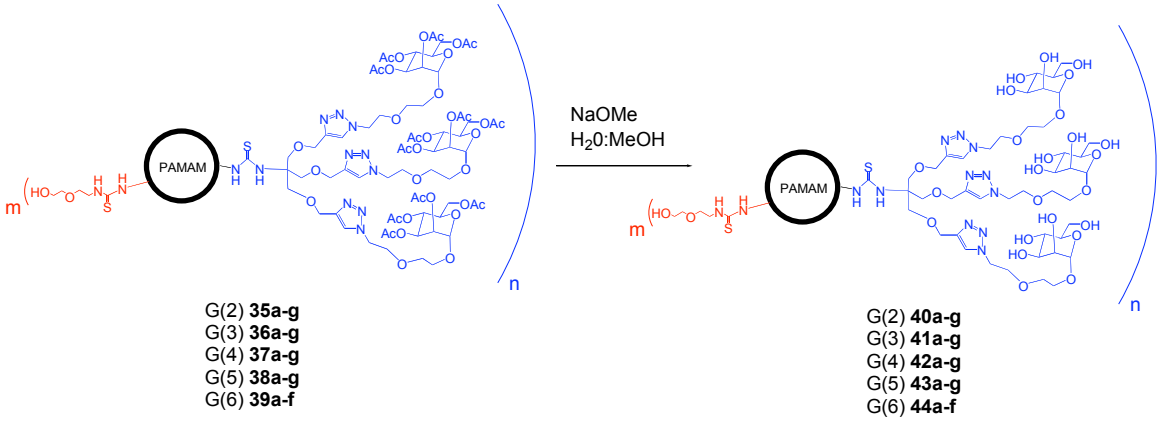

Scheme 2.14 Synthesis of deacetylated heterogeneously functionalized tris-mannose cluster and ethoxyethanol PAMAM dendrimers **40-44**.

Characterization by NMR

The ^{1}H NMR spectrum for compound **37e** and the corresponding deacetylated **42e** are shown in Figure 2.14. As expected, the signal from the spacer methylenes overlaps with the signal from the cluster linkers, because they are structurally very similar. As fewer clusters are added in each series, those overlapped signals become very large compared with the signal from the sugar protons. However, the hydroxyl group of the spacer is distinct, and is observed at 4.58 ppm. Figure 2.15 shows a stack plot of this region of the spectrum (including some sugar and linker signals) for **37g, 37e, 37c,** and **37b**. The compound of the top spectrum (**37g**) has no sugar clusters and the only signal in the region arises from the alcohol proton. As more clusters are appended to the dendrimer (moving downward through Figure 2.25: **37e**, **37c**, and **37b**) this signal becomes very broad and eventually indistinguishable. This is caused by effectively burying this proton into the macromolecular interior by adding the mannose clusters. As a result, the relative loading of spacers and clusters can be calculated by the relative

integrations in the ^{1}H NMR only at low mannose density. Where this signal is distinct, the calculation for the number of appended sugars is close to that calculated from the mass spectrometry data (Table 2.2). The number of clusters by mass spectrometry is used throughout the rest of this report.

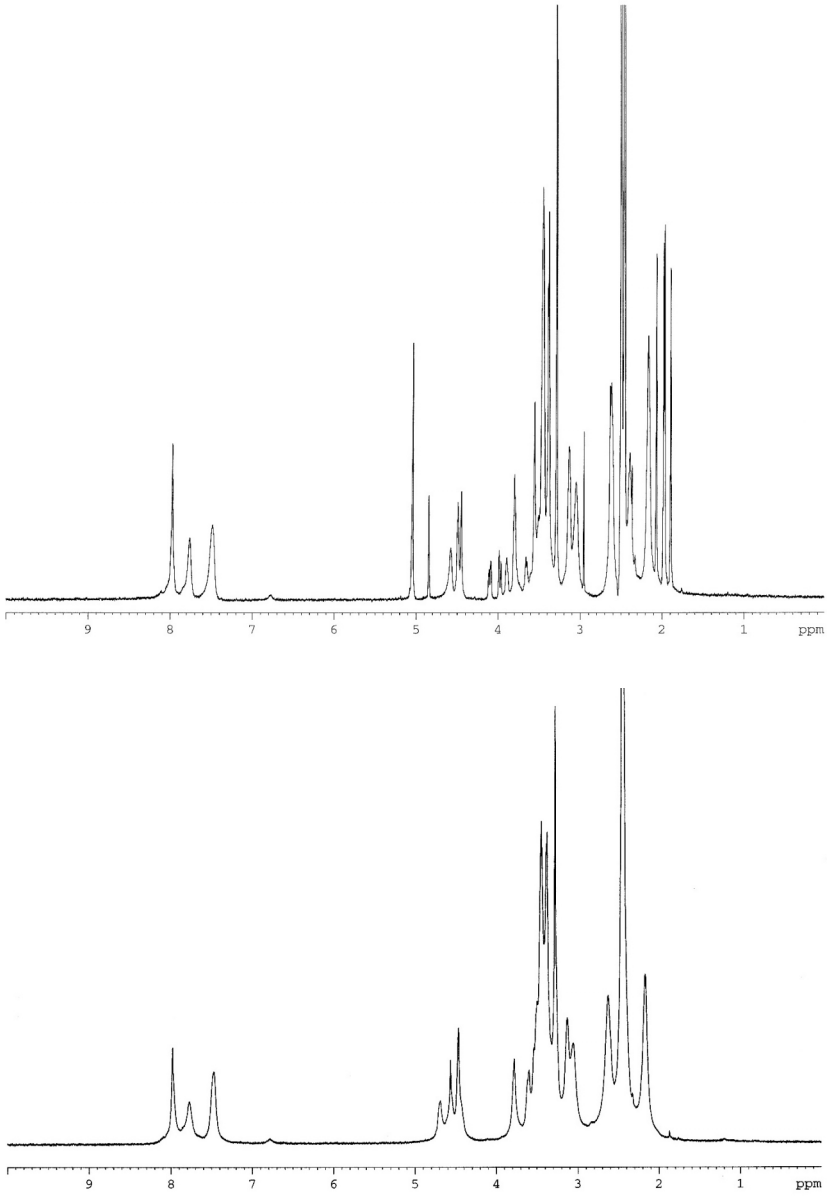

Figure 2.14 ^{1}H NMR spectra (500 MHz) of **37e** (top) and **42e** (bottom) in d_6-DMSO.

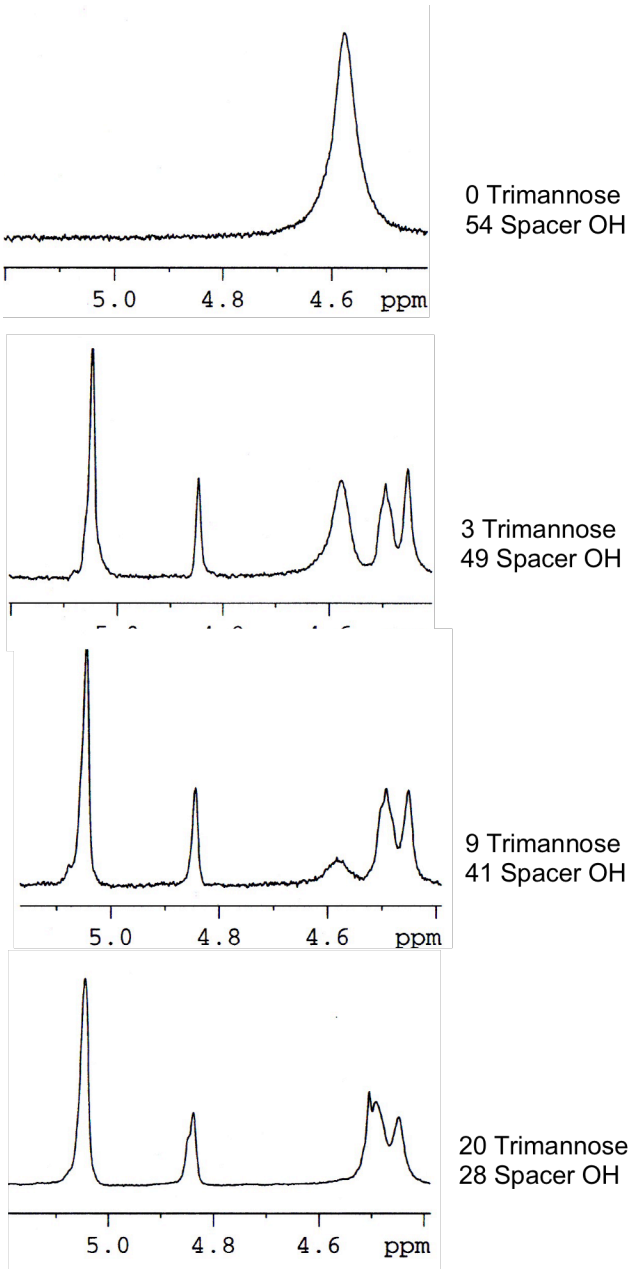

Figure 2.15 ^{1}H NMR spectra of **37g** (top), **37e, 37c**, and **37b** (bottom) indicating linebroadending of the signal from the hydroxyl group proton.

37	Number of Clusters by MS	Number of Clusters by NMR
a	26	ND
b	20	ND
c	9	15
d	5	7
e	3	4
f	2	2
g	0	0

Table 2.2 Sample comparison of relative loading of tris-mannose clusters on G(4) dendrimer **37** by MALDI-TOF MS and ^{1}H NMR. ND = not determined.

Characterization by MALDI-TOF MS

For each heterogeneous cluster functionalized PAMAM dendrimer, the M_W was measured after the addition of the ethoxyethanol isothiocyanate spacer, after the addition of the mannose cluster isothiocyanate, and after deacetylation of the carbohydrates. The mass spectrometry data for compounds **30-44** are reported in Table 2.3. The number of spacer isothiocyanates is directly measured from this data. The deacetylation reaction on the dendrimer presents an opportunity for a few distinct methods for the calculation of the number of appended sugars (Figure 2.16). First the number of clusters can be measured directly from the difference in average molecular weight between the partially functionalized dendrimer and the heterogeneously functionalized dendrimer. In the example shown in Figure 2.16a (**32c, 37c, 42c**) this difference is 36000 g/mol – 29600 g/mol, or 16400 g/mol. This corresponds to an addition of 10 clusters on average with a molecular weight of 1662 g/mol each. Second the removal of the acetyl group can be measured from the molecular weight difference in between the protected and deprotected dendrimers. In Figure 2.16b the difference is 3500 g/mol. Dividing this amount by the

loss the twelve-acetyl groups per cluster followed by reprotonation (12 x 42, or 504 g/mol) indicates the loss of acetyl groups from 7 clusters on average. Recall the very distinct acetyl group signal from the ^{1}H is completely absent after deprotection indicating this reaction went to completion. Finally, the number of added clusters can be measured indirectly from the difference in molecular weight between the final product and the partially functionalized dendrimer. From Figure 2.16c this difference is 12900 g/mol. This amount divided by the theoretical molecular weight of the deacetylated cluster (1157 g/mol) indicates an average of 11 clusters per dendrimer. The reported number of clusters is an average of these three calculations 10, 7, and 11 in the highlighted case of glycodendrimer 36d, this amounts to 9 mannose clusters on average (or 27 individual mannose units).

Upon completion of the library of heterogeneously mannose cluster functionalized dendrimers, it was apparent that a few compounds were effectively redundant. For example low loadings of G(2) dendrimer yielded compounds with an average of less than 1 cluster per dendrimers. These compounds are omitted from protein binding studies because the data simply would not be relevant.

Dendrimer Generation	Mw partially functionalized	# Spacers	Mw Acetylated	Mw Deacetylated	# Clusters	# Mannose
2	3750 (**30a**)	3	16400 (**35a**)	13300 (**40a**)	7	21
2	4520 (**30b**)	9	12300 (**35b**)	12300 (**40b**)	4	12
2	4920 (**30c**)	11	7600 (**35c**)	ND	2	6
2	5120 (**30d**)	13	6000 (**35d**)	ND	1	3
2	5460 (**30e**)	15	5900 (**35e**)	ND	0	0
2	5500 (**30f**)	16	6100 (**35f**)	ND	0	0
2	5280 (**30g**)	14	5300 (**35g**)	5300 (**40g**)	0	0
3	7930 (**31a**)	7	28800 (**36a**)	22300 (**41a**)	13	39
3	9260 (**31b**)	16	22000 (**36b**)	17300 (**41b**)	8	24
3	10570 (**31c**)	25	14900 (**36c**)	13400 (**41c**)	3	9
3	10880 (**31d**)	27	12900 (**36d**)	12400 (**41d**)	1	3
3	11400 (**31e**)	31	12500 (**36e**)	11200 (**41e**)	1	3
3	11300 (**31f**)	30	12100 (**36f**)	ND	1	3
3	11300 (**31g**)	30	11300 (**36g**)	10900 (**41g**)	0	0
4	15500 (**32a**)	14	60000 (**37a**)	48000 (**42a**)	26	78
4	17600 (**32b**)	28	51000 (**37b**)	41000 (**42b**)	20	60
4	19600 (**32c**)	41	36000 (**37c**)	32500 (**42c**)	9	27
4	20200 (**32d**)	46	28700 (**37d**)	26300 (**42d**)	5	15
4	20700 (**32e**)	49	25800 (**37e**)	25300 (**42e**)	3	9
4	20300 (**32f**)	46	23100 (**37f**)	22800 (**42f**)	2	6
4	21000 (**32g**)	51	21000 (**37g**)	21000 (**42g**)	0	0
5	29800 (**33a**)	29	92000 (**38a**)	69000 (**43a**)	39	117
5	32800 (**33b**)	50	81000 (**38b**)	64300 (**43b**)	30	90
5	34700 (**33c**)	63	55300 (**38c**)	49000 (**43c**)	12	36
5	36200 (**33d**)	73	55300 (**38d**)	46700 (**43d**)	12	36
5	37500 (**33e**)	81	52300 (**38e**)	45300 (**43e**)	10	30
5	38100 (**33f**)	86	50300 (**38f**)	44000 (**43f**)	8	24
5	41000 (**33g**)	106	41000 (**38g**)	41000 (**43g**)	0	0
6	60000 (**34a**)	48	174000 (**39a**)	135000 (**44a**)	66	198
6	70000 (**34b**)	116	122000 (**39b**)	107000 (**44b**)	31	93
6	71000 (**34c**)	122	108000 (**39c**)	98000 (**44c**)	22	66
6	72000 (**34d**)	129	88000 (**39d**)	85000 (**44d**)	9	27
6	76000 (**34e**)	156	82000 (**39e**)	ND	3	9
6	77000 (**34f**)	163	77000 (**39f**)	75000 (**44f**)	0	0

Table 2.3 MALDI-TOF MS data for compounds **30**-**44**.

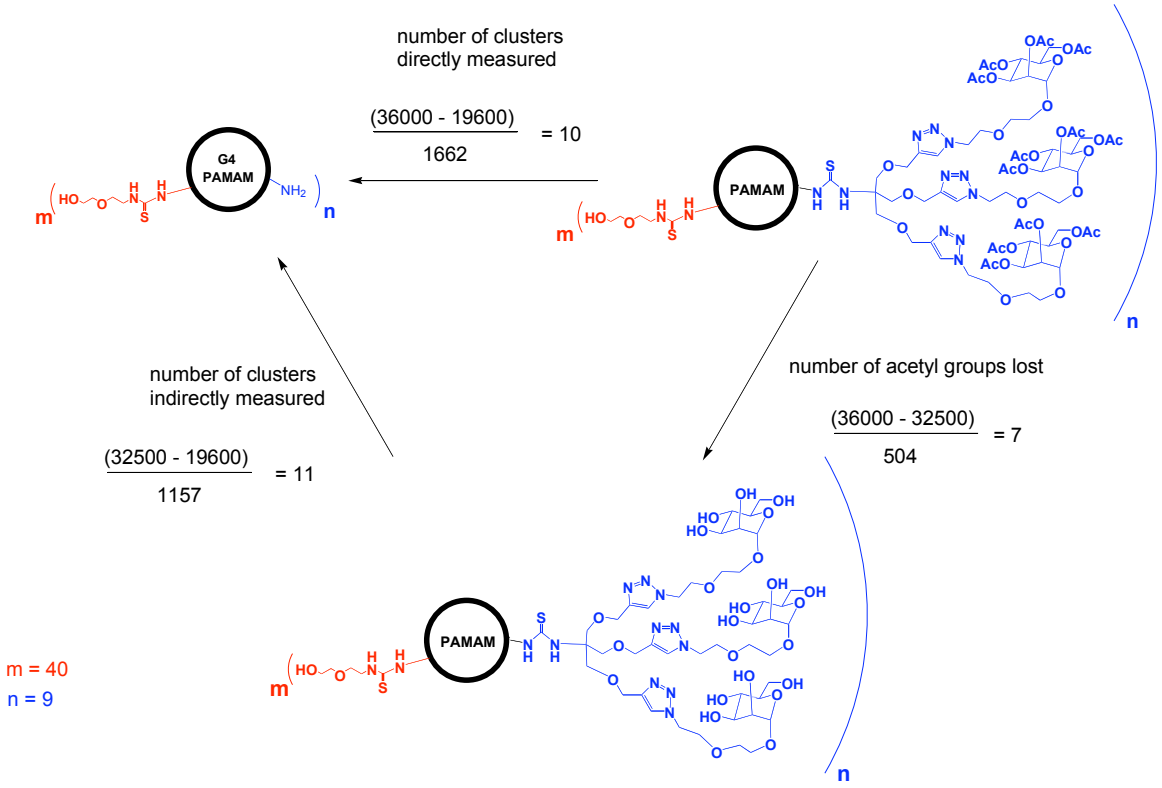

Figure 2.16 Calculation of the number of tris-mannose clusters on **37c**.

Summary

PAMAM dendrimers were functionalized with clusters, each with three linked mannose units. Utilizing a copper (I) catalyzed dipolar cycloaddition to form a regioselective disubstituted 1,2,3-triazole in the synthesis of glycodendrimers with new architectures was a significant advancement in this work.

The synthesis of the cluster isothiocyanate in 10 convergent steps provided the desired clean product with no mono- or bis- mannose clusters observed in either NMR or high-resolution mass spectrometry. The clusters were successfully appended to the PAMAM dendrimer periphery via a thiourea linkage, followed by global deprotection. The glycodendrimers were well characterized by NMR and extensive MALDI-TOF mass

spectrometry, despite a measurable population heterogeneity in the commercially available PAMAM dendrimers.

Next the clusters were effectively positioned across the macromolecular surface using a heterogeneous dendrimer functionalization strategy relying on random stoichiometric addition to give a bifunctional surface. Two ethylene glycol spacers of different lengths were synthesized, though only one was used for dendrimer functionalization. A library of glycodendrimers varying significantly in size and carbohydrate density was synthesized in preparation for protein binding studies (Chapter 5) that were designed to quantify the contribution of proximity effects toward multivalent binding.

Experimental Procedures

General Methods. General reagents were purchased from Fisher-Acros and Sigma-Aldrich. PAMAM dendrimers were purchased as aqueous solutions from Dendritech and lyophilized prior to use. Copper wire was purchase from Ace Hardware. Boron trifluoride etherate was freshly distilled from calcium hydride (40 °C at 9 mm Hg). Polystyrene crosslinked divinyl benzene resins were swelled prior to use; Wang resin in dimethyl formamide (DMF) overnight, and polymer bound ethylenediamine in tetrahydrofuran over 2 hours, and each was then thoroughly rinsed with solvent. Sephedex LH was swelled overnight in DMF. Dry DMF was prepared by stirring 24 hours with 4Å molecular sieves followed by filtration through a Millipore 0.45 μm nylon filter. *trans*-3-Indoleacrylic acid was crystallized from approximately 1:1 methanol and water. All other reagents were used as supplied.

NMR. ^{1}H NMR and ^{13}C NMR were acquired at 500 MHz and 125 MHz, respectively, on a Bruker DRX500 instrument in $CDCl_3$ or CD_3SOCD_3. Spectra are recorded for some compounds in both $CDCl_3$ and CD_3SOCD_3. All of the compounds were soluble in CD_3SOCD_3, yet the spectra in $CDCl_3$ had a better resolution. Where appropriate the data for spectra in both solvents are included to facilitate comparison of compounds.

MALDI-TOF MS. Matrix assisted laser desorption ionization (MALDI) mass spectra were acquired using a Bruker Biflex-III time-of-flight mass spectrometer. Spectra were obtained using a trans-3-indoleacrylic acid (IAA) matrix with a matrix-analyte ratio of 36,000: 1 to 1000:1. A 1 μL aliquot of the analyte (0.5-20 mg/mL) in DMF, DMA, or DMSO, was combined with 10 μL of IAA in DMF (20 mg/mL). A 1 μL aliquot was deposited on the laser target, drying in 1-4 hours. Bovine serum albumin (MW 66,431 g/mol) and laser promoted oligomers up to the tetramer and the M/Z peak where Z = 2, trypsinogen (MW 23,982 g/mol), cytochrome C (12,361 g/mol), and bradykinin (1061 g/mol) were used as external standards. Positive ion mass spectra were acquired in linear mode, and the ions were generated by using a nitrogen laser (337 nm) pulsed at 5 Hz with a pulse width of 3 nanoseconds. Ions were accelerated at 19-20,000 volts and amplified using a discrete dynode multiplier. Spectra (10 to 2000) were summed into a LeCroy LSA1000 high-speed signal digitizer. All data processing was performed using Bruker XMass/XTOF V 5.0.2. Molecular mass data and polydispersities of the broad peaks were calculated by using the Polymer Module included in the software package. The peaks were analyzed using the *continuous* mode. Delta values were set at minimum levels.

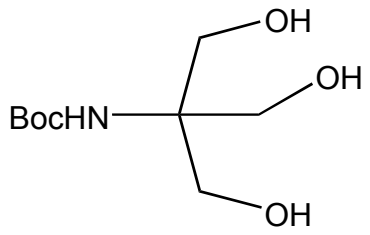

N-(*tert*-Butyloxycarbonyl)tris(hydroxymethyl)aminomethane (1).

Compound **1** was prepared using a modification of previously published methods.[88] Tris(hydroxymethyl)aminomethane (7.10 g, 58.5 mmol) was dissolved in DMF (100 mL) and combined with di-*tert*-butyl dicarbonate (14.0 g, 64.1 mmol) and TEA (13.0 g, 128 mmol) under a nitrogen atmosphere and stirred at 50 °C for 2 hours. DMF was removed *in vacuo* and the product was washed with, and filtered from, cold ethyl acetate to yield 10.4 g white solid (80% yield) **1**. ^{1}H NMR (CD_3SOCD_3, 500MHz) δ 5.73 (bs, 1H, N*H*), 4.46 (t, 3H, J = 5.3 Hz, OH), 3.48 (d, 6H, J = 5.6 Hz, CH_2), 1.33 (s, 9H, CH_3) ppm; ^{13}C NMR (CD_3SOCD_3, 125MHz) δ 155.5, 78.3, 60.9, 60.7, 28.7 ppm; IR (KBr) 3415, 3304 (br), 2986, 1679, 1549 cm^{-1}

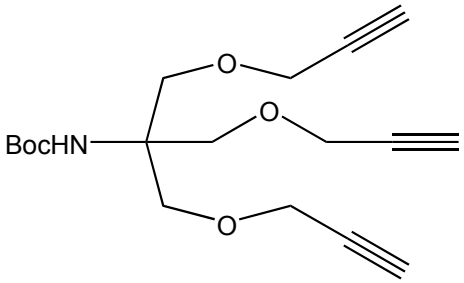

N-(*tert*-Butyloxycarbonyl)tris(propargyloxymethyl)aminomethane (2).

A solution of **1** (616 mg, 2.78 mmol) in DMF (10 mL) was added dropwise to a suspension of sodium hydride (282 mg, 11.8 mmol) in DMF (30 mL) at -50 °C. After

stirring 30 minutes, propargyl bromide (1.57 g, 13 mmol) was added as an 80% solution in toluene and the solution stirred at -50 °C for 4 hours. The reaction was quenched with the addition of 20 mL water, and was warmed to room temperature. The product was extracted with ethyl acetate (4 x 30 mL), and the organic layers were combined and washed with water (3 x 30 mL), then dried over $MgSO_4$. The solution was concentrated to leave a brown oil which was purified on silica gel (60:40 hexanes:ethyl acetate) to yield 433 mg (43% yield) slightly yellow oil **2**. ^{1}H NMR (CD_3SOCD_3, 500MHz) δ 6.12 (bs, 1H, N*H*) 4.08 (s, 6H, C*H*$_2$CCH), 3.55 (s, 6H NCC*H*$_2$O). 2.46 (s, 3H, CH_2CCH), 1.34 (s, 9H, C*H*$_3$) ppm; ^{13}C NMR (CD_3SOCD_3, 125 MHz) δ 154.7, 80.7, 78.3, 77.6, 68.4, 58.5, 28.6 ppm (missing NH*C*(CH_2)); ^{1}H NMR ($CDCl_3$, 500MHz) δ 4.89 (bs, 1H, N*H*) 4.12 (d, 6H, J = 1.8 Hz, C*H*$_2$CCH), 3.75 (s, 6H NCC*H*$_2$O). 2.40 (t, 3H, J = 2.3 Hz, CH_2CCH), 1.40 (s, 9H, C*H*$_3$) ppm; ^{13}C NMR ($CDCl_3$, 125MHz) δ 154.8, 79.6, 79.1, 74.6, 68.9, 58.7, 58.1, 28.4 ppm; IR ($CDCl_3$) 3436, 3308, 2981, 1711, 1501 cm^{-1}

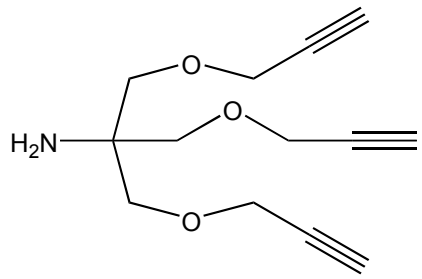

tris(propargyloxymethyl)aminomethane (4).

The protected amine **2** (2.2 g, 6.6 mmol) was dissolved in 18 mL chloroform, then 6 mL TFA was added to the stirring solution. After 30 min saturated sodium bicarbonate (100 mL) was added slowly, then the organic layer was removed, and was washed with

sodium bicarbonate (30 mL). The aqueous layers were extracted with chloroform (3 x 20 mL), and the combined organic layers were washed with water (2 x 30 mL) then dried over $MgSO_4$. The solvent was removed *in vacuo* leaving 1.5 g (97 %) **4** as an orange oil. ^1H NMR (CD_3SOCD_3, 500MHz) δ 4.10 (d, 6H, J = 2.3 Hz), 3.36 (t, 3H, J = 2.3 Hz), 3.27 (s, 6H), 1.44 (s, 2H) ppm; ^{13}C NMR (CD_3SOCD_3, 125MHz) δ 80.7, 77.6, 72.3, 58.6, 55.8 ppm; ^1H NMR ($CDCl_3$, 500MHz) δ 4.10 (s, 6H), 3.4 (s, 6H), 2.4 (s, 3H, OH), 1.4 (bs, 2H) ppm; ^{13}C NMR ($CDCl_3$, 125MHz) δ 79.7, 74.5, 71.9, 58.6, 55.5 ppm.

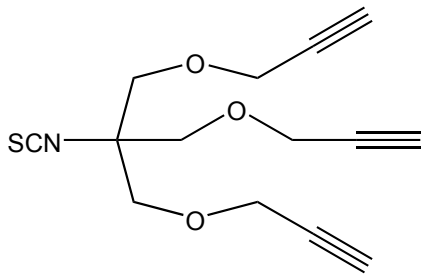

tris(propargyloxymethyl)isothiocyanatomethane (5).

A solution of thiophosgene (225 mg, 1.96 mmol) in 4 mL DCM was added dropwise over 20 min. to a solution of amine **4** (229 mg, 0.974 mmol) and triethylamine (400 μL, 2.85 mmol) in 9 mL DCM then stirred 1 hour. The solution was concentrated *in vacuo*, was taken up in 10 mL ethyl acetate, was washed with water (2 x 10 mL) and the combined organic extracts were dried over $MgSO_4$. The solution was concentrated *in vacuo* and the product purified on silica gel (6:4 hexanes : ethyl acetate) to give 170 mg **5** as a slightly yellow oil (63% yield). ^1H NMR ($CDCl_3$, 500 MHz) δ 4.19 (d, 6H, J = 2.3 Hz), 3.66 (s, 6H), 2.44 (t, 3H, J = 2.3Hz) ppm; ^{13}C NMR ($CDCl_3$, 125MHz) δ 137.4, 79.0 75.1, 69.6, 66.4, 58.9 ppm; ^1H NMR (CD_3SOCD_3, 500MHz) δ 4.19 (s, 6H), 3.66 (s, 6H), 3.3 (s, 3H)

ppm; ^{13}C NMR (CD_3SOCD_3, 125MHz) δ 134.7, 80.0, 78.2, 69.6, 66.9, 58.7 ppm; HRMS (micro-TOF) 278.0851 (M+H cacld 278.0845 for $C_{14}H_{16}O_3NS$); IR ($CDCl_3$) 3291, 2877, 2251, 2068 cm^{-1}

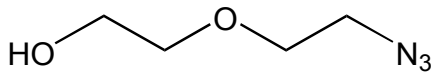

2-(2-azidoethoxy)ethanol (9).

Compound **9** was prepared using a modification of previously published methods.[108] 2-(2-chloroethoxy)ethanol (6.4 g, 51 mmol) was dissolved in dry DMF (40 mL) along with sodium azide (3.7 g, 57 mmol) and mixture was stirred at 80 °C for 2 days. Next 30 mL of water was added, and the solution was cooled to room temperature. The solvent was removed *in vacuo* to afford a mixture of clear oil and white solid. The product oil was dissolved in 80 mL DCM and filtered from the solid salts. The DCM was removed *vacuo* to afford 5.8 g (86% yield) **9** as a clear oil. ^{1}H NMR ($CDCl_3$, 500MHz) δ 3.68 (t, 2H, 4.6 Hz), 3.62 (t, 2H, 5.0 Hz), 3.54 (t, 2H, 4.6 Hz), 3.35 (t, 2H, 5.0 Hz) 2.60 (s, 1H, OH) ppm; ^{13}C NMR ($CDCl_3$, 125MHz) δ 72.4, 69.9, 61.6, 50.7 ppm; IR ($CDCl_3$) 3597, 2870, 2112 cm^{-1}

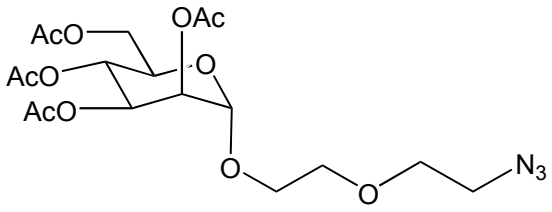

1-*O*-(5-azido-3-oxapentyl)-2,3,4,6-tetra-*O*-acetyl-α-D-mannopyranoside (10).

The trichloroacetimidate **8** (6.9 g, 14 mmol) was dissolved in 25 mL dry DCM and was mixed with azide **9** (1.84 g, 14.0 mmol) in 25 mL dry DCM and with 4Å molecular sieves. The solution was flushed with N_2 (g) and was capped under positive N_2 (g) pressure. Boron trifluoride etherate (2.0 g, 14 mmol) was added to the solution, which was stirred for 19 hours. Solid sodium bicarbonate (2.2g, 26 mmol) was then added, and the mixture was stirred for 30 minutes. The solid salts were removed by suction filtration, and solution was concentrated *in vacuo*. The product was purified on silica gel (1:1 ethyl acetate : hexanes to 100 % ethyl acetate) to yield a clear oil **10** (3.86 g, 60 % yield). ^{1}H NMR ($CDCl_3$, 500MHz) δ 5.29 (dd, 1H, J = 10.0 Hz, 3.3 Hz), 5.19-5.23 (m, 2H), 4.81 (s, 1H), 4.21 (dd, 1H, 12.4 Hz, 5.2 Hz), 3.99-4.06 (m, 2H), 3.7-3.8 (m, 1H), 3.61 (m, 5H), 3.32 (t, 2H, 4.8 Hz), 2.08 (s, 3H), 2.02 (s, 3H), 1.96 (s, 3H), 2.91 (s, 3H) ppm; ^{13}C NMR ($CDCl_3$, 125MHz) δ 170.6, 169.9, 169.8, 169.7, 97.7, 70.1, 70.0, 69.4, 69.0, 68.4, 67.2, 66.0, 62.4, 50.6, 20.9, 20.8, 20.7, 20.6 ppm; IR ($CDCl_3$) 2938, 2113, 1754 cm^{-1}; HRMS (micro-TOF) 500.1304 (M+K cacld 500.1277 for $C_{18}H_{27}O_{11}N_3K$)

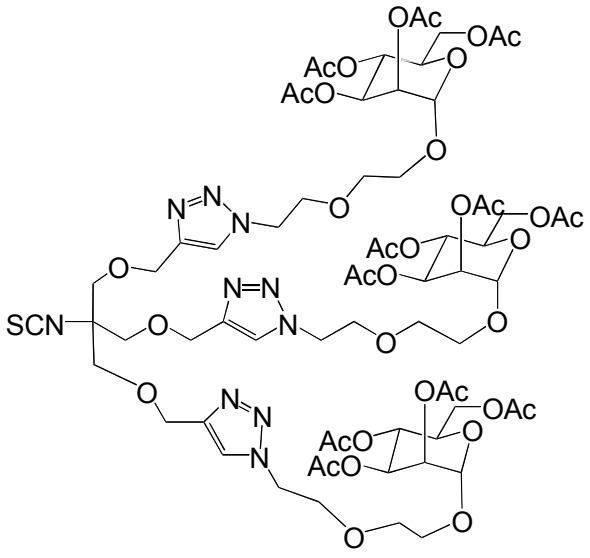

tris-Mannose Cluster Isothiocyanate (11).

Azidomannose **10** (1.794 g, 3.89 mmol) in 40 mL 1:1 THF:water was combined with a solution of isothiocyanate **5** (360 mg, 1.30 mmol) in 20 mL 3:1 THF:water. 974 μL of an aqueous solution of copper sulfate at 100 mg/mL concentration (97.4 mg, 0.390 mmol) was then added to the stirring solution followed by 1.55 mL of an aqeous solution of sodium ascorbate at 100 mg/mL (155 mg, 0.782 mmol) turning the yellow solution green. Stirring continued for 2 days followed by the addition of EDTA (291 mg, 0.782 mmol) in 15 mL water. Stirring continued for 1 hour as the solution became a translucent blue-green color. The product was extracted with ethyl acetate (3 x 30 mL), the combined organics were washed with water (2 x 30 mL), then dried over $MgSO_4$. The solvent was removed *in vacuo* leaving 2.2 g fluffy white solid **11** (100 % yield). ^{1}H NMR (CD_3SOCD_3, 500MHz) δ 8.01 (s, 1H), 5.05 (s, 3H), 4.85 (s, 1H), 4.51 (s, 4H), 4.08-4.13 (m, 1H), 3.95-4.02 (m, 1H), 3.90 (bs, 1H), 3.80 (m, 2H), 3.62-3.69 (m, 1H), 3.46-3.60 (m, 5H), 2.07 (s, 3H), 1.99 (s, 3H), 1.97 (s, 3H), 1.90 (s, 3H) ppm; ^{13}C NMR (CD_3SOCD_3, 125MHz) δ 170.5, 170.1, 169.9, 143.7, 134.4, 124.8, 97.1, 69.8, 69.4, 69.1, 68.3, 67.6, 66.8, 65.8, 64.5, 62.4, 49.7, 31.7, 21.0, 20.9, 20.8, 20.8 (one overlapped CH_3CO) ppm; HRMS (micro-TOF) 1661.5767 (M+K cacld 1661.5782 for $C_{68}H_{97}O_{36}N_{10}S$)

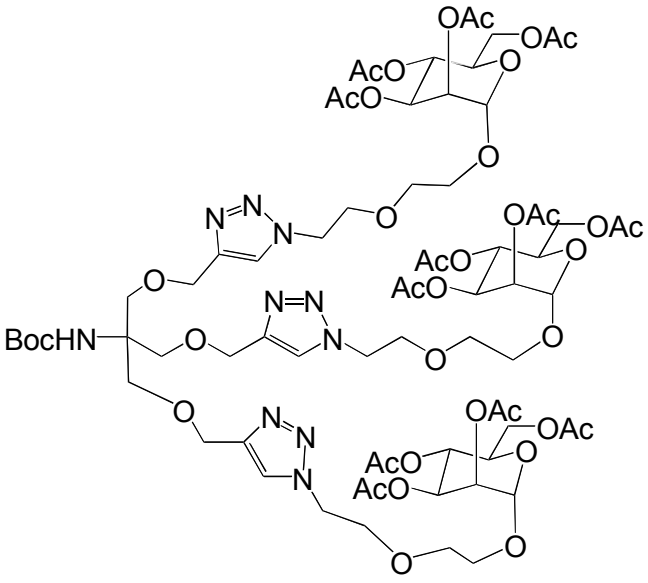

tris-Mannose Cluster (Boc) protected amine (13).

The mannose derivative **10** (556 mg, 1.21 mmol) was added to a stirring solution of tris-propargyl ether **2** (100 mg, 0.298 mmol) in 4 mL 5:3 *t*-butanol:water followed by copper sulfate (15 mg, 0.060 mmol) and an approximately 1 cm segment of 22 ga. copper wire. The solution was heated to 40 °C and stirred for four days. EDTA (44.7 mg, 0.12 mmol) was then added to the solution, and stirring was continued for 30 min. The product was extracted with chloroform (3 x 5 mL) and the solvent was removed *in vacuo* leaving orange soapy solid. The product was purified by size exclusion chromatography with Sephedex LH medium giving **13** as an orange oil (293 mg, 57 % yield). ^{1}H NMR ($CDCl_3$, 500MHz) δ 7.65 (s, 1H), 5.20-5.35(m, 3H), 5.0 (bs, 0.3H), 4.81 (m, 1H), 4.4-4.6 (m, 4H), 4.2-4.3 (m, 1H), 4.0-4.1 (m, 1H), 3.95 (bs, 1H), 3.86 (s, 2H), 3.65-3.8 (m, 3H), 3.59 (s, 4H), 2.12 (s, 3H), 2.05 (s, 3H), 2.01 (s, 3H), 1.96 (s, 3H), 1.35 (s, 3H) ppm; ^{13}C NMR (125MHz, $CDCl_3$) δ 170.6, 170.0, 169.9, 169.7, 154.7, 144.8, 124.7, 97.7, 70.0, 69.6, 69.5, 69.3, 69.0, 68.5, 67.2, 66.1, 64.7, 62.4, 60.3, 58.4, 50.0, 28.3, 20.8, 20.7 ppm

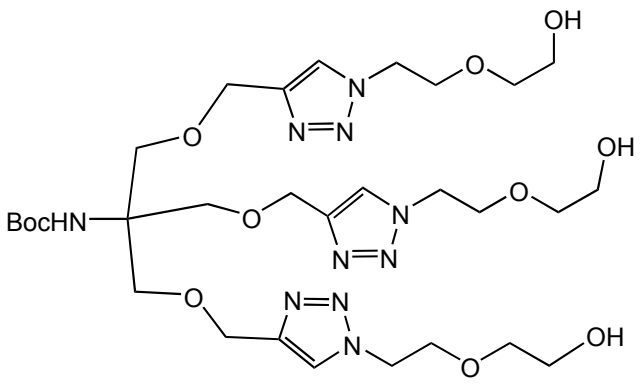

Ethoxyethanol Cluster (Boc protected amine) (14) with excess (9).

The azide **9** (167.5 mg, 1.28 mmol) was added to a stirring solution of tris-propargyl ether **2** (98.5 mg, 0.294 mmol) in 4 mL 5:3 *t*-butanol:water followed by copper sulfate (23 mg, 0.093 mmol) and an approximately 1 cm segment of 22 ga. copper wire. The solution was heated to 40 °C and stirred for one day. EDTA (69.6 mg, 0.187 mmol) was added to the solution, and stirring continued 30 min. The product was extracted with chloroform (3 x 5 mL) and the solvent was removed *in vacuo* leaving 103 mg orange oil mixture of **14** and **9**. The mixture was 28 mol % **14** (72 mol % **9**), and 68 weight % **14** by ^{1}H NMR (70 mg **14**, 33 % yield). ^{1}H NMR ($CDCl_3$, 500MHz) δ 7.78 (s, 1H), 5.1 (bs, 0.3H), 4.53 (s, 2H), 4.48 (t, 2H, J = 4.8 Hz), 3.79 (t, 2H, J = 4.9 Hz), 3.68 (t, 2H, J = 4.6 Hz), 3.60-3.65 (m, 6H), 3.54 (t, 2H, J = 4.6 Hz), 3.49 (t, 2H, J = 4.5 Hz), 3.34 (t, 2H, J = 5.0 Hz), 2.5 (bs, 4H), 1.34 (s, 3H) ppm; ^{13}C NMR (125MHz, $CDCl_3$) δ 144.7, 124.1, 72.6, 72.5, 69.9, 69.2, 69.1, 64.7, 61.6, 61.2, 58.4, 50.7, 50.2, 28.3 ppm (missing *C*ONH, one overlapped *C*H_2O).

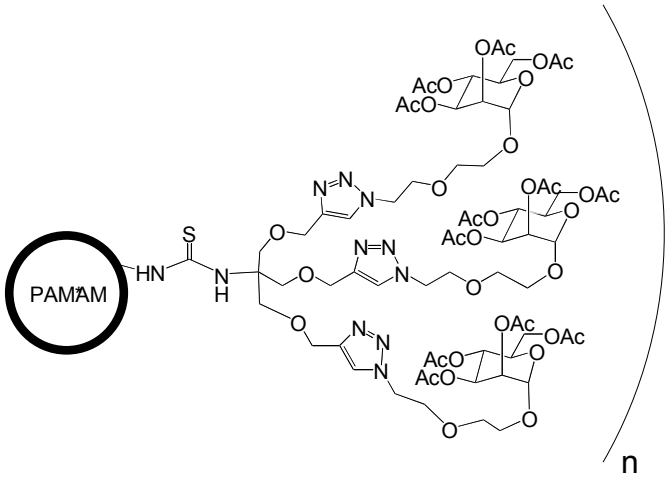

G(2) **15**
G(3) **16**
G(4) **17**
G(5) **18**
G(6) **19**

Representative procedure for the synthesis of PAMAM-based thiourea-linked tris-mannose clusters (15-19) (the following procedure is for **17**, see Table 2.4 for quantities of reactants and reaction yields for **15-19**). G(4) PAMAM dendrimer (13 mg, 0.96 μmol) was dissolved in 500 μL DMSO and mixed with mannose cluster **11** (88.1 mg, 53 μmol) in 1.8 mL DMSO. After 2 days the product was purified by dialysis in DMSO (MWCO 10,000 Da), and solvent was removed *in vacuo* to afford 61 mg **17** (77 % yield) as a soapy white solid.

Compound	Generation	Quantity of PAMAM (mg)	μmol PAMAM	Quantity of **11** (mg)	μmol **11**	yield (%)
15	2	17.0	5.22	138	83.2	101
16	3	21.4	3.1	165	99.3	111
17	4	13.0	0.963	88.1	53	77
18	5	10.1	0.396	62.5	37.6	91
19	6	11.5	0.217	62.0	37.3	89

Table 2.4 Quantities of reactants and product yields for compounds **15-19**.

PAMAM-based thiourea-linked tris-mannose clusters (15-19). Integration values have been set relative to the mannose cluster protons; for simple comparison the PAMAM protons are given as decimals.

15. ^{1}H NMR (CD_3SOCD_3, 500MHz) δ 7.7-8.2 (m, 2.3H), 6.8 (bs, 0.2H), 5.04 (s, 3H), 4.84 (s, 1H), 4.35-4.6 (m, 4H), 4.0-4.2 (m, 1H), 3.99 (m, 1H), 3.89 (bs, 1H), 3.80 (s, 3H), 3.67 (m, 1H), 3.55 (s, 4H), 3.25-3.35 (m, 1.3H), 3.0-3.25 (m, 1.5H), 2.55-2.7 (bs, 1.2H), 2.3-2.45 (bs, 0.7H), 2.12 (bs, 1.2H), 2.06 (s, 3H), 1.98 (s, 3H), 1.97 (s, 3H), 1.89 (s, 3H) ppm; ^{13}C NMR (CD_3SOCD_3, 125MHz) δ 182.1, 171.9, 170.5, 170.1, 169.9, 144.1, 124.6, 97.1, 69.4, 69.1, 68.8, 68.3, 66.8, 65.8, 64.4, 62.4, 61.7, 60.2, 50.0, 49.7, 43.3, 42.6, 38.5, 37.4, 33.6, 21.2, 21.0, 20.9, 20.8, 14.5 ppm; MALDI-TOF MS (pos) found 24,000 g/mol.

16. ^{1}H NMR (CD_3SOCD_3, 500MHz) δ 7.7-8.1 (m, 2.0H), 6.8 (bs, 0.2H), 5.05 (s, 3H), 4.84 (s, 1H), 4.4-4.55 (m, 4H), 4.09 (m, 1H), 3.97-3.99 (m, 1H), 3.89 (s, 1H), 3.80 (s, 4H), 3.66 (s, 1H), 3.56 (s, 3H), 3.2-3.4 (m, 2.0H), 3.0-3.15 (m, 1.6H), 2.55-2.7 (m, 1.2H), 2.39 (m, 0.8H), 2.16 (bs, 1.3H), 2.06 (s, 3H), 1.98 (s, 3H), 1.97 (s, 3H), 1.89 (s, 3H) ppm; ^{13}C NMR (CD_3SOCD_3, 125MHz) δ 182.1, 172.0, 170.5, 170.1, 169.9, 144.1, 124.5, 97.1, 69.4, 69.1, 68.8, 68.3, 66.8, 65.8, 64.4, 62.4, 61.7, 60.2, 52.9, 50.0, 49.7, 43.3, 42.6, 38.9, 38.5, 37.3, 33.6, 23.0, 21.2, 21.0, 14.5 ppm; MALDI-TOF MS (pos) found 44,000 g/mol.

17. ^{1}H NMR (CD_3SOCD_3, 500MHz) δ 7.6-8.3 (m, 2.6H), 6.8 (bs, 0.6H), 5.05 (s, 3H), 4.84 (s, 1H), 4.3-4.7 (m, 4H), 4.0-4.2 (m, 1H), 3.99 (m, 1H), 3.89 (s, 1H), 3.80 (bs, 3H),

3.66 (bs, 1H), 3.55 (bs, 3H), 3.3-3.4 (bs, 0.6H), 3.04 (m, 1.3H), 2.55-2.75 (m, 0.9H), 2.15 (bs, 1.1H), 2.06 (s, 3H), 1.96 (m, 6H), 1.88 (s, 3H) ppm; ^{13}C NMR (CD_3SOCD_3, 125MHz) δ 170.4, 170.1, 169.9, 144.1, 124.5, 97.1, 69.4, 69.1, 68.8, 68.5, 68.3, 66.8, 65.8, 64.4,63.3, 62.4, 60.2, 49.7, 43.3, 42.6, 38.5, 37.4, 33.6, 21.2, 20.9, 20.8, 20.8, 14.5 ppm; MALDI-TOF MS (pos) found 78,000 g/mol.

18. ^{1}H NMR (CD_3SOCD_3, 500MHz) δ 7.65-8.2 (m, 2.2H), 6.8 (bs, 0.4H), 5.04 (s, 3H), 4.83 (s, 1H), 4.3-4.6 (m, 4H), 4.05-4.15 (m, 1H), 3.96-4.00 (m, 1H), 3.89 (s, 1H), 3.79 (s, 3H), 3.65 (s, 1H), 3.55 (s, 3H), 3.0-3.2 (m, 1.8H), 2.55-2.75 (m,1.2H), 2.3-2.45 (m, 0.8H), 2.15 (bs, 1.2H), 2.05 (s, 3H), 1.9-2.0 (m, 6H), 1.88 (s, 3H) ppm; ^{13}C NMR (CD_3SOCD_3, 125MHz) δ 170.4, 170.1, 169.9, 144.1, 124.5, 97.1, 69.4, 69.1, 68.8, 68.5, 68.3, 66.8, 65.8, 64.4,63.3, 62.4, 60.2, 49.7, 38.5, 33.6, 20.9, 20.8, 20.8, 14.5 ppm; MALDI-TOF MS (pos) found 137,000 g/mol.

19. ^{1}H NMR (CD_3SOCD_3, 500MHz) δ 7.6-8.3 (m, 2.8H), 6.8 (bs, 0.5H), 5.04 (s, 3H), 4.84 (s, 1H), 4.3-4.6 (m, 4H), 4.0-4.15 (m, 1H), 3.96-3.98 (m, 1H), 3.89 (s, 1H), 3.79 (s, 3H), 3.65 (s, 1H), 3.30 (s, 2.8H), 3.04 (bs, 2.1H), 2.55-2.80 (m, 1.9H), 2.15 (bs, 1.4H), 2.06 (s, 2H), 1.9-2.0 (m, 5H), 1.88 (s, 2H) ppm; ^{13}C NMR (CD_3SOCD_3, 125MHz) δ 170.4, 170.1, 169.9, 144.1, 124.5, 97.1, 69.4, 69.1, 68.5, 68.3, 66.8, 65.8, 64.4, 62.4, 49.7, 20.9, 20.8 ppm; MALDI-TOF MS (pos) found 223,000 g/mol.

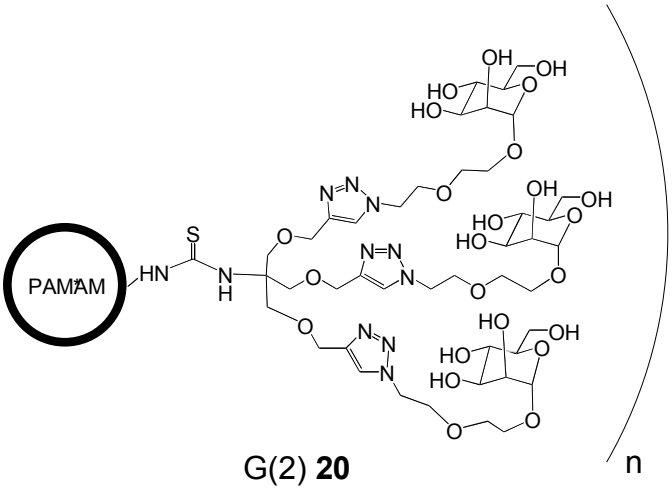

G(2) **20**
G(3) **21**
G(4) **22**
G(5) **23**
G(6) **24**

Representative procedure for the synthesis of PAMAM-based thiourea-linked tris-mannose clusters (20-24) (the following procedure is for **22**, see Table 2.5 for quantities of reactants and reaction yields for **20-24**). The acetylated glycodendrimer **17** (58 mg, 0.744 μmol) was mixed with 5 mL 1:1 methanol : water without dissolving. A 1.7 M solution of sodium methoxide in methanol (68 μL, 120 μmol) was then added to the stirring mixture. After stirring for 2 days the solid material was dissolved and the solution was neutralized with Amberlite IR-120 (acidic). Next the product solution was purified by dialysis (MWCO 1000 Da) in water, then the solvent was removed by lyophilization leaving 20.7 mg flaky white solid **22** (51 % yield).

Compound	Generation	Quantity of dendrimer (mg)	μmol dendrimer	Volume of NaOMe (1.7M) (mL)	μmol NaOMe	yield (%)
20	2	127.0	5.23	155	263	49
21	3	151	3.43	183	311	61
22	4	58.0	0.744	68	116	51
23	5	46	0.336	53	90	61
24	6	43	0.193	47.0	80	63

Table 2.5 Quantities of reactants and product yields for compounds **20-24**.

Deacetylated PAMAM-based thiourea-linked tris-mannose clusters (20-24). Integration values have been set relative to the mannose cluster protons; for simple comparison the PAMAM protons are given as decimals.

20. ^{1}H NMR (CD_3SOCD_3, 500MHz) δ 7.95-8.2 (m, 1.4H), 7.3-7.95 (m, 0.7H), 6.8 (bs, 0.1H), 4.73 (bs, 1H), 4.57 (s, 1H), 4.47 (s, 2H), 3.78 (s, 2H), 3.51-3.62 (3H), 3.2-3.5 (m, 7H), 3.10 (m, 1.0H), 2.84 (m, 1.6H), 2.32 (bs, 1.0H) ppm; MALDI-TOF MS (pos) found 17,200 g/mol.

21. ^{1}H NMR (CD_3SOCD_3, 500MHz) δ 7.7-8.2 (m, 1.0H), 6.8 (bs, 0.1H), 4.71 (bs, 1H), 4.57 (s, 1H), 4.47 (s, 2H), 3.78 (s, 2H), 3.62 (m, 1H), 3.5-3.6 (m, 2H), 3.40 (s, 1H), 3.30 (bs, 2H), 3.04 (m, 0.7H), 2.62 (bs, 0.7H), 2.16 (bs, 0.6H) ppm; MALDI-TOF MS (pos) found 30,000 g/mol.

22. ^{1}H NMR (CD_3SOCD_3, 500MHz) δ 7.7-8.2 (m, 1.0H), 6.8 (bs, 0.2H), 4.72 (bs, 1H), 4.57 (s, 1H), 4.48 (s, 2H), 3.78 (s, 2H), 3.62 (m, 1H), 3.5-3.6 (m, 1H), 3.2-3.45 (m, 3H),

3.05 (m, 0.6H), 2.62 (bs, 0.7H), 2.47 (0.2H), 2.16 (bs, 0.6H) ppm; MALDI-TOF MS (pos) found 59,000 g/mol.

23. ^{1}H NMR (CD_3SOCD_3, 500MHz) δ 7.5-8.2 (m, 1.5H), 4.70 (bs, 1H), 4.57 (s, 1H), 4.47 (s, 3H), 3.78 (s, 2H), 3.62 (m, 2H), 3.45-3.6 (m, 2H), 3.15-3.45 (m, 6H), 2.9-3.15 (m, 2.5H), 2.60 (bs, 2.0H), 2.38 (0.8H), 2.16 (bs, 01.8H) ppm; MALDI-TOF MS (pos) found 101,000 g/mol.

24. ^{1}H NMR (CD_3SOCD_3, 500MHz) δ 7.7-8.2 (m, 1.5H), 4.72 (bs, 1H), 4.56 (s, 1H), 4.47 (s, 2H), 3.78 (s, 2H), 3.45-3.7 (m, 3H), 3.40 (bs, 2H), 3.0-3.2 (m, 1.2H), 2.6-2.8 (bs, 0.9H), 2.05-2.4 (m, 1.1H) ppm; MALDI-TOF MS (pos) found 169,000 g/mol.

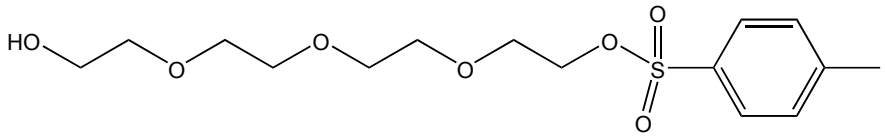

11-toluenesulfonyl-3,6,9-trioxaundecan-1-ol (25).

Compound **25** was prepared according to previously published methods. [106]

Tetraethyleneglycol (6.4g, 33 mmol) was dissolved in DCM (100 mL) and the solution was cooled to 0 °C then toluene sulfonyl chloride (6.9 g, 36 mmol) was added along with silver (I) oxide (11.4 g, 49 mmol) and potassium iodide (1.1 g, 6.6 mmol). After stirring for 15 minutes the reaction was complete by TLC (10% methanol, 90% chloroform) and the solution was filtered through a plug of silica and concentrated *in vacuo*. The product was purified on silica gel (4% methanol, 96% chloroform) to give 4.4 g **25** as a clear oil

(38% yield). ^{1}H NMR ($CDCl_3$, 500MHz) δ 7.69 (d, 2H, J = 8.2 Hz), 7.26 (d, 2H, J = 8.6 Hz), 4.06 (t, 2H, J = 4.7 Hz), 3.50-3.62 (m, 14H), 2.80 (s, 1H), 2.35 (s, 3H) ppm; ^{13}C NMR ($CDCl_3$, 125MHz) δ 144.9, 132.9, 129.9, 127.9, 72.5, 70.6, 70.6, 70.4, 70.3, 69.3, 68.6, 61.6, 21.6 ppm

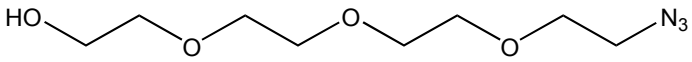

11-azido-3,6,9-trioxaundecan-1-ol (26).

Compound **26** was prepared using a modification of previously published methods.[108] Sodium azide (1.13 g, 17.4 mmol) was mixed with tosylate **25** in 60 mL DMF and the mixture was stirred at 80°C for 28 hours followed by the addition of 10 mL water. The solvent was removed *in vacuo* and the product was extracted with DCM (120 mL) and filtered from the solid salts. The solvent was removed *in vacuo* leaving 2.26 g **26** as a clear oil (94 % yield). ^{1}H NMR ($CDCl_3$, 500MHz) δ 3.54-3.71 (m, 14H), 3.41 (t, 2H, J = 5 Hz), 2.63 (t, 1H, J = 6 Hz) ppm; ^{13}C NMR ($CDCl_3$, 125MHz) δ 72.5, 70.7, 70.7, 70.6, 70.4, 70.0, 61.7, 50.7 ppm

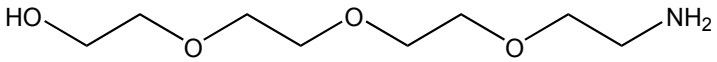

11-amino-3,6,9-trioxaundecan-1-ol (27).

The azide **26** (2.2 g, 10 mmol) was dissolved in ethanol (40 mL) and was combined with Pd/C (0.2 g). The reaction flask was flushed with H_2 (g) and was fitted with an H_2 (g) filled balloon. The mixture was stirred overnight followed by filtration of the catalyst and removal of the solvent *in vacuo* to yield the amine **27** (1.2 g, 62 % yield). ^{1}H NMR

($CDCl_3$, 500MHz) δ 3.66 (t, 3H, J = 4.4 Hz), 3.59-3.64 (m, 8H), 3.54 (t, 2H, J = 4.4 Hz), 3.48 (t, 2H, J = 5.1 Hz), 2.80 (t, 2H, J = 5.0 Hz) 2.52 (bs, 2H) ppm; ^{13}C NMR ($CDCl_3$, 125MHz) δ 73.2, 73.0, 70.6, 70.5, 70.3, 70.1, 61.4, 41.5 ppm; IR ($CDCl_3$) 3376, 2873, 1591 cm^{-1}. Characterization data agrees with literature values.[108]

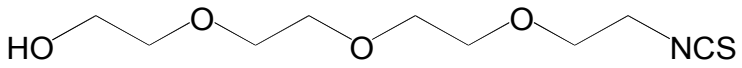

11-isothiocyanato-3,6,9-trioxaundecan-1-ol (28).

The amine **27** (1.2 g, 6.2 mmol) and triethylamine (1.4 g, 13.9 mmol) in 5 mL chloroform were added dropwise to a solution of thiophosgene (0.9 g, 7.8 mmol) in 40 mL chloroform via syringe pump over 1 hour then stirring continued 30 min. The solution was concentrated *in vacuo* and redissolved in 50 mL water and 50 mL chloroform. The aqueous layer was extracted with chloroform (3 x 50 mL), and the combined organic extracts were washed with water (2 x 50 mL) and dried over $MgSO_4$. After removal of the solvent the crude product was Kugelrohr distilled (125°C – 140°C) to afford 500 mg yellow oil (34% yield). The product **28** with minor impurities failed to be cleanly separated by further Kugelrohr distillation or chromatography with silica, alumina, or reversed-phase media. ^1H NMR ($CDCl_3$, 500MHz) δ 3.65 (t, 2H), 3.59-3.64 (m, 1H), 3.54 (t, 2H), 2.7 (s, 1H) ppm (and small signals from minor impurities 4.5 (m), 4.3 (s), 3.3 (m) ppm.).; ^{13}C NMR ($CDCl_3$, 125MHz) δ 132.3, 72.5, 70.6, 70.6, 70.4, 70.3, 69.2, 61.6, 45.4 ppm;

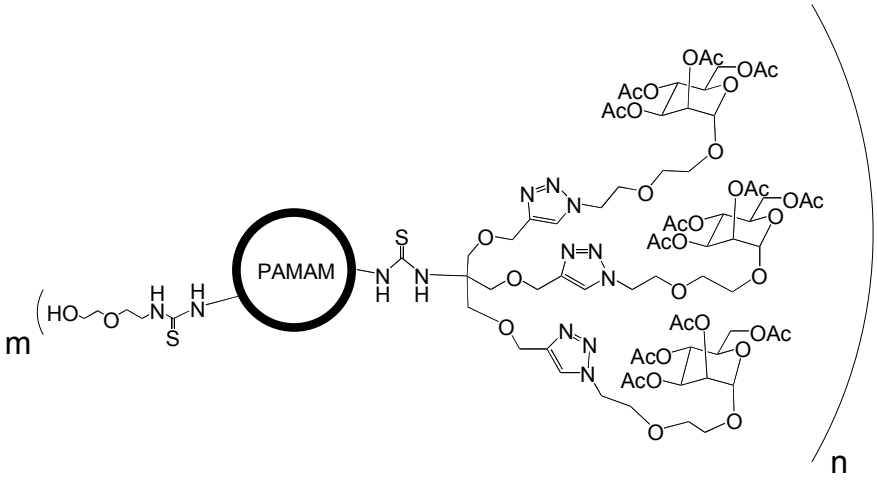

Step 1:	Step 2:
G(2) **30a-g**	G(2) **35a-g**
G(3) **31a-g**	G(3) **36a-g**
G(4) **32a-g**	G(4) **37a-g**
G(5) **33a-g**	G(5) **38a-g**
G(6) **34a-f**	G(6) **39a-f**

Representative procedure for the synthesis of heterogeneously functionalized PAMAM-based thiourea-linked ethoxyethanol and tris-mannose cluster dendrimers (30-39). (the following procedure is for **32e** and **37e,** see Table 2.6 for quantities of reactants and reaction yields for **30-39**). Step 1: G(4) PAMAM dendrimer (19.6 mg, 1.45 μmol) was dissolved in 200 μL DMSO and was mixed with the spacer isothiocyanate **29** (10.6 mg, 72 μmol) in 200 μL DMSO. After 2 days, a 5 μL aliquot of the partially functionalized **32e** was removed for MALDI-TOF MS analysis. Step 2: Next mannose cluster **11** (12.7 mg, 7.6 μmol) in 1.8 mL DMSO was added. After 2 days the product was purified by dialysis in DMSO (MWCO 10,000 Da), and solvent was removed *in vacuo* leaving 34.2 mg **37e** (92% yield).

Compound	Generation	of PAMAM (mg)	μmol PAMAM	Quantity of **29** (mg)	μmol **29**	Quantity of **11** (mg)	μmol **11**	yield (%)
30a, 35a	2	15.2	4.66	2.7	18	116	69.8	99
30b, 35b	2	15.5	4.76	5.6	38	76.6	46.1	41
30c, 35c	2	15.3	4.70	8.3	56	38.2	23.0	92
30d, 35d	2	15.4	4.73	9.5	65	23.3	14.0	103
30e, 35e	2	15.6	4.79	10.1	69	11.2	6.7	95
30f, 35f	2	15.5	4.76	10.6	72	15.2	9.1	76
30g, 35g	2	16.5	5.07	18.5	126	0	0	105
31a, 36a	3	13.5	1.95	2.3	16	96.8	58.2	91
31b, 36b	3	12.5	1.81	4.3	29	60.3	36.3	93
31c, 36c	3	13.8	2.00	7.0	48	37.2	22.4	105
31d, 36d	3	14	2.03	8.1	55	19.6	11.8	105
31e, 36e	3	13.9	2.01	8.5	58	6.3	3.8	85
31f, 36f	3	13.9	2.01	9.0	61	13.7	8.2	59
31g, 36g	3	16.8	2.43	18.6	127	0	0	104
32a, 37a	4	18.3	1.36	2.7	18	109	65.6	65
32b, 37b	4	18.7	1.39	5.5	37	75.4	45.4	65
32c, 37c	4	18.7	1.39	8.2	56	36.8	22.1	42
32d, 37d	4	19.1	1.41	9.9	67	18.6	11.2	106
32e, 37e	4	19.6	1.45	10.6	72	12.7	7.6	92
32f, 37f	4	20.7	1.53	11.7	80	6.4	3.9	67
32g, 37g	4	19.4	1.44	15.3	104	0	0	64
33a, 38a	5	13.2	0.52	1.8	12	84.5	50.8	95
33b, 38b	5	12.4	0.49	3.4	23	64.7	38.9	93
33c, 38c	5	13.5	0.53	5.6	38	35.7	21.5	95
33d, 38d	5	12.9	0.51	6.0	41	28.4	17.1	102
33e, 38e	5	12.4	0.49	6.1	41	21.0	12.6	95
33f, 38f	5	12.1	0.48	6.3	43	16.8	10.1	107
33g, 38g	5	12.6	0.50	10.0	68	0	0	116
34a, 39a	6	17.2	0.33	2.0	14	84.3	50.7	44
34b, 39b	6	19.5	0.37	4.6	31	42.5	25.6	36
34c, 39c	6	17.1	0.32	6.1	41	34.2	20.6	54
34d, 39d	6	17.4	0.33	8.3	56	18.9	11.4	69
34e, 39e	6	17.3	0.33	7.8	53	15.0	9.0	14
34f, 39f	6	17.7	0.33	15.6	106	0	0	75

Table 2.6 Quantities of reactants and product yields for compounds **30-39**.

Heterogeneously functionalized PAMAM-based thiourea-linked ethoxyethanol and tris-mannose cluster dendrimers (30-39). Integration values have been set relative to the mannose cluster protons, for simple comparison the ethoxyethanol protons and PAMAM protons are given as decimals.

30a. MALDI-TOF MS (pos) found 3750 g/mol.

35a. ^{1}H NMR (CD_3SOCD_3, 500MHz) δ 7.97 (m, 1.7H), 7.7-7.9 (m, 0.6H), 7.5 (bs, 0.2), 6.8 (bs, 0.3H), 5.04 (s, 3H), 4.84 (s, 1H), 4.35-4.6 (m, 4H), 4.0-4.2 (m, 1H), 3.96-3.99 (m, 1H), 3.89 (bs, 1H), 3.80 (s, 4H), 3.6-3.7 (m, 1H), 3.55 (s, 3H), 3.45 (bs, 0.84H), 3.38 (m, 1.08H), 3.0-3.2 (m, 1.76H), 2.6-2.7 (m, 2.04H), 2.3-2.45 (m, 1.2H), 2.16 (bs, 1.6H), 2.06 (s, 3H), 1.98 (s, 3H), 1.96 (s, 3H), 1.89 (s, 3H) ppm; MALDI-TOF MS (pos) found 16,400 g/mol.

30b. MALDI-TOF MS (pos) found 4520 g/mol.

35b. ^{1}H NMR (CD_3SOCD_3, 500MHz) δ 7.8-8.2 (m, 2.4H), 7.5 (bs, 0.5H), 6.8 (bs, 0.07H), 5.04 (s, 3H), 4.84 (s, 1H), 4.6 (bs, 0.25H), 4.4-4.55 (m, 4H), 4.08-4.12 (m, 1H), 3.96-3.98 (m, 1H), 3.89 (bs, 1H), 3.78 (s, 4H), 3.6-3.7 (m, 1H), 3.55 (s, 4H), 3.45 (s, 3H), 3.38 (s, 2H), 3.0-3.2 (m, 2.9H), 2.55-2.7 (m, 2.9H), 2.3-2.45 (m, 1.5H), 2.16 (bs, 2.8H), 2.07 (s, 3H), 1.98 (s, 3H), 1.97 (s, 3H), 1.89 (s, 3H) ppm; MALDI-TOF MS (pos) found 12300 g/mol.

30c. MALDI-TOF MS (pos) found 4920 g/mol.

35c. ^{1}H NMR (CD_3SOCD_3, 500MHz) δ 7.9-8.2 (m, 2.1H), 7.78 (m, 1.4H), 7.50 (bs, 1.7H), 5.04 (s, 3H), 4.85 (s, 1H), 4.59 (bs, 0.6H), 4.35-4.55 (m, 4H), 4.08-4.12 (m, 1H), 3.89-3.96 (m, 1H), 3.89 (bs, 1H), 3.80 (s, 4H), 3.6-3.7 (m, 1H), 3.56 (s, 5.0H), 3.45 (m, 7.2H), 3.38 (m, 5.1H), 3.31 (s, 6.5H), 3.13 (bs, 3.4H), 3.05 (bs, 3.5H), 2.55-2.75 (m, 5.8H), 2.3-2.45 (m, 3.9H), 2.17 (bs, 6.5H), 2.07 (s, 3H), 1.98 (s, 3H), 1.97 (s, 3H), 1.90 (s, 3H) ppm; MALDI-TOF MS (pos) found 7600 g/mol.

30d. MALDI-TOF MS (pos) found 5120 g/mol.

35d. ^{1}H NMR (CD_3SOCD_3, 500MHz) δ 7.9-8.2 (m, 4.6H), 7.8 (m, 2.6H), 7.51 (bs, 3.8H), 5.04 (s, 3H), 4.85 (s, 1H), 4.59 (bs, 2.3H), 4.4-4.55 (m, 3H), 4.08-4.11 (m, 1H), 3.96-3.98 (m, 1H), 3.89 (bs, 1H), 3.80 (s, 4H), 3.56 (s, 4.9H), 3.45 (m, 13.5H), 3.39 (m, 8.4H), 3.32 (s, 7.5H), 3.14 (s, 5.7H), 3.05 (s, 4.4H), 2.62 (s, 9.2H), 2.39 (m, 5.0H), 2.16 (bs, 8.9H), 2.07 (s, 3H), 1.98 (s, 2H), 1.97 (s, 3H), 1.89 (s, 2H) ppm; MALDI-TOF MS (pos) found 6000 g/mol.

30e. MALDI-TOF MS (pos) found 5460 g/mol.

35e. ^{1}H NMR (CD_3SOCD_3, 500MHz) δ 7.9-8.2 (m, 7.8H), 7.78 (m, 7.4H), 7.51 (bs, 12.7H), 5.04 (s, 3H), 4.85 (s, 1H), 4.60 (bs, 5.2H), 4.4-4.5 (m, 5H), 4.05-4.15 (m, 1H), 3.95-4.05 (m, 1H), 3.9 (bs, 1H), 3.7-3.85 (m, 4H), 3.5-3.7 (m, 17.0H), 3.45 (t, 42.2H), 3.38 (t, 30.6H), 3.31 (s, 33.0H), 3.13 (m, 20.8H), 3.05 (bs, 16.2H), 2.62 (bs, 31.2H), 2.3-2.45 (m, 18.5H), 2.17 (s, 32.3H), 2.07 (s, 5H), 1.98 (s, 4H), 1.97 (s, 4H), 1.90 (s, 4H) ppm; MALDI-TOF MS (pos) found 5900 g/mol.

30f. MALDI-TOF MS (pos) found 5500 g/mol.

35f. ^{1}H NMR (CD_3SOCD_3, 500MHz) δ 7.9-8.2 (m, 7.4H), 7.78 (m, 5.4H), 7.51 (bs, 8.5H), 5.04 (s, 3H), 4.85 (s, 1H), 4.60 (bs, 4.5H), 4.4-4.55 (m, 4H), 4.05-4.15 (m, 1H), 3.95-4.0 (m, 1H), 3.89 (bs, 1H), 3.80 (s, 5H), 3.5-3.7 (m, 9.3H), 3.45 (m, 31.7H), 3.39 (t, 18.3H), 3.30 (s, 29.8H), 3.14 (s, 12.8H), 3.05 (bs, 9.1H), 2.62 (s, 19.2H), 2.39 (s, 10.9H), 2.17 (s, 19.4H), 2.07 (s, 3H), 1.98 (s, 3H), 1.97 (s, 3H), 1.90 (s, 3H) ppm; MALDI-TOF MS (pos) found 6100 g/mol.

30g. MALDI-TOF MS (pos) found 5280 g/mol.

35g. ^{1}H NMR (CD_3SOCD_3, 500MHz) δ 7.9-8.2 (m, 1H), 7.78 (m, 1H), 7.50 (bs, 2H), 4.59 (bs, 1H), 3.4-3.6 (m, 8H), 3.38 (t, 4H), 3.31 (s, 5H), 3.14 (m, 3H), 3.05 (s, 2H), 2.62 (s, 4H), 2.39 (m, 2H), 2.17 (s, 4H) ppm; MALDI-TOF MS (pos) found 5300 g/mol.

31a. MALDI-TOF MS (pos) found 7930 g/mol.

36a. ^{1}H NMR (CD_3SOCD_3, 500MHz) δ 7.97 (m, 2.0H), 7.7-7.9 (m, 0.7H), 7.5 (bs, 0.2H), 6.8 (bs, 0.3H), 5.05 (s, 3H), 4.84 (s, 1H), 4.4-4.6 (m, 4H), 4.08-4.11 (m, 1H), 3.96-3.98 (m, 1H), 3.89 (bs, 1H), 3.80 (s, 4H), 3.66 (s, 1H), 3.55 (s, 4H), 3.45 (s, 1.0H), 3.38 (s, 0.9H), 3.0-3.2 (m, 2.0H), 2.55-2.7 (m, 1.8H), 2.3-2.45 (m, 1.3H), 2.16 (bs, 2.0H), 2.06 (s, 3H), 1.98 (s, 3H), 1.96 (s, 3H), 1.89 (s, 3H) ppm; MALDI-TOF MS (pos) found 28,800 g/mol.

31b. MALDI-TOF MS (pos) found 9260 g/mol.

36b. ^{1}H NMR (CD_3SOCD_3, 500MHz) δ 7.98 (m, 1.8H), 7.8 (m, 0.9H), 7.5 (bs, 0.6H), 5.04 (s, 3H), 4.84 (s, 1H), 4.6 (bs, 0.2H), 4.35-4.55 (m, 4H), 4.0-4.15 (m, 1H), 3.96-3.99 (m, 1H), 3.89 (bs, 1H), 3.80 (s, 4H), 3.6-3.7 (m, 1H), 3.56 (s, 4.0H), 3.45 (s, 2.9H), 3.38 (2.2H), 3.05 (s, 2.6H), 3.0-3.2 (m, 3.5H), 2.55-2.7 (m, 3.1H), 2.35-2.45 (m, 2.1H), 2.16 (bs, 3.3H), 2.07 (s, 3H), 1.98 (s, 3H), 1.97 (s, 4H), 1.89 (s, 3H) ppm; MALDI-TOF MS (pos) found 22,000 g/mol.

31c. MALDI-TOF MS (pos) found 10,570 g/mol.

36c. ^{1}H NMR (CD_3SOCD_3, 500MHz) δ 7.9-8.2 (m, 2.7H), 7.78 (bs, 1.7H), 7.50 (bs, 1.8H), 5.05 (s, 3H), 4.85 (s, 1H), 4.6 (bs, 1.0H), 4.4-4.55 (m, 4H), 4.09-4.11 (m, 1H),

3.96-3.99 (m, 1H), 3.89 (bs, 2H), 3.80 (s, 4H), 3.6-3.7 (m, 2H), 3.56 (s, 5.0H), 3.45 (m, 6.8H), 3.38 (m, 4.6H), 3.30 (m, 8.1H), 3-3.2 (m, 6.7H), 2.55-2.75 (m, 6.4H), 2.3-2.45 (m, 3.0H), 2.16 (bs, 5.5H), 2.07 (s, 3H), 1.98 (s, 3H), 1.97 (s, 3H), 1.90 (s, 3H) ppm; MALDI-TOF MS (pos) found 14,900 g/mol.

31d. MALDI-TOF MS (pos) found 10,880 g/mol.

36d. ^{1}H NMR (CD_3SOCD_3, 500MHz) δ 7.9-8.2 (m, 4.8H), 7.78 (bs, 5.1H), 7.51 (bs, 7.1H), 5.04 (s, 4H), 4.85 (s, 1H), 4.59 (bs, 2.5H), 4.4-4.55 (m, 6H), 4.05-4.15 (m, 1H), 3.95-4.0 (m, 1H), 3.89 (bs, 2H), 3.80 (s, 6H), 3.6-3.7 (m, 2H), 3.5-3.6 (m, 12.2H), 3.46 (s, 25.3H), 3.39 (m, 18.2H), 3.31 (s, 18.4), 3.14 (bs, 12.9H), 3.05 (bs, 11.5), 2.62 (m, 20.4), 2.35-2.4 (m, 14.2H), 2.16 (s, 22.3H), 2.07 (s, 6H), 1.98 (s, 4H), 1.97 (s, 6H), 1.90 (s, 5H) ppm; MALDI-TOF MS (pos) found 12,900 g/mol.

31e. MALDI-TOF MS (pos) found 11,400 g/mol.

36e. ^{1}H NMR (CD_3SOCD_3, 500MHz) δ 7.9-8.2 (m, 11.6H), 7.78 (bs, 10.3H), 7.51 (bs, 14.7H), 5.04 (s, 3H), 4.85 (s, 1H), 4.60 (bs, 6.7H), 4.4-4.55 (m, 4H), 4.05-4.15 (m, 1H), 3.95-4.0 (m, 1H), 3.90 (bs, 1H), 3.80 (m, 5.4H), 3.45-3.70 (m, 65.7H), 3.39 (m, 32.1H), 3.31 (s, 36.0H), 3.14 (s, 23.9H), 3.05 (s, 20.1H), 2.62 (s, 36.1H), 2.39 (s, 22.3H), 2.16 (s, 38.6H), 2.07 (s, 4H), 1.98 (s, 3H), 1.97 (s, 4H), 1.90 (s, 4H) ppm; MALDI-TOF MS (pos) found 12,500 g/mol.

31f. MALDI-TOF MS (pos) found 11,300 g/mol.

36f. ^{1}H NMR (CD_3SOCD_3, 500MHz) δ 7.7-8.5 (m, 16.1H), 7.59 (bs, 4.3H), 5.05 (s, 3H), 4.85 (s, 1H), 4.55-4.8 (bs, 3.7H), 4.4-4.55 (m, 4H), 4.05-4.15 (m, 1H), 3.96-3.99 (m, 1H), 3.89 (bs, 1H), 3.80 (s, 3H), 3.4-3.7 (m, 35.3H), 3.38 (s, 16.2H), 3.30 (m, 31.8H), 3.0-3.25 (m, 26.5H), 2.61 (s, 17.7H), 2.2-2.35 (m, 13.9H), 2.17 (s, 21.8H), 2.07 (s, 3H), 1.98 (s, 3H), 1.97 (s, 3H), 1.90 (s, 3H) ppm; MALDI-TOF MS (pos) found 12,100 g/mol.

31g. MALDI-TOF MS (pos) found 11300 g/mol.

36g. ^{1}H NMR (CD_3SOCD_3, 500MHz) δ 7.9-8.2 (m, 1H), 7.77 (bs, 1H), 7.49 (bs, 2H), 4.59 (bs, 1H), 3.4-3.65 (m, 8H), 3.38 (t, 4H), 3.31 (s, 4H), 3.14 (bs, 3H), 3.05 (bs, 2H), 2.63 (m, 4H), 2.38 (m, 3H), 2.16 (s, 5H) ppm; MALDI-TOF MS (pos) found 11,300 g/mol.

32a. MALDI-TOF MS (pos) found 15,500 g/mol.

37a. ^{1}H NMR (CD_3SOCD_3, 500MHz) δ 7.8-8.1 (m, 2.2H), 7.5 (bs, 0.2H), 6.8 (bs, 0.1H), 5.04 (s, 3H), 4.84 (s, 1H), 4.45-4.60 (m, 4H), 4.09-4.11 (m, 1H), 3.96-4.01 (m, 1H), 3.89 (s, 1H), 3.80 (s, 4H), 3.66 (m, 1H), 3.55 (s, 3H), 3.45 (bs, 0.95H), 3.38 (m, 1H), 3.0-3.2 (m, 2H), 2.55-2.75 (m, 1.7H), 2.3-2.45 (m, 1H), 2.16 (bs, 1.7H), 2.06 (s, 3H), 1.97 (s, 3H), 1.96 (s, 2H), 1.89 (s, 3H) ppm; MALDI-TOF MS (pos) found 60,000 g/mol.

32b. MALDI-TOF MS (pos) found 17,600 g/mol.

37b. ^{1}H NMR (CD_3SOCD_3, 500MHz) δ 7.9-8.1 (m, 2.1H), 7.75 (m, 0.9H), 7.48 (bs, 0.7H), 6.8 (bs, 0.3H), 5.05 (s, 3H), 4.84 (s, 1H), 4.57 (bs, 0.5H), 4.49 (s, 2H), 4.45 (s, 2H), 4.08-4.11 (m, 1H), 3.96-4.00 (m, 1H), 3.89 (bs, 1H), 3.80 (s, 4H), 3.60-3.70 (m,

1H), 3.56 (s, 3H), 3.45 (s, 2.2H), 3.38 (m, 1.8H), 3.14 (bs, 1.2H), 3.05 (bs, 1.8H), 2.55-2.88 (m, 2.5H), 2.30-2.40 (m, 1.5H), 2.16 (bs, 2.6H), 2.06 (s, 3H), 1.98 (s, 3H), 1.96 (s, 3H), 1.89 (s, 3H) ppm; MALDI-TOF MS (pos) found 51,000 g/mol.

32c. MALDI-TOF MS (pos) found 19,600 g/mol.

37c. ^{1}H NMR (CD_3SOCD_3, 500MHz) δ 7.97 (m, 2.4H), 7.76 (bs, 1.6H), 7.48 (bs, 1.8H), 6.8 (bs 0.1H), 5.05 (s, 3H), 4.85 (s, 1H), 4.58 (bs, 0.9H), 4.49 (s, 2H), 4.45 (s, 2H), 4.08-4.11 (dd, 1H), 3.96-4.01 (m, 1H), 3.89 (bs, 1H), 3.80 (s, 4H), 3.60-3.70 (m, 1H), 3.56 (s, 4H), 3.46 (m, 5.9H), 3.39 (m, 4.3H), 3.14 (bs, 2.8H), 3.05 (bs, 3.1H), 2.62 (bs, 5.3H), 2.39 (bs, 3H), 2.17 (bs, 5.3H), 2.07 (s, 4H), 1.98 (m, 6H), 1.89 (s, 3H) ppm; MALDI-TOF MS (pos) found 36,000 g/mol.

32d. MALDI-TOF MS (pos) found 20,200 g/mol.

37d. ^{1}H NMR (CD_3SOCD_3, 500MHz) δ7.98 (m, 4.8H), 7.76 (bs, 3.4H), 7.49 (bs, 4.8H), 5.05 (s, 3H), 4.85 (s, 1H), 4.58 (bs, 2.2H), 4.50 (s, 2H), 4.45 (s, 1H), 4.09-4.11 (app dd, 1H), 3.97-3.99 (m, 1H), 3.89 (bs, 1H), 3.80 (m, 4H), 3.66 (m, 1H), 3.35-3.60 (m, 21.6H), 3.14 (bs, 6.1H), 3.06 (bs, 6H), 2.50-2.70 (m, 10.4H), 2.30-2.40 (m, 7.8H), 2.17 (bs, 11.4H), 2.07 (s, 4H), 1.98 (s, 3H), 1.97 (s, 3H), 1.90 (s, 3H) ppm; MALDI-TOF MS (pos) found 28,700 g/mol.

32e. MALDI-TOF MS (pos) found 20,700 g/mol.

37e. ^{1}H NMR (CD_3SOCD_3, 500MHz) δ 7.98 (bs, 6.1H), 7.76 (bs, 5.3H), 7.48 (bs, 8.7H), 5.05 (s, 3H), 4.85 (s, 1H), 4.58 (bs, 4H), 4.50 (s, 2H), 4.45 (s, 2H), 4.09-4.11 (app dd,

1H), 3.95-4.05 (m, 1H), 3.90 (bs, 1H), 3.80 (m, 4H), 3.65-3.66 (m, 1H), 3.3-3.6 (m, 53.7H), 3.14 (bs, 11.5H), 3.05 (bs, 10.8H), 2.55-2.7 (m, 19.5H), 2.3-2.4 (m, 13.1H), 2.17 (bs, 21.5H), 2.07 (s, 4H), 1.98 (s, 4H), 1.97 (s, 4H), 1.90 (s, 4H) ppm; MALDI-TOF MS (pos) found 25,800 g/mol.

32f. MALDI-TOF MS (pos) found 20,300 g/mol.

37f. ^{1}H NMR (CD_3SOCD_3, 500MHz) δ 7.9-8.0 (m, 11.7H), 7.76 (bs , 11.4H), 7.48 (bs, 21.5H), 5.05 (s, 3H), 4.85 (s, 1H), 4.58 (s, 1H), 4.51 (s, 4H), 4.10 (app dd, 1H), 4.0 (m, 1H), 3.90 (bs, 1H), 3.80 (m, 3H), 3.35-3.60 (m, 124H), 3.14 (bs, 27.4H), 3.05 (bs, 23H), 2.5-2.7 (m, 45H), 2.3-2.4 (m, 27.6H), 2.17 (bs, 47.2H), 2.07 (s, 5H), 1.99 (s, 4H), 1.97 (s, 4H), 1.90 (s, 4H) ppm; MALDI-TOF MS (pos) found 23,100 g/mol.

32g. MALDI-TOF MS (pos) found 21,000 g/mol.

37g. ^{1}H NMR (CD_3SOCD_3, 500MHz) δ 7.97 (bs, 1H), 7.76 (bs, 1H), 7.47 (bs, 2H), 4.58 (bs, 1H), 3.2-3.6 (m, 7H), 3.14 (bs, 3H), 3.05 (bs, 2H), 2.62 (bs, 5H), 2.39 (s, 3H), 2.17 (s, 5H) ppm; MALDI-TOF MS (pos) found 21,000 g/mol.

33a. MALDI-TOF MS (pos) found 29,800 g/mol.

38a. ^{1}H NMR (CD_3SOCD_3, 500MHz) δ 7.6-8.2 (m, 3.2H), 6.8 (bs, 0.3H), 5.04 (s, 3H), 4.84 (s, 1H), 4.35-4.60 (m, 4H), 4.05-4.15 (m, 1H), 3.9-4.0 (m, 1H), 3.89 (bs, 1H), 3.79 (s, 3.5H), 3.65 (s, 1.4H), 3.55 (s, 3.6H), 3.2-3.4 (m, 5.5H), 3.0-3.2 (m, 2.4H), 2.55-2.7 (m, 1.9H), 2.16 (bs, 2.2H), 2.06 (s, 3H), 1.97 (s, 3H), 1.96 (s, 4H), 1.89 (s, 3H) ppm; MALDI-TOF MS (pos) found 92,000 g/mol.

33b. MALDI-TOF MS (pos) found 32,800 g/mol.

38b. ^{1}H NMR (CD_3SOCD_3, 500MHz) δ 7.5-8.3 (m, 3.7H), 6.8 (bs, 0.3H), 5.04 (s, 3H), 4.84 (s, 1H), 4.35-4.6 (m, 4H), 4.0-4.15 (m, 1H), 3.9-4.0 (m, 1H), 3.89 (bs, 1H), 3.80 (s, 3H), 3.65 (s, 1.3H), 3.55 (s, 3.3H), 3.45 (s, 1.8H), 3.37 (s, 1.2H), 3.31 (s, 4.9H), 3.0-3.2 (m, 2.8H), 2.55-2.7 (m, 2.3H), 2.16 (bs, 2.6H), 2.06 (s, 3H), 1.98 (s, 2H), 1.96 (s, 3H), 1.89 (s, 3H) ppm; MALDI-TOF MS (pos) found 81,000 g/mol.

33c. MALDI-TOF MS (pos) found 34,700 g/mol.

38c. ^{1}H NMR (CD_3SOCD_3, 500MHz) δ 7.5-8.3 (m, 5.8H), 6.8 (bs, 0.1H), 5.04 (s, 3H), 4.84 (s, 1H), 4.4-4.55 (m, 4H), 4.08-4.11 (m, 1H), 3.96-3.98 (m, 1H), 3.89 (s, 1H), 3.80 (s, 4H), 3.66 (m, 1H), 3.55 (s, 3.8H), 3.45 (s, 6.7H), 3.38 (s, 3.7H), 3.31 (s, 9.3H), 3.0-3.2 (m, 6.5H), 2.55-2.75 (m, 6.2H), 2.16 (bs, 6.2H), 2.07 (s, 3H), 1.98 (s, 2H), 1.97 (s, 3H), 1.89 (s, 3H) ppm; MALDI-TOF MS (pos) found 55,300 g/mol.

33d. MALDI-TOF MS (pos) found 36,200 g/mol.

38d. ^{1}H NMR (CD_3SOCD_3, 500MHz) δ 7.9-8.6 (m, 4.6H), 7.85 (bs, 2.2H), 7.6 (bs, 1.3H), 6.8 (bs, 0.2H), 5.04 (s, 2H), 4.84 (s, 1H), 4.4-4.6 (m, 4H), 4.05-4.15 (m, 1H), 3.96-3.99 (m, 1H), 3.89 (s, 1H), 3.80 (s, 3H), 3.64 (m, 1H), 3.55 (s, 3.9H), 3.45 (s, 6.8H), 3.38 (s, 4.0H), 3.31 (s, 8.6H), 3.0-3.2 (m, 7.3H), 2.55-2.75 (m, 5.6H), 2.16 (bs, 7.2H), 2.07 (s, 3H), 1.98 (s, 2H), 1.97 (s, 4H), 1.89 (s, 3H) ppm; MALDI-TOF MS (pos) found 55,300 g/mol.

33e. MALDI-TOF MS (pos) found 37,500 g/mol.

38e. ^{1}H NMR (CD_3SOCD_3, 500MHz) δ 7.9-8.6 (m, 3.9H), 7.86 (bs, 2.7H), 7.6 (bs, 1.4H), 5.04 (s, 2H), 4.84 (s, 1H), 4.35-4.60 (m, 4H), 4.05-4.15 (m, 1H), 3.96-3.98 (m, 1H), 3.89 (s, 1H), 3.80 (s, 3H), 3.65 (m, 1H), 3.56 (s, 4.3H), 3.45 (s, 8.8H), 3.38 (s, 5.2H), 3.31 (s, 12.0H), 3.0-3.2 (m, 9.3H), 2.55-2.75 (m, 7.8H), 2.16 (bs, 9.0H), 2.07 (s, 3H), 1.98 (s, 3H), 1.97 (s, 4H), 1.89 (s, 3H) ppm; MALDI-TOF MS (pos) found 52,300 g/mol.

33f. MALDI-TOF MS (pos) found 38,100 g/mol.

38f. ^{1}H NMR (CD_3SOCD_3, 500MHz) δ 7.9-8.6 (m, 4.1H), 7.85 (bs, 2.8H), 7.6 (bs, 1.2H), 5.04 (s, 2H), 4.84 (s, 1H), 4.35-4.65 (m, 4H), 4.05-4.15 (m, 1H), 3.96-3.98 (m, 1H), 3.89 (s, 1H), 3.80 (s, 3H), 3.66 (m, 1H), 3.55 (s, 4.5H), 3.45 (s, 9.7H), 3.38 (s, 5.3H), 3.31 (s, 11.7H), 3.0-3.2 (m, 9.4H), 2.55-2.70 (m, 7.9H), 2.17 (bs, 9.3H), 2.07 (s, 3H), 1.98 (s, 3H), 1.97 (s, 4H), 1.89 (s, 4H) ppm; MALDI-TOF MS (pos) found 50,300 g/mol.

33g. MALDI-TOF MS (pos) found 41,000 g/mol.

38g. ^{1}H NMR (CD_3SOCD_3, 500MHz) δ 8.00 (bs, 1H), 7.78 (bs, 1H), 7.51 (bs, 2H), 4.60 (bs, 1H), 3.45 (s, 8H), 3.39 (m, 4H), 3.31 (s, 3H), 3.14 (bs, 3H), 3.05 (bs, 2H), 2.55-2.70 (m, 4H), 2.3-2.4 (m, 4H), 2.17 (bs, 7H) ppm; MALDI-TOF MS (pos) found 41,000 g/mol.

34a. MALDI-TOF MS (pos) found 60,000 g/mol.

39a. ^{1}H NMR (CD_3SOCD_3, 500MHz) δ 7.9-8.2 (m, 2.4H), 7.7-7.9 (m, 0.6H), 7.6 (bs, 0.5H), 6.8 (bs, 0.5H), 5.04 (s, 2H), 4.83 (s, 1H), 4.4-4.7 (m, 3H), 4.05-4.15 (m, 1H), 3.96-3.98 (m, 1H), 3.89 (s, 1H), 3.80 (s, 3H), 3.65 (s, 1.2H), 3.55 (s, 2.4H), 3.46 9 (s, 1.0H), 3.39 (s, 0.9H), 3.30 (s), 3.0-3.2 (m, 2.1H), 2.55-2.75 (m, 1.3H), 2.16 (bs, 1.6H), 2.05 (s, 2H), 1.9-2.0 (m, 5H), 1.88 (s, 3H) ppm; MALDI-TOF MS (pos) found 174,000 g/mol.

34b. MALDI-TOF MS (pos) found 70,000 g/mol.

39b. ^{1}H NMR (CD_3SOCD_3, 500MHz) δ 7.97 (m, 2.7H), 7.78 (m, 1.6H), 7.51 (bs, 1.2H), 6.8 (bs, 0.2H), 5.04 (s, 3H), 4.84 (s, 1H), 4.35-4.6 (m, 4H), 4.05-4.15 (m, 1H), 3.95-4.0 (m, 1H), 3.89 (s, 1H), 3.80 (s, 3H), 3.66 (m, 1H), 3.55 (s, 3.5H), 3.46 (s, 3.8H), 3.38 (s, 3.0H), 3.30 (s, 5.4H), 3.0-3.2 (m, 5.3H), 2.55-2.75 (m, 4.4H), 2.16 (bs, 4.4H), 2.06 (s, 3H), 1.9-2.0 (m, 6H), 1.89 (s, 3H) ppm; MALDI-TOF MS (pos) found 122,000 g/mol.

34c. MALDI-TOF MS (pos) found 71,000 g/mol.

39c. ^{1}H NMR (CD_3SOCD_3, 500MHz) δ 7.97 (bs, 3.8H), 7.78 (bs, 1.6H), 7.5 (bs, 1.8H), 6.8 (bs, 0.5H), 5.04 (s, 2H), 4.84 (s, 1H), 4.4-4.7 (m, 4H), 4.05-4.15 (m, 1H), 3.96-3.98 (m, 1H), 3.89 (s, 1H), 3.80 (s, 3H), 3.66 (m, 1H), 3.55 (s, 2.8H), 3.46 (s, 5.3H), 3.39 (s, 3.4H), 3.30 (s, 4.6 H), 3.0-3.2 (m, 5.2H), 2.62 (bs, 4.3H), 2.16 (bs, 4.4H), 2.06 (s, 3H), 1.9-2.0 (m, 5H), 1.89 (s, 3H) ppm; MALDI-TOF MS (pos) found 108,000 g/mol.

34d. MALDI-TOF MS (pos) found 72,000 g/mol.

39d. ^{1}H NMR (CD_3SOCD_3, 500MHz) δ 7.98 (m, 5.3H), 7.77 (bs, 4.0H), 7.49 (bs, 6.6H), 5.05 (s, 2H), 4.84 (s, 1H), 4.59 (bs, 2.7H), 4.35-4.55 (m, 4H), 4.05-4.15 (m, 1H), 3.96-3.99 (m, 1H), 3.89 (s, 1H), 3.80 (s, 4H), 3.3-3.7 (m, 39.1H), 3.0-3.2 (m, 16.3H), 2.62 (bs,

14.9H), 2.17 (bs, 14.5H), 2.07 (s, 5H), 1.9-2.0 (m, 6H), 1.89 (s, 4H) ppm; MALDI-TOF MS (pos) found 88,000 g/mol.

34e. MALDI-TOF MS (pos) found 76,000 g/mol.]

39e. ^{1}H NMR (CD_3SOCD_3, 500MHz) δ 7.98 (bs, 9.9H), 7.77 (bs, 8.4H), 7.48 (bs, 15.3H), 5.04 (s, 4H), 4.84 (s, 1H), 4.60 (bs, 5.7H), 4.35-4.5 (m, 7H), 4.05-4.15 (m, 1H), 3.96-3.99 (m, 1H), 3.89 (s, 1H), 3.80 (s, 6H), 3.65 (m, 2H), 3.55 (s, 8.9 H), 3.46 (s, 44.6H), 3.39 (s, 29.6H), 3.14 (s, 21.0H), 3.06 (s, 16.5H), 2.62 (bs, 32.1H), 2.17 (bs, 37.0H), 2.07 (s, 11H), 1.97 (m, 16H), 1.89 (s, 10H) ppm; MALDI-TOF MS (pos) found 82,000 g/mol.

34f. MALDI-TOF MS (pos) found 77,000 g/mol.

39f. ^{1}H NMR (CD_3SOCD_3, 500MHz) δ 7.98 (bs, 1H), 7.76 (bs, 1H), 7.48 (s, 2H), 4.60 (bs, 1H), 3.46 (s, 7H), 3.39 (m, 4H), 3.11 (s, 3H), 3.06 (bs, 2H), 2.62 (bs, 4H), 2.40 (bs, 2H), 2.17 (bs, 4H) ppm; MALDI-TOF MS (pos) found 77,000 g/mol.

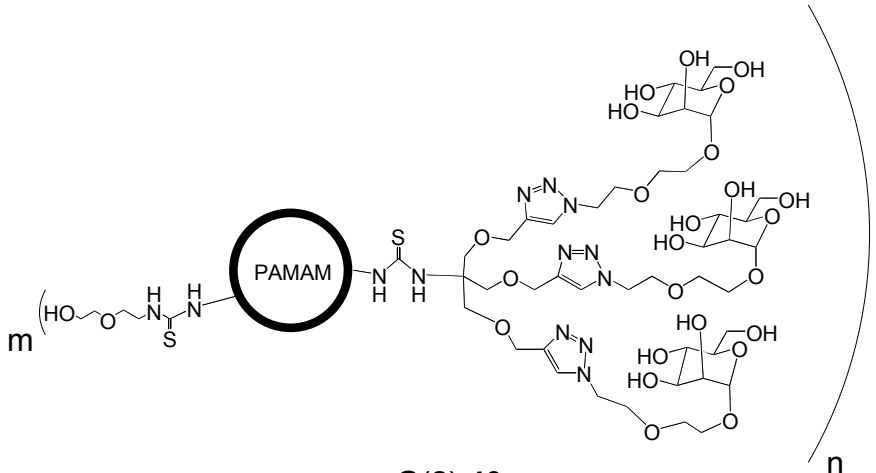

G(2) **40a-g**
G(3) **41a-g**
G(4) **42a-g**
G(5) **43a-g**
G(6) **44a-f**

Representative procedure for the synthesis of deacetylated heterogeneously functionalized PAMAM-based thiourea-linked ethoxyethanol and tris-mannose cluster dendrimers (40-44). (the following procedure is for **42e**, see Table 2.7 for quantities of reactants and reaction yields for **40-44**). The acetylated glycodendrimer **37e** (34.2 mg, 1.33 μmol) was mixed with 3 mL 1:1 methanol : water without dissolving. A 1.2 M solution of sodium methoxide in methanol (52 μL, 62 μmol) was then added to the stirring mixture. After stirring for 2 days the solid material was dissolved and the solution neutralized with Amberlite IR-120 (acidic). Next the product solution was purified by dialysis (MWCO 1000 Da) in water, then the solvent removed by lyophilization leaving 12.9 mg flaky tan solid **42e** (38% yield).

Compound	Generation	Quantity of dendrimer (mg)	mmol dendrimer	Volume of NaOMe (1.2M) (mL)	mmol NaOMe	yield (%)
40a	2	76.2	4.65	265	318	36
40b	2	23.7	1.93	68	82	17
40c	2	32.8	4.32	52	62	ND
40d	2	29.5	4.92	20	24	ND
40e	2	27	4.58	10	12	ND
40f	2	22.1	3.62	10	12	ND
40g	2	28.1	5.30	0	0	90
41a	3	51.3	1.78	168	202	56
41b	3	36.9	1.68	96	115	58
41c	3	31.3	2.10	41	49	64
41d	3	27.6	2.14	20	24	65
41e	3	21.5	1.72	9	11	64
41f	3	14.4	1.19	4	5	ND
41g	3	28.4	2.51	0	0	94
42a	4	52.5	0.88	176	211	42
42b	4	45.5	0.89	124	149	58
42c	4	20.8	0.58	42	50	45
42d	4	42.9	1.49	58	70	59
42e	4	34.2	1.33	52	62	38
42f	4	23.8	1.03	14	17	34
42g	4	19.8	0.92	0	0	35
43a	5	45.6	0.49	138	166	51
43b	5	36.7	0.45	99	119	66
43c	5	28	0.51	47	56	62
43d	5	28.6	0.52	44	53	77
43e	5	24.2	0.46	31	37	75
43f	5	25.5	0.51	28	34	74
43g	5	2.33	0.57	0	0	80
44a	6	25.1	0.14	75	90	44
44b	6	16	0.13	33	40	61
44c	6	19.2	0.17	29	35	47
44d	6	19.9	0.23	22	26	37
44e	6	3.8	0.05	1	1	ND
44f	6	18.7	0.25	0	0	43

Table 2.7 Quantities of reactants and product yields for compounds **40-44**. ND = not determined.

Deacetylated heterogeneously functionalized PAMAM-based thiourea-linked ethoxyethanol and tris-mannose cluster dendrimers (40-44). Integration values have

been set relative to the mannose cluster protons, for simple comparison the ethoxyethanol protons and PAMAM protons are given as decimals.

40a. ^{1}H NMR (CD_3SOCD_3, 500MHz) δ 7.95-8.2 (m, 1.2H), 7.7-7.95 (m, 0.2H), 7.4-7.8 (m, 0.3H), 6.8 (bs, 0.2H), 4.73 (bs, 1H), 4.57 (s, 1H), 4.47 (s, 2H), 3.78 (s, 2H), 3.54-3.60 (1.1H), 3.51-3.54 (m, 1.7H), 3.40 (m, 2.3H), 3.33 (m, 2.3H), 3.27 (m, 1.2H), 3.10 (m, 1.2H), 2.84 (m, 1.5H), 2.28 (bs, 1.2H) ppm; MALDI-TOF MS (pos) found 13300 g/mol.

40b. ^{1}H NMR (CD_3SOCD_3, 500MHz) δ 7.95-8.4 (m, 1.7H), 7.4-7.95 (m, 1.2H), 6.8 (bs, 0.3H), 4.72 (s, 1H), 4.57 (s, 1H), 4.48 (s, 2H), 3.78 (s, 2H), 3.60-3.62 (m, 1.2H), 3.51-3.54 (m, 1.7H), 3.45 (m, 3.1H), 3.14 (bs, 0.8H) ppm; MALDI-TOF MS (pos) found 12,300 g/mol.

40c. ^{1}H NMR (CD_3SOCD_3, 500MHz) δ 7.95-8.4 (m, 1.9H), 7.4-7.95 (m, 1.4H), 6.8 (bs, 0.2H), 4.72 (s, 1H), 4.57 (s, 1H), 4.47 (s, 2H), 3.78 (s, 2H), 3.60-3.62 (m, 1.2H), 3.52-3.54 (m, 1.8H), 3.35-3.45 (m, 3.7H), 3.14 (bs, 1.7H) ppm.

40d. ^{1}H NMR (CD_3SOCD_3, 500MHz) δ 7.8-8.3 (m, 2.0H), 7.4-7.8 (m, 1.4H), 4.72 (bs, 1H), 4.57 (s, 1H), 4.47 (s, 2H), 3.78 (s, 2H), 3.60-3.62 (m, 1.4H), 3.2-3.6 (m, 23H), 3.13 (bs, 3.1H), 2.75 (bs, 3.1H), 2.25 (bs, 2.1H) ppm.

40e. ^{1}H NMR (CD_3SOCD_3, 500MHz) δ 7.8-8.3 (m, 4.2H), 7.4-7.8 (m, 3.3H), 4.7 (bs, 1H), 4.57 (s, 1H), 4.47 (s, 2H), 3.78 (m, 2H), 3.15-3.65 (m, 48H), 3.14 (bs, 7.6H), 2.75 (bs, 7.0H), 2.25 (bs, 5.4H) ppm.

40f. ^{1}H NMR (CD_3SOCD_3, 500MHz) δ 7.8-8.3 (m, 3.4H), 7.4-7.8 (m, 2.8H), 6.52 (s, 0.2H), 4.72 (bs, 1H), 4.57 (s, 1H), 4.47 (s, 2H), 3.78 (s, 2H), 3.2-3.7 (m, 72H), 3.14 (s, 6.6H), 2.75 (bs, 6.5H), 2.25 (bs, 4.9H) ppm.

41a. ^{1}H NMR (CD_3SOCD_3, 500MHz) δ 7.8-8.4 (m, 1.4H), 7.4-7.8 (m, 0.7H), 6.8 (bs, 0.2H), 4.73 (bs, 1H), 4.57 (s, 1H), 4.47 (s, 2H), 3.78 (s, 2H), 3.60-3.62 (m, 1.2H), 3.51-3.54 (m, 1.7H), 3.40 (m, 2.7H), 3.33 (m, 4.8H), 3.11 (m, 1.2H), 2.55-3.0 (m, 1.4H), 2.33 (bs, 1.0H) ppm; MALDI-TOF MS (pos) found 22,300 g/mol.

41b. ^{1}H NMR (CD_3SOCD_3, 500MHz) δ 7.8-8.3 (m, 1.8H), 7.4-7.8 (m, 0.8H), 4.73 (bs, 1H), 4.57 (s, 1H), 4.47 (s, 2H), 3.78 (s, 2H), 3.60-3.62 (1.3H), 3.2-3.6 (m, 13H), 3.14 (bs, 2.1H), 2.8 (bs, 2.1H), 2.29 (bs, 1.7H) ppm; MALDI-TOF MS (pos) found 17,300 g/mol.

41c. ^{1}H NMR (CD_3SOCD_3, 500MHz) δ 7.8-8.3 (m, 2.0H), 7.4-7.8 (m, 1.2H), 4.72 (bs, 1H), 4.57 (s, 1H), 4.47 (s, 2H), 3.78 (s, 2H), 3.2-3.7 (m, 15H), 3.14 (bs, 2.9H), 2.76 (bs, 2.4H), 2.25 (bs, 1.9H) ppm; MALDI-TOF MS (pos) found13,400 g/mol.

41d. ^{1}H NMR (CD_3SOCD_3, 500MHz) δ 7.8-8.4 (m, 3.8H), 7.4-7.8 (m, 2.0H), 4.72 (bs, 1H), 4.57 (s, 1H), 4.47 (s, 1H), 3.78 (s, 2H), 3.2-3.7 (m, 21H), 3.13 (m, 7.1H), 2.69 (bs, 3.9H), 2.21 (bs, 4.2H) ppm; MALDI-TOF MS (pos) found 12,400 g/mol.

41e. MALDI-TOF MS (pos) found 11,200 g/mol.

]

42a. ^{1}H NMR (CD_3SOCD_3, 500MHz) δ 7.8-8.3 (m, 1.5H), 7.4-7.6 (m, 0.3H), 6.8 (bs, 0.3H), 4.71 (s, 1H), 4.57 (s, 1H), 4.48 (s, 2H), 3.78 (s, 2H), 3.60-3.62 (m, 1.2H), 3.3-3.6 (4.7H), 3.10 (bs, 1.3H), 2.0-2.4 (m, 0.9H) ppm; MALDI-TOF MS (pos) found 48,000 g/mol.

42b. ^{1}H NMR (CD_3SOCD_3, 500MHz) δ 7.7-8.2 (m, 2.0H), 7.4-7.6 (bs, 0.5H), 6.8 (bs, 0.2H), 4.71 (bs, 1H), 4.57 (s, 1H), 4.48 (s, 2H), 3.78 (s, 2H), 3.60-3.62 (m, 1.2H), 3.3-3.6 (m, 6.2H), 2.95-3.2 (m, 2.0H), 2.55-2.9 (m, 1.7H), 2.0-2.3 (m, 1.7H) ppm; MALDI-TOF MS (pos) found 41,000 g/mol.

42c. ^{1}H NMR (CD_3SOCD_3, 500MHz) δ 7.7-8.3 (m, 3.4H), 7.4-7.65 (1.1H), 4.72 (bs, 1H), 4.57 (s, 1H), 4.48 (s, 2H), 3.78 (s, 2H), 3.60-3.62 (m, 1.4H), 3.3-3.6 (7.6H), 3.15 (bs, 2.5H), 2.6-2.9 (m, 2.7H), 2.1-2.3 (m, 2.4H) ppm; MALDI-TOF MS (pos) found 32,500 g/mol.

42d. ^{1}H NMR (CD_3SOCD_3, 500MHz) δ 8.00 (bs, 1.6H), 7.78 (bs, 1.5H), 7.48 (bs, 2.0H), 4.69 (bs, 1H), 4.57 (s, 1H), 4.48 (s, 2H), 3.78 (s, 2H), 3.3-3.7 (m, 15H), 2.9-3.2 (m, 5.4H), 2.64 (bs, 5.6H), 2.18 (bs, 4.9H) ppm; MALDI-TOF MS (pos) found 26,300 g/mol.

42e. ^{1}H NMR (CD_3SOCD_3, 500MHz) δ 8.00 (bs, 2.1H), 7.85 (m, 1.4H), 7.48 (bs, 2.6H), 4.70 (bs, 1H), 4.57 (s, 1H), 4.48 (s, 2H), 3.78 (s, 2H), 3.3-3.7 (m, 18H), 3.14 (m, 6.7H), 2.55-2.9 (m, 6.4H), 2.05-2.3 (m, 5.6H) ppm; MALDI-TOF MS (pos) found 25,300 g/mol.

42f. ^{1}H NMR (CD_3SOCD_3, 500MHz) δ 7.99 (bs, 3.4H), 7.6-7.9 (m, 3.4H), 7.47 (m, 7.1H), 4.35-4.8 (m, 4H), 3.7-3.85 (m, 1H), 3.3-3.65 (m, 38H), 2.95-3.2 (m, 17H), 2.55-2.85 (m, 15H), 2.20 (bs, 14H) ppm; MALDI-TOF MS (pos) found 22,800 g/mol.

43a. ^{1}H NMR (CD_3SOCD_3, 500MHz) δ 7.7-8.3 (m, 1.9H), 6.8 (bs, 0.2H), 4.72 (bs, 2H), 4.57 (s, 1H), 4.47 (s, 3H), 3.78 (s, 2H), 3.60-3.62 (m, 1.3H), 3.5-3.6 (m, 2.4H), 3.2-3.4 (m, 7.1H), 2.9-3.2 (m, 2.8H), 2.60 (bs, 2.0H), 1.9-2.4 (m, 2.5H) ppm; MALDI-TOF MS (pos) found 69,000 g/mol.

43b. ^{1}H NMR (CD_3SOCD_3, 500MHz) δ 8.00 (m, 1.2H), 7.82 (bs, 0.8H), 7.56 (bs, 0.2H), 4.72 (bs, 1H), 4.57 (s, 1H), 4.47 (s, 4H), 3.78 (s, 3H), 3.60-3.62 (m, 1.6H), 3.15-3.6 (m, 13.4H), 2.9-3.15 (m, 4.2H), 2.61 (bs, 3.3H), 2.39 (bs, 1.3H), 2.16 (bs, 3.3H) ppm; MALDI-TOF MS (pos) found 64,300 g/mol.

43c. ^{1}H NMR (CD_3SOCD_3, 500MHz) δ 8.00 (m, 3.0 H), 7.85 (bs, 1.2H), 7.6 (bs, 0.8H), 4.8 (bs, 2H), 4.57 (s, 1H), 4.47 (s, 2H), 3.78 (s, 3H), 3.60-3.62 (m, 1.6H), 3.15-3.6 (m, 17.8H), 2.9-3.15 (m, 5.5H), 2.61 (bs, 4.2H), 2.16 (bs, 5.7H) ppm; MALDI-TOF MS (pos) found 49,000 g/mol.

43d. ^{1}H NMR (CD_3SOCD_3, 500MHz) δ 7.9-8.3 (m, 2.0H), 7.83 (bs, 1.4H), 7.61 (bs, 1.1H), 4.72 (bs, 1H), 4.57 (s, 1H), 4.47 (s, 3H), 3.78 (s, 2H), 3.2-3.7 (m, 19.9H), 2.9-3.2 (m, 6.3H), 2.55-2.9 (m, 6.1H), 2.39 (bs, 2.1H), 2.17 (bs, 5.4H) ppm; MALDI-TOF MS (pos) found 46,700 g/mol.

43e. ^{1}H NMR (CD_3SOCD_3, 500MHz) δ 7.8-8.3 (m, 3.0H), 7.4-7.8 (m, 1.4H), 4.74 (bs, 1H), 4.57 (s, 1H), 4.47 (s, 2H), 3.78 (s, 2H), 3.2-3.7 (m, 21.4H), 3.10 (5.7H), 2.66 (bs, 5.2H), 2.20 (bs, 4.2H) ppm; MALDI-TOF MS (pos) found 45,300 g/mol.

43f. ^{1}H NMR (CD_3SOCD_3, 500MHz) δ 7.3-8.6 (m, 5.8H), 4.74 (bs, 1H), 4.57 (s, 1H), 4.3-4.55 (m, 4H), (3.78 (s, 2H), 2.9-3.7 (m, 30.6H), 2.64 (bs, 5.7H), 2.18 (bs, 5.2H) ppm; MALDI-TOF MS (pos) found 44,000 g/mol.

44a. ^{1}H NMR (CD_3SOCD_3, 500MHz) δ 7.8-8.3 (m, 1.8H), 7.4-7.8 (m, 0.4H), 6.8 (bs, 0.3H), 4.74 (bs, 1H), 4.57 (s, 1H), 4.47 (s, 2H), 3.78 (s, 1H), 3.35-3.7 (m, 4.4H), 3.09 (1.9H), 2.69 (bs, 1.1H), 2.21 (bs, 1.7H) ppm; MALDI-TOF MS (pos) found 135,000 g/mol.

44b. ^{1}H NMR (CD_3SOCD_3, 500MHz) δ 7.9-8.3 (m, 1.4H), 7.85 (m, 0.6H), 7.53 (m, 0.7H), 6.8 (bs, 0.2H), 4.74 (bs, 1H), 4.57 (s, 1H), 4.47 (s, 2H), 3.78 (s, 1H), 3.45-3.7 (m, 3.0H), 3.0-3.2 (m, 1.6H), 2.64 (bs, 1.6H), 2.22 (bs, 1.5H) ppm; MALDI-TOF MS (pos) found 107,000 g/mol.

44c. ^{1}H NMR (CD_3SOCD_3, 500MHz) δ 8.00 (m, 1.2H), 7.87 (m, 0.7H), 7.53 (m, 1.0H), 6.8 (bs, 0.2H), 4.74 (bs, 1H), 4.57 (s, 1H), 4.47 (s, 2H), 3.78 (s, 1H), 3.4-3.7 (m, 8.9H), 3.0-3.2 (m, 2.1H), 2.68 (bs, 2.0H), 2.22 (bs, 1.9H) ppm; MALDI-TOF MS (pos) found 98,000 g/mol.

44d. ^{1}H NMR (CD_3SOCD_3, 500MHz) δ 7.9-8.2 (m, 1.7H), 7.7-79 (m, 1.7H), 7.51 (bs, 3.5H), 4.74 (bs, 1H), 4.57 (s, 2H), 4.47 (s, 2H), 3.78 (s, 1H), 3.4-3.7 (m, 28.4H), 3.14 (bs, 8.3H), 2.67 (bs, 7.7H), 2.21 (bs, 5.6H) ppm; MALDI-TOF MS (pos) found 85,000 g/mol.

CHAPTER 3

N-ACETYL GALACTOSAMINE FUNCTIONALIZED DENDRITIC POLYMERS

Introduction

Synthetic multivalent ligands bearing mannose or glucose that bind with Concanavalin A are great tools to use for understanding fundamentals of carbohydrate protein interactions. However, simple models of physiological events in humans may help in understanding the specific roles of carbohydrates-protein interactions in disease states, and may aid in the development of potential therapeutics. In this section the synthesis of multivalent ligands bearing N-acetyl galactosamine is described. These compounds may be used to study Galectin-3, in order to gain insight into the mechanism of cancer metastasis on a molecular level.[21, 22]

Lipid rafts are microdomains on the cell surface enriched with cholesterol, and glycolipids.[109] Carbohydrate components of lipid rafts participate in cell adhesion processes, like cell surface glycans, including adhesion of pathogens and bacteria.[110] Lipid raft microdomains are also involved in signal transduction and protein trafficking.[111] These domains have been reported with diameters from the angstrom scale to the micrometer scale. Dendrimers alone cannot span this size differential. Instead, dendritic polymers could be made, which cluster many glycodendrimers together. The use of dendrons in polymer chemistry has precedence in recent literature as dendronized linear polymers (Figure 3.1) are structurally like “molecular cylinders”,[112, 113] also

dendrons and dendrimers have been integrated in various other large supramolecular structures such as micelles and dendrimer-block polymer aggregates.[114]

The goal of the work in this section is the synthesis of heterogeneous N-acetyl galactosamine and azide functionalized PAMAM dendrimers, followed by tethering multiple glycodendrimers together using the copper (I) catalyzed Huisgen dipolar cycloaddition.[81, 82]

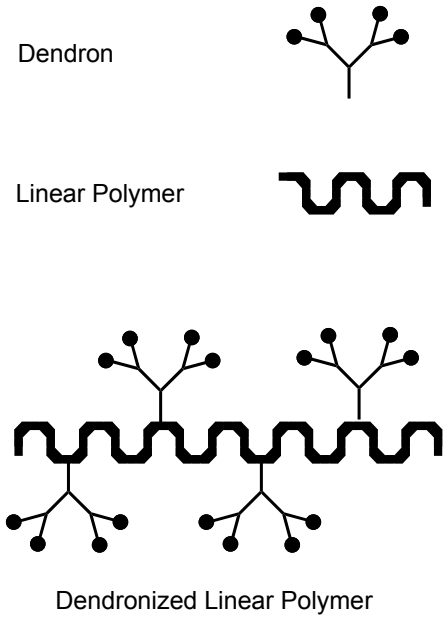

Figure 3.1 Dendronized linear polymers.

N-Acetyl Galactosamine

The synthesis of an N-acetyl galactosamine glycodendrimer requires first an N-acetyl galactosamine isothiocyanate. Fortunately the glycosylation of peracetylated N-acetyl galactosamine doesn't require two separate synthetic steps to deprotect and activate the anomeric position as in the case of mannose (Chapter 2).[115]

The first step in the synthesis is the protection of the alcohol groups on the sugar (Scheme 3.1). Acetylation of either galactosamine hydrochloride or N-acetyl galactosamine (as a mixture of anomers) was first performed with acetic anhydride to form **45**.[116] The addition of alcohols to protected N-acetyl galactosamine with a number of different lewis catalysts have been reported. Of the reported methods, one straightforward approach used iron (III) chloride to activate the sugar.[117] Glycosylation of **29** did not occur in the presence of iron (III) chloride. Comparison of the ^{1}H NMR of **45** with data from the literature confirmed that **45** was predominantly the α anomer. This anomeric geometry isn't suited for neighboring group assistance in the glycosylation step. Preparation of the β anomer **46** was done using a modification of a method reported by Stacey, using zinc (II) chloride (Scheme 3.2).[118] Although the reaction is lower yielding than the formation of **45,** the anomeric geometry was conducive to simple glycosylation. When **46** was mixed with isopropanol in anhydrous conditions the desired **47** was obtained as previously reported, presumably through the formation of the oxazolium intermediate indicated in Scheme 3.2, and purified by recrystallization. If no alcohol is present, in the reaction the corresponding oxazole could be isolated if desired.[117, 119]

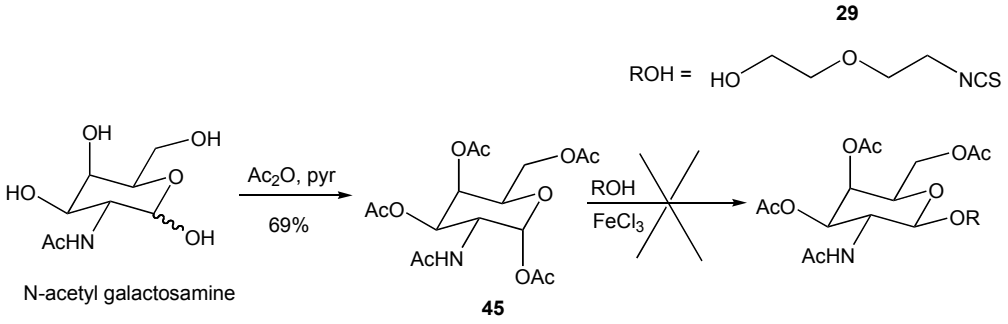

Scheme 3.1 Synthesis of **45** and subsequent failed glycosylation of **29**.

As expected, the reaction between **46** activated with iron (III) chloride and **29** went forward smoothly forming isothiocyanate **48** (Scheme 3.3). The product wasn't readily recrystallized like some reported simple glycosylation products (including **47**) and purification by chromatography was required.

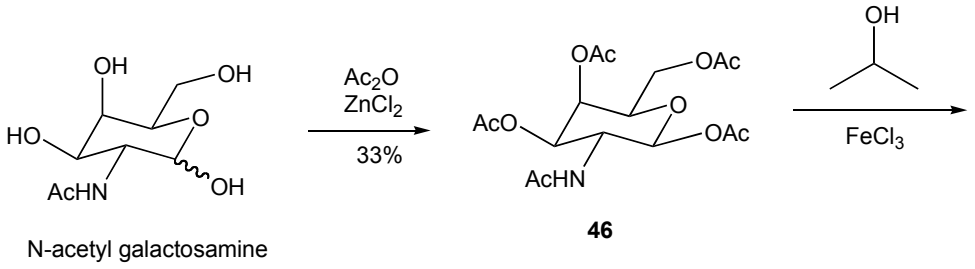

Scheme 3.2 Synthesis of **47** from β-N-acetyl galactosamine **46**.

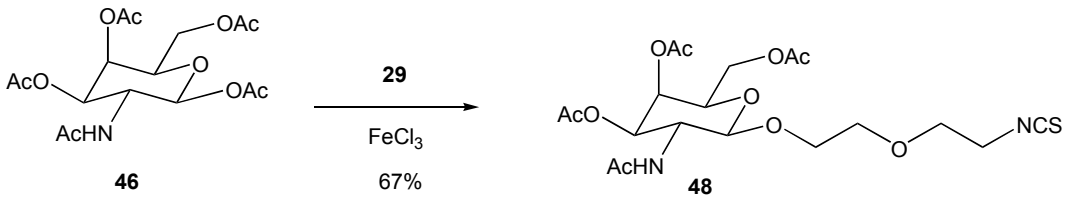

Scheme 3.3 Synthesis of N-acetyl galactosamine isothiocyanate **48**.

N-Acetyl Galactosamine and Phenyl Azide Heterogeneously Functionalized PAMAM Dendrimers

To tether the dendrimers together using the copper (I) catalyzed Huisgen dipolar cycloaddition required azide functionality on the dendrimer surface. The first planned route was the formation of azidoethyl isothiocyanate (Scheme 3.4). Azidoethyl amine **49** was made according to a previously reported procedure.[120] The product was difficult to completely purify, and the synthesis possibly created the hazardous byproduct hydrazoic acid. A simple solution was to replace the azidoethyl isothiocyanate with the commercially available 4-azidophenyl isothiocyanate. While the presence of a large number of aromatic groups on the PAMAM surface leads to undesirable solubility properties, it was hoped that a small number of aromatic rings could be added without deleterious effects.

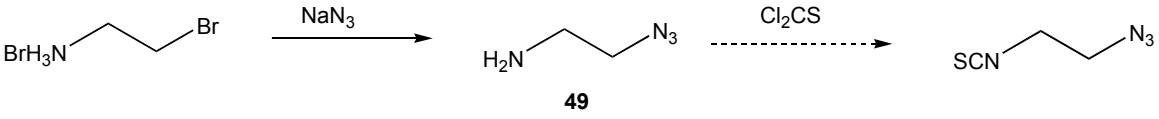

Scheme 3.4 Synthesis of **49**, and the proposed synthesis of azidoethyl isothiocyanate.

The synthesis of partially functionalized (G3) PAMAM dendrimers with 4-azidophenyl isothiocyanate (**50**) is shown in Scheme 3.5. The addition of four equivalents of the azide was observed using ^{1}H NMR in d_6-DMSO by a shift in the signal protons on the aromatic ring (Figure 3.2). Integration of the aromatic signals compared with the dendrimer amide signal indicates approximately five phenyl azides per

dendrimer, although the error on this measurement is quite high due to the breadth of the amide signal and relatively small size of the phenyl azide signals. Next the addition of an excess of **48** saturated the remaining dendrimer amines, and the macromolecule was purified by dialysis (MWCO 3500 Da) to give the heterogeneously functionalized dendrimer **51**.

To tether the dendrimers a linker was needed with two alkyne groups. Tetraethylene glycol underwent a bis-propargylation reaction at -50 ºC using sodium hydride in DMF with propargyl bromide (Scheme 3.6) to form **52** as an orange oil.

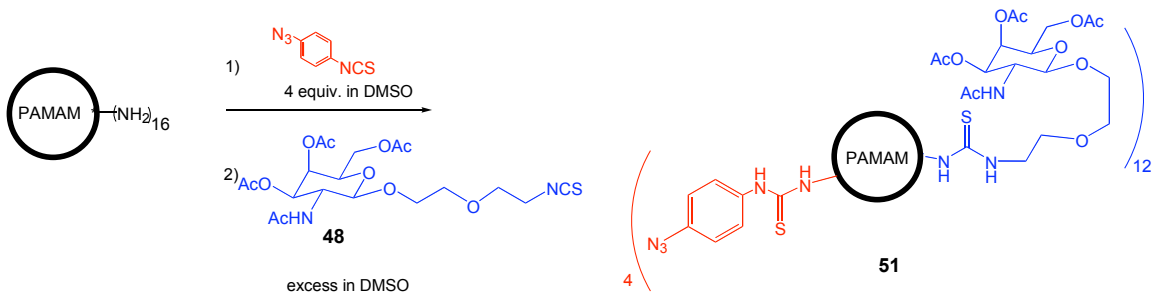

Scheme 3.5 The synthesis of azidophenyl and N-acetyl galactosamine heterogeneously functionalized PAMAM dendrimer **51**.

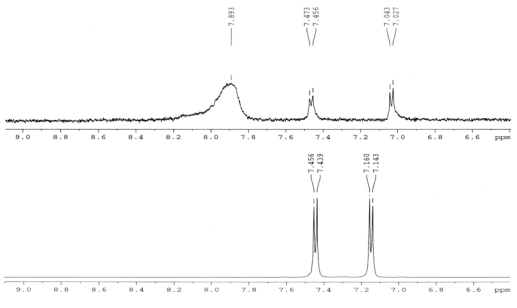

Figure 3.2 ^{1}H NMR spectra of partially functionalized azidophenyl PAMAM dendrimer **50** (top) and the starting compound 4-azidophenyl isothiocyanate (bottom) in d_6-DMSO.

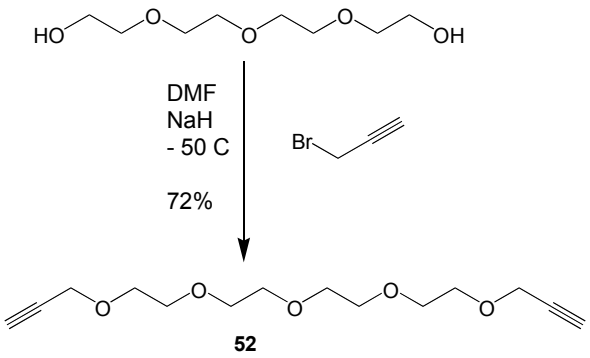

52

Scheme 3.6 Synthesis of bis-alkyne linker **52**.

Dendritic Polymers

The copolymerization of a heterogeneously functionalized N-acetyl galactosamine and phenyl azide dendrimer (**51**) with linker **52** was done using the copper (I) catalyzed dipolar cycloaddition conditions as before (Chapter 2). At low loading of azide on the dendrimer (two equivalents) and a typical concentration for the reaction (1 mM in dendrimer), no polymerization occurred. We speculate that after the addition of a single linker molecule the next cycloaddition was intramolecular. Little difference was observed in the MALDI-TOF MS calculated M_W or the retention times in gel permeation chromatography (GPC).

Increasing the number of azides per dendrimer, and/or increasing the concentration of the cycloaddition reactants was required for the apparent polymerization (Scheme 3.7).

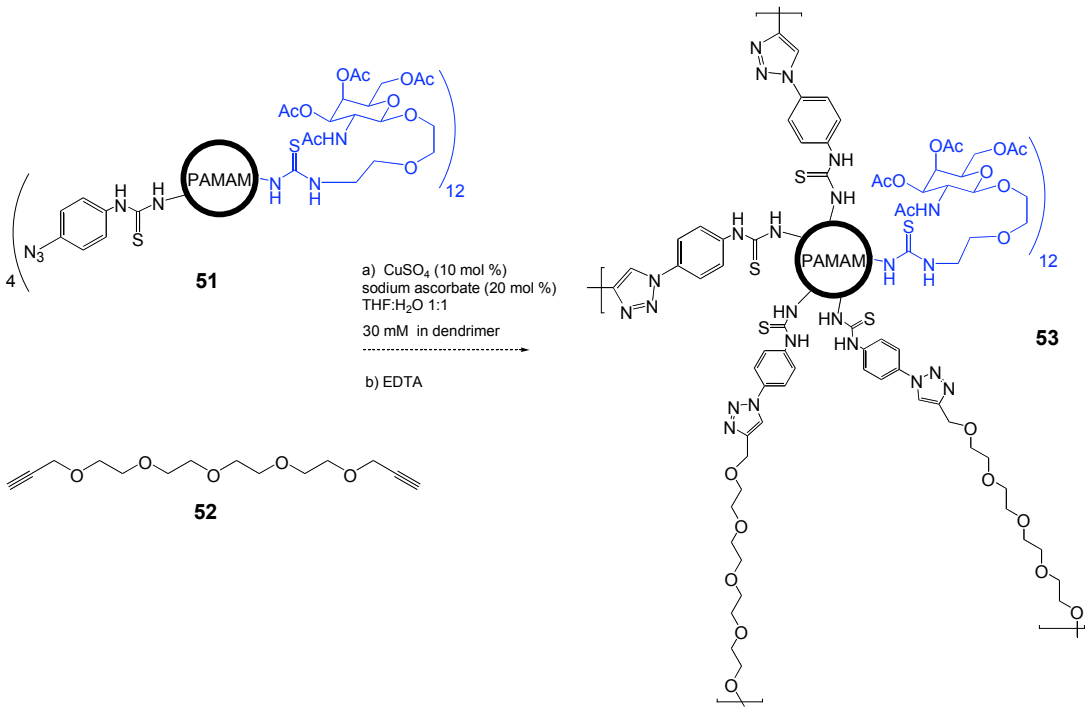

Scheme 3.7 Synthesis N-acetyl galactosamine functionalized dendritic polymer **53**.

There was some evidence the polymerization reaction succeeded. Aside from visible differences between the flakey solid product **53** and the sticky gel-like starting material **51**, there was a difference in the solubility properties of **51** and **53**. While **51** was soluble in 95:5 THF and water, **53** wasn't soluble until a 75:25 mixture of THF and water was used as a solvent. Even in the preparation of the sample for NMR analysis, **51** was readily soluble in d_6-DMSO, while **53** required an hour of stirring in d_6-DMSO for some solubility. The ^{1}H NMR spectra of **51** and **53** are shown in Figure 3.3. Although the resolution of the ^{1}H NMR spectrum prohibits significant interpretation, the severe line broadening is consistent with the formation of a large macromolecule. The ^{13}C NMR spectra provide little information on the polymerization reaction, other than to indicate possible triazole formation, which could occur intramolecularly.

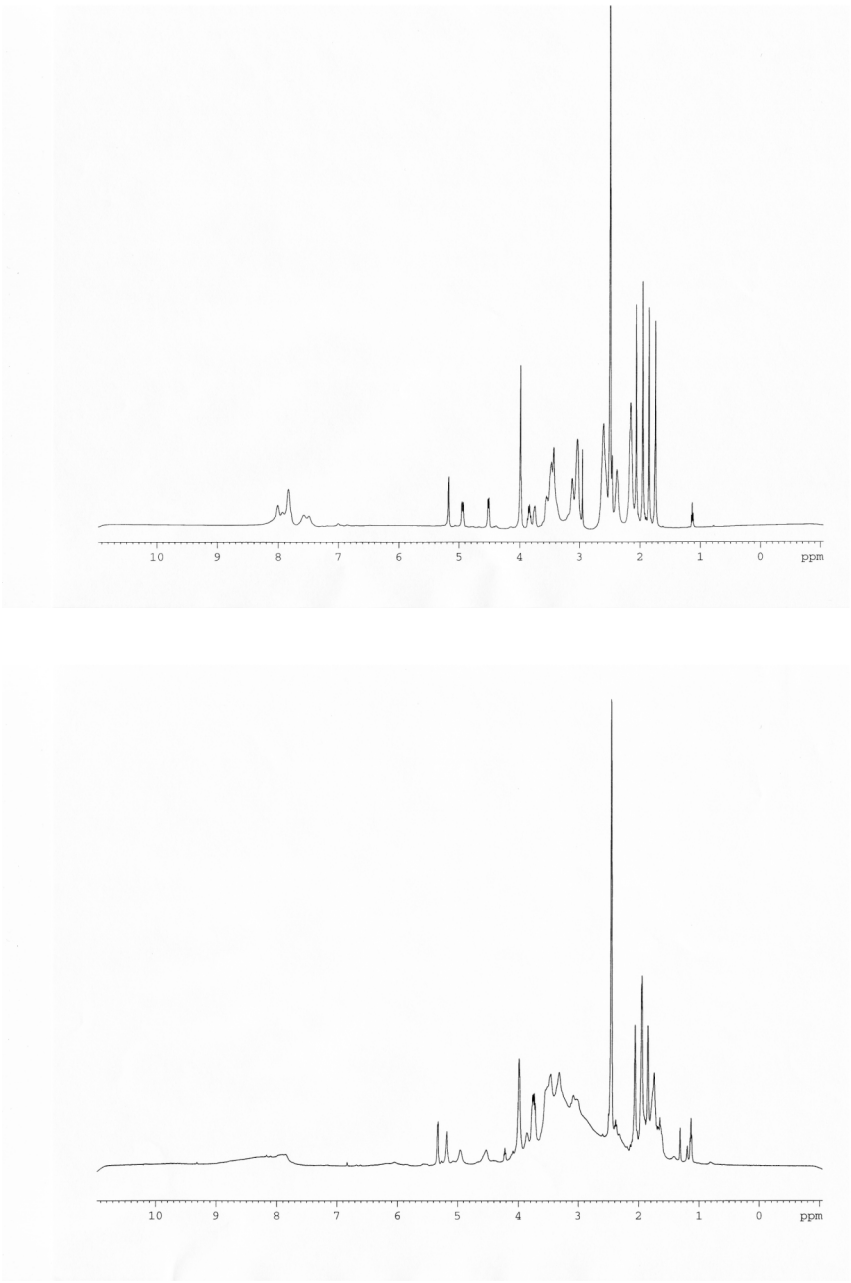

Figure 3.3 The ^{1}H NMR spectra of **51** (top) and **53** (bottom) in d_6-DMSO.

Next MALDI-TOF MS was attempted to characterize **53**. Under the standard conditions used in our labs **51** could be characterized using MALDI-TOF MS (M_W =

13500 g/mol), giving a weight average molecular weight consistent with the addition of 4 azidophenyl groups and 12 N-acetyl galactosamine groups. Under the same conditions **53** gave no signal for product or starting macromonomers. This suggests either the monomer was degraded in the reaction, or the reaction product had a large molecular mass.

Dynamic light scattering (DLS) was also used a means to possibly characterize **53**. As a control compound of known structure, Con A, was measured by DLS giving the histogram shown in Figure 3.4. The average diameter of Con A was 6.2 nm over a 5-minute experiment time, near the expected diameter of approximately 6.5 nm. To obtain quality DLS data multiple experiments over longer durations are common, so the small error from above was within reason. Unfortunately **51** was below the size threshold for particle analysis by DLS. After multiple tests with **53** no appreciable signal was observed, perhaps due to the absence of polymer, or the presence of a large distribution of particle sizes.

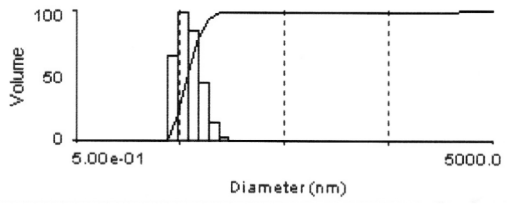

d	G(d)
2.66	0
3.34	0
4.18	67
5.25	100
6.58	86
8.25	46
10.34	15
12.96	3
16.25	0
20.38	0
25.55	0

Figure 3.4 DLS histogram, and corresponding data table, of Con A at 0.1 mg/mL.

Summary

Classical carbohydrate chemistry provided a route to new derivatives of N-acetyl galactosamine that were used for dendrimer surface functionalization. A heterogeneous dendrimer functionalization with N-acetyl galactosamine and azidophenyl groups provided one monomer, and a bis-alkyne tether provided another monomer for a copolymerization reaction to make lipid raft microdomain mimics. While no direct characterization yielded information on the polymer, the indirect evidence for polymer formation indicates the click chemistry route to lipid raft mimics was successful.

Experimental Procedures

General Methods. General reagents were purchased from Fisher-Acros and Sigma-Aldrich. PAMAM dendrimers were purchased as aqueous solutions from Dendritech and lyophilized prior to use. Dry DMF was prepared by stirring 24 hours with 4Å molecular sieves followed by filtration through a Millipore 0.45 μm nylon filter. *trans*-3-Indoleacrylic acid was crystallized from approximately 1:1 methanol and water. All other reagents were used as supplied.

NMR. ^{1}H NMR and ^{13}C NMR were acquired at 500 MHz and 125 MHz, respectively, on a Bruker DRX500 instrument in $CDCl_3$ or CD_3SOCD_3.

MALDI-TOF MS. Matrix assisted laser desorption ionization (MALDI) mass spectra were acquired using a Bruker Biflex-III time-of-flight mass spectrometer. Spectra were

obtained using a trans-3-indoleacrylic acid (IAA) matrix with a matrix-analyte ratio of 36,000: 1 to 1000:1. A 1 μL aliquot of the analyte (0.5-20 mg/mL,) in DMF, DMA, or DMSO, was combined with 10 μL of IAA in DMF (20 mg/mL). A 1 μL aliquot was deposited on the laser target, drying in 1-4 hours. Bovine serum albumin (MW 66,431 g/mol) and laser promoted oligomers up to the tetramer and the M/Z peak where Z = 2, trypsinogen (MW 23,982 g/mol), cytochrome C (12,361 g/mol), and bradykinin (1061 g/mol) were used as external standards. Positive ion mass spectra were acquired in linear mode, and the ions were generated by using a nitrogen laser (337 nm) pulsed at 5 Hz with a pulse width of 3 nanoseconds. Ions were accelerated at 19-20,000 volts and amplified using a discrete dynode multiplier. Spectra (10 to 2000) were summed into a LeCroy LSA1000 high-speed signal digitizer. All data processing was performed using Bruker XMass/XTOF V 5.0.2. Molecular mass data and polydispersities of the broad peaks were calculated by using the Polymer Module included in the software package. The peaks were analyzed using the *continuous* mode. Delta values were set at minimum levels.

Gel Permeation Chromatography. Mixtures of tetrahydrofuran and water (50:50 to 95:5) were filtered through Millipore nylon filters (0.45 μm). The GPC system consisted of a Waters 515 HPLC pump, Waters Styragel HR4 and HR4E columns, and a Waters 996 photodiode array detector that was ran with Waters Empower 2 software. Runs were performed at room temperature with 0.3 mL/min to 0.7 mL/min flow rates. Sample concentrations of 0.10 mg/mL to 10 mg/mL were analyzed.

Dynamic Light Scattering (DLS). A Brookhaven Instrument Corporation 90Plus dynamic light scattering instrument was used to collect data, and analysis was performed using the dynamic light scattering software from Brookhaven Instruments. Light from a 661 nm diode laser at 15 mW of power illuminated the sample and diffraction was detected at 90 degrees using a photomultiplier detector. A correlation function was determined by a BI-9000At autocorrelator and the correlation function was fit using a non-linear least squares fit to give a particle size histogram. Quartz crystal cuvettes were used to analyze samples at a concentration of 0.1 mg/mL to 1 mg/mL in 1:1 THF and water.

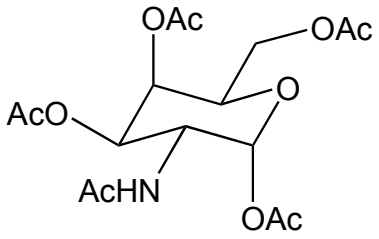

2-acetamido-2-deoxy-1,3,4,6-tetra-O-acetyl-α-D-galactopyranose 45.

Compound **45** was prepared according to previously published methods.[116]

N-acetyl galactosamine (1.13 g, 5.1 mmol) was combined with acetic anhydride (11 mL) in pyridine (15 mL). After stirring two hours the sugar had dissolved, and stirring continued 24 hours. Water (100 mL) was added, though no crystallization was induced. The solvent was removed *in vacuo* to give crude **45** as a fluffy white solid, which was used without further purification (1.36 g, 69% yield). The product was 92 mol % **45** and 8 mol % **46** by ^{1}H NMR. ^{1}H NMR ($CDCl_3$, 500MHz) δ 6.20 (d, 1H, J = 3.4 Hz), 5.6 (m, 0.09H, from **46**), 5.36-5.40 (m, 2H), 5.20 (dd, 1H, J = 11.5 , 3.0 Hz), 5.05 (m, 0.10H,

from **46**), 4.67-4.75 (m, 1H), 4.18-4.25 (m, 1H), 4.01-4.13 (m, 2H), 2.16 (s, 6H), 2.01 (s, 6H), 1.93 (s, 3H) ppm.

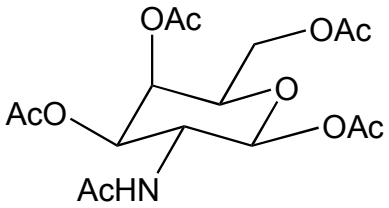

2-acetamido-2-deoxy-1,3,4,6-tetra-O-acetyl-β-D-galactopyranose 46.

Compound **46** was prepared using a modification of previously published methods. [118] Galactosamine hydrochloride (2.15 g, 9.97 mmol) was combined with acetic anhydride (30 mL). Zinc (II) chloride (1.36 g, 9.98 mmol) was added to the stirring mixture. After stirring overnight the material had all dissolved. The solution was added to ice (approx. 30 mL) and neutralized with saturated sodium bicarbonate, then made basic (pH = 9-10) with sodium hydroxide and the product was extracted with chloroform (6 x 40 mL), washed with water (1 x 50 mL) and dried over $MgSO_4$. The solvent was removed *in vacuo* until precipitation occurred, then ethanol was added (20 mL) and the product crystallized overnight to give 1.04 g **46**. A second recrystallization of the mother liquor yielded 0.25 g **46** for a yield of 33 %. M.p. 235 °C (lit. 235 °C); ^{1}H NMR (CD_3SOCD_3, 500 MHz) δ 7.87 (d, 1H, 9.2 Hz), 5.60 (d, 1H, 8.8 Hz), 5.22 (d, 1H, 2.9 Hz), 5.02 (dd, 1H, 11.3 Hz, 3.3 Hz), 4.19 (t, 1H, 6.0 Hz), 4.9-4.1 (m, 3H), 2.08 (s, 3H), 2.00 (s, 3H), 1.95 (s, 3H), 1.87 (s, 3H), 1.74 (s, 3H) ppm; ^{13}C NMR (CD_3SOCD_3, 125 MHz) δ 170.0, 169.4, 92.9, 71.2, 70.5, 66.9, 61.8, 48.6, 23.1, 21.0, 20.9 (missing/overlapped 3 CH_3CO, 2 CH_3CO) ppm.

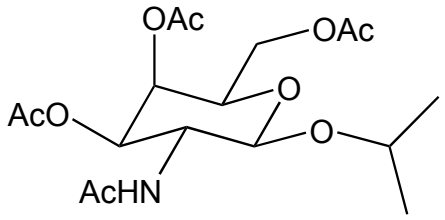

1-*O*-isopropyl-2-acetamido-2-deoxy-3,4,6-tri-O-acetyl-β-D-galactopyranose 47.

Compound **47** was prepared according to previously published methods.[117]

Iron (III) chloride (113 mg, 0.70 mmol) was added to DCM (2 mL) and stirred with anhydrous $CaSO_4$ (400 mg) for 10 minutes. Sugar **46** (97.8 mg, 0.25 mmol) was then added followed by isopropanol (115 mg, 1.9 mmol) and the mixture stirred overnight. Next cold saturated sodium bicarbonate was added (5 mL) along with cold chloroform (5 mL). These stirred together overnight then the layers were separated. The aqueous layers were further extracted with chloroform (3 x 10 mL) until clear. The combined organic layers were dried over $MgSO_4$ and solvent removed *in vacuo* to yield a clear oil. The product was recrystallized overnight from ethanol to give **47** (42 mg, 43% yield) as a white solid. M.p. 173-175 °C (lit. 174-175); ^{1}H NMR (CD_3SOCD_3, 500 MHz) δ 7.76 (d, 1H, 9.2 Hz), 5.17 (d, 1H, 3.0 Hz), 4.96 (dd, 11.2 Hz, 3.2 Hz), 4.53 (d, 1H, 8.4 Hz), 3.96-4.03 (m, 3H), 3.70-3.80 (m, 2H), 2.07 (s, 3H), 1.95 (s, 3H), 1.85 (s, 3H), 1.72 (s, 3H), 1.07 (d, 3H, 6.2 Hz), 1.01 (d, 3H, 5.9 Hz) ppm; ^{13}C NMR (CD_3SOCD_3, 125 MHz) δ 170.5, 170.3, 170.1, 169.6, 100.2, 72.0, 70.9, 70.2, 67.2, 61.9, 50.2, 23.7, 23.2, 22.3, 20.9, 20.9 ppm.

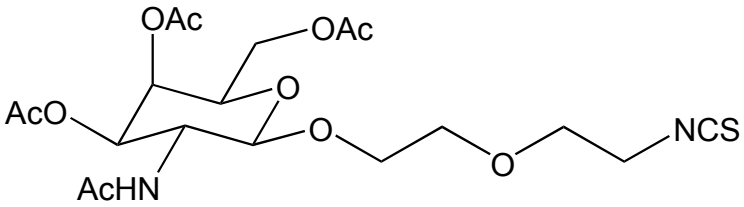

1-*O*-(5-isothiocyanato-3-oxapentyl)-2-acetamido-2-deoxy-3,4,6-tri-O-acetyl-β-D-galactopyranose 48.

Iron (III) chloride (634 mg, 3.91 mmol) was added to DCM (15 mL) and stirred with anhydrous $CaSO_4$ (1.4 g) for 10 minutes. Sugar **46** (941 mg, 2.42 mmol) was then added followed by **29** (831 mg, 5.65 mmol), and the mixture stirred overnight. Cold saturated sodium bicarbonate was added (25 mL) along with cold chloroform (25 mL). These stirred together overnight at room temperature, then the layers were separated. The aqueous layers were further extracted with chloroform (3 x 25 mL) until clear. The combined organic layers were washed with water (2 x 25 mL) then dried over $MgSO_4$ and solvent was removed *in vacuo* to yield a yellow oil. The product was purified on silica gel (100% ethyl acetate to 5% methanol : 95% ethyl acetate) giving 765 mg (67% yield) **48** as a foamy white solid. ^{1}H NMR (CD_3SOCD_3, 500 MHz) δ 7.79 (d, 1H, 9.2 Hz), 5.18 (d, 1H, 3.1 Hz), 4.94 (dd, 1H, 11.2 Hz, 3.2 Hz), 3.99 (d, 1H, 10.0 Hz), 3.94-4.03 (m, 4H), 3.70-3.81 (m, 3H), 3.49-3.63 (m, 5H), 2.07 (s, 3H), 1.97 (s, 3H), 1.89 (s, 3H), 1.75 (s, 3H) ppm; ^{13}C NMR (CD_3SOCD_3, 125 MHz) δ 170.4, 170.4, 170.1, 169.7, 129.3, 101.3, 70.9, 70.4, 69.7, 68.9, 68.7, 67.1, 61.9, 49.7, 45.5, 23.2, 20.9, 20.9, 20.9 ppm; HRMS (micro-TOF) 477.1542 (M+H cacld 477.1537 for $C_{19}H_{29}O_{10}N_2S$).

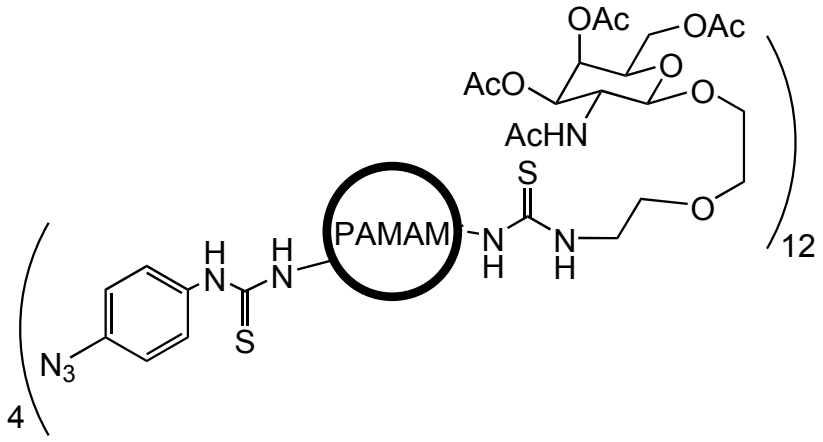

Azidophenyl and N-acetyl galactosamine heterogeneously functionalized G(3) PAMAM dendrimer 51.

4-Azidophenyl isothiocyanate (4.7 mg, 27 μmol) in 470 μL d_6-DMSO was added to G(3) PAMAM dendrimer (46.3 mg, 6.4 μmol) in 750 μL d_6-DMSO and was stirred for one day. ^{1}H NMR (CD_3SOCD_3, 500 MHz) δ 7.89 (bs, 6H), 7.46 (d, 1H, J = 8.8 Hz), 7.04 (d, 8.3 Hz), 3.21 (bs, 25H), 3.04 (m, 24H), 2.60 (s, 20H), 2.52 (s, 9H), 2.33 (s, 9H), 2.16 (s, 20H) ppm.

The solution was then mixed with sugar **48** (68.6 mg, 140 μmol) and was stirred for 2 days and was dialyzed (MWCO 3500 Da) against DMSO, followed by removal of most of the solvent *in vacuo* giving 109 mg of **51** as a white/orange solid (125% yield due to excess solvent). ^{1}H NMR (CD_3SOCD_3, 500 MHz) δ 8.0 (bs, 2H), 7.93 (bs, 1H), 7.83 (bs, 3H), 7.4-7.8 (m, 1.5H), 5.17 (s, 1H), 4.94 (d, 1H, J = 11.1 Hz), 4.51 (d, 1H, J = 8.1 Hz), 3.99 (s, 3H), 3.74 (m, 1H), 3.3-3.7 (m, 11H), 3.12 (bs, 4H), 3.04 (bs, 6H), 2.60 (bs, 9H), 2.38 (bs, 4H), 2.16 (bs, 8H), 2.07 (s, 4H), 1.96 (s, 4H), 1.90 (s, 4H), 1.75 (s, 4H) ppm; ^{13}C NMR (CD_3SOCD_3, 125 MHz) δ 172.2, 171.7, 170.4, 170.3, 170.0, 169.9, 125.3,

101.4, 70.9, 70.4, 69.7, 69.3, 68.7, 67.5, 67.2, 61.9, 52.6, 50.0, 49.8, 37.4, 33.7, 30.8, 25.6, 23.2, 20.9, 20.8 ppm; MALDI-TOF MS (pos) found 13,500 g/mol.

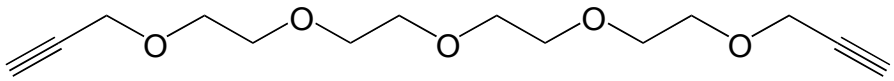

1,11-propargyloxy-3,6,9-trioxaundecane 52.

A suspension of sodium hydride (182 mg, 7.58 mmol) in 5 mL dry DMF was cooled to 50 ºC and a solution of tetraethylene glycol (377 mg, 1.94 mmol) in 5 mL dry DMF was added to the stirring suspension. After 30 minutes, propargyl bromide (966 mg, 8.12 mmol) was added to mixture and stirring continued at -50 ºC for four hours, followed by quenching with water (10 mL), and then the solution was slowly warmed to room temperature. The product was extracted with ethyl acetate (3 x 20 mL), was washed with brine (3 x 5 mL), and with water (2 x 10 mL) and was dried over $MgSO_4$. The product was purified on silica gel (ethyl acetate) to give 378 mg orange oil **52** (72 % yield). ^{1}H NMR ($CDCl_3$, 500 MHz) δ 4.12 (d, 2H, J = 1.8 Hz), 3.58-3.61 (m, 8H), 3.38 (t, 1H, J = 1.8 Hz) ppm; ^{13}C NMR ($CDCl_3$, 125 MHz) δ 79.6, 74.5, 70.5, 70.5, 70.3, 69.0, 58.3 ppm;HRMS (micro-TOF) 271.1540 (M+H cacld 271.1510 for $C_{14}H_{23}O_5$).

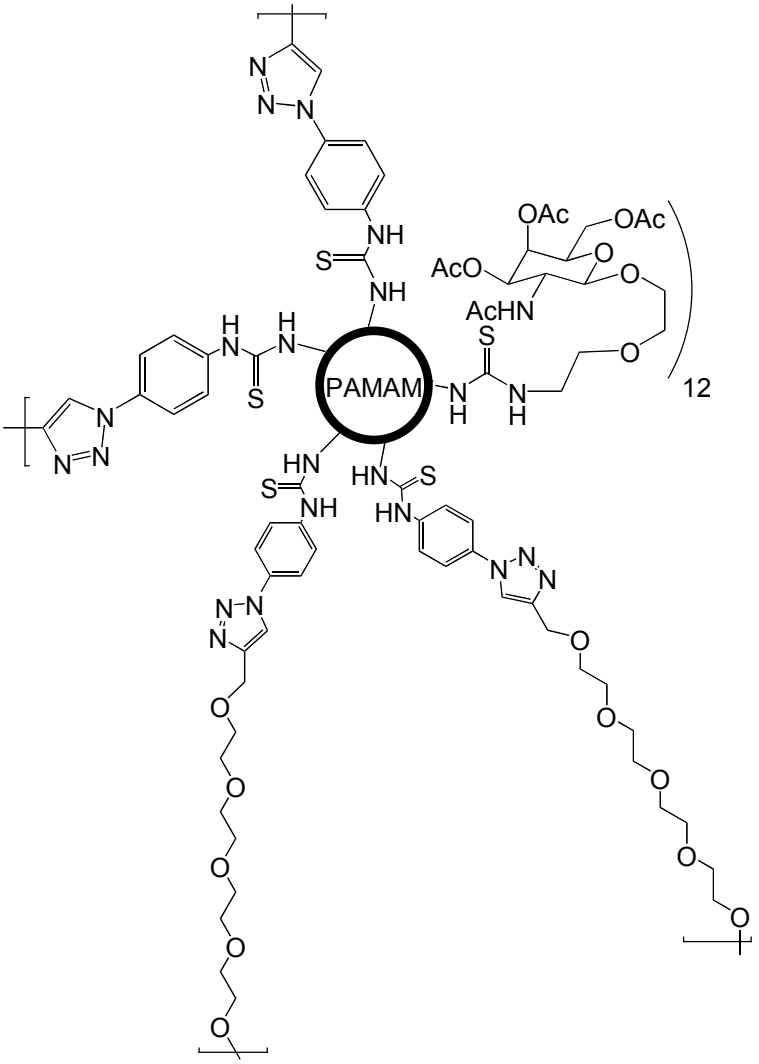

N-acetyl galactosamine functionalized PAMAM based dendritic polymer 53.

The bis-propargyl ether **52** (1.42 mg, 52.4 μmol) in 14.2 μL 1:1 THF:water was mixed with sodium ascorbate (0.42 mg, 2.1 μmol) in 4.2 μL water and copper (II) sulfate (0.26 mg, 1.0 μmol) in 2.6 μL of water, making a bright yellow colloid. The heterogeneously functionalized N-acetyl galactosamine and azidophenyl PAMAM dendrimer **51** (34.9 mg, 2.62 μmol) in 60 μL 1:1 THF:water was then added to the colloid, and the thick slurry stirred vigorously for 2 days, followed by the addition of EDTA (0.8 mg, 2.1 μmol) in 80

μL water which stirred for 30 minutes. The product was purified by dialysis (MWCO 3500 Da) against 1:1 THF:water, then the solvent removed *in vacuo* leaving 21.7 mg white solid **53**. ^{1}H NMR (CD_3SOCD_3, 500 MHz) δ 7.5-9.1 (m, 8H), 5.34 (m, 1H), 5.18 (s, 1H), 4.96 (bs, 1H), 4.53 (bs, 1H), 2.55-4.3 (m, 57H), 2.2-2.45 (m, 5H), 1.5-2.2 (m, 24 H) ppm; ^{13}C NMR (CD_3SOCD_3, 125 MHz) δ 171.2, 170.4, 170.1, 107.4, 101.5, 70.9, 70.5, 70.4, 70.2, 69.6, 69.3, 68.7, 67.1, 67.1, 61.9, 52.4, 49.8, 32.1, 30.9, 29.3, 24.0, 23.3, 21.2, 21.0, 20.9 ppm.

CHAPTER 4

DIMANNOSE FUNCTIONALIZED PAMAM DENDRIMERS

Introduction

The envelope glycoprotein GP120 is heavily glycosylated.[121] The termini of the glycans are predominantly composed of manα1-2man epitopes. This particular disaccharide is responsible for the adhesion of the virus to the cell, and to Cyanovirin N, an HIV inactivating protein.[20] To mimic the multiantennary display of the manα1-2man portions of the GP120 surface, we synthesized manα1-2man functionalized PAMAM dendrimers.[122] These glycodendrimers were used for binding studies with Cyanovirin-N. Used as synthetic antigens, dimannose functionalized dendrimers may also be useful for producing general antibodies for GP120.

Manα1-2Man Functionalized PAMAM Dendrimers[122]

The preparation of the disaccharide began with the synthesis of the mannose trichloroacetimidate **8** as previously described[94] (Chapter 2) and the synthesis of the tetra-acetylated mannose derivative with a deprotected hydroxyl group at the number 2 carbon **54** as described in literature reports (Scheme 4.1).[123] The two halves of the disaccharide were combined using trimethylsilyl trifluoromethane sulfonate,[124] although it was later discovered in our labs that boron trifluoride etherate is a better Lewis acid in this coupling reaction.[122] The octa-acetyl dimannose **55** was selectively deprotected as the

remaining anomeric acetyl group was cleaved using hydrazine acetate to **56**.[124] The anomeric group was activated as a trichloroacetimidate **57** then trimethylsilyl trifluoromethane sulfonate mediated addition of **29** yielded the desired manα1-2man isothiocyanate **58**.

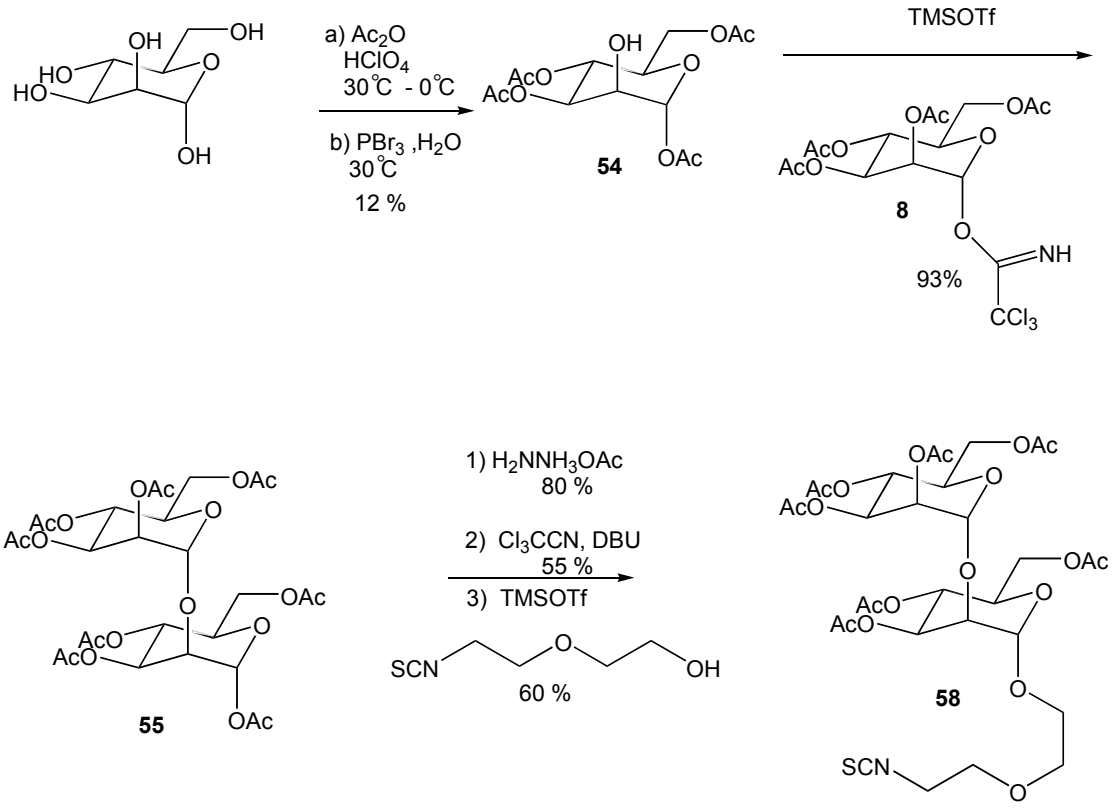

Scheme 4.1 Synthesis of a manα1-2man isothiocyanate **58.**

The dimannose isothiocyanate was added to G(3) and G(4) PAMAM dendrimers in order to saturate the surface with the disaccharide, by the formation of a thiourea bond, forming dendrimers **59** and **60** (Scheme 4.2). After purification of the glycodendrimers by dialysis against DMSO, the acetyl protecting groups were cleaved using Zemplén

conditions, and further dialysis against water provided the deacetylated dendrimers **61** and **62.** As with the glycodendrimers discussed in Chapter 2, care was taken to avoid removing all of the solvent after dendrimer functionalization, resulting in inflated yields after dendrimer functionalization (85%-120%), yet for both steps combined the yields were 35%-50%, due to loss of dendrimer from dialysis after each reaction.

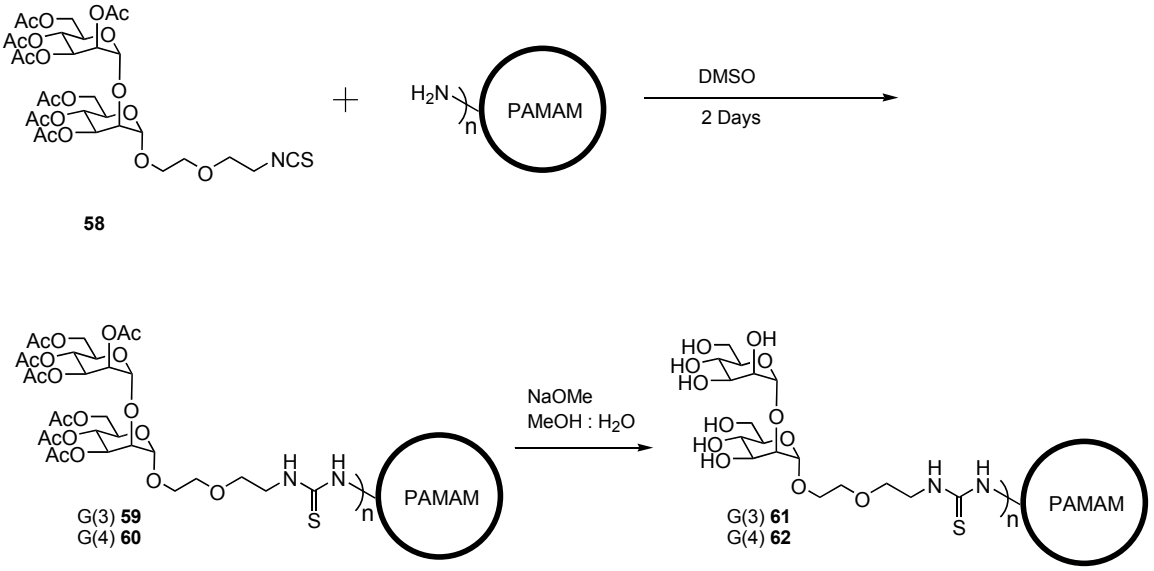

Scheme 4.2 Synthesis of dimannose functionalized PAMAM dendrimers **61** and **62**.

Characterization by NMR

The ^{1}H NMR (500MHz) spectra of the acetyl-protected dendrimers **59** and **60** in d_6-DMSO are shown in Figure 4.1. From Figure 4.1, the signals farthest downfield at 7.96 and 7.75 ppm correspond to the interior amide protons of the dendrimer, while the peak at 7.47 ppm corresponds to the thiourea protons. These assignments were based on

a simple experiment following the synthesis of **32g**, an ethoxyethanol functionalized PAMAM dendrimer with no carbohydrates.

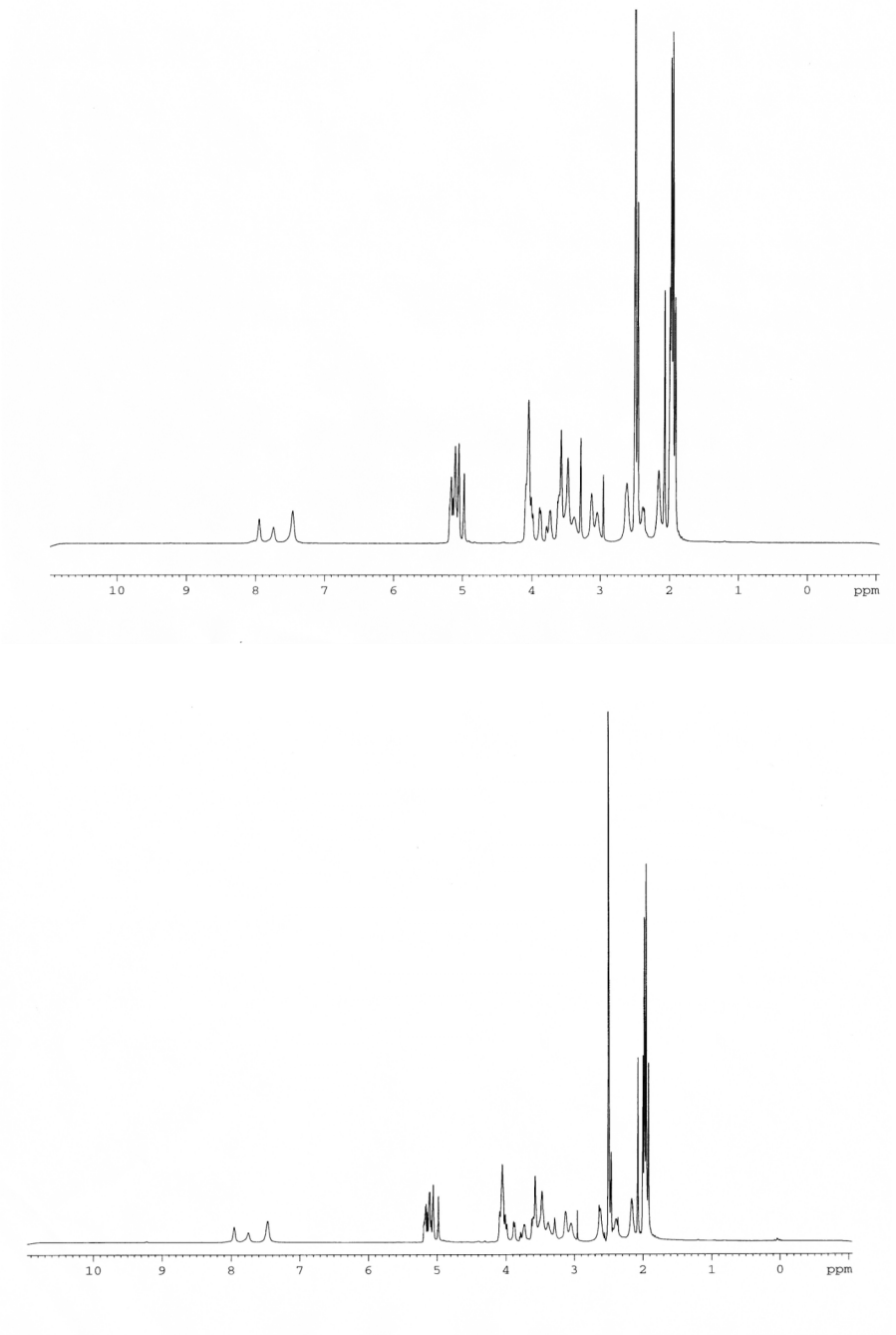

Figure 4.1 ^{1}H NMR spectra of **59** (top) and **60** (bottom) in d_6-DMSO.

The syntheses of **31g**, and **32g**, were repeated in this series of compounds so they could be used as non-Cyanovirin-N specific controls in protein binding experiments. The ^{1}H NMR of the downfield region of the spectrum was measured at different times (Figure 4.2) before and after the addition of a small excess of **29** to a G(4) PAMAM dendrimer. This time-course indicated that the peak growing in at around 7.5 ppm was likely due to the newly forming thiourea protons. Notice the reaction between a PAMAM dendrimer and the small linker **29** occurred rather quickly by NMR, yet with larger isothiocyanates, such as **58,** the reaction isn't complete for 2 days (by MALDI-TOF MS).

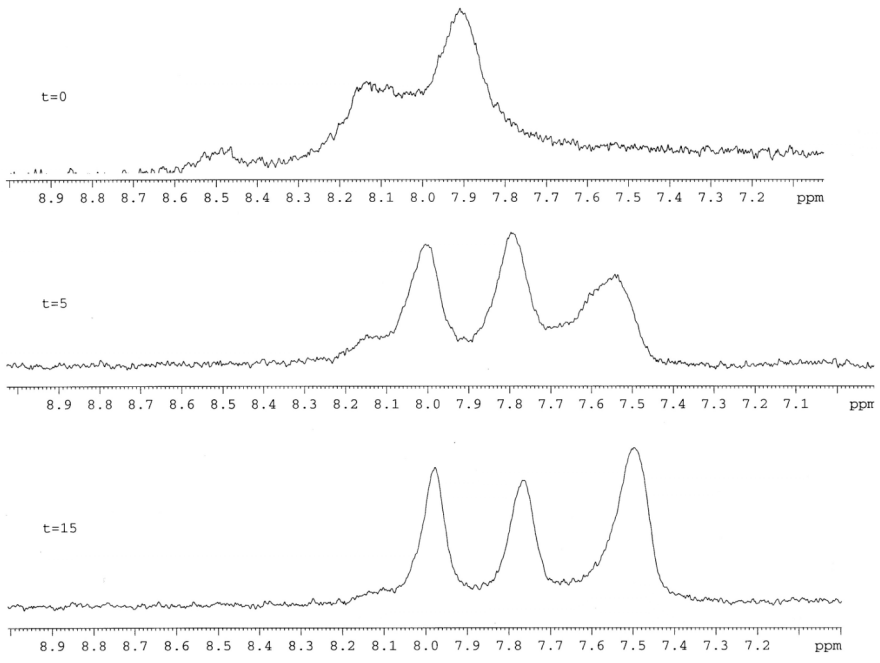

Figure 4.2 A ^{1}H NMR spectrum in d_6-DMSO from 7.0 ppm to 9.0 ppm of a G(4) PAMAM dendrimer (top), and then 5 minutes after the addition of an excess of **29** (middle), and 15 minutes after the addition of **29** (bottom) indicating the upfield peak at 7.5 ppm was most likely caused by the forming thiourea protons.

The ^{1}H NMR (500MHz) spectra of the deacetylated dendrimers **61** and **62** in D_2O are shown in Figure 4.3. The thiourea and amide proton signals were solvent exchanged in this spectrum, but the important information was the clear disappearance of the signal from the acetyl groups at 1.8 to 2.1 ppm (a transformation also supported by the solubility of the compounds in D_2O, and ^{13}C NMR spectra). The presence of two distinct anomeric protons around 5.0 ppm was helpful as well because these peaks are not distinct in Figure 4.1

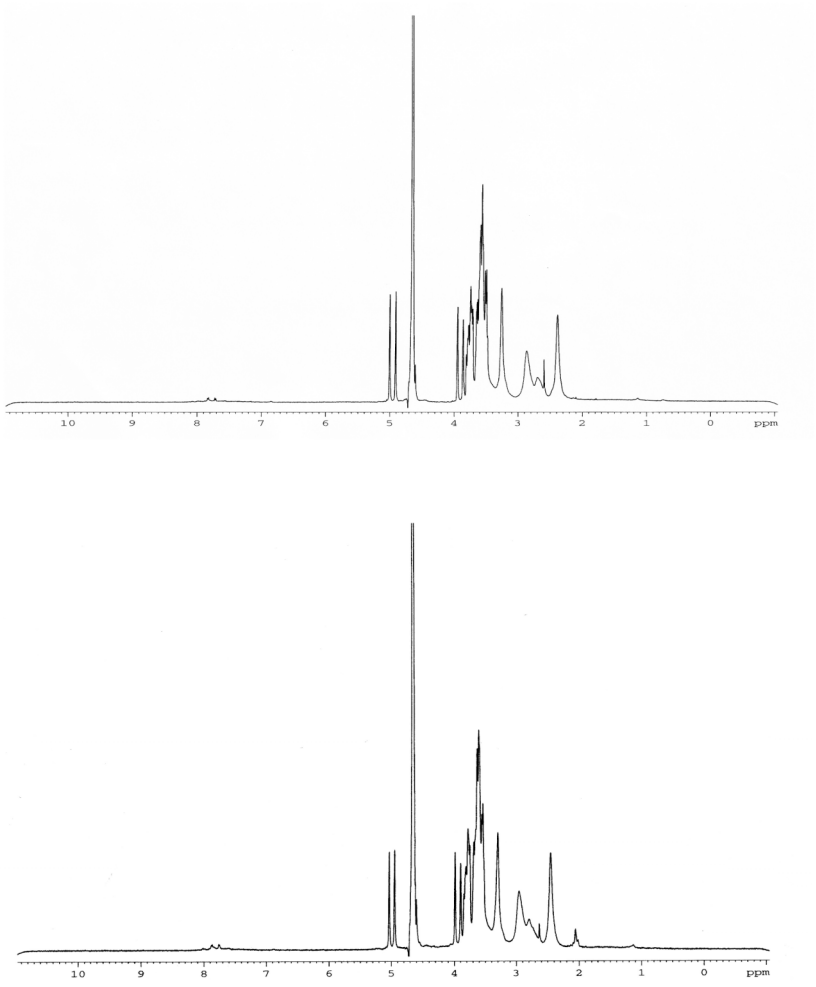

Figure 4.3 The ^{1}H NMR spectra of **61** and **62** in D_2O.

Characterization by MALDI-TOF MS

Example MALDI-TOF MS spectra for compounds **59** and **60** are given in Figure 4.4. The number of manα1-2man units was simply measured directly from the average M_W of three individual measurements. The weight average molecular weight and number of appended disaccharides are reported in Table 4.1. As with the tris-mannose cluster functionalized PAMAM dendrimers (Chapter 2), since fewer isothiocyanates are appended to the dendrimer than available primary amine attachment sites, despite an excess of the sugar, we presume a sterically allowed maximum number of disaccharides was added to the dendrimer surface.

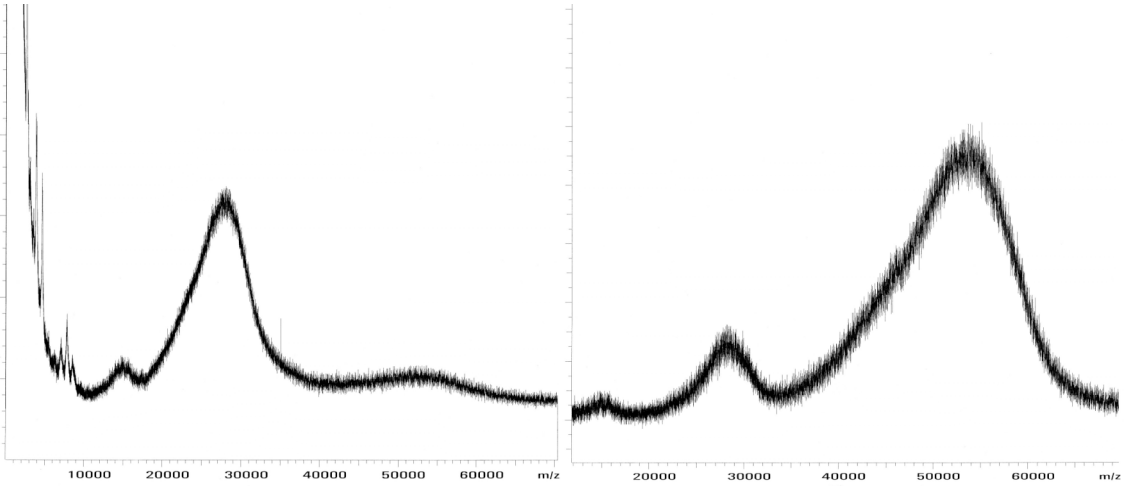

Figure 4.4 MALDI-TOF spectra of **59** and **60**.

Dendrimer Generation	M_W Acetylated (g/ mol)	# Dimannose
3	27100 (**59**)	26
4	51000 (**60**)	48

Table 4.1 MALDI-TOF MS data for dimannose functionalized PAMAM dendrimers.

Summary

Dimannose functionalized G(3) and G(4) PAMAM dendrimers were synthesized and characterized. In this section, classical mannose manipulation was combined with isothiocyanate functionality in the synthesis of these glycodendrimers. The manα1-2man moieties are larger than the monosaccharides added to the PAMAM dendrimers in the early work in this area (Chapter 1), yet smaller than tris-mannose clusters (Chapter 2). Thus it was expected that the number of appended isothiocyanates lay in between the glycodendrimers presented earlier. The number of appended isothiocyanates, for example in the G(4) series, were 55 mannose > 48 dimannose > 39 tris-mannose clusters. The strategy presented here could also be used for higher order oligomannose based glycodendrimers, as are observed in high-mannose type N-glycans.

The dimannose glycodendrimers synthesized here were sent to Dr. Angela Gronenborn, a collaborator at the National Institutes of Health (now at the University of Pittsburgh). Dr. Gronenborn performed precipitation assays with the manα1-2man specific HIV-inactivating protein Cyanovirin N. This work is presented in Chapter 5.

Experimental Procedures

General Methods. General reagents were purchased from Fisher-Acros and Sigma-Aldrich. PAMAM dendrimers were purchased as aqueous solutions from Dendritech and lyophilized prior to use. *trans*-3-Indoleacrylic acid was crystallized from approximately 1:1 methanol and water. All other reagents were used as supplied.

NMR. ^{1}H NMR and ^{13}C NMR were acquired at 500 MHz and 125 MHz, respectively, on a Bruker DRX500 instrument in $CDCl_3$ or CD_3SOCD_3.

MALDI-TOF MS. Matrix assisted laser desorption ionization (MALDI) mass spectra were acquired using a Bruker Biflex-III time-of-flight mass spectrometer. Spectra were obtained using a trans-3-indoleacrylic acid (IAA) matrix with a matrix-analyte ratio of 36,000: 1 to 1000:1. A 1 μL aliquot of the analyte (0.5-20 mg/mL,) in DMF, DMA, or DMSO, was combined with 10 μL of IAA in DMF (20 mg/mL). A 1 μL aliquot was deposited on the laser target, drying in 1-4 hours. Bovine serum albumin (MW 66,431 g/mol) and laser promoted oligomers up to the tetramer and the M/Z peak where Z = 2, trypsinogen (MW 23,982 g/mol), cytochrome C (12,361 g/mol), and bradykinin (1061 g/mol) were used as external standards. Positive ion mass spectra were acquired in linear mode, and the ions were generated by using a nitrogen laser (337 nm) pulsed at 5 Hz with a pulse width of 3 nanoseconds. Ions were accelerated at 19-20,000 volts and amplified using a discrete dynode multiplier. Spectra (10 to 2000) were summed into a LeCroy LSA1000 high-speed signal digitizer. All data processing was performed using Bruker XMass/XTOF V 5.0.2. Molecular mass data and polydispersities of the broad peaks were calculated by using the Polymer Module included in the software package. The peaks were analyzed using the *continuous* mode. Delta values were set at minimum levels.

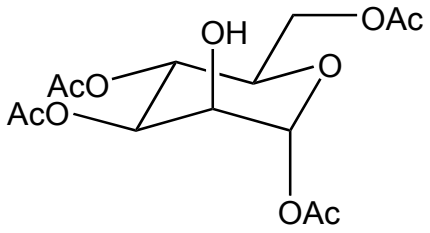

1,3,4,6-tetra-*O*-acetyl-α-D-mannopyranoside (54).

Compound **54** was prepared according to published literature methdods.[123] A 70% solution of perchloric acid in water (12 drops) was added to a solution of α-D-mannose (10 mg, 60 μmol) in acetic anhydride (75 mL). To this stirring yellow solution α-D-mannose (18.48g, 103 mmol) was slowly added, cooling in an ice bath as necessary so T ≤ 45 °C. The dark brown solution was stirred at 30 °C for 30 minutes, then 0 °C for 1 hour. Phosphorous tribromide (13 mL, 37 g, 140 mmol) was then added followed by H_2O (7 mL). This orange solution was stirred for 75 minutes at 30 °C followed by the addition of an 80% w/v solution of sodium acetate (75 mL), cooling as necessary so T ≤ 45 °C. Stirring continued for an additional 25 minutes. The product was extracted with chloroform (3 x 75 mL) and washed with saturated $NaHCO_3$ (aq) (2 x 75 mL) and water (2 x 75 mL) then dried over $MgSO_4$. The chloroform was removed *in vacuo* leaving an orange oil. Addition of cold ether (500 mL) led to the formation of a white solid **54**, which was filtered and dried to 4.11 g (11.8 mmol, 11.5% yield). ^{1}H NMR (500 MHz, CDCl3) δ 5.77 (s, 1H), 5.37 (t, 1H, J = 9.8 Hz), 5.01 (dd, 1H, J =9.5, 3.0 Hz), 4.29 (dd, 1H, J = 12.0, 5.0 Hz), 4.12 (bs, 1H), 4.11 (dd, 1H, J = 12.0, 2.5 Hz), 3.76 (dq, 1H, J = 10.0, 2.5 Hz), 2.55 (bs, 1H), 2.16 (s, 3H), 2.10 (s, 3H), 2.07 (s, 3H), 2.03 (s, 3H) ppm.

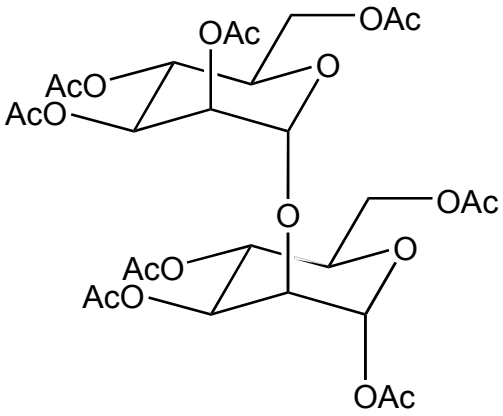

1,3,4,6-tetra-*O*-acetyl-2-*O*-(2,3,4,6-tetra-*O*-acetyl-α-D-mannopyranosyl)-α-D-mannopyranose (55).

Compound **55** was prepared according to published literature methods.[124] A solution of **54** (1.09 g, 3.1 mmol) in CH_2Cl_2 (10 mL) was combined with a solution of **8** (3.04 g, 6.2 mmol) in CH_2Cl_2 (10 mL) and 4Å molecular sieves and was cooled to –50 °C under Ar (g). A trimethylsilyl trifluoromethane sulfonate (675 μL, 830 mg, 3.7 mmol) solution in CH_2Cl_2 (10 mL) was added and this was stirred for 1 hour at –50 °C under Ar (g) then warmed to 0 °C then pyridine (5 mL) was added. The solution was filtered through celite and concentrated *in vacuo* to an orange oil. The product was purified on silica gel (70:30 ethyl acetate:hexanes) to yield 1.98 g white fluffy solid **55** (93% yield). ^{1}H NMR (500 MHz, $CDCl_3$) δ 5.77 (s, 1H), 5.46 (dd, J=2.5, 9.5 Hz, 1H), 5.29-5.37 (m, 3H), 5.10 (dd, J=2.5, 9.5 Hz, 1H), 4.99 (s, 1H), 4.40-4.42 (m, 1H), 4.31 (dd, J=4, 13 Hz, 1H), 4.02-4.25 (m, 4H), 3.77-3.78 (m, 1H), 2.13 (m, 6H), 2.11 (s, 3H), 2.08 (m, 6H), 2.02 (bs, 6H), 2.00 (s, 3H) ppm.

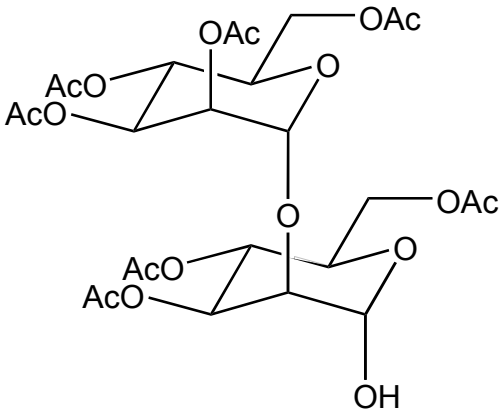

3,4,6-tri-*O*-acetyl-2-*O*-(2,3,4,6-tetra-*O*-acetyl-α-D-mannopyranosyl)-α-D-mannopyranose (56).

Compound **56** was prepared according to previously published methods.[124]

A solution of **55** (2.28 g, 3.4 mmol), hydrazine acetate (800 mg, 8.7 mmol) and DMF (140 mL) was stirred at 50 °C for 30 minutes. Ethyl Acetate was added (100 mL) and washed with water (100 mL). The aqueous layer was washed with Ethyl Acetate (3 x 75 mL). The combined organic extracts were washed with saturated $NaHCO_3$ (aq) (3 x 75 mL) and brine (2 x 75 mL) then dried over $MgSO_4$. The solvent was removed *in vacuo* to give 1.8 g of **56** (82% yield). ^{1}H NMR (500 MHz, $CDCl_3$) δ 5.26-5.40 (m, 6H), 4.92, (s, 1H), 4.05-4.20 (m, 7H), 3.25 (bs, 1H), 1.99-2.12 (m, 21H) ppm.

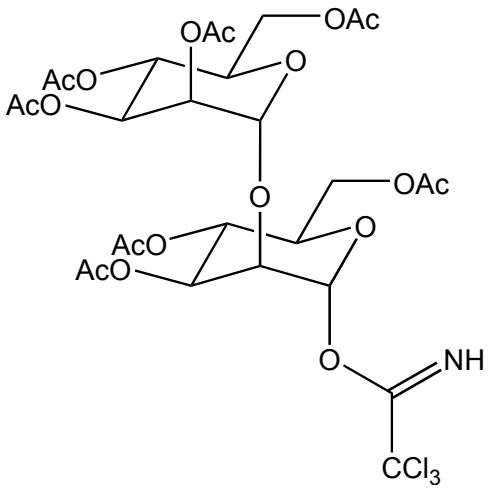

3,4,6-tri-*O*-acetyl-2-*O*-(2,3,4,6-tetra-*O*-acetyl-α-D-mannopyranosyl)-α-D-mannopyranosyl trichloroacetimidate (57).

Compound **57** was prepared according to previously published methods.[124] A solution **56** (1.8 g, 2.80 mmol) in CH_2Cl_2 was cooled to 0 °C then trichloroacetonitrile (2.80 mL, 4.03 g, 27.9 mmol) and 1,8-diaza-bicyclo[5.4.0]undec-7-ene (DBU) (146 mg, 960 μmol) were added and the solution stirred 1 hour. The solvent was removed *in vacuo* and product was purified on silica gel (75:25 ethyl acetate:hexanes) to 1.2 g yellow solid (54% yield). ^{1}H NMR (500 MHz, $CDCl_3$) δ 8.71 (s, 1H), 6.41 (s, 1H), 5.34-5.56 (m, 2H), 5.27-5.31 (m, 3H), 4.98 (s, 1H), 4.27 (s, 1H), 4.10-4.23 (m, 6H), 2.14 (s, 3H), 2.12 (s, 3H), 2.09 (s, 3H), 2.06 (s, 3H), 2.03-2.04 (m, 6H), 2.00 (s, 3H) ppm.

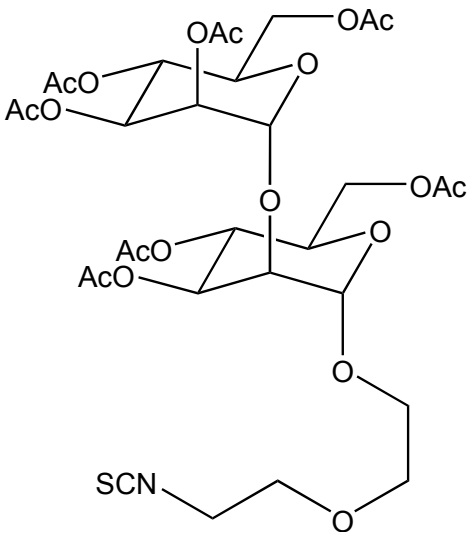

1-*O*-(5-isothiocyanato-3-oxapentyl)-3,4,6-tri-*O*-acetyl-2-*O*-(2,3,4,6-tetra-*O*-acetyl-α-D-mannopyranosyl)-α-D-mannopyranose (58). A solution of **57** (633 mg, 810 μmol) and **29** (418 mg, 2.8 mmol) in CH_2Cl_2 were combined with 4Å molecular sieves and cooled to –50 °C under Ar (g). After stirring 1 hour, trimethylsilyl trifluoromethane sulfonate (140 μL, 172 mg, 775 μmol) was added and the reaction solution was warmed to room temperature over 4 hours followed by addition of benzene (12 mL) and pyridine (7.5 mL). The solution was filtered through celite and solvents removed *in vacuo*. The product was purified on silica gel (95:5 ethyl acetate:hexanes) and recrystallized (3:1 ether:pet ether) to 386 mg white solid **57** (62% yield). MP 67-68 °C; ^{1}H NMR (500 MHz, $CDCl_3$) δ 5.18-5.35 (m, 5H), 4.93 (s, 1H), 4.87 (s, 1H), 4.01-4.19 (m, 6H), 3.92 (m, 1H), 3.79 (m, 1H), 3.58-3.64 (m, 7H), 2.08 (s, 3H), 2.07 (s, 3H), 2.02 (s, 3H), 2.1 (s, 3H), 1.97 (s, 3H), 1.97 (s, 3H), 1.94 (s, 3H) ppm; ^{13}C NMR (125 MHz) 170.8, 170.4, 170.3, 169.8, 169.7, 169.3, 133.1, 99.1, 98.3, 77.0, 70.2, 70.0, 69.7, 69.4, 69.1, 68.5, 68.4, 67.3,

66.4, 66.1, 62.5, 62.1, 45.3, 20.8, 20.7, 20.6 ppm; IR (KBr) 1737, 2109, 3044; HRMS: Calcd for $(M+Na)^+$ $C_{31}H_{43}O_{19}NSNa$ 788.2048, found 788.2031.

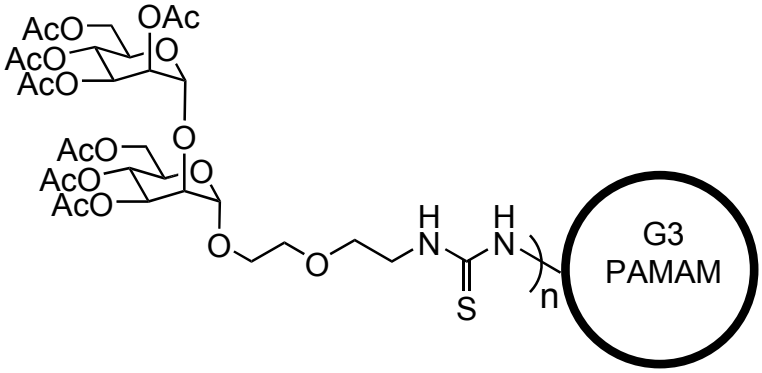

Generation 3.0 PAMAM-based 1-*O*-(5-thiourea-3-oxapentyl)-3,4,6-tri-*O*-acetyl-2-*O*-(2,3,4,6-tetra-*O*-acetyl-α-D-mannopyranosyl)-α-D-mannopyranose (59). A solution of **58** (35mg, 46 μmol) in 1 mL DMSO was added to amine terminated Starburst PAMAM dendrimer (generation 3) (6.3 mg, 0.91 μmol) and the solution was stirred for 2 days. Dialysis against DMSO (MWCO 3500 Da) followed by lyopholization afforded 30 mg slightly yellow thick solid (121% yield). ^{1}H NMR (CD_3SOCD_3, 500MHz) δ 7.96 (bs, 1H), 7.75 (bs, 1H), 7.47 (bs, 2H), 5.06-5.20 (m, 7H), 4.98 (s, 1H), 3.99-4.09 (m, 7H), 3.87-3.89 (m, 1H), 3.73-3.79 (m, 2H), 3.58-3.62 (m, 5H), 3.48 (bs, 5H), 3.38 (m, 2H), 3.29 (bs, 2H), 3.13 (bs, 3H), 3.05 (bs, 2H), 2.54-2.70 (m, 4H), 2.47 (s, 2H), 2.33-2.45 (m, 3H), 2.16 (bs, 4H), 2.08 (s, 4H), 2.00 (s, 3H), 1.98 (s, 7H), 1.95 (s, 7H), 1.92 (s, 4H) ppm; ^{13}C NMR (125 MHz) δ 170.5, 170.4, 170.2, 170.0, 169.9, 169.7, 98.5, 97.9, 76.3, 69.9, 69.5, 69.2, 68.9, 68.5, 68.3, 67.2, 66.0, 62.5, 62.0, 50.0, 33.7, 21.0, 20.9, 20.8, 20.7 ppm; MALDI-TOF MS (pos) 27,100.

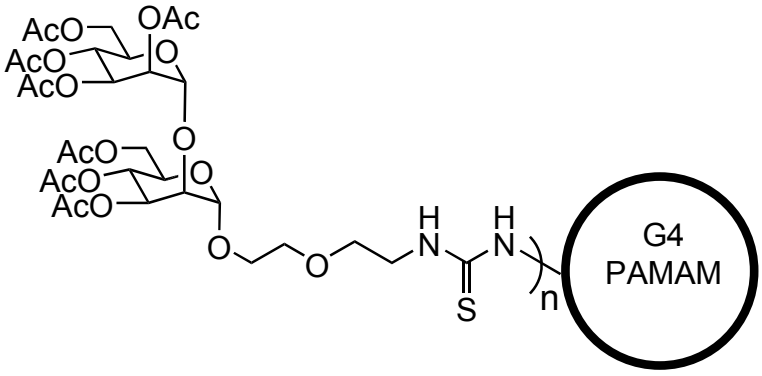

Generation 4.0 PAMAM-based 1-*O*-(5-thiourea-3-oxapentyl)-3,4,6-tri-*O*-acetyl-2-*O*-(2,3,4,6-tetra-*O*-acetyl-α-D-mannopyranosyl)-α-D-mannopyranose (60). A solution of **58** (35mg, 46 μmol) in 1 mL DMSO added to amine terminated Starburst PAMAM dendrimer (generation 4) (6.3 mg, 0.47 μmol) and the solution stirred 2 days followed by dialysis against DMSO (MWCO 3500 Da). The solvent was removed by lyopholization to 20 mg slightly yellow thick solid (85% yield). ^{1}H NMR (500MHz, CD_3SOCD_3) δ 7.93 (bs, 1H, amide N*H*), 7.72 (bs, 1H, amide N*H*), 7.44 (bs, 2H, $CH_2NHC(S)NHCH_2$), 5.05-5.20 (m, 7H), 4.98 (bs, 1H), 3.99-4.09 (m, 7H). 3.88-3.89 (m, 1H), 3.74-3.79 (m, 2H), 3.56-3.63 (m, 5H), 3.48 (bs, 5H), 3.39 (m, 2H), 3.37 (s, 3H), 3.14 (bs, 3H), 3.05 (bs, 2H), 2.96 (s, 1H), 2.56-2.70 (m, 4H), 2.47 (s, 5H), 2.33-2.43 (m, 3H), 2.11-2.27 (bs, 5H), 2.07 (s, 4H), 2.00 (s, 4H), 1.98 (s, 8H), 1.95 (s, 8H), 1.92 (s, 4H) ppm; ^{13}C NMR (125 MHz) δ 172.2, 171.7, 170.5, 170.4, 170.2, 170.0, 169.9, 169.9, 169.7, 98.5, 97.9, 76.3, 69.9, 69.5, 69.2, 69.0, 68.9, 68.5, 68.3, 67.4, 67.2, 66.0, 62.5, 62.0, 50.0, 45.5, 43.7, 42.6, 38.6, 37.3, 33.7, 21.0, 21.0, 20.9, 20.9, 20.8, 20.7 ppm; MALDI-TOF MS (pos) 50,400.

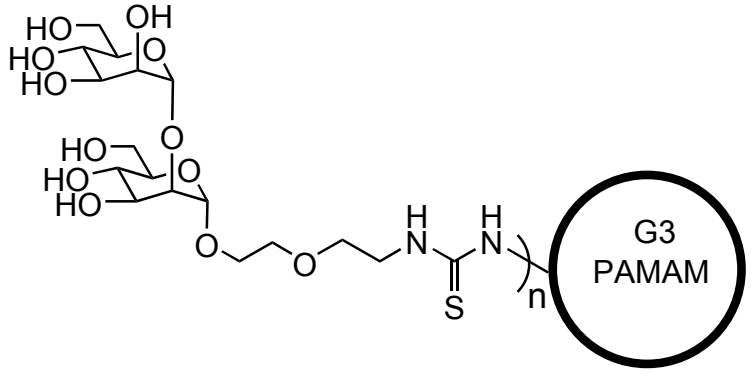

Generation 3.0 PAMAM-based 1-*O*-(5-thiourea-3-oxapentyl)-2-*O*-(α-D-mannopyranosyl)-α-D-mannopyranose (61).

Methanolic NaOMe (0.31 M, 93 μL) was added to a suspension of **59** in MeOH:H_2O (1:1, 3 mL) and stirred until all the solid dissolved (~12 h). The solution was neutralized with Amberlite IR-120 (acidic), dialyzed against water (MWCO 3500 g/mol), and filtered (Acrodisc 13mm inline syringe with 0.2 μm membrane). Lyophilization afforded 9.5 mg of **61** as a pale tan oily solid. ^{1}H NMR (500MHz, CD_3SOCD_3) δ 5.00 (s, 1H), 4.91 (s, 1H), 3.95 (s, 1H), 3.86 (s, 1H), 3.71-3.81 (m, 5H). 3.50-3.65 (m, 14H), 3.26, (bs, 5H), 2.52-3.00 (m, 6H), 2.39 (bs, 4H) ppm; ^{13}C NMR (125 MHz) δ 102.3, 98.4, 78.7, 73.3, 72.8, 70.4, 70.3, 70.0, 69.5, 68.9, 67.0, 67.0, 66.6, 61.2, 61.0, 51.7, 49.4, 43.2, 36.4, 31.8 ppm

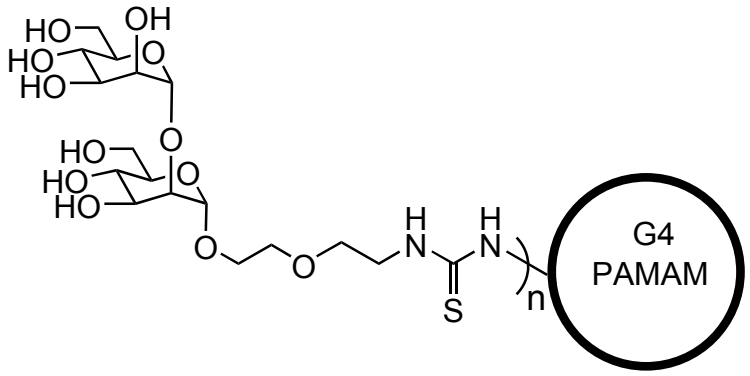

Generation 4.0 PAMAM-based 1-*O*-(5-thiourea-3-oxapentyl)-2-*O*-(α-D-mannopyranosyl)-α-D-mannopyranose (62).

Methanolic NaOMe (0.31 M, 93 μL) was added to a suspension of **60** in MeOH:H_2O (1:1, 3 mL) and stirred until all the solid dissolved (~12 h). The solution was neutralized with Amberlite IR-120 (acidic), dialyzed against water (MWCO 3500 g/mol), and filtered (Acrodisc 13mm inline syringe with 0.2 μm membrane). Lyophilization afforded 6.8 mg of **62** as a pale tan oily solid. ^{1}H NMR (500MHz, CD_3SOCD_3) δ 5.04, (s, 1H), 4.95 (s, 1H), 3.99 (s, 1H), 3.90 (s, 1H), 3.75-3.85 (m, 6H), 3.54-3.69 (m, 15H), 3.30 (bs, 5H), 2.60-3.10 (m, 7H), 2.46 (bs, 4H) ppm; ^{13}C NMR (125 MHz) δ 173.9, 102.3, 98.4, 78.7, 73.3, 72.9, 70.4, 70.3, 70.0, 69.5, 68.9, 67.0, 67.0, 66.6, 61.2, 61.0, 49.5, 31.5 ppm

CHAPTER 5

ANALYZING CARBOHYDRATE-PROTEIN INTERACTIONS USING GLYCODENDRIMERS

Introduction

To gain insight into the mechanism of protein carbohydrate interactions, the glycodendrimers that were synthesized as described in the preceding chapters were analyzed as ligands in lectin binding experiments. This chapter describes experiments in transmission electron microscopy (TEM), precipitation assays, isothermal titration microcalorimetry (ITC), and hemagglutination inhibition assays (HIA).

Transmission Electron Microscopy[73]

The G(6) mannose functionalized glycodendrimers **63-68** were synthesized as previously described, more information on this synthesis is given in Chapter 6 (Figure 5.1).[72] The largest glycodendrimer **68** was analyzed by transmission electron microscopy (TEM) before and after incubation with the mannose specific lectin Con A in the presence of a tungstate stain.[125] The images from this work are shown in Figure 5.2.

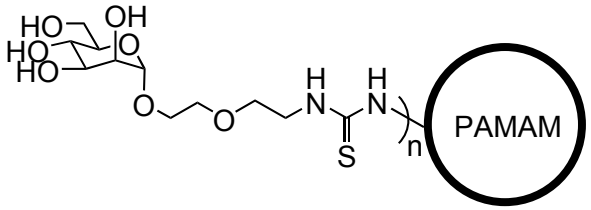

G(1) = **63**
G(2) = **64**
G(3) = **65**
G(4) = **66**
G(5) = **67**
G(6) = **68**

Figure 5.1 Mannose-functionalized PAMAM dendrimers **63-68**.

Scientists from other research groups report that affinity enhancements for synthetic multivalent ligands over monosaccharides arise from primarily aggregative effects.[27] This is undoubtedly true in certain model systems and physiological events as discussed in Chapter 1. TEM images were taken to determine if similar aggregation effects caused the enhancements observed for glycodendrimers **63-68** over methyl mannose in the hemagglutination inhibition assay. From Figure 5.2a, the glycodendrimers alone were observed, although the edges of the particles appear roughened due to resolution of the method,[125] at around 10 nm (the actual diameter of these dendrimers in solution based on electron paramagnetic resonance experiments, EPR, is 13 nm). When the glycodendrimer was incubated with Con A, with dendrimer and lectin concentrations matching those used in the hemagglutination inhibition assay, discrete clusters of lectin appeared to form around the glycodendrimer roughly doubling the diameter of the observed particle, as was expected with the lectin 6.5 nm in diameter (Figure 5.2b).

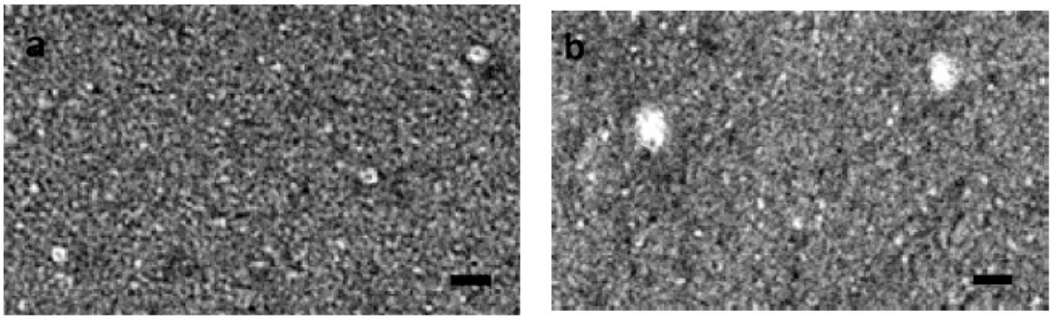

Figure 5.2 TEM images of aqueous solutions of a) **68** at a concentration of 0.023 mg/mL and b) **68** (0.023 mg/mL) and Con A (0.18 mg/mL). Scale bar = 20 nm. Solutions in potassium phosphotungstate stain (2% w/v).

Precipitation Assays

The dendrimers **61** and **62** (Figure 5.3) were analyzed by a precipitation assay by Dr. Angela Gronenborn, at the NIH, with the carbohydrate binding protein Cyanovirin-N.[122]

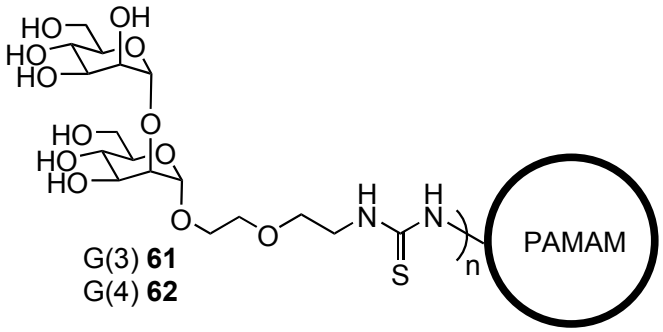

Figure 5.3 Dimannose functionalized PAMAM dendrimers **61** and **62**.

Separately, the dendrimers **63-68** were analyzed by precipitation assay with Con A by other members of our research group according to a method from by Brewer.[73, 126] The assay measurements for compounds **61** and **62** are given in Figure 5.4. A linear decrease in the UV absorbance at 280 nm, from Cyanovirin-N, is observed upon titration with the glycodendrimers (Figure 5.4a) corresponding to an increase in the amount of protein precipitated. These data correspond to binding stoichiometries of 8:1 and 11:1 Cyanovirin N to dendrimers **61** and **62** respectively (Figure 5.4b). The precipitation assay data for **61** and **62** are given in Table 5.1 and are compared with the precipitation assay data for **65-66**, dendrimers of the same generation.

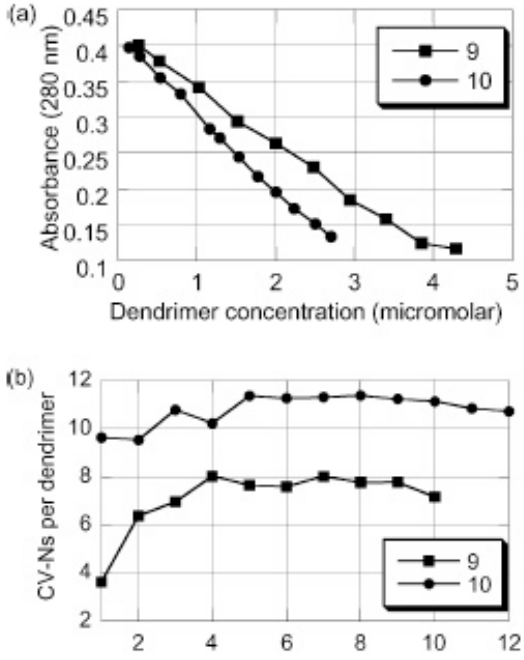

Figure 5.4 Precipitation Assay data for compounds **61** and **62** including a) absorbance vs dendrimer concentration and b) the number of Cyanovirin N per dendrimer.

Compound	Protein	Observed protein bound	Theoretical protein bound
59	Cyanovirin-N	8	13
60	Cyanovirin-N	11	15
65	Con A	10	10
66	Con A	12	12

Table 5.1 Precipitation Assay data for compounds **61** and **62** with Cyanovirin N and compounds **65** and **66** with Concanavalin A.

The maximum number of Con A lectins recruited by **65-66** as determined by the precipitation assay matches the calculated maximum, however, the maximum amount of Cyanovirin-N was not recruited by **61** and **62** (Table 5.1). This disparity is rationalized based on affinity. The high affinity of Cyanovirin-N for **61** and **62** forms a tightly bound

complex, unable to rearrange on the timescale of the assay (Figure 5.5a). By contrast, the relatively lower affinity of Con A for **65-66** results in optimal packing of Con A through rearrangements of the ligand and receptor (Figure 5.5b).

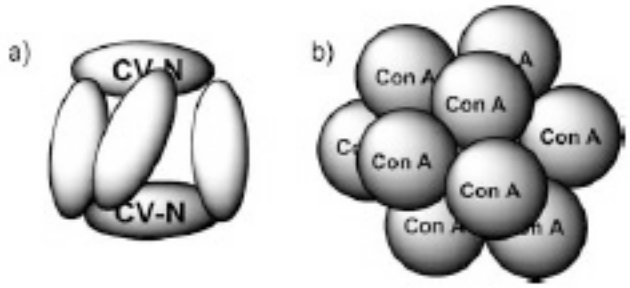

Figure 5.5 Schematic representation of a) unoptimized dendrimer coverage by Cyanovirin N and b) complete dendrimer coating by Concanavalin A.

Isothermal Titration Microcalorimetry (ITC)

ITC measures the heat evolved as a consequence of a series of injections of a ligand solution into a receptor solution, forming a binding isotherm from which the thermodynamic data of the interaction can be calculated. [127] The thermodynamic data is calculated from the isotherm using a least squares fitting. ITC has been used in recent reports to measure the thermodynamics of binding lectins with synthetic ligand with great success.[128, 129]

First, a titration of dimeric Con A with methyl mannose was performed according to literature methods.[130] Con A dimers are formed at lower pH (around 5.2), while tetramers are formed at physiological pH.

Con A was dissolved overnight in a 3,3-dimethylglutaric acid (DMG) buffer (50 mM) at pH = 5.2 containing 1 mM $MnCl_2$, 1 mM $CaCl_2$ and NaCl (0.15 M). The

concentration of Con A was determined spectrophotometrically at 280 nm using $A^{1\%}_{1cm}$ = 12.4 at pH = 5.2 and is reported in terms of monomer (MW = 26,500).[129]

Following a procedure by Dam *et. al.*, Con A from 290 μM to 5 μM was titrated with methyl mannose (Figure 5.6).[130] The concentration of Con A was varied to determine the optimum concentration for ITC experiments. As observed in Figure 5.6a, at high concentration of Con A, the isotherm is incomplete, which would lead to inaccurate thermodynamics calculations. Also, when the protein concentration was low (Figure 5.6c and Figure 5.6d) the signal (μcal/sec) was reduced, leading to lower signal to noise and larger error in the least squares fitting.

Con A titration with mannose functionalized G(6) PAMAM dendrimer **68** was performed next. A solution of **68** (25 μM) was titrated into a solution of Con A (20 μM), giving the isotherm in Figure 5.7. Examining the solution, it was clear that after mixing precipitation had occurred. This event was also observed in the titration measurement, as noise in the baseline in the top portion of Figure 5.7. Aggregation results in thermodynamic measurements independent of ligand-receptor binding, therefore only soluble solutions may be analyzed using this method.

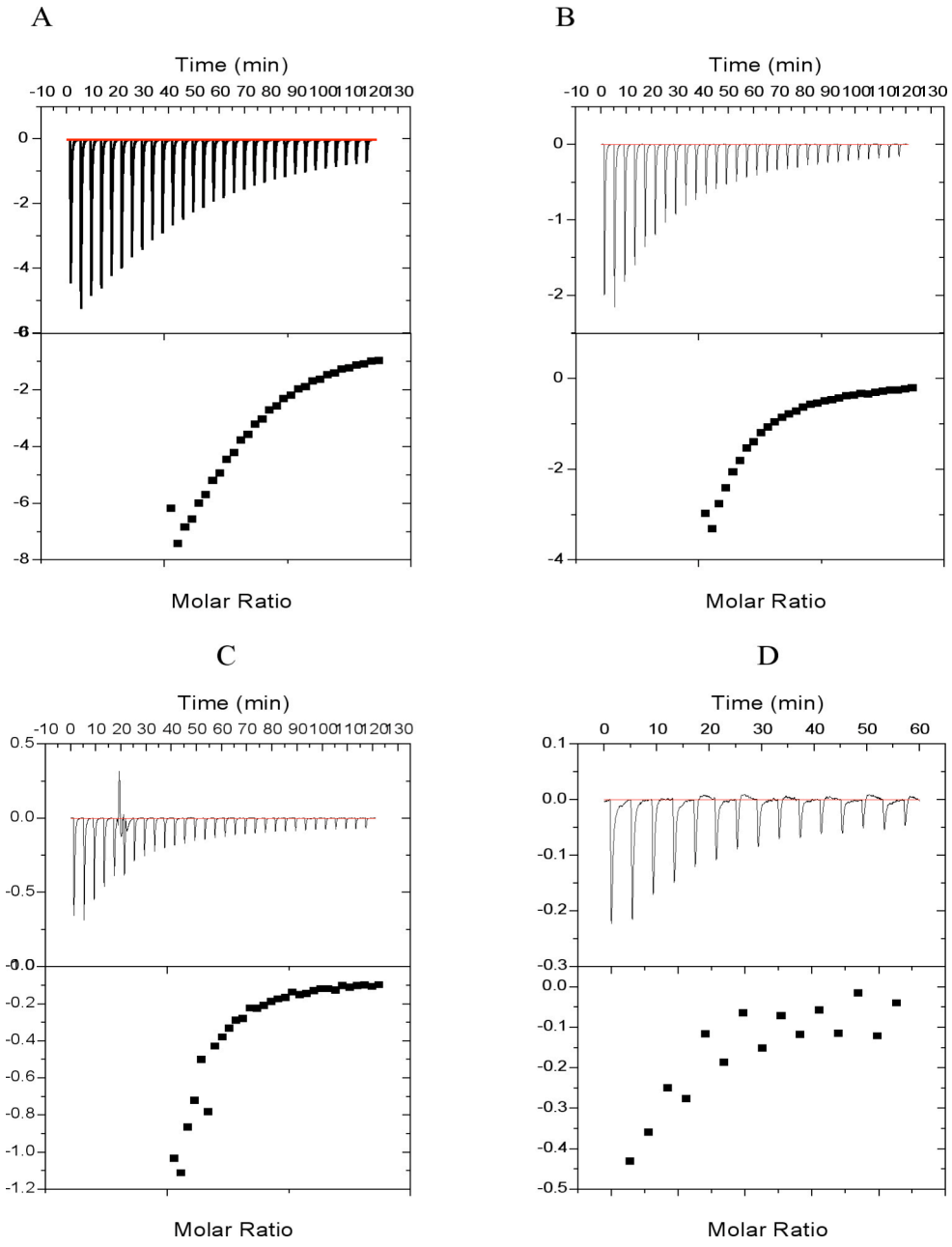

Figure 5.6 ITC profiles of Concanavalin A titration with methyl-α-D-mannose. With Con A concentrations at a) 290 μM, b) 72 μM, c) 18 μM, and d) 5 μM.

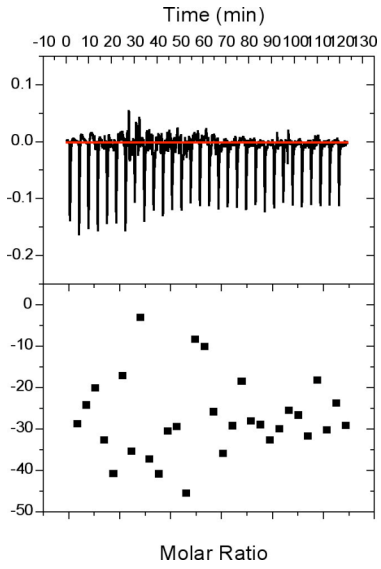

Figure 5.7 ITC profile of a precipitating Concanavalin A and mannose functionalized G(6) PAMAM dendrimer **68.**

Next glycodendrimer **66** was analyzed because the smaller dendrimer might be less apt to form large aggregates, and low concentrations of dendrimer and Con A were used to avoid aggregation. Unfortunately, very low concentrations of the binding components didn't produce any significant signal. The highest possible non-aggregating concentration of **66** (7μM) was titrated into Con A (26 μM) giving the binding isotherm in Figure 5.8. Manual mixing of the binding partners and evaluation of the solution or colloid under a handheld laser pointer was used to determine these maximum concentrations. Inspection of the signal from Figure 5.8, which is less than 0.2 μcal/sec, indicates that these concentrations were still too low to make a reliable measurement.

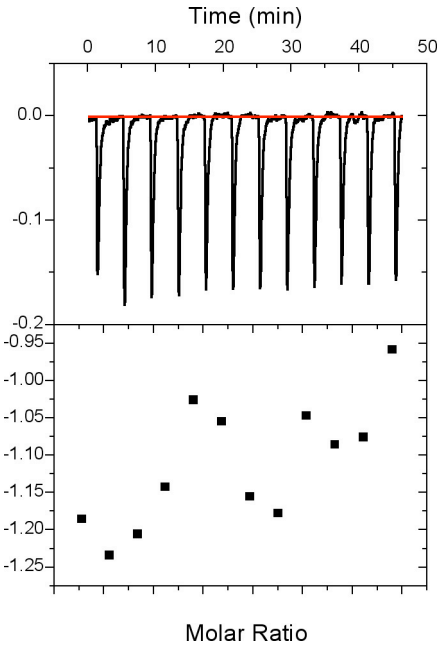

Figure 5.8 ITC profile of a soluble mixture of Concanavalin A and a mannose functionalized G(4) PAMAM dendrimer **66.**

Another method employed was reverse-ITC, where the ligand was present in the sample cell and Con A was added in a stepwise fashion.[129] This variation of ITC required high concentrations of Con A for injection, made using Amicon Ultra centrifugal filtration devices with an MWCO of 5000 Da. With this tool, Con A solutions up to 920 μM were made. When **66** (0.26 μM) was titrated with Con A (920 μM) the binding isotherm in Figure 5.9 was produced. Again, aggregation was observed even in the early stages of binding as evident from the excess noise in the baseline.

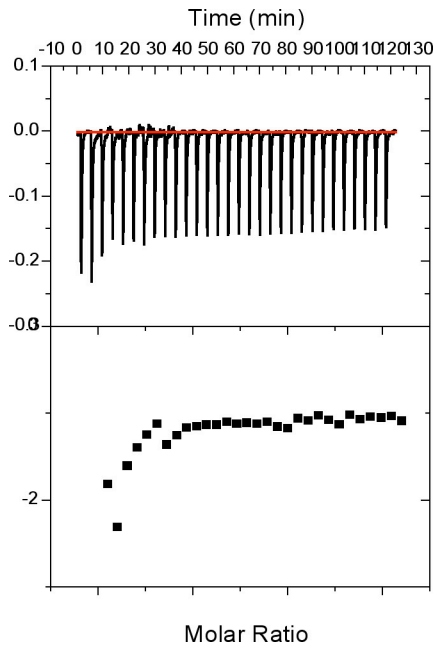

Figure 5.9 Reverse ITC profile of **68** titrated by Concanavalin A.

Next, a series of changes to the experiment were done that were designed to reduce aggregation at concentrations where significant signal might be observed. Temperatures up to 50 °C were used without reducing aggregation. The NaCl was omitted from the buffer and separately a different buffer (sodium acetate 0.1 M, 1 mM $MnCl_2$, 1 mM $CaCl_2$) was tried without improvement to the ITC results. Next, a detergent, TWEEN-20, was included, although this failed to reduce aggregation as well. The conclusion from these experiments was that at submicromolar concentrations of Con A and mannose functionalized PAMAM dendrimers, such as the concentrations used in a hemagglutination inhibition assay, no appreciable signal was obtained from ITC and when the solutions were mixed at higher concentrations, aggregation occurred.

Hemagglutination Inhibition Assay (HIA)

Lectins are defined, in part, by their ability to agglutinate erythrocytes. One simple method of evaluating synthetic multivalent ligands is by measuring their ability to inhibit this process. The HIA does not directly provide association constants or other thermodynamic information, yet it does provide a useful comparison of the activity of a series of synthetic multivalent ligands.[27, 131, 132] The HIA is diagrammed in Figure 5.10.

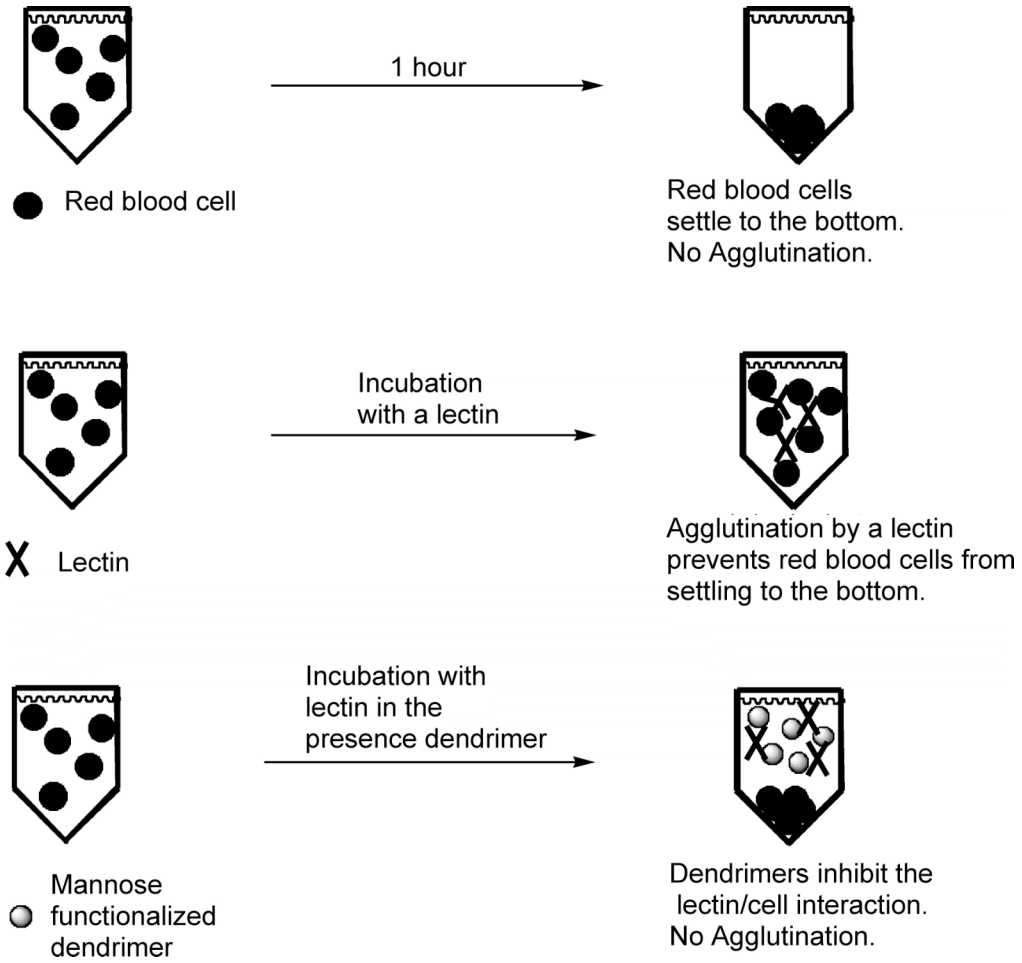

Figure 5.10 A schematic description of the hemagglutination inhibition assay.

A solution of red blood cells in a V-bottom well plate will settle to the bottom of the plate over the course of about two hours, forming a bead surrounded by clear buffer. When a lectin such as Con A is added to the well, agglutination is observed as the lectin forms cross-links between the cells through binding the cell surface glycoproteins, preventing bead formation. If an inhibitor is added to the lectin solution, such as methyl mannose or mannose functionalized PAMAM dendrimers, then the carbohydrate recognition domains of the lectin are blocked, and the red blood cells are allowed to again precipitate into a bead, as no agglutination is observed.

In a 96-well V-bottom microtiter plate, a serial dilution of the inhibitor is prepared and at a certain point the concentration will be too low to inhibit agglutination. The last well in the serial dilution that inhibits agglutination is called the minimum inhibitory concentration and this is the observable measurement. The possible error in the measurement arises in that the minimum inhibitory concentration is ±1 well, and since a two-fold serial dilution is used, the standard deviation is relatively large.

In the first experiment mannose functionalized dendrimers **63-65** were evaluated for binding pea lectin (from *pisum sativum*).[133] This lectin is a dimer specific for mannose. The first step in the HIA is the determination of the appropriate concentration of lectin. For Con A, 8 times the minimum required concentration was used in the HIA, yet for pea lectin, which didn't interact with the inhibitor as well, only 2 times the minimum agglutination concentration was used in the assay to increase the sensitivity.

The results of the HIA using **63-65** and pea lectin are reported in Table 5.2. The minimum inhibitory concentration of the glycodendrimers is compared with that of methyl mannose. A lower concentration of mannose-functionalized dendrimer is

required to inhibit agglutination in each case. However, since each dendrimer has multiple copies of mannose, a more relevant concentration is reported in valency corrected terms. In other words, the valency corrected minimum inhibitory concentration of a mannose-functionalized G(2) PAMAM dendrimer, with 16 sugars, is 16 times the concentration of the dendrimer. In Table 5.2, this is organized as the concentration per dendrimer, and the valency corrected concentration, per mannose.

Compound	Concentration of dendrimer (μM)	Relative activity per dendrimer	Concentration of mannose (μM)	Relative activity per mannose
methyl mannose	402	1	400	1.0
63	40	10	320	1.2
64	19	21	300	1.3
65	5	82	160	2.6

Table 5.2 Hemagglutination Inhibition Assay data for compounds **63-65** with Pea Lectin.

From the relative activity of each, on a per mannose basis, the mannose-functionalized PAMAM dendrimers were only as active or less active than methyl mannose. This is in contrast to the HIA data using the same lectins with Con A, where an increase in activity relative to methyl mannose was observed with the mannose-functionalized G(3) PAMAM dendrimer. Perhaps due too the lack of shape complementarity between the lectin and the glycodendrimer, or the flexibility of pea lectin compared with Con A, no enhancement in activity compared with methyl mannose was observed.[134]

An HIA was also performed analyzing the inhibition of the interaction between Con A and red blood cells using tris-mannose cluster functionalized glycodendrimers **20-24** and **40-44**. The HIA data for this series of compounds is given in Table 5.3.

Dendrimer Generation	Compound	Loading %	Activity relative to methyl mannose	Standard Deviation
2	**20**	100	3000	1500
2	**40a**	56	5900	5000
2	**40b**	29	2700	1200
2	**40g**	0	0	0
3	**21**	100	3400	1600
3	**41a**	57	3900	1000
3	**41b**	34	4000	1300
3	**41c**	11	2300	800
3	**41e**	4	1300	300
3	**41g**	0	0	0
4	**22**	100	2500	900
4	**42a**	67	2800	600
4	**42b**	51	3600	1600
4	**42c**	24	7200	1300
4	**42d**	13	5100	4300
4	**42e**	7	3900	1300
4	**42f**	4	300	100
4	**42g**	0	0	0
5	**23**	100	2400	1100
5	**43a**	57	3200	1500
5	**43b**	44	2400	1300
5	**43c**	18	2000	800
5	**43f**	12	1800	700
5	**43g**	0	0	0
6	**24**	100	1800	1100
6	**44a**	64	1600	500
6	**44b**	30	3900	1100
6	**44c**	21	4700	3700
6	**44d**	9	8000	2800
6	**44f**	0	0	0

Table 5.3 Results from the HIA of compounds **20-24**, and **40-44**.

To determine if there was a trend in the relative activity per mannose of the glycodendrimers versus the degree of loading of these glycodendrimers, a graph was made of the data and is shown in Figure 5.11.

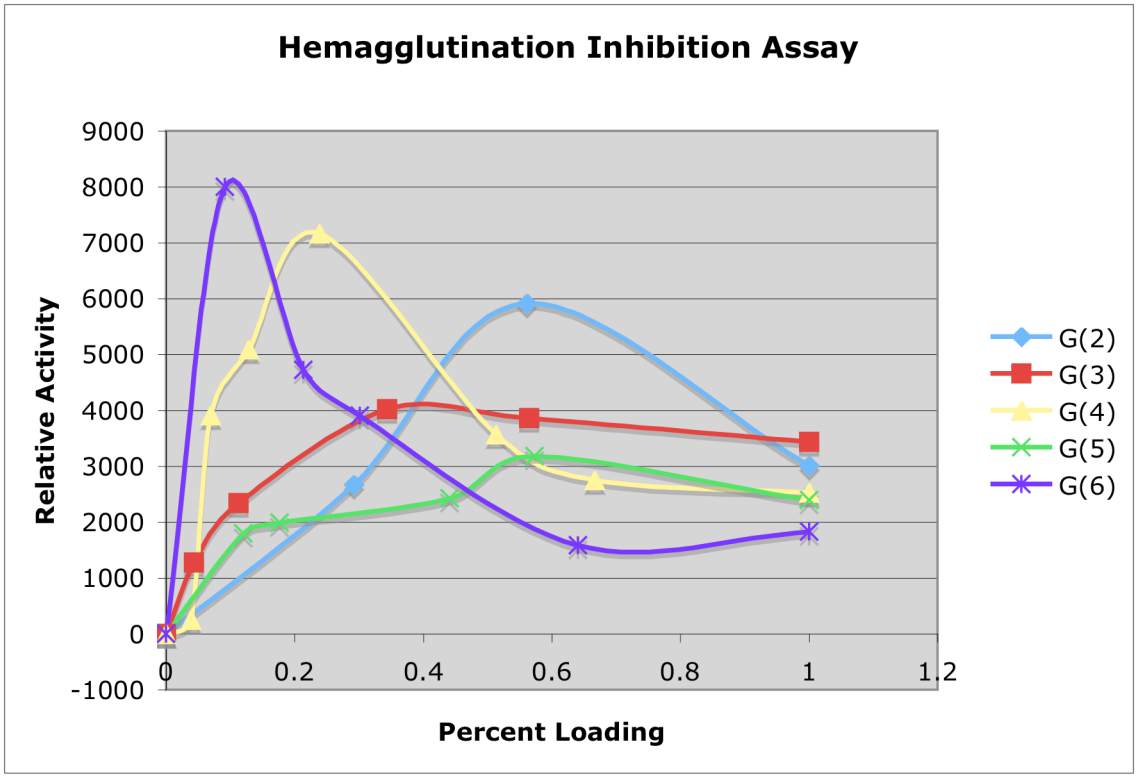

Figure 5.11 Activity of the glycodendrimers **40-44** relative to methyl mannose vs dendrimer loading.

The HIA was repeated 6-8 times for each dendrimer, and the reported activities are averages of these trials with the standard deviation measured from each series. The large standard deviations for the HIA arise from inherent error in the assay due to the two-fold dilution each measurement is ± 1 well, or a four-fold difference in measured inhibiting concentration.

From the HIA data it appears that most of the dendrimers had a similar activity, 1500 to 8000 times more active than methyl mannose. The control dendrimers with no mannose had no inhibiting activity in the assay. The indication is that the size of the dendrimer and dendrimer loading had relatively little effect on Con A binding, except at very low loading where the clusters were relatively far apart from one another on the dendrimer surface.

If the large and small dendrimers were both able to bind to Con A bivalently, little difference would be expected in their relative activities. If the small dendrimers were, in fact, too small to span the 65 Å between the Con A carbohydrate recognition domains, then this assay suggests the ability to bind bivalently has a relatively smaller role in the activity enhancement, and that the enhancement from proximity effects was a greater determinant of activity.

In previous work using heterogeneously functionalized mannose glycodendrimers, unclustered, the maximum relative activity was at 50% loading.[73] At lower loadings a significant reduction in activity occurred. With the tris-cluster functionalized glycodendrimers above there was not a significant reduction in activity until loadings of less than 10%. This indicates cluster spacing was not a relatively large determinant of activity either.

The large measurement error in the HIA reported here means that these conclusions should be considered carefully, and emphasizes the requirement for quantitative assays in the analysis of carbohydrate-protein interactions using synthetic multivalent ligands. With that considered, it appears from this assay that synthetic multivalent ligands may be just as effective, or more effective, when the pendant

carbohydrates are clustered rather than singular. The activity enhancements observed above were not very dependent on macromolecule size or cluster spacing.

Summary

Transmission electron microscopy images of the interaction of **68** with Con A appear to show distinct clusters of single dendrimers saturated with lectin. This suggests aggregation is not be occurring at the concentrations used to evaluated glycodendrimers using the HIA, and that the binding model between glycodendrimers and lectins in this system rely on multivalency and cluster effects for activity enhancements.

The precipitation assay using dendimers **61** and **62** indicate these bind Cyanovirin N with a very high affinity when compared to mannose functionalized dendrimers binding with Con A. The high affinity of the dimannose functionalized dendrimers for Cyanovirin N could be very useful in studying how Cyanovirin N binds with GP120, and is also a positive indication that these glycodendrimers could be used as synthetic antigens.

Isothermal titration microcalorimetry analysis of the glycodendrimers synthesized in our labs failed to provide adequate signal to noise at concentrations of the ligand and receptor that did not aggregate. However, it was demonstrated that this technique might be used in analysis of lectin-monosaccharide interactions in our labs.

The hemagglutination inhibition assay was used to evaluate the interaction of mannose functionalized PAMAM dendrimers **63-65** with pea lectin. The glycodendrimers exhibited only a small degree of ehancement over methyl mannose.

Evaluation of tris-mannose cluster functionalized PAMAM dendrimers with a HIA indicated that carbohydrates in forced proximity result in an assay activity greater than 1000 times the assay activity of methyl mannose, somewhat independent of macromolecule size or loading.

Experimental Procedures

General Methods. General reagents were purchased from Fisher-Acros and Sigma-Aldrich. Con A and pea lectin were purchased from Calbiochem. All other reagents were used as supplied.

Buffer Preparation.

Alsever's solution was prepared by combining NaCl (4.2 g, 72 mmol), sodium citrate (8.0 g, 2.7 mmol), and glucose (20.5 g, 114 mmol) in 1 L water, followed by titration with HCL (6 M) to pH = 6.0.

HEPES buffer was prepared by combining N-[2-hydroxyethyl]piperazine-N'-[2-ethanesulfonic acid] (HEPES) (2.38 g, 10 mmol), $CaCl_2 \bullet 2H_2O$ (14.7 mg, 1mmol) with 1 L water followed by titration with NaOH to pH = 8.5.

Phosphate buffered saline (PBS) was prepared by combining NaCl (35 g, 0.6 mol), sodium phosphate monobasic monohydrate (3.86 g, 28 mmol), and sodium phosphate dibasic heptahydrate (19.3 g, 72 mmol) in 4 L water, pH = 7.2.

Hemagglutination inhibition assay buffer was prepared by dissolving bovine serum albumin in PBS (0.5% w/v).

TRIS buffered saline was prepared by combining Trizma•HCl (26.4 g, 168 mmol), tris(hydroxymethyl)aminomethane (TRIS) (3.88 g, 32 mmol), and NaCl (35 g, 0.6 mol) in 4 L water, pH = 7.5.

3,3-dimethylglutaric acid buffer was prepared by titrating a 0.05 M solution with NaOH until the pH = 5.2. Next solid $MnCl_2$ and $CaCl_2$ were added to make the concentration of each 1 mM.

Sodium acetate buffer was prepared by making a sodium acetate solution (0.1 M), which was titrated with HCl until pH = 5.2. Next, solid $MnCl_2$ and $CaCl_2$ were added to make the concentration of each 1 mM.

Transmission Electron Microscopy.

Images for **68** and **68**/Con A complexes were taken on a LEO 912AB transmission electron microscope at an acceleration voltage of 100 kV with potassium phosphotungstate (2 wt %) stain. A 30 second glow discharged carbon-coated copper grid was used. Con A was dialyzed away from excess salt before use.

Isothermal Titration Microcalorimetry.

ITC experiments were performed using a VP model ITC instrument from MicroCal, LLC (Northhampton, MA). Injections of ligand solutions were performed using a 250 μL computer controlled syringe. The reference power was 25 μCal/sec, and the initial delay was 60 sec. A 5% methanol solution (aq) was added to water resulting in a linear isotherm of positive slope. Next the instrument was calibrated using a protocol provided by the instrument manufacturer in a document titled "The Preparation of RNase A and 2'CMP solutions for Isothermal Titration Calorimetry". The titrations were performed at 30 °C, 3 μL per injection (2 μL for the first injection only), 3.5 minutes per injection, 30 injections, 2 second filter, 6 second injection duration, 300-400 rpm stirring speed, and a reference offset of 20.

Hemagglutination Inhibition Assay.

Lectin Preparation. Approximately 10 mg Con A, or pea lectin, was dissolved over 8 hours in 15 mL HEPES buffer without agitation at 4 °C. The solution was dialyzed (MWCO 1000 Da) against tris-buffered saline (1 L) for 4 hours, then twice against phosphate buffered saline (1 L) for 8 hours to remove excess Ca^{2+} from the solution. The lectin stock solution was stored at 4 °C.

Blood Preparation. Fresh whole rabbit blood in EDTA was added to Alsever's solution to make a 10-20% (v/v) blood solution. The cells were pelleted by centrifugation (2000 rpm, 5 min). Care was taken to avoid hemolysis of the red blood cells. The layer of white blood cells and plasma proteins was removed. Next PBS solution (12 mL) was

added and carefully mixed with the red blood cells, and then the mixture was centrifuged again. This step was repeated, and then a 2% to 8% (v/v) solution of blood was prepared in HIA assay buffer. The assay was easier to visualize at 6-8% (v/v) blood solution.

Lectin titration. Serial two-fold dilutions of the stock lectin solution were made in a Costar 96 well V-bottom microtiter plate by mixing 50 μL lectin solution with 50 μL assay buffer in the first well. Next 50 μL from well 1 was mixed with 50 μL assay buffer in well 2. Next 50 μL from well 2 was mixed with 50 μL assay buffer in well 3, and this was repeated for 24 wells, emptying the excess 50 μL into a separate waste container. To each well 50 μL of the red blood cell suspension was added. After 2 hours (at 25 °C) Each well was examined to determine if agglutination had occurred. If a bead had formed surrounded by clear solution no agglutination occurred. This can be visualized easily in a cell with no lectin. If the solution remained red throughout the well this indicates cell agglutination occurred. The minimum concentration required to agglutinate the red blood cells was determined, called the 1 unit concentration. In the inhibition assays 2 x this concentration (2 unit) or 8 times this concentration (8 unit) lectin was used. The concentration of Con A was determined spectrophotometrically at 280 nm using $A^{1\%}_{1cm}$ = 13.7 at pH = 7.2 and is reported in terms of monomer (MW = 26,500). The concentration of pea lectin was determined spectrophotometrically at 280 nm using $A^{1\%}_{1cm}$ = 15.0 at pH = 7.2, (MW = 49,000).

Inhibiting dose determination. Serial two-fold dilutions of inhibitor were prepared by mixing with assay buffer as done above for lectin dilutions. To each well 50 μL of lectin solution (2 unit for pea lectin, 8 unit for Con A) was added. These were incubated for 3 hours after which 50 μL of blood solution was added to each well. After 2 hours the wells were examined to determine the minimum inhibitory concentration of each inhibitor (the last well where agglutination failed to occur).

CHAPTER 6

POLY(POLYOXOMETALATE) GLYCODENDRIMERS AND POLYOXOMETALATES AS OXIDATION CATALYSTS

Introduction

Metal oxides, anions of early transition metals such as molybdenum, tungsten, vanadium, and niobium, MO_y^{n-}, can self-assemble in solution into discrete clusters $M_xO_y^{n-}$ called isopolyanions, or more generally, polyoxometalates.[135] The structure and properties of polyoxometalates (POMs) bridge small molecule solution phase metal oxide chemistry and large lattice solid-state chemistry. [136] Although the metal atoms may differ, the basic structural principles are the same. Bridging oxygen atoms connect the metal centers, and no metal-metal bonds are formed upon assembly (for example see Figure 6.1). The assembly process remains largely unknown, however, semi-rational synthetic methods are used to construct POMs of different composition, structure, and size. The cluster formation is generally directed by controlling pH and temperature. POMs containing differernt atoms with the general structure $H_wM_xO_y^{n-}$, are also common structures within the class, and they are called heteropolyanions. The most common heteropolyanion atoms are P(V) and Si(IV), yet other metal centers like Co(II,III), Cu(I,II), Al(III), Ti(IV), Zr(IV), Mn(IV), and Fe(III) are often integrated to impart specific properties to the molecules such as magnetism or certain redox character. Heteropolyoxometalate structures include the Keggin anion (Figure 6.2b) and the Wells-Dawson anion (Figure 6.2c).

In 1920 Wu reported the synthesis of an ammonium salt of $P_2W_{18}O_{62}^{6-}$, formed by refluxing sodium tungstate in phosphoric acid.[137] This molecule is composed of eighteen tungstate octahedra encapsulating two phosphate tetrahedra.

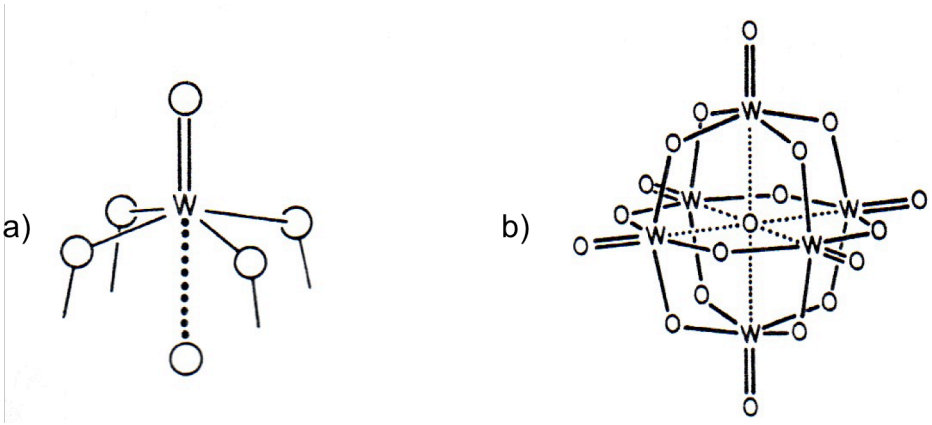

Figure 6.1 A (a) close up of the WO_6 octahedron building block, and the (b) $W_6O_{19}^{2-}$ cluster anion (figure from reference 136).

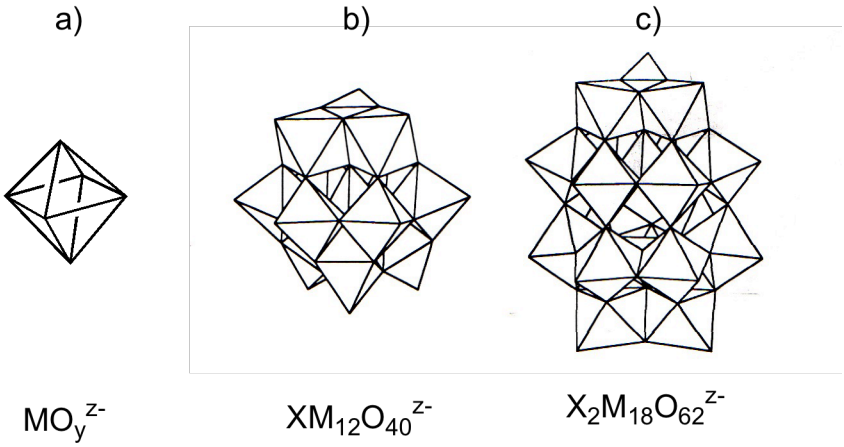

Figure 6.2 Polyhedral representation of (a) a metal oxide octahedron, (b) Keggin, and (c) Wells-Dawson heteropolyoxometalate structures (figure from reference 140).

The major product was later shown to have the Wells-Dawson type structure by x-ray crystallography studies.[138] A minor isomer was also reported differing in the orientation of the cap triad (Figure 6.3[139]). Wu separated the isomers (termed A and B based on differences in their color, ease of reduction, and crystal structure) using forceps. In the 1970's B and A isomers became α and β respectively. Rather than a direct transliteration, the more stable B isomer was labeled α and the less stable A isomer was labeled β to become consistent with accepted POM nomenclature. Modern labs utilize a pH sensitive isomerization reaction to re-orient the cap octahedra in solution.

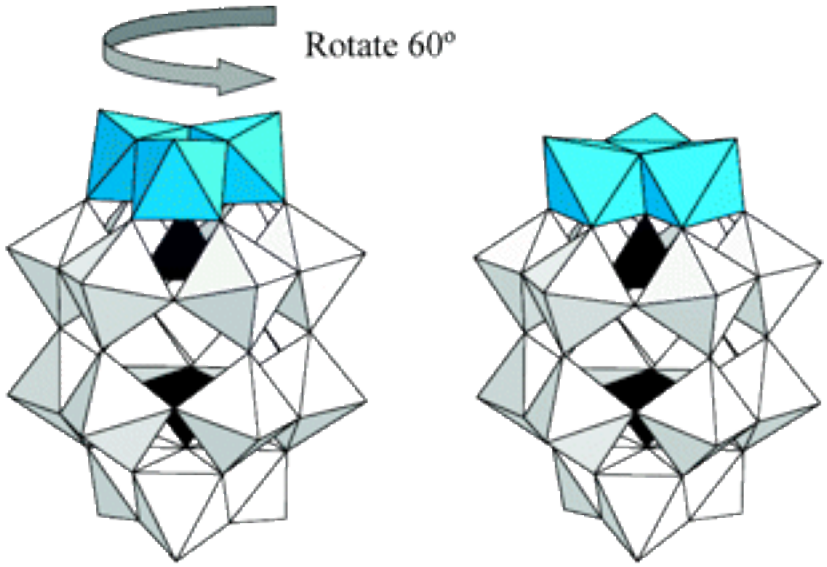

Figure 6.3 α and β Wells-Dawson isomers, differing in the orientation of the cap triad (figure from reference 139).

Through pH changes the clusters in solution can undergo specific partial degradations to lacunary molecules.[140] A single metal oxide, or multiple metal oxides can be removed, and replaced with others (Figure 6.4a) as is done to isomerize Wu's α and β

isomers in solution. The cap triad of octahedra on either the Keggin or Wells-Dawson structure can be chemically removed (Figure 6.4b and 6.4c). These lacunary compounds are the components for a variety of synthetically complex POM structures. For example many POMs are sandwich type clusters (Figure 6.5).

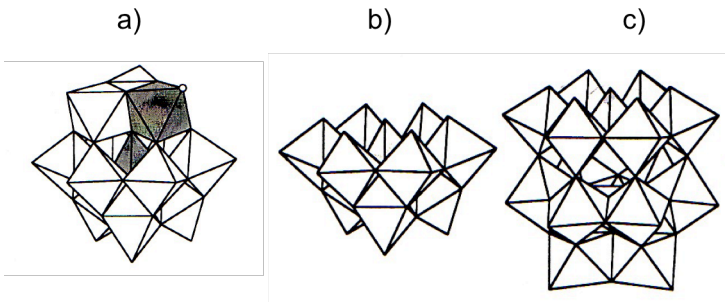

Figure 6.4 A (a) monosubstituted Keggin anion, (b) trivacant Keggin anion, and (c) trivacant Wells-Dawson structures (figure from reference 140).

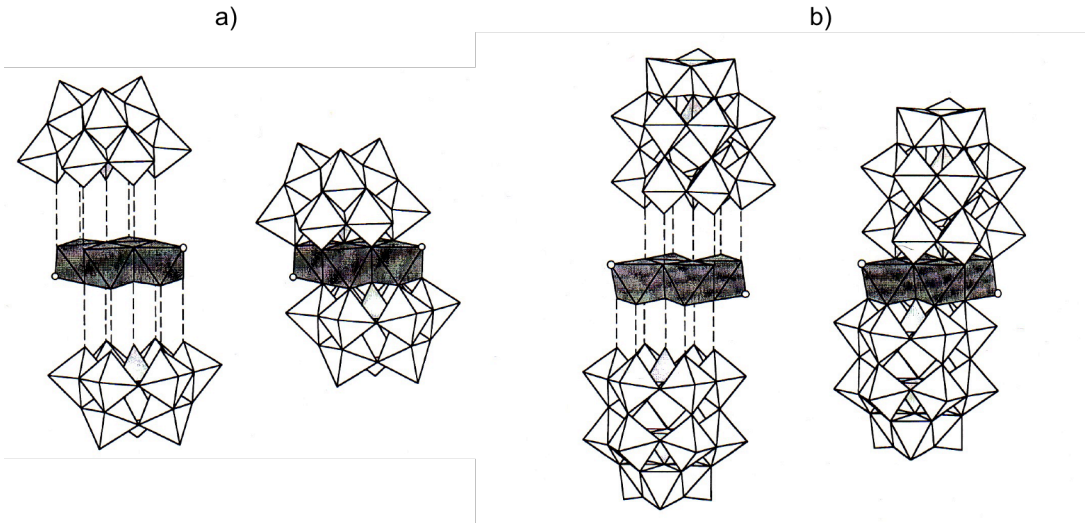

Figure 6.5 Polyhedral representation of a sandwich type heteropolyoxometalates (a) from lacunary Keggin anions i.e. $[M_4(H_2O)_2(P_2W_9O_{34})O_2]^{10-}$, and from lacunary Wells-Dawson anions i.e. $[M_4(H_2O)_2(P_2W_{15}O_{56})O_2]^{16-}$, M(II) = Mn, Ni, Co, Cu or Zn (figure from reference 140).

Solubility properties, and catalytic activity to some extent, can generally be tuned by choice of counter-ions for the metal anion clusters. Proton counter-ions with heteropolyoxometalates make up the class called heteropoly-acids (HPAs). The HPA class of POM catalysts is relatively large and heavily researched.[141] HPAs can have very strong Brönsted acidity and fast multi-electron redox transformations, making them suitable catalysts. In several industrial settings HPAs are used as catalysts. A popular example is HPAs used in the bleaching of wood pulp; a task formerly performed using chlorine leading to chlorinated aromatics and dioxins, which pose more serious environmental hazards.

Non-acidic POMs are sometimes highly active catalysts as well. Neumann *et. al.*, demonstrated the utility of the sandwich type POM $Na_{12}[ZnW(VO)_2(ZnW_9O_{34})_2]$ in conjunction with chiral hydroperoxides and hydrogen peroxide in the epoxidation of allylic alcohols (Scheme 6.1).[142] High enantiomeric excess (>90) and high yields (>90%) were achieved on a variety of allylic alcohols using only 0.002 mol % to 0.01 mol % of catalyst POM. Along with alkene epoxidation, POM catalysts oxidize alcohols, sulfides, and aromatic functionalities as well.[143, 144]

In the same class with HPAs and sandwich complexes, transition metal substituted POMs have demonstrated catalytic activity. In these cases lacunary precursors are exposed to other metal oxides that assemble to fill in the gaps left from cleavage.

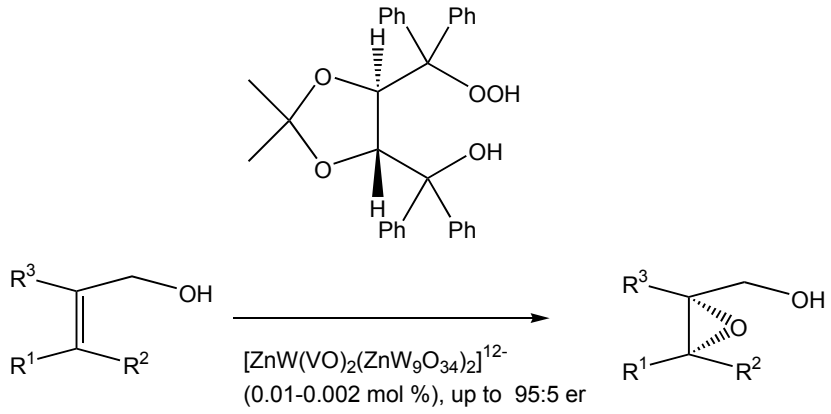

Scheme 6.1 Oxidation of allylic alcohols by a chiral peroxide and catalytic sandwich type polyoxometalate.

Harlemarker and Pope first synthesized mono, di, and tri vanadium substituted $P_2W_{18}O_{62}^{6-}$ to form $P_2W_{17}VO_{62}^{n-,}$ $P_2W_{16}V_2O_{62}^{n-,}$ and $P_2W_{15}V_3O_{62}^{n-}$ (charge, n, varies with vanadium oxidation state) polyoxanions with vanadium in both V(IV) and V(V) states.[145] Finke later refined the synthesis of the trivanadium substituted analog, composed with tetrabutyl ammonium counter-ions for organic solvent solubility.[146] In this report the authors indicated "this compound $[[Bu_4N]_5H_4P_2W_{15}V_3O_{62}]$ appears to be extremely sensitive to alcohols, with the irreversible development of multiple species indicated by ^{31}P NMR immediately following exposure to methanol". Taking advantage of this observation, Hill *et. al.* reported the alkyloxy-bound vanadium substituted POM $[RC(CH_2O)_3V_3P_2W_{15}O_{59}]^{9-}$ and its use in the catalysis of tetrahydrothiophene to tetrahydrothiophene oxide with a variety of oxidants including aqueous hydrogen peroxide (Scheme 6.2).[147] The organic triol bound the vanadium-substituted cap by the formation of a tri-vanadium ester. The catalytic activity of these polyoxometalates were dependent on counter-ion: H^+/alkylated > TBA/alkylated > TBA/POM nonalkylated > no catalyst (TBA = tetrabutyl ammonium).

In these papers many important properties of alkylated vanadium substituted polyoxophosotungstates were introduced, among them:

1) The vanadium esters formed by these POMs with alcohols were hydrolytically stable and irreversibly formed.

2) The complete alkylated POM cluster was the active catalytic species and decomposition products were minimal, even in the presence of hydrogen peroxide.

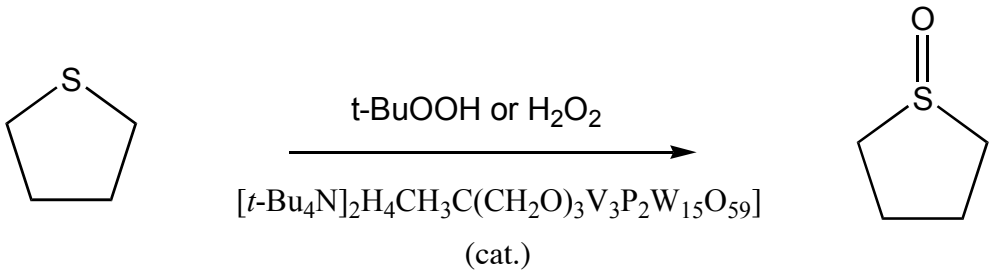

Scheme 6.2 Oxidation of tetrahydrothiophene to tetrahydrothiophene oxide.

The proposed mechanism of catalysis of tetrahydrothiophene oxidation using t-butyl peroxide and $[CH_3C(CH_2O)_3V_3P_2W_{15}O_{59}]^{6-}$ (labeled 1-CH_3) is shown in Figure 6.6. The expected cooperation of two catalytic sites is very interesting. If two or more catalyst monomers were bound covalently to one another on the surface of a dendrimer, enhanced catalytic activity may be expected. Dendrimers are nicely suited scaffolds for catalysts for other reasons as well.[148-150] Heterogeneous catalysts are easily separated from the reaction mixture though low catalytic activities are usually observed. Homogeneous catalysts are generally more active and specific, but more difficult to remove. Dendrimers as catalyst and catalyst scaffolds can bridge this gap by remaining soluble in the reaction medium, yet easily separable based on size exclusion techniques.

As mention earlier in reference to POMs, dendrimers combine the attributes of small soluble and large insoluble molecules.

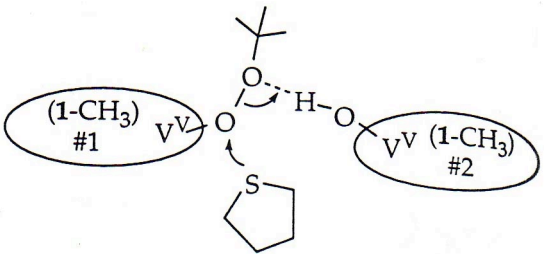

Figure 6.6 Proposed transition state in the oxidation of THT by vanadium substituted POMs. (1-CH_3) represents $[CH_3C(CH_2O)_3V_3P_2W_{15}O_{59}]^{6-}$ (figure from reference 147).

By judicious choice of a dendrimer scientists can control the microenvironment of a reaction. In a case presented by Twyman and Martin a simple deacetylation reaction (Scheme 6.3) in water was accelerated using a PAMAM dendrimer with surface primary amines, versus N-acetyl ethylenediamine, an amine substrate selected to match the structure of the dendrimer arms.[151] The p-nitrophenol acetate is first bound within the dendrimer, and primary amine from the dendrimer surface initiates the amide bond formation, in a transition state stabilized by the dendrimer amide N-H bonds (Figure 6.7). The p-nitrophenolate leaving group is measure by UV-Vis Spectrometry at 390 nm, the measured rate profiles of the different amines are shown in figure 6.8. The proposed explanation for the dramatic increase in the rate of aminolysis is the hydrophobic p-nitrophenol acetate is encapsulated within the relatively hydrophobic dendrimer interior in buffered aqueous solution, and with the chemically very similar N-acetyl ethylenediamine, no such encapsulation occurs.

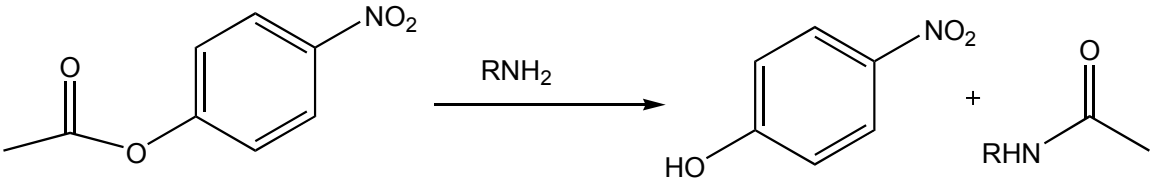

Scheme 6.3 Aminolysis of p-nitrophenol acetate, R represents N-acetyl ethylenediamine or PAMAM dendrimer interiors.

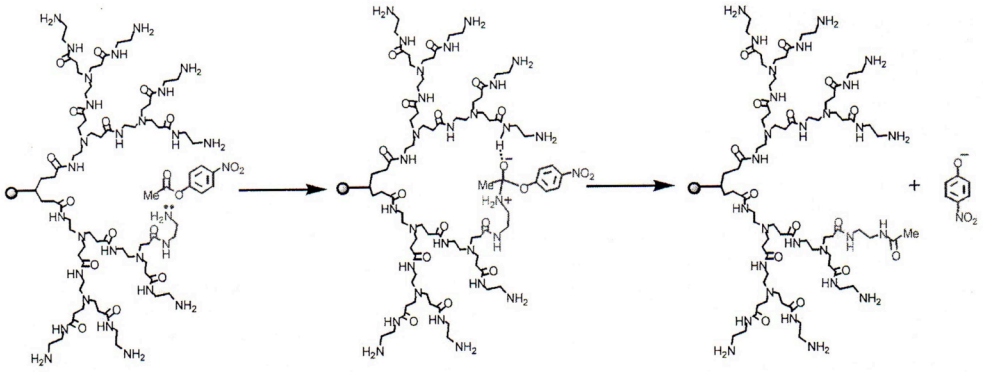

Figure 6.7 Proposed mechanism of aminolysis encapsulated in a PAMAM interior (figure from reference 149).

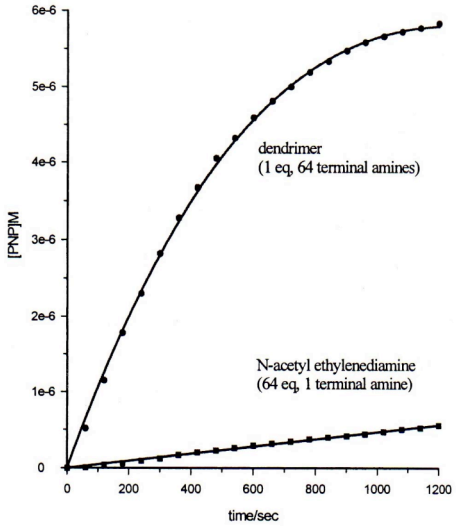

Figure 6.8 Rate profile for aminolysis reactions using PAMAM dendrimer and N-Acetyl ethylenediamine (figure from reference 149).

In one case presented by Newkome and Hill, Generation(0) hydroxylated dendrimers were functionalized with four copies of the $P_2V_3W_{15}O_{59}^{6-}$ anion.[152] Again the oxidation of tetrahydrothiophene was used as an example reaction, however the reaction was affirmed in this study to be completely acid-catalyzed. There was no comparison in catalytic activity between the POM functionalized dendrimer and POM alone, nor was there any demonstrated catalytic advantage for using the small dendrimer, as the authors proposed this study as a model for later using commercially produced polyhydroxylated polymers such as polyvinyl alcohol.

While this work is the only known precedent for poly(POM) dendrimers, metallodendrimers are an increasingly versatile class of molecules and other types of metal clusters have been used to decorate the dendrimer periphery, even with large dendrimers. Astruc *et. al.* bound $[Ru_3(CO)_{12}]$ clusters, known to catalyze the cyclocarbonylation of yne-aldehydes,[153] to G(3.0) diaminobutane (DAB) dendrimers with a phosphine linker.[154]

POMs and dendrimers have been used together for mutual advantages in catalysis in a few research publications, such as the construction of multilayer nanocomposite surfaces on electrodes with PAMAM dendrimers and a phosphomolybdate. These functionalized electrodes were used as bifunctional catalysts for the reduction of nitrite or the oxidation of arsenite.[155, 156] In these cases the PAMAM dendrimer serves to increase the surface permeability and enables layer by layer deposition into a multilayer assembly surface.

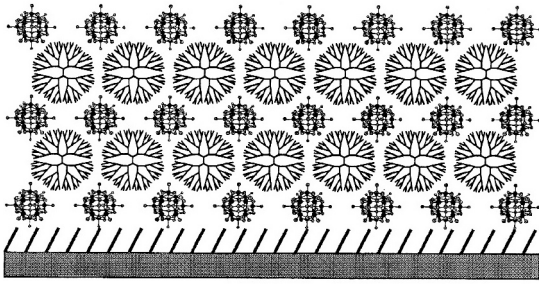

Figure 6.9 Multilayer nanocomposite formed from layer by layer deposition of $PMo_{12}O_{40}^{3-}$ and PAMAM dendrimers on a gold electrode coated with 4-aminothiophenol (figure from reference 155).

Hyperbranched polymers are quite similar to dendrimers, as branched macromolecules. Neumann *et. al.* combined alkylated polyethylenimine (Alk-PEI) polymer cations, a hyperbranched polymer, and POMs $[PO_4[WO(O_2)_2]_4]^{3-}$ or $[ZnWZn_2(H_2O)_2(ZnW_9O_{34})_2]^{12-}$ anions for use in aqueous biphasic catalysis (Figure 6.10).[157] The catalyst POM and Alk-PEI form a water-soluble complex electrostatically bound together. The complex has hydrophobic regions able to solubilize organic, water-insoluble, substrates. The enzyme like complexes were combined with hydrogen peroxide in water with "very hydrophobic" substrates, such as diphenyl sulfide, cyclooctene, or styrene. The oxidation reaction products diphenyl sulfone, cyclooctene oxide, and benzaldehyde were formed, respectively, with very high conversion percentage, and if the PEI is unmodified (nonionic), or absent, the reaction yields were negligible. Aqueous biphasic catalysis is highly desirable, particularly for industrial applications.[158]

As shown in Figure 6.10, the substrate can be coordinated with the catalyst in an enzyme like fashion and the product can be easily removed while the aqueous catalyst phase is recycled. In this manner homogeneous catalysts can be used effectively without

more complex separation methods. On smaller laboratory scale the organic products are extracted from the mixture with an organic solvent, however on the industrial scale organic solvents may be bypassed altogether, and this environmental benefit is also highly desirable.

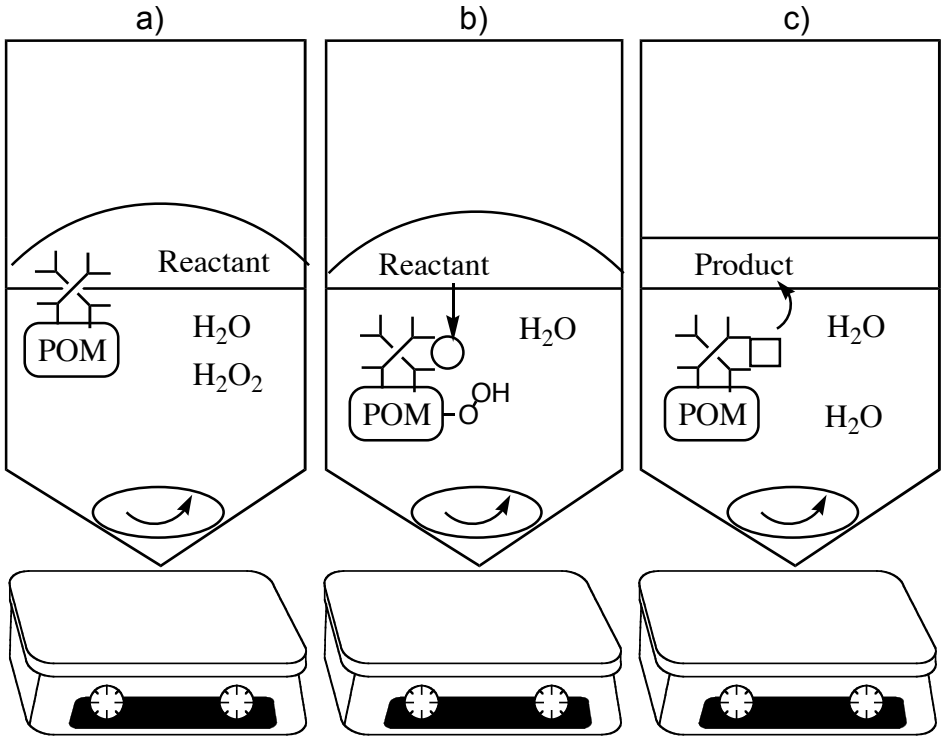

Figure 6.10 Aqueous biphasic catalysis using hyperbranched polymers or dendrimers. The a) POM/macromolecule complex in water b) coordinates the hydrophobic reactant with the active catalyst and oxidation occurs in the aqueous phase (circle to square) c) expelling the product into an organic phase upon completion.

Research Goals

The goal of this project was to synthesize poly(POM) dendrimers in order to coordinate catalysts and substrates for increased catalytic activity, taking advantage of the

hydrophobic dendrimer interior for substrate encapsulation, catalyst proximity for cooperative effects in a bis-catalyst transition state, the use of mild oxidants for organic oxidation, and size separation for clean removal of the catalyst from the reaction mixture, or phase separation of products from aqueous biphasic reactions.

In addition it was necessary to explore new oxidation reactions on which to test the poly(POM) dendrimer catalyst that occur at near normal pH, because dendrimers degrade under the acidic conditions employed in the alkoxy-POM examples described above, and POMs are often unstable under basic conditions. Oxidation at neutral conditions would presumably also increase the generality of substrates substantially.

A secondary goal was to develop a method to bind POMs onto a dendrimer scaffold for future experiments in magnetics. Some POMs, such as polyoxovanadates (IV) are comprised of magnetic ions, also, nonmagnetic POMs can encapsulate small clusters of magnetic ions such as Ni(II) and Co(II).[159] These clusters are being explored for novel magnetic properties, and new magnetic materials. The Cloninger and Singel research groups have demonstrated that spin-spin interactions on a dendrimer surface occur,[74] and magnetically active POMs interacting on dendrimers may aid in bridging the gap between large scale and molecular scale magnetics.

Polyoxometalate Synthesis

The polyoxometalate $(Bu_4N)_5H_4P_2W_{15}V_3O_{62}$ **74** was prepared as previously described and shown in Scheme 6.4.[146, 160, 161] Refluxing sodium tungstate with concentrated phosphoric acid formed the phosphotungstate cluster **70**. Precipitation as

the potassium salt to both α (major) and β (minor) isomers completed the first step, a reaction first discovered by Wu in 1920.[137] The mixture was treated with base, partially degrading the cluster anion, followed by cluster regeneration in hydrochloric acid. This reaction transformed much of the β isomer into the desired α form **71**. This isomerization is observable by ^{31}P NMR (Figure 6.11) where the minor peaks at -11.2 and 12.0 ppm in figure 6.11a corresponding to the β isomer, asymmetrical about the interior phosphates, are nearly gone in figure 6.11b. The resulting major signal at -12.7 ppm results from the symmetrical α isomer. The crystal structure of the α isomer was first published in 1953.[138]

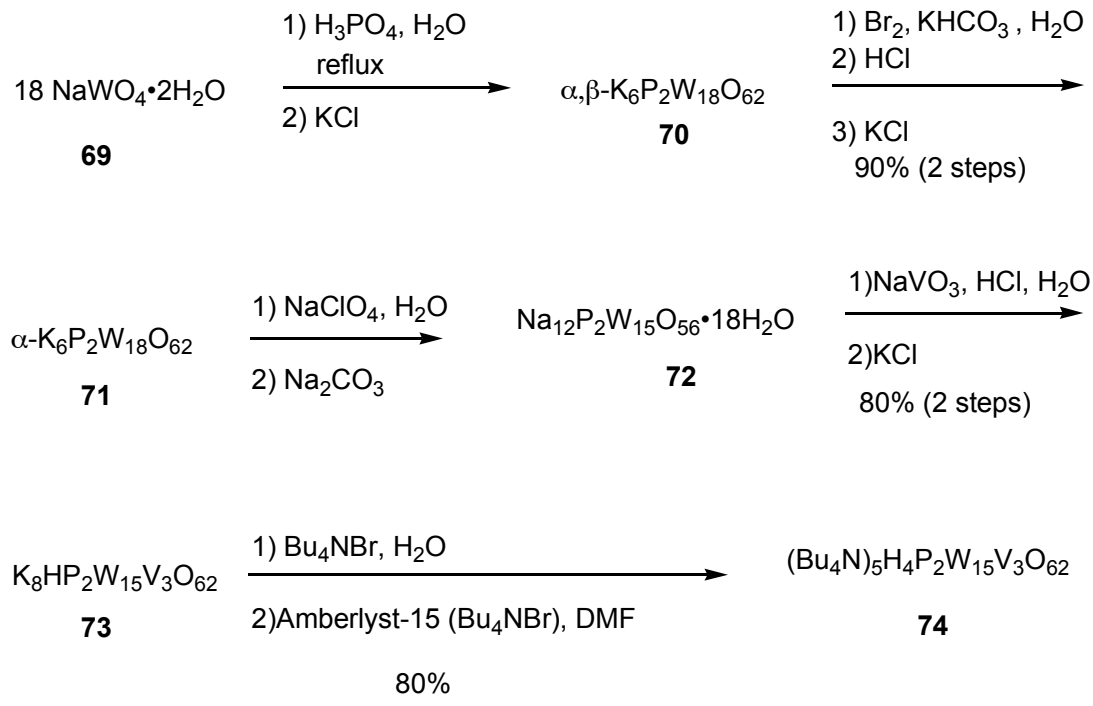

Scheme 6.4: Synthesis of $(Bu_4N)_5H_4P_2W_{15}V_3O_{62}$ (**74**).

Sodium perchlorate addition displaced the potassium cations, followed by treatment with base precipitated the lacunary precursor **72** as a sodium salt. This metastable intermediate was the topic of an important report by Finke *et. al.* in 2002 wherein multiple published syntheses were investigated and compared.[161] The tests concluded Contant published the best synthesis in 1990.[162] Our later synthesis of this material reflected the updated procedure, altering the rate of base addition, the amount of base added, and the reaction temperature. NMR is inadequate to reliably characterize this cluster, as discussed in Finke's report, due to poor stability.

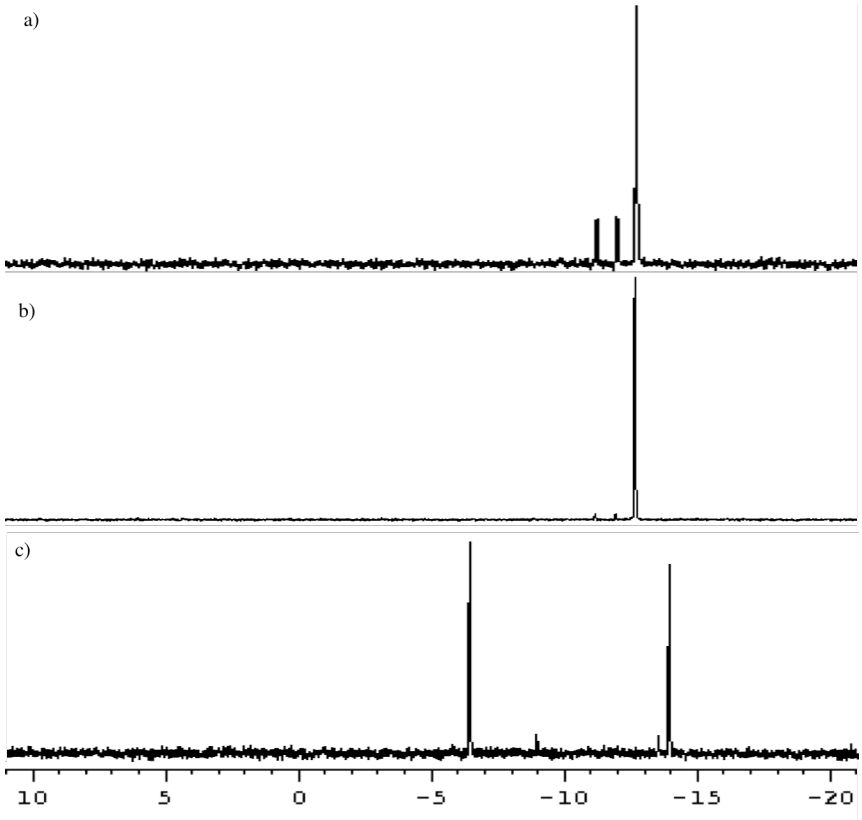

Figure 6.11: ^{31}P NMR spectra of a) αβ-$K_6P_2W_{18}O_{62}$ **70**, b) α-$K_6P_2W_{18}O_{62}$ **71** and c) $K_8HP_2W_{15}V_3O_{62}$ **73**.

In the presence of sodium metavanadate at low pH the lacunary species **72** bound vanadates forming the trivanadium-substituted polyoxotungstate anion (Figure 6.12). This cluster was readily recrystallized as the octapotassium salt into large orange red crystals **73**, 94% pure by ^{31}P NMR (Figure 6.11c), where two distinct phosphorous signals are observed. The minor peaks seen in Figure 6.11c are due to primarily $P_2W_{16}V_2O_{62}^{8-}$.

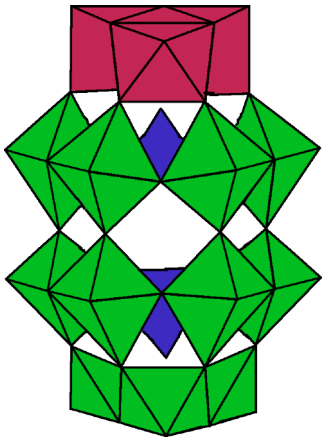

Figure 6.12: Polyhedral representation of the $P_2W_{15}V_3O_{62}^{9-}$ anion. Red represents vanadates, blue represents phosphates, and green represents tungstates; counter-ions not shown.

Exposure of a solution of **73** to tetrabutylammonium bromide (TBAB), followed by cation exchange in DMF with an Amberlyst 15 cation exchange resin charged with TBA cations resulted in the pale orange powder **74**. The TBA salt of the anion shown in Figure 6.12 was soluble in organic solvents such as dimethylformamide or acetonitrile and insoluble in water. Slow drying and careful protection from light proved to be essential for the isolation of the orange product. ^{31}P NMR yielded major peaks at –8.7

ppm (phosphorous proximal to vanadium triad) and –14.3 ppm (phosphorous distal from vanadium triad).

In solid or solution phase **74** may undergo a color change from orange to green. This corresponds to the photosensitive reduction of V(V) to V(IV). Reduction rate appears to depend also on solvent: DMF > CH_3CN > DMA. In the presence of organic molecules the reduction rate also increases, for example ethanol > isopropanol ≥ triethylamine.

Vanadium Esterification Reactions

Hill *et. al.* reported binding various alcohols to the trivanadium substituted POM **74** by the formation of vanadium esters.[147, 152] These experiments were successfully examined in our labs (Scheme 6.5) using methanol binding to POM **74** using ^{51}V and ^{31}P and ^{1}H NMR (Figure 6.13). The relative amounts of triester, diester, and monoester (**75-77**) could be controlled with alcohol concentration.

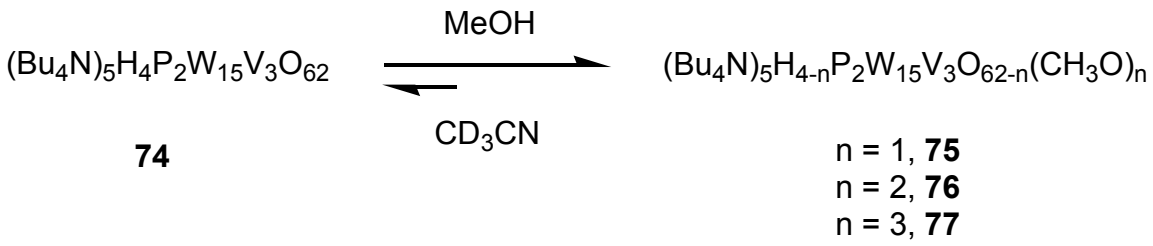

Scheme 6.5: Vanadium esterification of POM **74** with methanol in CD_3CN forming mono, di, and triesters 6a, 6b, and 6c.

POM counter-ions may be changed although this affects reactivity. For example, the water-soluble potassium salt **73** (see Scheme 6.4) failed to bind methanol even in the

presence of 18-crown-6. Finke *et. al.* developed a method to replace TBA cations with sodium cations in transition metal substituted POMs.[163, 164]

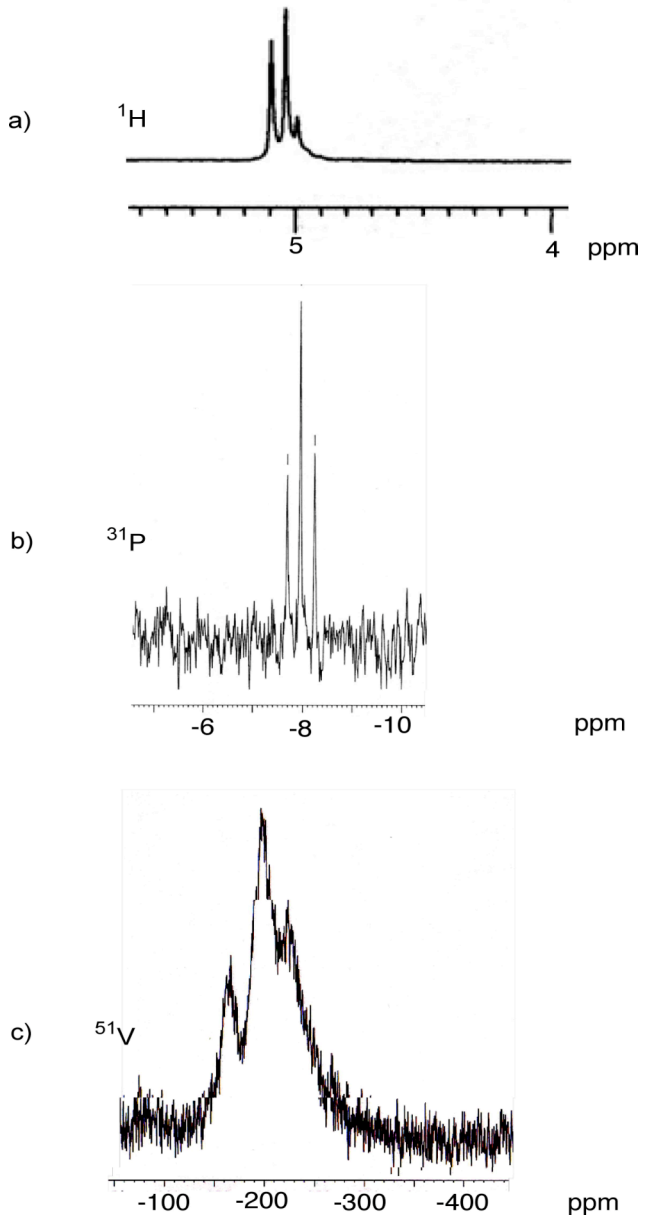

Figure 6.13: a) ^{1}H NMR of mono **75**, di **76**, and triester **77**, b) ^{31}P NMR mono **75**, di **76**, and triester **77** and c) ^{51}V NMR mono **75**, di **76**, and triester **77**.

The TBA-POM **74** was mixed with sodium tetrafluoroborate in acetonitrile and dilute sodium hydroxide was added. A yellow water-soluble precipitate formed and was purified by dialysis. The yield for this reaction was very low (< 8%) yet it resulted in a water soluble POM with ^{31}P NMR signals at –6.5 ppm and –13.7 ppm and a MALDI-TOF MS parent ion at m/z = 2136, corresponding to what may have been a doubly charged $Na_9P_2W_{15}V_3O_{62}\bullet 9H_2O$ (**78**). To verify the formation of this product, elemental analysis should be performed. However prior to that analysis, it was discovered that the water-soluble POM did not react with methanol. Further studies of this cluster were therefore postponed.

Synthesis of Alcohol Surface Functionalized Dendrimers

Dendrimers with alcoholic surface functionality were required for POM surface attachment. In each case PAMAM dendrimers with surface primary amines was bound using an appropriate isothiocyanate (Chapter 1). Three different isothiocyanato alcohols were bound: *p*-isothiocyanato-α-D-mannopyranoside **80** (Scheme 6.6a), 2-(2-isothiocyanatoethoxy)ethanol **29** (Scheme 6.6b), and 1-O-(5-isothiocyanato-3-oxapentyl-2,3,4,6-tetra-o-acetyl-α-D-mannopyranoside **81** (Scheme 6.6c), deacetylation was performed after addition to the dendrimer. Each dendrimer was made according to recently published methods.

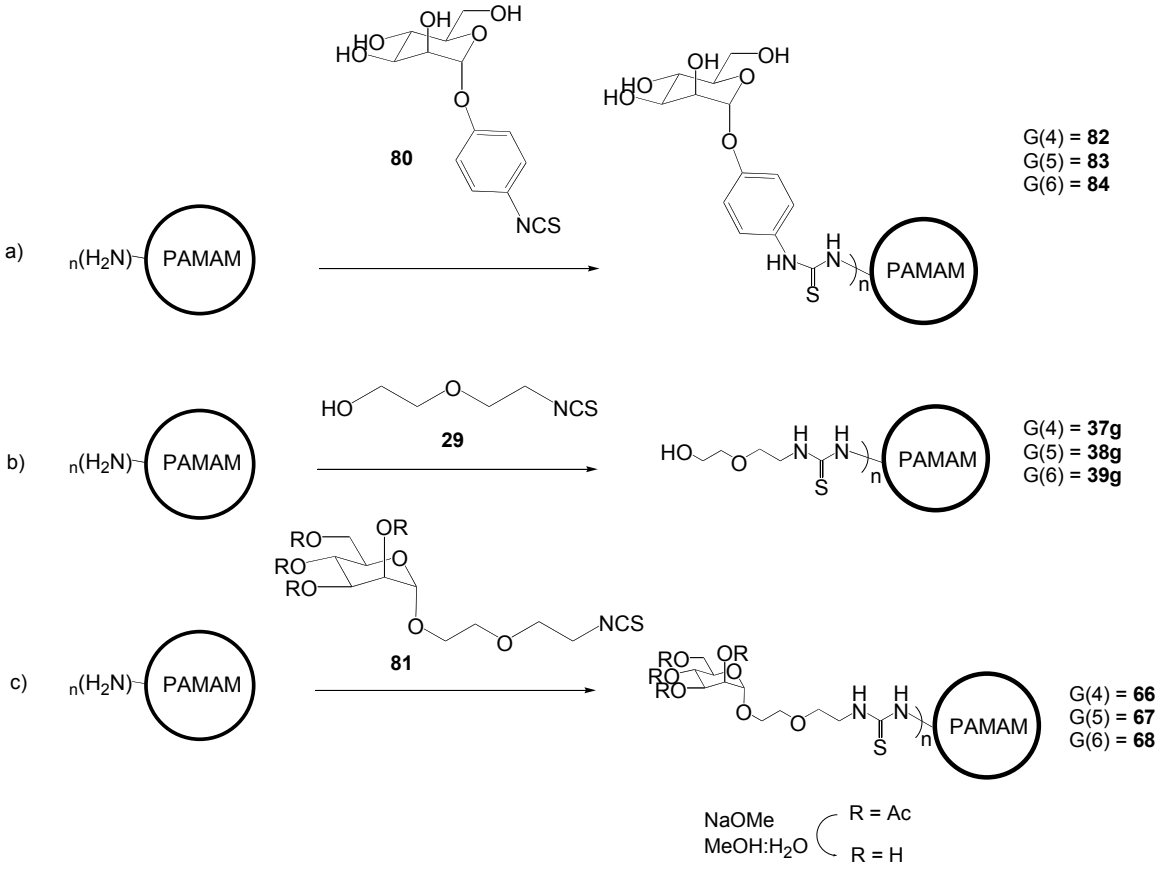

Scheme 6.6 Synthesis of (a) phenyl mannoside dendrimers **82-84**,[161] (b) ethoxyethanol dendrimers **37g**, **38g**, and **39g**, and (c) ethoxyethanol linked acetylated mannoside dendrimers **66-68**.[72]

The phenyl linked mannose was made in two steps from the commercially available nitro compound by reduction, using hydrogen with Pd/C, to the amine **79**, followed by formation of the isothiocyanate **80** using thiophosgene, in a procedure slightly modified from literature reports (Scheme 6.7).[71] The ethoxy-ethanol linker **29** was made synthesized in one step from the primary amine using thiophosgene (Chapter 2).

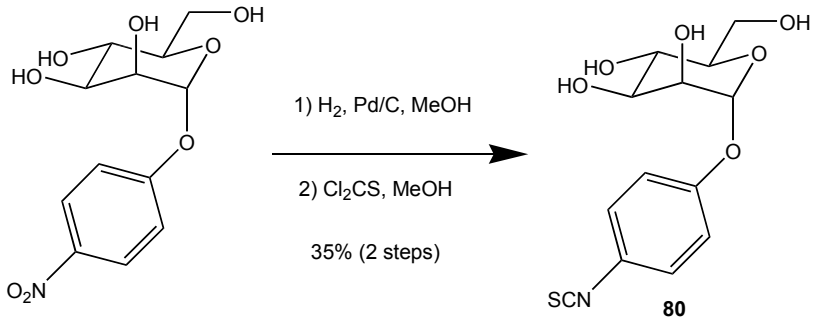

Scheme 6.7 Synthesis of *p*-phenyl mannose isothiocyanate **80**.

The mannose isothiocyanate **81** was synthesized as previously reported in one step from mannose trichloroacetimidate **8** (Scheme 6.8).[72]

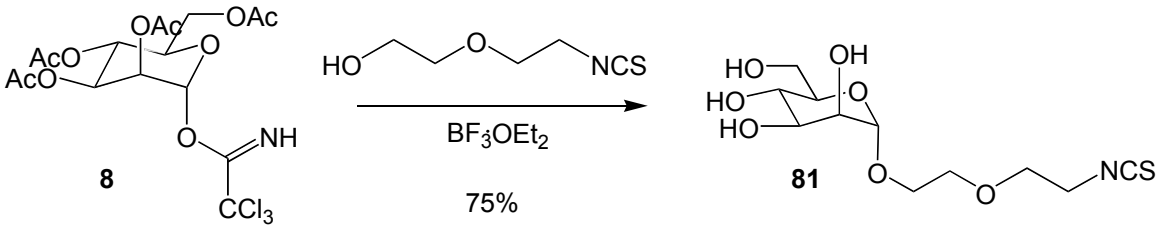

Scheme 6.8 Synthesis of isothiocyanato-ethoxyethyl mannoside **81**.

These isothiocyanates were used to functionalize generations 4,5, and 6 PAMAM surfaces as previously described (Chapter 2) by the formation of a thiourea (Scheme 6.6) followed by purification by dialysis. Acetylated mannose functionalized dendrimers N underwent global deacetylation using Zemplen conditions. Alcohol surface functionalized dendrimers were characterized by ^{1}H and ^{13}C NMR and MALDI-TOF MS (Table 6.1), scaffolds were used for POM binding. The number of endgroups was calculated from the difference in weight average molecular weight between the starting PAMAM dendrimer and the final hydroxy-functionalized dendrimer divided by the molecular weight of the corresponding isothiocyanate.

Compound	M_W (Da)	# Endgroups
82	29400	51
83	54000	91
84	85000	102
37g	21400	54
38g	43000	119
39g	77000	163
66	30500	54
67	57500	102
68	101000	153

Table 6.1 Characterization data for dendrimers **82-84**, **37g**, **38g**, **39g**, and **66-68**.

Synthesis of Poly(POM) Dendrimers[165]

Vanadium esterification between the polyoxometalate **74** and hydroxylated dendrimers (Scheme 6.9) was straightforward in planning, and less simple in practice. One particular hurdle was the light sensitivity of POM **74**, a solvent dependent feature. The dendrimers **82-84, 37g-39g, 66-68,** also have a narrow window of appropriate solvents. Using dimethyl acetamide (DMA) as the primary reaction solvent was optimum for solubility and the prevention of vanadium reduction, except for phenyl linked mannose dendrimers **82-84**, where reduction remained problematic. Careful elimination of solvents used in dendrimer synthesis, such as DMSO, and minimization of light exposure were techniques that were refined as these efforts proceeded.

Scheme 6.9a shows the synthesis of **8**5-**87** and Scheme 6.9b shows the synthesis of **88**–**90**, although the scheme is not meant to imply that the number identity of the hydroxyl groups on mannose or the number of ethoxyethanol units that tether to **74** is known.

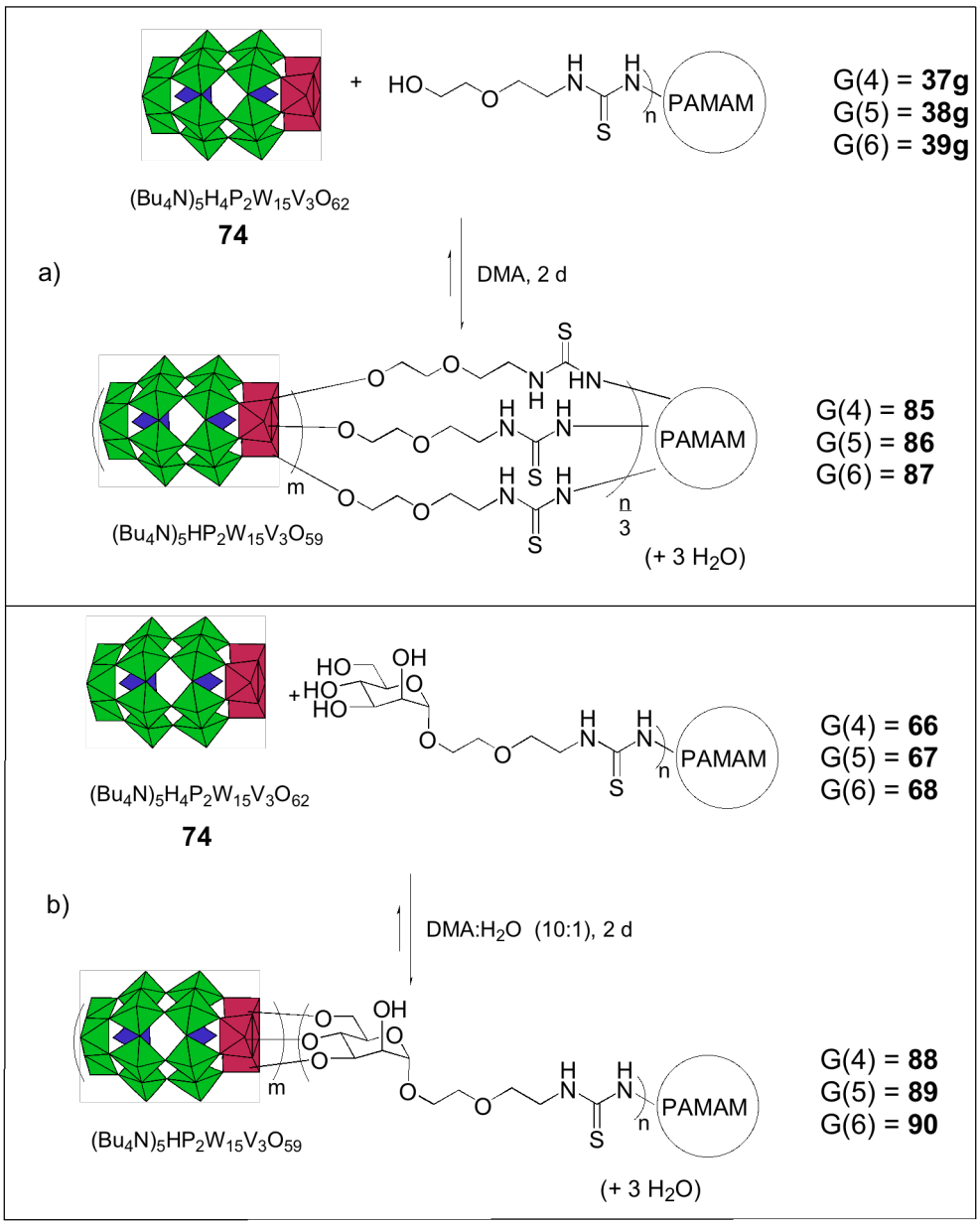

Scheme 6.9 Syntheses of metallodendrimers (a) **85-87** and (b) **88-90**. The number of dendrimer endgroups, n, is given in Table 6.1. The number of POMs, m, was determined by MALDI-TOF MS and is reported in Table 6.2.

Another facet of this synthesis was the equilibrium of vanadium esterification in solution, a feature learned belatedly. Literature precedent seemed to clearly indicate an

irreversible covalent bond formation,[146, 147] but attempts to purify compounds **85-90** from free polyoxometalate in solution were unsuccessful due to equilibration. The most commonly attempted purification route was separation by size, because POM **74** weighed 5181 g/mol and the poly(POM) dendrimers weighed 21,400 g/mol to 257,000 g/mol. Dialysis was unsuccessful and commonly led to a dark green product indicative of V^{V} to V^{IV} reduction. Solvent extraction of free POM, using acetonitrile for example, failed as well. Conversely, precipitation of the dendrimer products could possibly have been used, but solution characterization would remain a problem, and dendrimer solubility is typically determined by surface functionality. Size exclusion gel media such as Sephedex G50 was employed in both column chromatography (fractions monitored by MALDI-MS) and centrifugation methods, and both failed to yield poly(POM) dendrimers.

Gel Permeation Chromatography (GPC) on a Waters HPLC instrument provided at least some product identification. Dendrimers **82-84** were mixed with POM **74** in DMSO and then were analyzed by GPC. Figure 6.14 is data derived from the analysis of dendrimers **82-84** alone, initially intended to serve as calibration data. When dendrimer-POM conjugates were analyzed the resulting retention times matched the retention for dendrimer alone. No signal for individual POMs was observed. We postulate the dendrimer-bound POM interacted with the exclusion cavities in the medium of the column, promoting the release of POM from the dendrimer. The result after GPC was simply dendrimer lacking any bound POMs.

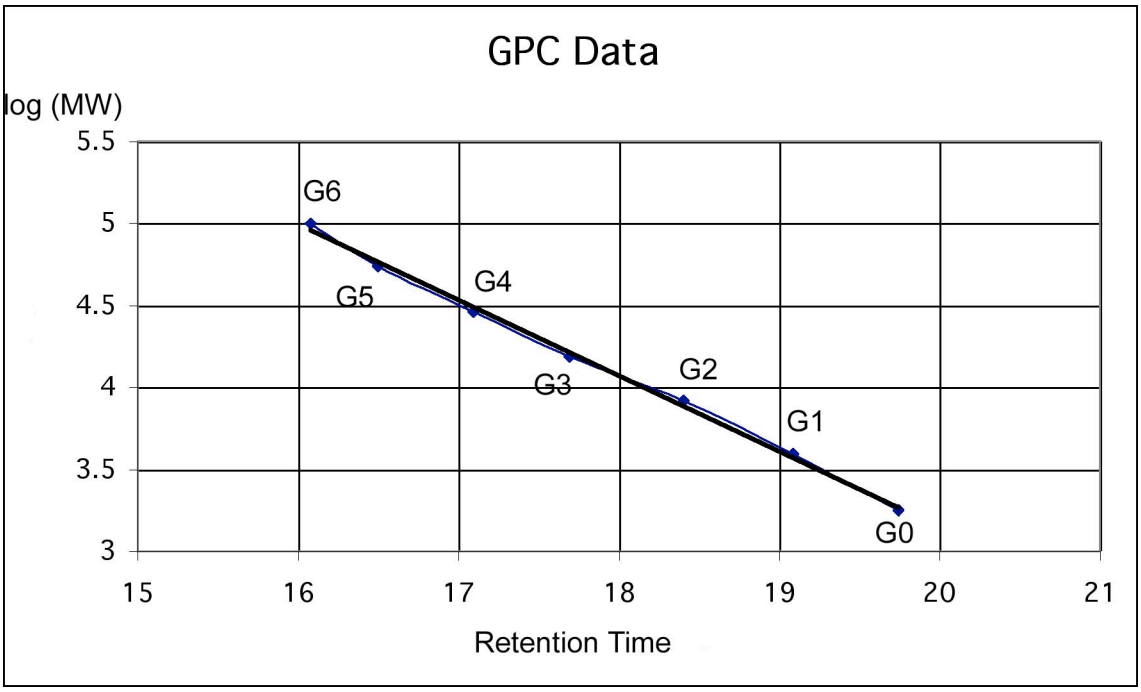

Figure 6.14 Gel Permeation Chromatography data for *p*-phenyl mannose functionalized dendrimer Generation **82-84**.

Accepting the nature of the equilibrium based on discussions with experts in vanadium chemistry and a thorough re-analysis of pertinent literature was essential to moving forward.

The physical limitations of NMR also added complexity in the analysis of the poly(POM) dendrimers **85-90**, even given the mixture of poly(POM) dendrimers and free POM **74**. The large particle size resulted in fast T_2 and dramatically increased line broadening. ^{1}H and ^{51}V NMR, while interesting in analysis of vanadium esterification with methanol, were far less revealing when analyzing dendritic materials. ^{31}P NMR also exhibits linebroadening effects, though less severe. Figure 6.15 is an example of ^{31}P NMR of compound **85** in DMA. This spectrum indicates two major broadened peaks (A

and B), which may result from bound POM, and a single large sharp peak (C). The latter signal (C) could be assigned to free POM **74**. This signal is observed near where the phosphorus more distant from the vanadium cap is expected. However, there is no complementary large sharp peak observed corresponding to the phosphorus proximal to the vanadium end. The synthesis of POM **74** includes trace amounts of different polyoxometalate species, such as the heptadecatungstate divanadate, that may be responsible for the less significant peaks (D). These minor peaks represent 3% to 11% of the ^{31}P relative to A, B, and C in dendrimers **85-90**.

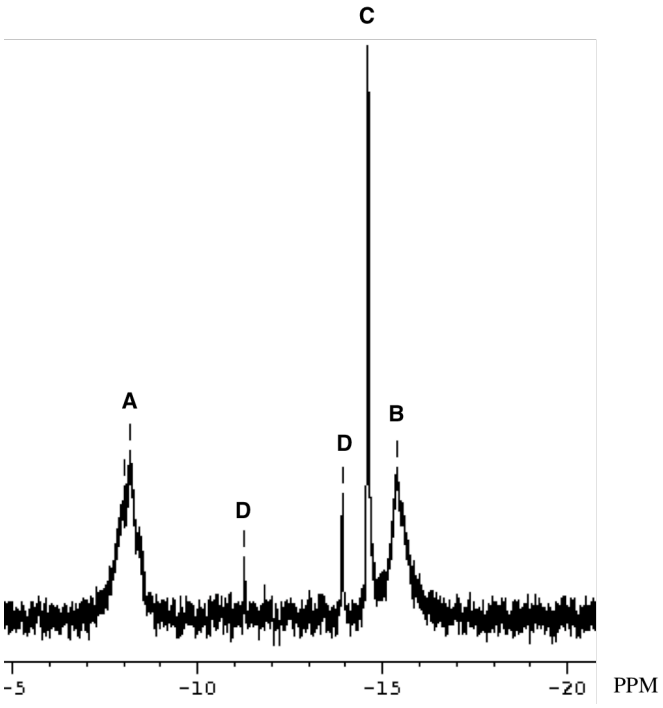

Figure 6.15 ^{31}P spectrum of compound **85**.

While this data is certainly interesting, it was necessary to rely on dried analyte techniques for product characterization such as MALDI-TOF MS and Transmission Electron Microscopy (TEM).

Multiple TEM images were acquired for generation (6) poly(POM) dendrimer **90**, the largest synthesized, to obtain the best possible resolution (Figure 6.16). The particle diameters were measured using the instrument software. The edges of each particle appear roughened because the scale of the dendrimers approaches the scale of the background.[166] The average measured diameter (eighty individual measurements) of poly(POM) dendrimer **90** was 11nm, slightly smaller than expected possibly due to drying effects. Also apparent is the darker interior of each particle. Unstained images like Figure 6.16 will not display the organic portions of these molecules.

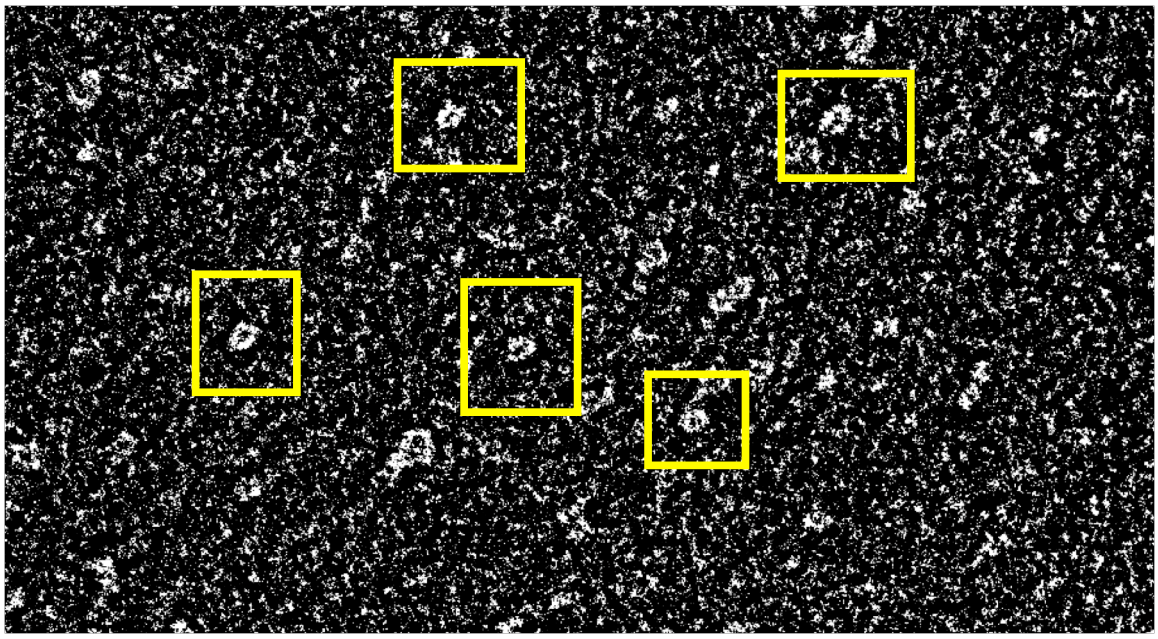

Figure 6.16 Transmission electron micrograph of compound **90**, average particle diameter = 11nm.

MALDI-TOF spectra of poly(POM) dendrimers provided perhaps the most information on the particles constructed, such as the number of POM clusters bound to each hydroxylated dendrimer (Table 6.2, Figure 6.17). To better optimize the MALDI-TOF MS signal a variety of analyte concentrations were examined spanning from 36,000:1 to 1000:1 analyte to matrix ratio. The number of polyoxometalate clusters bound to each dendrimer was calculated from the difference of poly(POM) dendrimer M_W and hydroxyl-functionalized/mannose-functionalized dendrimer M_W followed by division by 5181 g/mol, the molecular weight of POM **74**. The MALDI-TOF MS data for compounds **85-90** are reported in Table 6.2 as the average of three individual measurements (except **88** where two identical measurements was considered adequate). The polydispersity index for the experimental molecular weights of each compound are less than 1.05 and the peak shapes of the product dendrimers are very similar to those of hydroxyl-functionalized/mannose-functionalized dendrimers, indicating the broad peaks arise from defects in the dendrimer starting materials.

Compound	M_W (kDa)	Polydispersity	# POM
85	72	1.01	10
86	125	1.02	16
87	223	1.02	28
87	84.5	1.01	10
89	149	1.02	18
90	257	1.02	30

Table 6.2 MALDI-TOF data of compounds **85-90**.

The number of POM clusters bound is equal to or slightly less for ethoxyethanol than mannose-functionalized dendrimers of the same generation, as would be expected

from the small difference in surface area. In the cases of G(4) dendrimers **85** and **88** the number of clusters added closely reflects the amount of POM **74** added. In G(5) dendrimers **86** and **89,** 80-90% of the available POMs were bound. Finally, in G(6) dendrimers **87** and **90**, only around 75% of the available POMs bound added suggesting maximum possible POM addition in these reactions.

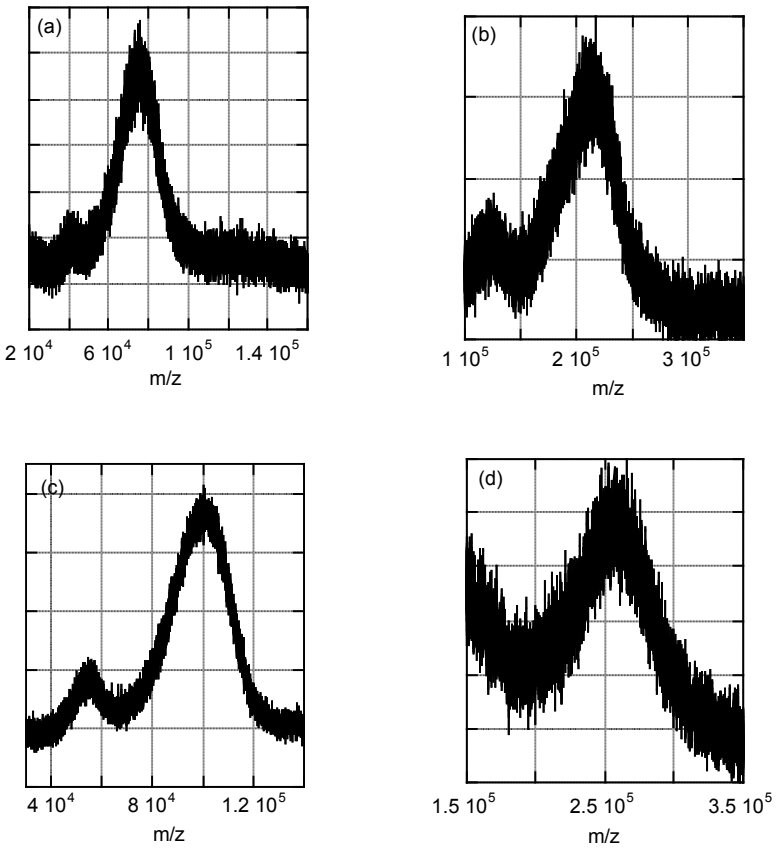

Figure 6.17 MALDI-TOF MS spectra of compounds (a) **39g**, (b) **87**, (c) **68**, and (d) **90**.

Polyoxometalate Catalysis

Many different types of POMs are used as oxidation catalysts in a variety of chemical reactions.[143, 144] Bleaching reactions, oxidative degradation of organic dyes by hydrogen peroxide, are easily monitored, and were previously reported.[167] In a series of publications from Spiro *et. al.* (see references 167 and 168 for leading citations) a number of POM catalysts were used in the oxidative degradation of methyl orange and crocetin, and the reactions were compared with catalysis by sodium molybdate and sodium tungstate, however vanadium substituted tungstate POMs were not included. Separately, transition metal oxides were used as catalysts in the oxidative degradation of phenolphthalein.[168] We chose this reaction to first test the activity of poly(POM) dendrimers because it's easy to monitor, and while POMs of the type **74** have not been used as catalysts for this reaction, there is excellent precedent with similar POMs.

The polyoxometalate catalyzed oxidative degradation of phenolphthalein by hydrogen peroxide (Scheme 6.10) could be monitored visually, and kinetics could be followed by simple UV/Visible spectroscopy.

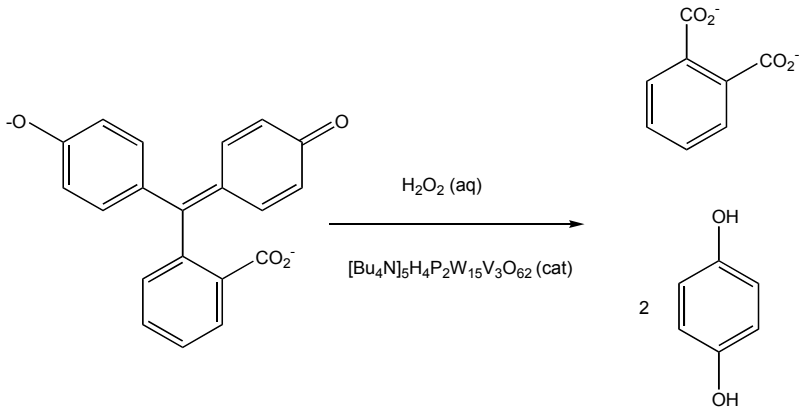

Scheme 6.10 Oxidative degradation of phenolphthalein.

Poly(POM) dendrimers, and POM **74** (solutions in DMSO), were separately mixed with aqueous solutions of phenolphthalein (made basic to elicit a bright pink color) and hydrogen peroxide. The evidence for the reaction was a color change from pink to clear. The first time the reaction was examined, the color change occurred within minutes when the catalyst, either on dendrimer or alone, was present. Without catalyst, the reaction took more than an hour. The relative concentrations were adjusted so that the catalyzed degradation occurred in approximately one hour, and the uncatalyzed reaction was not observed by the naked eye on this timeframe. No significant difference was observed in the reaction times between poly(POM) dendrimer and POM **74** alone (equally concentrated on a per-POM basis). An obvious concern was that, as a pH indicator, phenolphthalein would perform the same color change if the solution became acidic.

Catalyst stability was also a concern since during POM synthesis, low pH is maintained. A quick titration of the catalyst solution with sodium hydroxide followed by ^{31}P NMR analysis confirmed that the cluster quickly degrades in the pH range (9.5 – 11) required for oxidative degradation of phenolphthalein to occur.

With the very simple example above ruled out, a small survey of common polyoxometalate catalyzed oxidations was performed. Either oxygen gas or aqueous hydrogen peroxide (35%) was used as the oxidant with POM **74** as the catalyst without the dendrimer. Some of these reactions, the ones performed in NMR tubes in deuterated acetonitrile, are shown in Scheme 6.11.

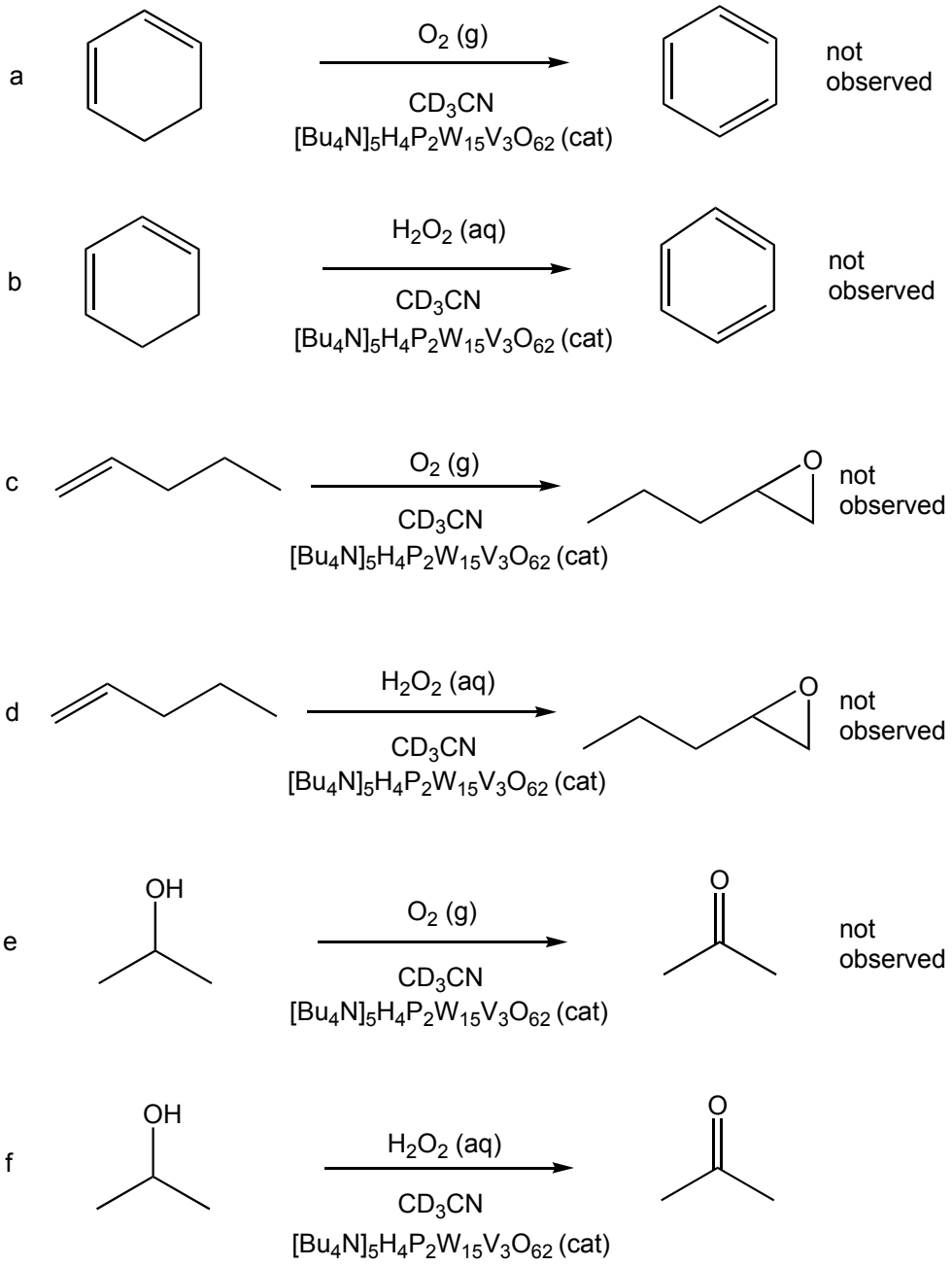

Scheme 6.11 Example oxidation reactions performed. (a) and (b) the dehydration of cyclohexadiene; (c) and (d) the epoxidation of pentene; and (e) and (f) ketone formation from isopropanol. In each case the POM $(Bu_4N)_5H_4P_2W_{15}V_3O_{62}$ (**74**) was used as a catalyst (2 mol %).

Epoxidation is a commonly employed reaction in POM catalyzed oxidations.[142] However, no epoxide formation was observed in our studies. Dehydrogenation of

cyclohexadienes to aromatic benzenes, typically employs vanadium substituted heteropolyanions,[169] but no reaction was observed using POM **74** as the catalyst with either oxygen or peroxide oxidants. The oxidation of simple alcohols, such as isopropanol, by POM catalysis has also been reported in recent literature,[170] and the peroxide oxidation of the isopropanol (Scheme 6.11f) singularly showed any signs of reactivity in our studies. Optimizing the reaction involved heating the solution to 40° C in a sealed tube. While the ^{13}C and ^{1}H NMR indicated acetone formation (Figure 6.18), the extraordinarily large water peak in the proton spectrum inhibited good peak identification or integration, particularly after the very early stages of the reaction. Neither the use of 4Å sieves nor magnesium sulfate in the reaction adequately resolved the spectra. To effectively monitor the oxidation of a secondary alcohol to a ketone, clearer spectroscopic monitoring was desired. Benzhydrol aromatic protons could facilitate reaction monitoring. While this new reactivity of POM **74** was encouraging, the unfortunate result from the survey was that the most appropriate substrate (alcohols) for further examination formed vanadium esters with the cluster – reactivity we harnessed to construct the metallodendrimers.

At this point, it became clear that more understanding of the vanadium esterification was needed. Would excess alcohol replace the oxygen-vanadium bond between the dendrimer and the cluster? Indeed vanadium esterification is in equilibrium, an important point relating to the following experiments.

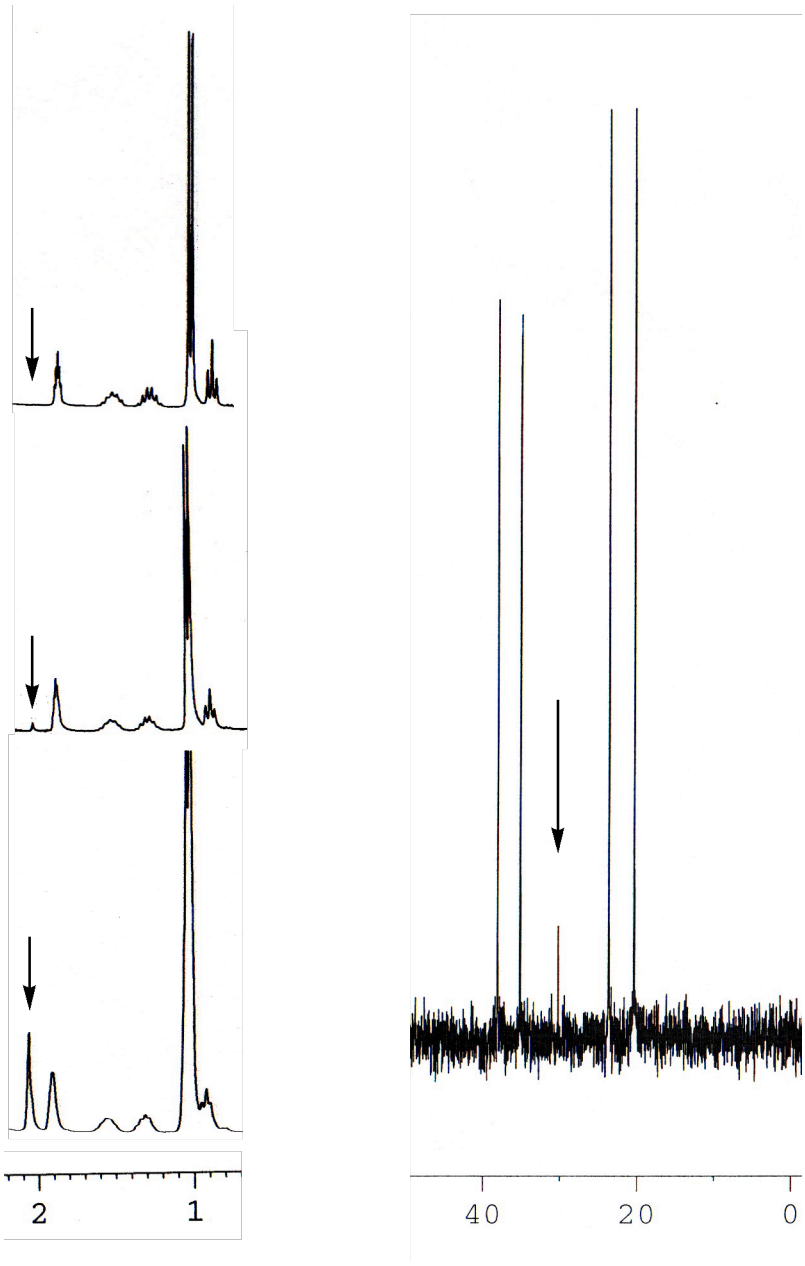

Figure 6.18 ^{1}H and ^{13}C NMR spectra from the early stages of isopropanol oxidation in CD_3CN, the arrows indicate peaks likely resulting from acetone formation.

First a variety of alcohols were mixed with **85** in acetonitrile. Ethanol, isopropanol, t-butanol, benzyl alcohol, and ethylene glycol were added to separate solutions of **85**, then after stirring overnight the poly(POM) dendrimer was analyzed by

MALDI-TOF MS. Since the measured M_W didn't change before and after exposure to the alcohols, transesterification did not seem to have occurred. Yet, due to the reaction equilibrium there was likely a balance between free POM, dendrimer bound POM, and alcohol bound POM. As a non-solution measurement, MALDI-TOF was inadequate. The working assumption became that some of the POM is bound to the dendrimer in solution, and this will be adequate in determining the differences in catalytic activity between dendrimer bound POM and free POM.

The oxidation of benzhydrol (**91**) to benzophenone (**92**) by hydrogen peroxide, catalyzed by POM **74** was quite useful (Scheme 6.12). Without any catalyst, benzophenone formation was not seen in NMR. With free POM **74** as the catalyst, small amounts of benzophenone were typically observed within hours at room temperature (Figure 6.19). Cluster functionalized dendrimers were not very soluble in deuterated acetonitrile. Over the period of the reaction (two days) the dendrimers would precipitate. The larger generation dendrimers were less soluble, but over a two each dendrimer was, at best, only somewhat soluble.

The oxidation was then attempted in DMF to improve dendrimer solubility. Unfortunately the reduction of vanadium from light (changing the color from red-orange to green) was a solvent sensitive reaction. Under normal lab conditions (lab lights off, ambient light from hallway on, reactions performed under foil) a POM solution in DMA may not turn green for weeks, a solution in acetonitrile turns green in days, and in DMF the reduction takes only hours or minutes. Thus, a solution in DMF will not survive in the necessary oxidation state for the duration of the reaction. This result was observed

again when attempting to oxidize benzhydrol in d_7-DMF. Unfortunately deuterated DMA wasn't commercially available.

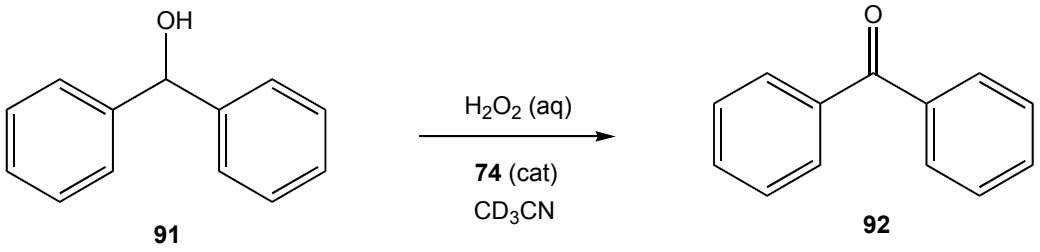

Scheme 6.12 The oxidation of benzhydrol (**91**) to benzophenone (**92**) by aqueous hydrogen peroxide in deuterated acetonitrile using POM **74** catalyst.

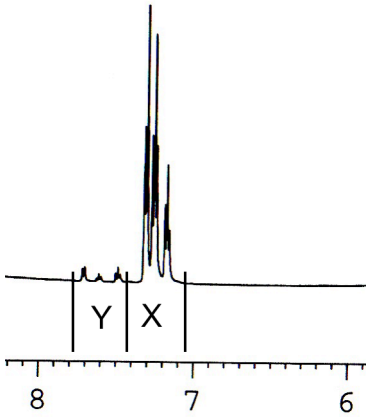

Figure 6.19 The aromatic region of a ^{1}H NMR spectrum after two hours from the reaction in Scheme 6.12. Peaks in the X area represent benzhydrol (**91**), and in the Y area represent benzophenone (**92**).

The choice of benzophenone as a target suggested the possibility of monitoring the reaction in DMA by UV-Vis spectroscopy. Attempts at oxidizing benzhydrol in DMA did not produce any significant signal at 340 nm, which would correspond to benzophenone. Perhaps the oxidation does not occur in DMA, or the addition of aqueous peroxide creates such a large slope into the UV region of the spectrum, that any product

signal is overwhelmed. The latter was seen to be the case when the same experiment was performed using acetonitrile as the reaction solvent.

Catalyst solubility continued to be a problem, so rather than using the poly(polyoxometalate) dendrimers as homogeneous catalyst, we next focused on heterogeneous catalysis as another possible application for poly(POM) dendrimers. Benzhydrol was melted at 70° C and partially converted to benzophenone in the presence of POM **74** and aqueous hydrogen peroxide. The reaction was monitored by TLC, and the resulting product mixture was analyzed by NMR. Since the PAMAM dendrimer may degrade at these high temperatures, some room temperatures liquids were examined as possible substrates. *t*-Butyl peroxide was tested as a potential oxidizing agent along with aqueous hydrogen peroxide (for examples see Scheme 6.13). These reactions failed to produce oxidized products, as monitored by NMR.

Next the dendrimers were added to a new reaction with the POM, including mesitylene and toluene, which along with benzhydrol are susceptible to oxidation in deuterated acetonitrile, a matter discussed in more detail later. To explore aqueous biphasic reaction conditions, mesitylene, hexanol, benzyl alcohol, pentene or toluene were combined with dendrimer **68** and POM **74** in water and were stirred for one day. The organic products were extracted with deuterated chloroform (Scheme 6.14). In each case, only starting material was observed with no oxidation products.

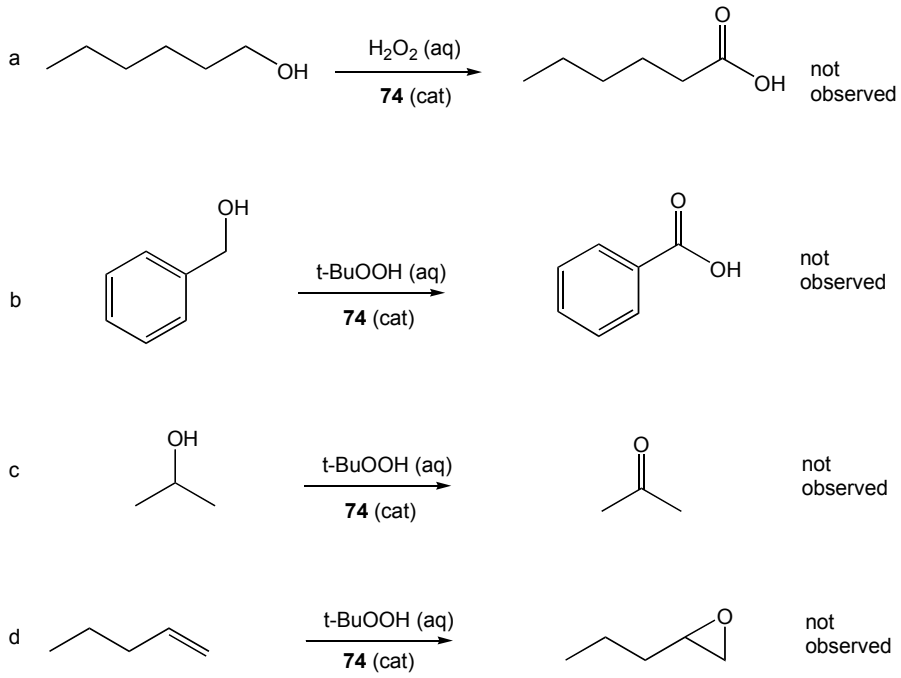

Scheme 6.13 Attempted oxidation of liquids (a) n-hexanol with hydrogen peroxide and (b) benzyl alcohol, (c) isopropanol, and (d) pentene with t-butyl peroxide.

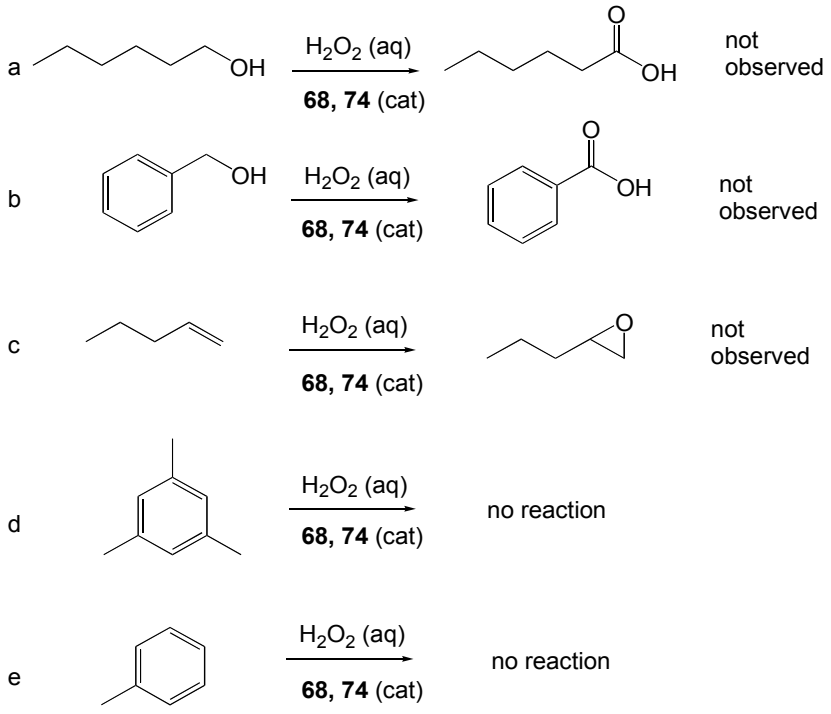

Scheme 6.14 Attempted aqueous biphasic reactions.

Returning to the most successful catalyst system yet seen, the oxidation of benzhydrol by hydrogen peroxide in CD_3CN, two significant issues remained. First, the poly(POM) dendrimers were not very soluble. Yet in both the homogeneous case (POM **74** in acetonitrile) and the heterogeneous case (**74** in neat benzhydrol) the benzophenone product formed in the presence of POM and didn't form without any catalyst. Accepting that dendrimer bound POM may be in or out of solution but active in either state, we pressed forward. Second, though benzophenone was formed, other side products emerged as well.

Examination of the aromatic region from the reaction run inside an NMR tube (with stirring for semi-soluble poly(POM) dendrimers, stir bars removed before NMR measurement) indicated benzhydrol peaks (Figure 6.20) at time 0, and as the reaction proceeded incoming peaks corresponding to benzophenone (d, 7.7, t, 7.6, t, 7.5 ppm). As the reaction proceeds many more aromatic peaks are observed. After 60 hours, many of the peaks are overlapped, making discrete integration difficult. The reaction's kinetic profile can be estimated as shown in Figure 6.21, relating only the identifiable benzhydrol and benzophenone relative integrations. The small slope at the start followed by a somewhat linear increase in product formation observed could be explained by a mechanism where the active catalyst is itself the product of a separate degradation reaction. Note also the catalyst bound to dendrimer is slower to contribute to the oxidation, possibly taking longer to degrade. In the absence of catalyst no reaction occurs even after 2.5 days.

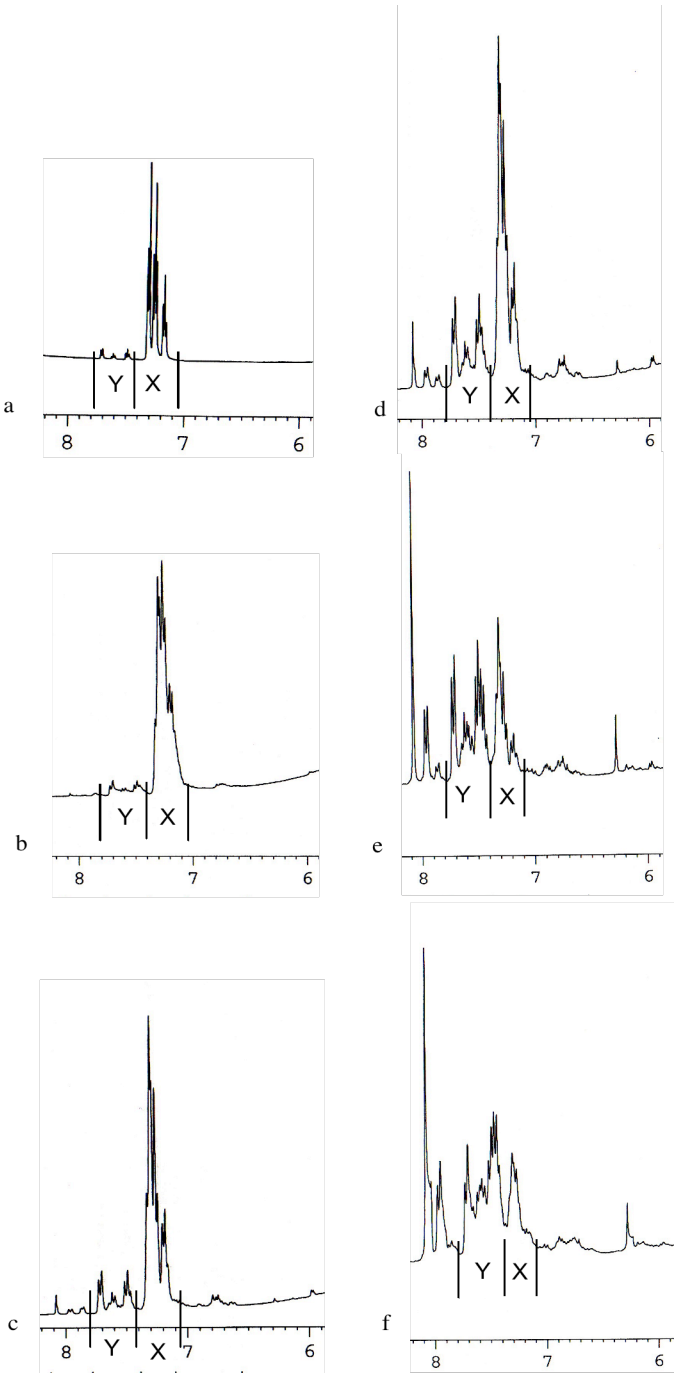

Figure 6.20 ^{1}H NMR spectrum of reaction products from the oxidation of benzhydrol over time (a) 2 hours, (b) 6 hours, (c) 12 hours, (d) 24 hours, (e) 48 hours, and (f) 60 hours. X represents peaks corresponding to benzhydrol (**91**), Y represents peaks corresponding to benzophenone (**92**).

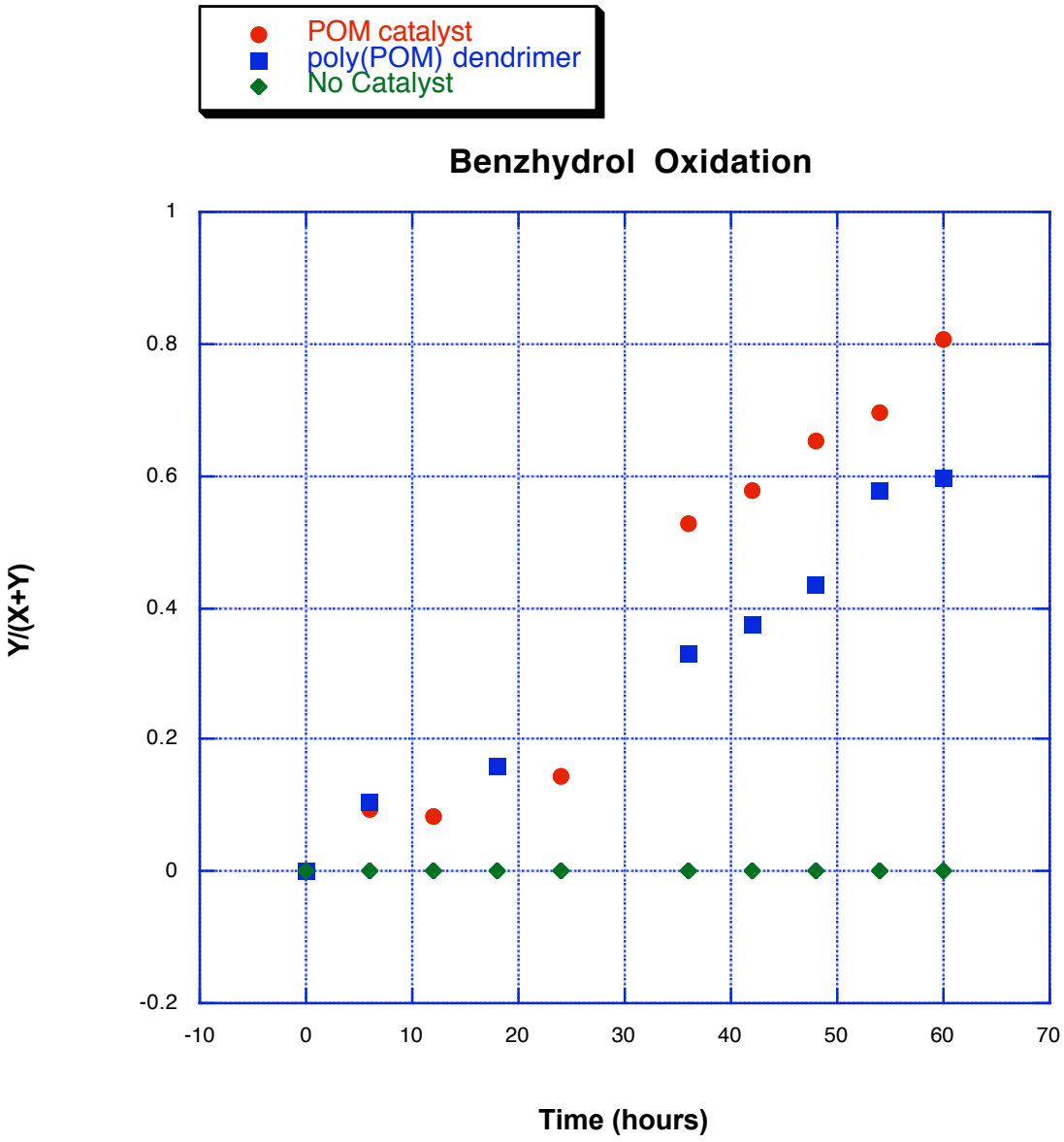

Figure 6.21 Rate profile of benzophenone formation by NMR. Time (X-axis) vs. benzophenone (**92**) integration value as a percentage of benzophenone (**92**) and benzhydrol (**91**) together (Y-axis). POM **74** (red), poly(POM)dendrimer **85** (blue), no catalyst (green).

The apparent doublet of benzophenone at 7.7 ppm (Figure 6.20) was reasonably clear of overlap, yet good kinetic data for the reaction required the use of an internal standard of known concentration against which the concentration of benzophenone could

be calculated. Choosing the appropriate standard was difficult because the water peak, and peroxide peak were so large, Mesitylene was selected as a potential standard because of the clear aromatic proton signal at around 6.8 ppm.

Unfortunately, over the course of the reaction, the relative integration for mesitylene became smaller, indicating that mesitylene was being consumed. This result was surprising due to the lack of functionality on the molecule. Toluene and benzene were then subjected to the same reaction conditions (minus the benzhydrol of course) to see if a singe product could be obtained by their oxidation. Benzene did not appear to readily oxidize, but toluene yielded at least 4 products (by COSY), in a similar fashion to the benzhydrol oxidation.

A significant peak at 8.1 ppm appeared consistently in both benzhydrol and toluene oxidations. To determine if this signal was derived from a POM bound proton or an unidentified product, the POM **74** was allowed to react with only hydrogen peroxide for over a day. The results were startling. The peak at 8.1 ppm in the ^{1}H spectrum did not seem to evolve as before. Yet more importantly, ^{31}P NMR was performed on this product to see if a peroxo-vanadium species would significantly shift the signal from the interior phosphates of the POM. Along with the two typical POM phosphorous signal, an intense peak appeared at 0 ppm. The most likely source of free phosphate is from the degradation of POM **74**.

To verify these results, about one fifth the usual amount of POM was combined with twice the usual amount of hydrogen peroxide. Within a day, both the POM ^{31}P signals were gone, and replaced with a peak at 0 ppm. Hoping a vanadium ester may be less susceptible to degradations, an ethyl ester of POM **74** (predominantly bi-ester and tri-

ester) was formed and subjected to aqueous hydrogen peroxide. This POM also degraded. Interestingly t-BuOOH did not seem to have the same effect, keeping the POM intact after prolonged exposure. However the butyl peroxide did not appear to oxide toluene (nor benzyl alcohol) even in the presence of POM **74**.

Summary

The vanadium-substituted heteropolyoxometalate **74** was constructed using literature procedures. In the presence of hydroxyl- and mannose-functionalized dendrimers, up to 40 individual POMs were bound to the dendrimer surface by a reversible vanadium esterification reaction. The MALDI-TOF MS, TEM, and ^{31}P NMR results provide substantial evidence for the product formation. However, in contrast to previous reports using similar vanadium esters, [146, 147] the product was quite susceptible to hydrolytic cleavage as shown in particular from the GPC traces. Despite this setback, the oxidation of some simple alcohols to ketones and the oxidative degradation of phenolphthalein each occurred, and neither has been reported using POM **74** to our knowledge. The active catalyst in both cases was likely itself a degradation product such as a vanadium oxide or tungsten oxide, another unexpected result considering the reported reactions of POM **74** with hydrogen peroxide. Potential improvements to the new catalyst materials would include a different POM, stable under oxidation conditions, and irreversibly bound to the dendrimer. Also, new linkers could be synthesized to more accurately mimic reportedly stable vanadium triesters, or a different dendrimer could be used that is stable to acidic conditions, which are prevalent in POM oxidation chemistry.

Experimental Procedures

General reagents were purchased from Aldrich, Sigma, Strem, and Acros. PAMAM dendrimers were purchased from Dendritech as aqueous solutions, and mannose-functionalized PAMAM dendrimer **66-68**[72] and polyoxometalate **74**[160-162] were made as previously reported. Reactions were not stirred unless so indicated. In the synthesis, reactions, and product characterizations using compound **74**, exposure to light was minimized because **74** is susceptible to vanadium reduction in the presence of light. Solvents and reagents were used as supplied.

MALDI-TOF MS. Matrix assisted laser desorption ionization (MALDI) mass spectra were acquired using a Bruker Biflex-III time-of-flight mass spectrometer. Spectra were obtained using a trans-3-indoleacrylic acid (IAA) matrix with a matrix-analyte ratio of 36,000: 1 to 1000:1. A 1 μL aliquot of the analyte (0.5-20 mg/mL) in DMF, DMA, or DMSO, was combined with 10 μL of IAA in DMF (20 mg/mL). A 1 μL aliquot was deposited on the laser target, drying in 1-4 hours. Bovine serum albumin (MW 66,431 g/mol) and laser promoted oligomers up to the tetramer and the M/Z peak where Z = 2, trypsinogen (MW 23,982 g/mol), cytochrome C (12,361 g/mol), and bradykinin (1061 g/mol) were used as external standards. Positive ion mass spectra were acquired in linear mode, and the ions were generated by using a nitrogen laser (337 nm) pulsed at 5 Hz with a pulse width of 3 nanoseconds. Ions were accelerated at 19-20,000 volts and amplified using a discrete dynode multiplier. Spectra (10 to 2000) were summed into a LeCroy LSA1000 high-speed signal digitizer. All data processing was performed using Bruker

XMass/XTOF V 5.0.2. Molecular mass data and polydispersities of the broad peaks were calculated by using the Polymer Module included in the software package. The peaks were analyzed using the *continuous* mode. Delta values were set at minimum levels.

Gel Permeation Chromatography. HPLC grade DMSO was filtered through Millipore nylon filters (0.45 μm). The GPC system consisted of a Waters 515 HPLC pump, Waters Styragel HR4 and HR4E columns, and a Waters 996 photodiode array detector that was ran with Waters Empower 2 software. Runs were performed at from 25 °C to 50 °C with 0.3 mL/min to 0.7 mL/min flow rates. Sample concentrations of 0.10 mg/mL to 10 mg/mL were analyzed.

Transmission Electron Microscopy. Images of **90** were taken on a LEO 912AB transmission electron microscope at an acceleration voltage of 100 kV with no stain at 40,000X magnification and 1 second exposure time. Samples were prepared by dropping a 5 μL spot of a 0.10 mg/mL solution in acetonitrile onto a 15 second glow discharge copper grid.

NMR. ^{1}H NMR and ^{31}P NMR were acquired at 500 MHz and 202.6 MHz, respectively, on a Bruker DRX500 instrument in CD_3CN or DMA. ^{51}V NMR were acquired at 66 MHz on a Brucker DRX 250 instrument. ^{31}P experiments were performed in DMA and externally referenced with 4% H_3PO_4 in DMA. ^{51}V NMR were externally reference with vanadium (V) trichloride oxide in CD_3CN.

$Na_9P_2W_{15}V_3O_{62}•9H_2O$ (78). (Procedure modified from reference 163). The POM **74** (71 mg, 14 μmol) in 30 mL acetonitrile was mixed with sodium tetrafluoroborate (13.8 mg, 130 μmol). Both compounds dissolved after bringing the solution to a boil. The solution was cooled to room temperature and an aqueous sodium hydroxide solution was added (44 μL, 5% solution, 55 μmol). After stirring for 24 hours a precipitate had formed. The solid was centrifuged and the solvent was removed. The yellow solid was redissolved in water, and was dialzyzed (MWCO 1000 Da) against water, then the water was removed by lyophilization to afford 4.6 mg **78** (8% yield). ^{31}P NMR (202.6 MHz, CD_3CN) δ -6.5, -13.7 ppm; MALDI-TOF MS measured 2136 g/mol.

Representative procedure for the synthesis of poly(polyoxometalate) dendrimers 85–87: formation of 85. A 20 mg/mL solution of hydroxyl-functionalized dendrimer **37g** was prepared in DMA. 53.5 μL of this solution (1.1 mg, 0.05 μmol) was added to 130 μL of POM **74** in DMA (20 mg/mL, 2.6 mg, 0.50 μmol). After two days, solvent was removed *in vacuo* to afford an orange solid **85**. ^{31}P NMR (202.6 MHz, DMA) δ -5.6, -8.4(bs), -12.3, -13.5, -14.3, -15.1(bs) ppm. IR (KBr) 3330, 2962, 2875, 1640, 1550, 1465, 1398, 1292, 1085, 945, 914, 817 cm^{-1}. MALDI-TOF MS measured 72,000 Da.

Characterization data for compound **86**. ^{31}P NMR (202.6 MHz, DMA) δ -5.7, -8.4(bs), -12.3, -13.6, -14.3, -15.3(bs) ppm. IR 3322, 2961, 2874, 1640, 1545, 1464, 1397, 1292, 1084, 1012, 940, 912, 810 cm^{-1}. MALDI-TOF MS measured 125,000 Da.

Characterization data for compound **87**. ^{31}P NMR (202.6 MHz, DMA) δ-5.6, -7.0, -8.3(bs), -12.3, -13.6, -13.9, -14.3, -15.3(bs) ppm. IR (KBr) 3320, 3070, 2961, 2873, 1652,

1540, 1457, 1396, 1292, 1084, 1012, 937, 911, 832, 756 cm^{-1}. MALDI-TOF MS measured 223,000 Da.

Representative procedure for the synthesis of poly(polyoxometalate) dendrimers 88-90: formation of 90. A 100 mg/mL solution of mannose-functionalized dendrimer **7** was prepared in millipore water. 12.6 μL of this solution (1.26 mg, 12.5 nmol) was added to 130 μL of POM **74** in DMA (20 mg/mL, 2.6 mg, 0.50 μmol). After two days, solvent was removed *in vacuo* to afford an orange solid **90**. ^{31}P NMR (202.6 MHz, DMA) δ -8.2(bs), -13.9, -14.6, -15.4(bs) ppm. IR (KBr) 3328, 2961, 1639, 1548, 1397, 1492, 1292, 1188, 1136, 1080, 1012, 935, 812 cm^{-1}, TEM images are shown in Figure 6.16. MALDI-TOF MS measured 257,000 Da.

Characterization data for compound **88**. ^{31}P NMR (202.6 MHz, DMA) δ -8.1(bs), -13.9, -14.6, -15.3(bs) ppm. IR (KBr) 3318, 2961, 1637, 1547, 1398, 1292, 1188, 1135, 1083, 1012, 938, 809 cm^{-1}, MALDI-TOF MS measured 84,500 Da.

Characterization data for compound **89**. ^{31}P NMR (202.6 MHz, DMA) δ-8.2(bs), -11.3, -13.9, -14.6, -15.4(bs) ppm. IR (KBr) 3322, 3073, 2960, 2874, 1640, 1547, 1461, 1397,1293, 1189, 1135, 1080, 934, 908, 878, 819 cm^{-1}, MALDI-TOF MS measured 149,000 Da.

Representative aqueous biphasic oxidation reaction: oxidation of toluene. Polyoxometalate **74** (6.0 mg, 1.2 μmol) was mixed with 200 μL water. A solution of mannose-functionalized PAMAM dendrimer **88** (3.1 mg, 0.10 μmol) in 153 μL water was added followed by toluene (54 μL, 500 μmol) and hydrogen peroxide (35% aq, 2.0

mmol). The biphasic mixture stirred gently for 22 h. The organic products were extracted with $CDCl_3$ (800 μL), dried over Mg_2SO_4 which was removed by centrifugation, and characterized by ^1H and ^{13}C NMR. Toluene starting material was the only compound recovered, suggesting that no reaction occurred.

Representative organic oxidation reaction: oxidation of benzhydrol. Polyoxometalate **74** was dissolved in 800 μL CD_3CN (5.2 mg, 1.0 μmol) and this solution was added to benzhydrol in 100 μL CD_3CN (1.8 mg, 10.0 1.0 μmol) followed by the addition of 100 μL H_2O_2 (35% aq, 1.0 mmol). The reaction was monitored by ^1H NMR.

CHAPTER 7

CONCLUDING REMARKS

The synthesis of the glycodendrimers in this report represents advancement in the synthetic control of the carbohydrate architectures of synthetic multivalent ligands. The efficiency and fidelity of the copper (I) catalyzed Huisgen dipolar cycloaddition of an azide and an alkyne was needed in the synthesis of tris-mannose cluster functionalized dendrimers. In what was essentially the penultimate step in the synthesis of these macromolecules, 'click chemistry' allowed for the synthesis of a perfectly formed clusters of three individual mannose units. A heterogeneous PAMAM dendrimer functionalization strategy afforded a level of control over the spatial relationship of the clusters on the dendrimer surface, and the macromolecule size was easily controlled by varying the dendrimer generation. In analysis of the interaction between the tris-mannose functionalized glycodendrimers with Con A using a hemagglutination inhibition assay it seemed that neither size nor varying the spatial relationship of the cluster was a determinant of activity in the assay. Rather, proximity effects from the cluster of sugars was likely responsible for the enhancement in activity of the glycodendrimers over methyl mannose. There was a significant amount of error in the hemagglutination inhibition assay. As a result the conclusion above should be considered lightly, and a quantitative assay should be used for a more reliable analysis of the interaction of these glycodendrimers Con A. Other assay methods such as ITC were attempted without

success, still other assays using techniques such as surface plasmon resonance and fluorescence spectroscopy are underway in our labs.

The synthesis of dimannose functionalized PAMAM dendrimers represents a straightforward method for making synthetic multivalent ligands for binding studies with the HIV-inactivating protein Cyanovirin N. These glycodendrimers were shown to have a high enough affinity for Cyanovirin N, such that optimal packing of the protein around the dendrimer wasn't achieved on the time scale of the precipation assay. This was in contrast to mannose-functionalized dendrimers bound with Con A in the precipitation assay, where optimal packing density was observed. The model of distinct clusters of Con A around a single glycodendrimer, rather than high order aggregation in the hemagglutination inhibition assay was verified by TEM.

The synthesis of an N-acetyl galactosamine isothiocyante represented a challenge in our labs. Only after an in depth study of the literature was a simple route to this compound discovered. Heterogeneous PAMAM dendrimer functionalization afforded N-acetyl galactosamine functionalized PAMAM dendrimers with a small number of phenyl azide groups on the dendrimer surface as well. This functionality was used in a copolymerization reaction with a bis-alkyne tether using 'click chemistry'. The physical evidence of polymerization suggested a large N-acetyl galactosamine functionalized macromolecule was synthesized, and this strategy could be used later for the synthesis of lipid raft domain mimics of various sizes and functionality. The evaluation of N-acetyl galactosamine functionalized dendrimers, made using the strategy reported here, with Galectin-3 is underway in our labs.

Finally, poly(POM) dendrimers were synthesized for applications in oxidation catalysis. The synthesis and characterization of these metallodendrimers represents advancement in metallodendrimers synthesis. Although the poly(POM) dendrimers themselves didn't display an enhanced catalytic effect over the monomeric POM due to POM stability, the design elements and synthetic methods from this work may be used in the future to make an efficient, easily separable catalyst that utilizes microenvironment control and monomer cooperativity .

REFERENCES CITED

1. Fukoda, M.; Hindsgaul, O., *Molecular Glycobiology*. Oxford University Press: New York, NY, 1994.

2. Gorelik, E.; Galili, U.; Raz, A., On the role of cell surface carbohyhdrates and their binding proteins (lectins) in tumor metastasis. *Cancer Metast. Rev.* **2001,** 20, (245-277).

3. Dwek, R. A., Glycobiology: Toward Understanding the Function of Sugars. *Chem. Rev.* **1996,** 96, 683-720.

4. Bertozzi, C. R.; Kiessling, L. L., Chemical Glycobiology. *Science* **2001,** 291, 2357-2364.

5. Morell, A. G.; Irvine, R. A.; Sternlieb, I.; Scheinberg, I. H.; Ashwell, G., Physical and Chemical Studies on Ceruloplasmin. *J. Biol. Chem.* **1968,** 243, (1), 155-159.

6. Ashwell, G.; Harford, J., Carbohydrate-Specific Receptors of the Liver. *Ann. Rev. Biochem.* **1982,** 51, 531-554.

7. Mammen, M.; Choi, S. K.; Whitesides, G. M., Polyvalent Interactions in Biological Systems: Implications for Design and Use of Multivalent Ligands and Inhibitors. *Angew. Chem. Int. Ed.* **1998,** 37, 2754-2794.

8. Nangia-Makker, P.; Conklin, J.; Hogan, V.; Raz, A., Carbohydrate-binding proteins in cancer, and their ligands as therapeutic agents. *Trends Mol. Med.* **2002,** 8, 187-192.

9. Pusztai, A., *Plant Lectins*. Cambridge University Press: Cambridge, 1991.

10. Bøg-Hansen, T. C., *Lectins Biology Biochemistry Clinical Biochemistry*. Walter de Gruyter: Berlin, 1981.

11. Lis, H.; Sharon, N., Lectins: Carbohydrate Specific Proteins That Mediate Cellular Recognition. *Chem. Rev.* **1998,** 98, 637-674.

12. Nilsson, C. L., Lectins: Proteins That Interpret the Sugar Code. *Anal. Chem.* **2003,** 75, (15), 348A-353A.

13. Bittiger, H.; Schnebli, H. P., *Concanavalin A as a Tool*. John Wiley & Sons: New York, 1976.

14. Kanellopoulos, P. N.; Pavlou, K.; Perrakis, A.; Agianian, B.; Vorgias, C. E.; Mavrommatis, C.; Soufi, M.; Tucker, P. A.; Hamodrakas, S. J., The crystal structure of the complexes of concanavalin A with 4'-nitrophenyl-alpha-D-mannopyranoside and 4'-nitrophenyl-alpha-D-glucopyranoside. *J. Struct. Biol.* **1996,** 116, 345-355.

15. Boyd, M. R.; Gustafson, K. R.; McMahon, J. B.; Shoemaker, R. H.; O'Keefe, B. R.; Mori, T.; Gulakowski, R. J.; Wu, L.; Rivera, M. I.; Laurencot, C. M.; Currens, M. J.; Cardellina, J. H.; Buckheit Jr., R. W.; Nara, P. L.; Pannell, L. K.; Sowder, R. C.; Henderson, L. E., Discovery of Cyanovirin-N, a Novel Human Immunodeficiency Virus-Inactivating Protein That Binds Viral Surface Envelope Glycoprotein gp120: Potential Applications to Microbicide Development. *Antimicrob. Agents Chemother.* **1997,** 41, 1521-1530.

16. Botos, I.; O'Keefe, B. R.; Shenoy, S. R.; Cartner, L. K.; Ratner, D. M.; Seeberger, P. H.; Boyd, M. R.; Wlodawer, A., Structures of the Complexes of a Potent Anti-HIV Protein Cyanovirin-N and High Mannose Oligosaccharides. *J. Biol. Chem.* **2002,** 277, (37), 34336-34342.

17. Barrientos, L. G.; Louis, J. M.; Ratner, D. M.; Seeberger, P. H.; Gronenborn, A. M., Solution Structure of a Circular-permuted Variant of the Potent HIV-inactivating Protein Cyanovirin-N: Structural Basis for Protein Stability and Oligosaccharide Interaction. *J. Mol. Biol.* **2003,** 325, 211-223.

18. O'Keefe, B. R.; Shenoy, S. R.; Xie, D.; Zhang, W.; Muschik, J. M.; Currens, M. J.; Chaiken, I.; Boyd, M. R., Analysis of the Interaction between the HIV-Inactivating Protein Cyanovirin-N and Soluble Forms of the Envelope Glycoproteins gp120 and gp41. *Mol. Pharmacol.* **2000,** 58, (5), 982-992.

19. Chan, D. C.; Kim, P. S., HIV Entry and Its Inhibition. *Cell* **1998,** 93, 681-684.

20. Shenoy, S. R.; Barrientos, L. G.; Ratner, D. M.; O'Keefe, B. R.; Seeberger, P. H.; Gronenborn, A. M.; Boyd, M. R., Multisite and Multivalent Binding between

Cyanovirin-N and Branched Oligomannosides: Calorimetric and NMR Characterization. *Chem. Biol.* **2002,** 9, 1109-1118.

21. Califice, S.; Castronovo, V.; van den Brule, F., Galectin-3 and Cancer. *Int. J. Onc.* **2004,** 25, 983-992.

22. Takenaka, Y.; Fukumori, T.; Raz, A., Galectin-3 and metastasis. *Glycocongate J.* **2004,** 19, (543-549).

23. Ochieng, J.; Furtak, V.; Lukyanov, P., Extracellular functions of galectin-3. *Glycocongate J.* **2002,** 19, 527-535.

24. Sörme, P.; Arnoux, P.; Kahl-Knutsson, B.; Leffler, H.; Rini, J. M.; Nilsson, U. J., Structural and Thermodynamic Studies on Cation-π Interactions in Lectin-Ligand Complexes: High-Affinity Galectin-3 Inhibitors through Fine-Tuning of an Arginine-Arene Interaction. *J. Am. Chem. Soc.* **2005,** 127, 1737-1743.

25. Lee, Y. C.; Lee, T. L., Carbohydrate-Protein Interactions: Basis of Glycobiology. *Acc. Chem. Res.* **1995,** 28, (8), 321-327.

26. Kiessling, L. L.; Pohl, N. L., Strength in numbers: non-natural polyvalent carbohydrate derviatives. *Chem. Biol.* **1996,** 3, (2), 71-77.

27. Lundquist, J. J.; Toone, E. J., The Glycoside Cluster Effect. *Chem. Rev.* **2002,** 102, 555-578.

28. Lee, Y. C.; Townsend, R. R.; Hardy, M. R.; Lönngren, J.; Arnarp, J.; Haraldsson, M.; Lönn, H., Binding of Synthetic Oligosaccharides to the Hepatic Gal/GalNAc Lectin. *J. Biol. Chem.* **1983,** 258, 199-202.

29. Brewer, C. F.; Brown, R. D., Binding of Mono- and Oligosaccharides to Concanavalin A as Studied by Solvent Proton Magnetic Resonance Dispersion. In *Carbohydrate-Protein Interaction*, Goldstein, I. J., Ed. American Chemical Society: Washington, D. C., 1979; pp 27-43.

30. Choi, S. K., *Synthetic Multivalent Molecules*
Concepts and Biomedical Applications. John Wiley & Sons: Hoboken, 2004.

31. Kitov, P. I.; Bundle, D. R., On the Nature of the Multivalency Effect: A Thermodynamic Model. *J. Am. Chem. Soc.* **2003,** 125, 16271-16284.

32. Huskens, J.; Mulder, A.; Auletta, T.; Nijhuis, C. A.; Ludden, M. J. W.; Reinhoudt, D. N., A Model for Describing the Thermodynamics of Multivalent Host-Guest Interactions at Interfaces. *J. Am. Chem. Soc.* **2004,** 126, 6784-6797.

33. Ercolani, G., Assesment of Cooperativity in Self-Assembly. *J. Am. Chem. Soc.* **2003,** 125, 16097-16103.

34. Burke, S. D.; Zhao, Q.; Schuster, M. C.; Kiessling, L. L., Synergistic Formation of Soluble Lectin Clusters by a Templated Multivalent Saccharide Ligand. *J. Am. Chem. Soc.* **2000,** 122, 4518.

35. Lees, W. J.; Spaltenstein, A.; Kingery-Wood, J. E.; Whitesides, G. M., Polyacrylamides Bearing Pendant α-Sialoside Groups Strongly Inhibit Agglutination of Erythrocytes by Influenza A Virus: Multivalency and Steric Stabilization of Particulate Biological Systems. *J. Med. Chem.* **1994,** 37, 3419-3433.

36. Perillo, N. L.; Pace, K. E.; Seilhamer, J. J.; Baum, L. G., Apoptosis of T cells mediated by galectin-1. *Nature* **1995,** 378, 736-739.

37. Pace, K. E.; Lee, C.; Stewart, P. L.; Baum, L. G., Restricted Receptor Segregation into Membrane Microdomains Occurs on Human T Cells During Apoptosis Induced by Galectin-1. *J. Immunol.* **1999,** 163, 3801-3811.

38. Okada, M., Molecular design and synthesis of glycopolymers. *Prog. Polym. Sci.* **2001,** 26, 67-104.

39. Nagahori, N.; Nishimura, S. I., Tailored Glycopolymers: Controlling the Carbohydrate-Protein Interaction Based on Template Effect. *Biomacromolecules* **2001,** 2, 22-24.

40. Ladmiral, V.; Mantovani, G.; Clarkson, G. J.; Cauet, S.; Irwin, J. L.; Haddleton, D. M., Synthesis of Neoglycopolymers by a Combination of a "Click Chemistry" and Living Radical Polymerization. *J. Am. Chem. Soc.* **2006,** 128, 4823-4830.

41. Arranz-Plaza, E.; Tracy, A. S.; Siriwardena, A.; Pierce, J. M.; Boons, G. J., High-Avidity, Low-Affinity Multivalent Interactions and the block to Polyspermy in *Xenopus laevis*. *J. Am. Chem. Soc.* **2002,** 124, 13035-13046.

42. Kim, B. S.; Hong, D. J.; Bae, J.; Lee, M., Controlled Self-Assembly of Carbohydrate Conjugate Rod-Coil Amphiphiles for Supramolecular Multivalent Ligands. *J. Am. Chem. Soc.* **2005,** 127, 16333-16337.

43. Röckendorf, N.; Lindhorst, T. K., Glycodendrimers. *Top. Curr. Chem.* **2001,** 217, 201-238.

44. Kensinger, R. D.; Yowler, B. C.; Benesi, A. J.; Schengrund, C. L., Synthesis of Novel, Multivalent Glycodendrimers as Ligands for HIV-1 gp120. *Bioconjugate Chem.* **2004,** 15, 349-358.

45. Ashton, P. R.; Hounsell, E. F.; Jayaraman, N.; Nilsen, T. M.; Spencer, N.; Stoddart, J. F.; Young, M., Synthesis and Biological Evaluation of α-D-Mannopyranoside-Containing Dendrimers. *J. Org. Chem.* **1998,** 63, 3429-3437.

46. Lin, C. C.; Yeh, Y. C.; Yang, C. Y.; Chen, G. F.; Chen, Y. C.; Wu, Y. C.; Chen, C. C., Quantitative analysis of multivalent interactions of carbohydrate-encapsulated gold nanoparticles with concanavalin A. *Chem. Commun.* **2003,** 23, 2920-2921.

47. Fulton, D. A.; Stoddart, J. F., Neoglycoconjugates Based on Cyclodextrins and Calixarenes. *Bioconjugate Chem.* **2001,** 12, (8), 655-672.

48. Mellet, C. O.; Defaye, J.; Garcia-Fernandez, J. M. C., Multivalent Cyclooligosaccharides: Versatilee Carbohydrate Clusters with Dual Role as Molecular Receptors and Lectin Ligands. *Chem. Eur. J.* **2002,** 8, (9), 1982-1990.

49. Gomez-Garcia, M.; Benito, J. M.; Rodriguez-Lucena, D.; Yu, J. X.; Chmurski, K.; Ortiz Mellet, C.; Gutierrez Gallego, R.; Maestre, A.; Defaye, J.; Garcia-Fernandez, J. M. C., Probing Secondary Carbohydrate-Protein Interactions with Highly Dense Cyclodextrin-Centered Heteroglycoclusters: The Heterocluster Effect. *J. Am. Chem. Soc.* **2005,** 127, 7970-7971.

50. Kitov, P. I.; Sadowska, J. M.; Mulvey, G.; Armstrong, G. D.; Ling, H.; Pannu, N. S.; Read, R. J.; Bundle, D. R., Shiga-like toxins are neutralized by tailored multivalent carbohydrate ligands. *Nature* **2000,** 403, 669-672.

51. Matsuura, K.; Akasaka, T.; Hibino, M.; Kobayashi, K., Facile Synthesis of Stable and Lectin-Recognizable DNA-Carbohydrate Conjugates via Diazo Coupling. *Bioconjugate Chem.* **2000,** 11, 202-211.

52. Singh, Y.; Renaudet, O.; Defrancq, E.; Dumy, P., Preparation of a Multitopic Glycopeptide-Oligonucleotide Conjugate. *Org. Lett* **2005,** 7, 1359-1362.

53. Wang, Y.; Kiick, K. L., Monodisperse Protein-Based Glycopolymers via a Combined Biosynthetic and Chemical Approach. *J. Am. Chem. Soc.* **2005,** 127, 16392-16393.

54. Spaltenstein, A.; Whitesides, G. M., Polyacrylamides bearing pendant α-sialoside groups strongly inhibit agglutination of erythrocytes by influenza virus. *J. Am. Chem. Soc.* **1991,** 113, 686-687.

55. Mortell, K. H.; Weatherman, R. V.; Kiessling, L. L., Recognition Specificity of Neoglycopolymers Prepared by Ring-Opening Metathesis Polymerization. *J. Am. Chem. Soc.* **1996,** 118, 2297-2298.

56. Schuster, M. C.; Mortell, K. H.; Hegeman, A. D.; Kiessling, L. L., Neoglycopolymers produced by aqueous ring-opening metathesis polymerization: decreasing saccharide density increases activity. *J. Mol. Cat. A* **1997,** 116, 209-216.

57. Kanai, M.; Mortell, K. H.; Kiessling, L. L., Varying the Size of Multivalent Ligands: The Dependence of Concanavalin A Binding on Neoglycopolymer Length. *J. Am. Chem. Soc.* **1997 ,** 119, 9931-9932.

58. Nelson, A.; Belitsky, J. M.; Vidal, S.; Joiner, C. S.; Baum, L. G.; Stoddart, J. F., A Self-Assembled Multivalent Pseudopolyrotaxane for Binding Galectin-1. *J. Am. Chem. Soc.* **2004,** 126, 11914-11922.

59. Hasegawa, T.; Kondoh, S.; Matsuura, K.; Kobayashi, K., Rigid Helical Poly(glycosyl phenyl isocyanide)s: Synthesis, Conformational Analysis, and Recognition by Lectins. *Macromolecules* **1999,** 32, 6595-6603.

60. Kalovidouris, S. A.; Blixt, O.; Nelson, A.; Vidal, S.; Turnbull, W. B.; Paulson, J. C.; Stoddart, J. F., Chemically Defined Sialoside Scaffolds for Investigation of Multivalent Interactions with Sialic Acid Binding Proteins. *J. Org. Chem.* **2003,** 68, 8485-8493.

61. Dudkin, V. Y.; Orlova, M.; Geng, X.; Mandal, M.; Olson, W. C.; Danishefsky, S. J., Toward Fully Synthetic Carbohydrate-Based HIV Antigen Design: On the Critical Role of Bivalency. *J. Am. Chem. Soc.* **2004,** 126, 9560-9562.

62. Polizzotti, B. D.; Kiick, K. L., Effects of Polymer Structure on the Inhibition of Cholera Toxin by Linear Polypeptide-Based Glycopolymers. *Biomacromolecules* **2006,** 7, 483-490.

63. Connolly, D. T.; Townsend, R. R.; Kawaguchi, K.; Bell, W. R.; Lee, Y. C., Binding and Endocytosis of Cluster Glycosides by Rabbit Hepatocytes. *J. Biol. Chem.* **1982,** 257, 939-945.

64. Kötter, S.; Krallmann-Wenzel, U.; Ehlers, S.; Lindhorst, T. K., Multivalent ligands for the mannose-specific lectin on type 1 fimbriae of *Escherichia coli*: syntheses and testing of trivalent α-D-mannoside clusters. *J. Chem. Soc. Perkin Trans. 1* **1998**, 2193-2200.

65. Al-Mughaid, H.; Grindley, T. B., Synthesis of a Nonavalent Mannoside Glycodendrimer Based on Pentaerythritol. *J. Org. Chem.* **2006,** 71, 1390-1298.

66. Grayson, S. M.; Frechet, J. M. J., Convergent Dendrons and Dendrimers: from Synthesis to Applications. *Chem. Rev.* **2001,** 101, 3819-3867.

67. Morgan, J. R.; Cloninger, M. J., Heterogeneously Functionalized Dendrimers. *Curr. Opin. Drug. Discovery Dev.* **2002,** 5, (6), 966-973.

68. Newkome, G. R.; Moorefield, C. N.; Vögtle, F., *Dendrimers and Dendrons: Concepts, Synthesis, Applications*. Wiley-VCH: New York, 2001.

69. Vögtle, F.; Gestermann, S.; Hesse, R.; Schwierz, H.; B., W., Functional Dendrimers. *Prog. Polym. Sci.* **2000,** 25, 987-1041.

70. Tomalia, D. A.; Hurst, H. D., Genealogically Directed Synthesis: Starburst/Cascade Dendrimers and Hyperbranched Structures. *Top. Curr. Chem.* **1993,** 165, 193-313.

71. Woller, E. K.; Cloninger, M. J., Mannose Functionalization of a Sixth Generation Dendrimer. *Biomacromolecules* **2001,** 2, 1052.

72. Woller, E. K.; Cloninger, M. J., The Lectin-Binding Properties of Six Generations of Mannose-Functionalized Dendrimers. *Org. Lett.* **2002,** 4, (1), 7.

73. Woller, E. K.; Walter, E. D.; Morgan, J. R.; Singel, D. J.; Cloninger, M. J., Altering the Strength of Lectin Binding Interactions and Controlling the Amount of Lectin Clustering Using Mannose/hydroxyl Functionalized Dendrimers. *J. Am. Chem. Soc.* **2003,** 125, 8820-8826.

74. Walter, E. D.; Sebby, K. B.; Usselman, R. J.; Singel, D. J.; Cloninger, M. J., Characterization of Heterogeneously Functionalized Dendrimers by Mass Spectrometry and EPR Spectroscopy. *J. Phys. Chem. B.* **2005,** 109, 21532-21538.

75. Han, H. J.; Sebby, K. B.; Singel, D. J.; Cloninger, M. J., Manuscript in preparation.

76. Kolb, H. C.; Finn, M. G.; Sharpless, K. B., Click Chemistry: Diverse Chemical Function from a Few Good Reactions. *Angew. Chem. Int. Ed.* **2001,** 40, 2004-2021.

77. Kolb, H. C.; Sharpless, K. B., The growing impact of click chemistry on drug discovery. *Drug Discovery Today* **2003,** 8, (24), 1128-1137.

78. Grieco, P. A., *Organic Synthesis in Water*. Blakie Academic & Professional: London, 1998.

79. Narayan, S.; Muldoon, J.; Finn, M. G.; Fokin, V. V.; Kolb, H. C.; Sharpless, K. B., "On Water": Unique Reactivity of Organic Compounds in Aqueous Suspension. *Angew. Chem. Int. Ed.* **2005,** 44, 3275-3279.

80. Finley, K. T., *Triazoles 1,2,3*. Wiley: New York, 1980; Vol. 39.

81. Rostovtsev, V. V.; Green, L. G.; Fokin, V. V.; Sharpless, K. B., A Stepwise Huisgen Cycloaddition Process: Copper(I)-Catalyzed Regioselective "Ligation" of Azides and Terminal Alkynes. *Angew. Chem. Int. Ed.* **2002,** 41, 2596-2599.

82. Tornøe, C. W.; Christensen, C.; Meldal, M., Peptidotriazoles on Solid Phase: [1,2,3]-Triazoles by Regiospecific Copper(I)-Catalyzed 1,3-Dipolar Cycloadditions of Terminal Alkynes to Azides. *J. Org. Chem.* **2002,** 67, 3057-3064.

83. Wang, Q.; Chan, T. R.; Hilgraf, R.; Fokin, V. V.; Sharpless, K. B.; Finn, M. G., Bioconjugation by Copper(I)-Catalyzed Azide-Alkyne [3+2] Cycloaddition. *J. Am. Chem. Soc.* **2003,** 125, 3192-3193.

84. Whiting, M.; Muldoon, J.; Lin, Y., C.; Silverman, S. M.; Lindstrom, W.; Olson, A. J.; Kolb, H. C.; Finn, M. G.; Sharpless, K. B.; Elder, J. H.; Fokin, V. V., Inhibitors of HIV-1 Protease by Using In Situ Click Chemistry. *Angew. Chem. Int. Ed.* **2006,** 45, 1435-1439.

85. Fazio, F.; Bryan, M. C.; Blixt, O.; Paulson, J. C.; Wong, C. H., Synthesis of Sugar Arrays in Microtiter Plate. *J. Am. Chem. Soc.* **2002,** 124, 14397-14402.

86. Chittiboina, S.; Xie, F.; Wang, Q., One-pot synthesis of triazole-linked glycoconjugates. *Tetrahedron Lett.* **2005,** 46, 2331-2336.

87 Perez-Balderas, F.; Ortega-Muñoz, M.; Morales-Sanfrutos, J.; Hernandez-Mateo, F.; Calvo-Flores, F. G.; Calvo-Asin, J. A.; Isac-Garcia, J.; Santoyo-Gonzalez, F., Multivalent Neoglycoconjugates by Regiospecific Cycloaddition of Alkynes and Azides Using Organic-Soluble Copper Catalysts. *Org. Lett* **2003,** 5, (11), 1951-1954.

88. Seto, C. T.; Mathias, J. P.; Whitesides, G. M., Molecular Self-Assembly through Hydrogen Bonding: Aggregation of Five Molecules To Form a Discrete Supramolecular Structure. *J. Am. Chem. Soc.* **1993,** 115, 1321-1329.

89. McPhee, M. M.; Kerwin, S. M., Synthesis and Metal Ion Binding Studies of Enediyne-Containing Crown Ethers. *J. Org. Chem.* **1996,** 61, 9385-9393.

90. Kokotos, G.; Verger, R.; Chiou, A., Synthesis of 2-Oxo Amide Triacylglycerol Analogues and Study of Their Inhibition Effect on Pancreatic and Gastric Lipases. *Chem. Eur. J.* **2000,** 6, 4211-4217.

91. Martín-Matute, B.; Nevado, C.; Cárdenas, D. J.; Echavarren, A. M., Intramolecular Reactions of Alkynes with Furans and Electron Rich Arenes Catalyzed by $PtCl_2$: The Role of Platinum Carbenes as Intermediates. *J. Am. Chem. Soc.* **2003,** 125, 5757.

92. Reppe, W., Mitarbeitern, Äthinylierung. *Liebigs Ann. Chem.* **1955,** 596, 1-158.

93. Shapiro, R.; DiCosimo, R.; Hennessey, S. M.; Steieglitz, G.; Campopiano, O.; Chiang, G. C., Discovery and development of a commercial synthesis of azafendin. *Org. Process Res. Dev.* **2001,** 5, 593-598.

94. Ren, R.; Liu, D., Synthesis of targetable cationic amphiphiles. *Tetrahedron Lett.* **1999,** 40, 7621-7625.

95. Chan, T. R.; Hilgraf, R.; Sharpless, K. B.; Fokin, V. V., Polytriazoles as Copper(I)-Stabilizing Ligands in Catalysis. *Org. Lett* **2004,** 6, (17), 2853-2855.

96. Lewis, W. G.; Magallon, F. G.; Fokin, V. V.; Finn, M. G., Discovery and Characterization of Catalysts for Azide-Alkyne Cycloaddition by Fluorescence Quenching. *J. Am. Chem. Soc.* **2004,** 126, 9152-9153.

97. Perrin, D. D., *Stability Contstants of Metal-Ion Complexes Part B Organic Ligands*. Pergamon Press: Oxford, 1979.

98. Qi, L.; Meijler, M. M.; Lee, S. H.; Sun, C.; Janda, K. D., Solid-Phase Synthesis of Anandamide Analogues. *Org. Lett* **2004,** 6, (10), 1673-1675.

99. Joralemon, M. J.; O'Reilly, R. K.; Matson, J. B.; Nugent, A. K.; Hawker, C. J.; Wooley, K. L., Dendrimers Clicked Together Divergently. *Macromolecules* **2005,** 38, 5436-5443.

100. Ryu, E. H.; Zhao, Y., Efficient Synthesis of Water-Soluble Calixarenes Using Click Chemistry. *Org. Lett* **2005,** 7, (6), 1035-1037.

101. Bodine, K. D.; Gin, D. Y.; Gin, M. S., Synthesis of Readily Modifiable Cyclodextrin Analogues via Cyclodimerization of an Alkynyl-Azido Trisaccharide. *J. Am. Chem. Soc.* **2004,** 126, 1638-1639.

102. Zanini, D.; Roy, R., Practical Synthesis of Starburst PAMAM α-Thiosialodendrimers for Probing Multivalent Carbohydrate-Lectin Binding Properties. *J. Org. Chem.* **1999,** 63, 3486-3491.

103. Tolic, L. P.; Anderson, G. A.; Smith, R. D.; Brothers II, H. M.; Spindler, R.; Tomalia, D. A., Electrospray Ionization Fourier Transform Ion Cyclotron Resonance Mass Spectrometric Characterization of High Molecular Mass Starburst Dendrimers. *Int. J. Mass Spec. and Ion Processes* **1997,** 165, 405-418.

104. Billmeyer Jr., F. W., *Textbook of Polymer Science*. Wiley: New York, 1984.

105. Morgan, J. R.; Cloninger, M. J., Heterogeneously Functionalized Dendrimers. *Curr. Opin. Drug Discovery Dev.* **2002,** 5, 966-973.

106. Bouzide, A.; Sauve, G., Silver (I) Oxide Mediated Highly Selective Monotosylation of Symmetrical Diols. Application to the synthesis of Polysubstituted Cyclic Ethers. *Org. Lett* **2002,** 4, (14), 2329-2332.

107. Tanabe, M.; Peters, R. H., (R,S)-Mevalonolactone-2-^{13}C. In *Organic Syntheses*, Wiley: New York, 1990; Vol. VII, pp 386-392.

108. Lebeau, L.; Oudet, P.; Mioskowski, C., Synthesis of New Phospholipids Linked to Steroid-Horomone Derivatives Designed for Two-Dimensional Crystallization of Proteins. *Helv. Chim. Acta* **1991,** 74, 1697-1706.

109. Edidin, M., The State of Lipid Rafts: From Model Membranes to Cells. *Annu. Rev. Biophys. Biomol. Struct.* **2003,** 32, 257-283.

110. Fivaz, M.; Abrami, L.; van der Goot, F.; Gisou, F., Landing on lipid rafts. *Trends Cell Biol.* **1999,** 9, (6), 212-213.

111. Matkó, J.; Szöllôsi, J., Landing of immune receptors and signal proteins on lipid rafts: a safe way to be spatio-temporally coordinated? *Immunol. Lett.* **2002,** 82, (1-2), 3-15.

112. Helms, B.; Mynar, J. L.; Hawker, C. J.; Fréchet, J. M. J., Dendronized Linear Polymers via "Click Chemistry". *J. Am. Chem. Soc.* **2004,** 126, 15020-15021.

113. Shu, J.; Schlüter, A. D.; Ecker, C.; Severin, N.; Rabe, J. P., Extremely Long Dendronized Polymers: Synthesis, Quantification of Structure Perfection, Individualization, and SFM Manipulation. *Angew. Chem. Int. Ed.* **2001,** 40, 4666-4669.

114. Al-Jamal, K. T.; Ramaswamy, C.; Florence, A. T., Supramolecular structures from dendrons and dendrimers. *Adv. Drug Del. Rev.* **2005,** 57, 2238-2270.

115. Banoub, J., Synthesis of Oligosaccharides of 2-Amino-2-deoxy Sugars. *Chem. Rev.* **1992,** 92, 1167-1195.

116. Findeis, M. A., Stepwise synthesis of a GalNAc-containing cluster glycoside ligand of the asialoglycoprotein receptor. *Int. J. Peptide Protein Res.* **1994,** 43, 477-485.

117. Kiso, M.; Anderson, L., The ferric chloride-catalyzed glycosylation of alcohols by 2-acylamido-2-deoxy-β-D-glucopyranose 1-acetates. *Carbohydrate Res.* **1979,** 72, C12-C14.

118. Stacey, J., Derivatives of Chondrosamine. *J. Chem. Soc.* **1944**, 272.

119. Matta, K. L.; Johnson, E. A.; Barlow, J. J., A simple method for the synthesis of 2-acetamido-2-deoxy-β-D-galatopyranosides. *Carbohydrate Res.* **1973,** 26, 215-218.

120. Benalil, A.; Carboni, B.; Vaultier, M., Synthesis of 1,2-Aminoazides. Conversion to Unsymmetrical Vicinal Diamines by Catalytic Hydrogenation or Reductive Alkylation with Dichloroboranes. *Tetrahedron* **1991,** 47, (38), 8177-8194.

121. Geyer, H.; Holschbach, C.; Hunsmann, G.; Schneider, J., Carbohydrates of Human Immunodeficiencey Virus. *J. Biol. Chem.* **1988,** 263, 11760-11767.

122. Mangold, S. L.; Morgan, J. R.; Strohmeyer, G. C.; Gronenborn, A. M.; Cloninger, M. J., Cyanovirin-N binding to Manα1-2Man functionalized dendrimers. *Org. Biomol. Chem.* **2005,** 3, 2354-2358.

123. Deferrari, J. O.; Gros, E. G.; Mastronardi, I. O., Methylation of carbohydrates bearing base-labile substituents, with diiazomethane-boron-trifluoride etherate II. A new synthesis of 2-*O*-methyl-D-mannose. *Carbohydrate Res.* **1967,** 4, 432-434.

124. Upreti, M.; Ruhela, D.; Vishwakarma, R. A., Synthesis of the Tetrasaccharide Cap Domain of the Antigenic Lipophosphoglycan of *leishmania donovani* Parasite. *Tetrahedron* **2000,** 56, 6577-6584.

125. Jackson, C. L.; Chanzy, H. D.; Booy, F. P.; Drake, B. J.; Tomalia, D. A.; Bauer, B. J.; Amis, E. J., Visualization of Dendrimer Molecules by Transmission Electron Microscopy (TEM): Staining Methods and Cryo-TEM of Vitrified Solutions. *Macromolecules* **1998,** 31, 6259-6265.

126. Khan, M. I.; Mandal, D. K.; Brewer, C. F., Interactions of Concanavalin-a with Glycoproteins - a Quantitatitve Precipitation Study of Concanavalin-a with the Soybean Agglutinin. *Carbohydrate Res.* **1991,** 213, 69-77.

127. Dam, T. K.; Brewer, C. F., Thermodynamic Studies of Lectin-Carbohydrate Interactions by Isothermal Titration Calorimetry. *Chem. Rev.* **2002,** 102, 387-429.

128. Dam, T. K.; Roy, R.; Pagé, D.; Brewer, C. F., Negative Cooperativity Associated With Binding of Multivalent Carbohydrates to Lectins, Thermodynamic analysis of the "Multivalency Effect". *Biochemistry* **2002,** 41, 1351-1358.

129. Dam, T. K.; Roy, R.; Pagé, D.; Brewer, C. F., Thermodynamic Binding Parameters of Individual Epitopes of Multivalent Carbohydrates to Concanavalin A As Determined by "Reverse" Isothermal Titration Microcalorimetry. *Biochemistry* **2002,** 41, 1359-1363.

130. Mandal, D. K.; Kishore, N.; Brewer, C. F., Thermodynamics of Lectin-Carbohydrate Interactions. Titration Microcalorimetry Measurements of the Binding of N-Linked Carbohydrates and Ovalbumin to Concanavalin A. *Biochemistry* **1994,** 33, 1149-1156.

131. Osawa, T.; Matsumoto, I., Gorse (*Ulex europeus*) Phytohemagglutinins. *Meth. Enzymol.* **1972,** 28, 323-327.

132. Dimick, S. M.; Powell, S. C.; McMahon, S. A.; Moothoo, D. N.; Naismith, J. H.; Toone, E. J., On the Meaning of Affinity: Cluster Glycoside Effects and Concanavalin A. *J. Am. Chem. Soc.* **1999,** 121, 10286-10296.

133. Trowbridge, I. S., Isolation and Chemical Characterization of a Mitogenic Lectin from *Pisum sativum*. *J. Biol. Chem.* **1974,** 249, 6004-6012.

134. Schlick, K. H.; Udelhoven, R. A.; Strohmeyer, G. C.; Cloninger, M. J., Binding of Mannose-Functionalized Dendrimers with Pea (*Pisum Sativum*) Lectin. *Mol. Pharmacol.* **2005,** 2, 295-301.

135. Pope, M. T.; Muller, A., *Polyoxometalates: From Platonic Solids to Anti-Retroviral Activity*. Kluwer Academic: Dordrecht, 1994.

136. Day, V. W.; Klemperer, W. G., Metal Oxide Chemistry in Solution: The Early Transition Metal Polyoxoanions. *Science* **1985,** 228, 533-541.

137. Wu, H., Contribution to the chemistry of phosphomolybdic acids, phosphotungstic acids, and allied substances. *J. Biol. Chem.* **1920,** 43, 189-220.

138. Dawson, B., The Structure of the 9(18)-Heteropoly Anion in Potassium 9(18)-Tungstophosphate, $K_6(P_2W_{18}O_{62})\cdot 14H_20$. *Acta. Cryst.* **1953,** 6, 113.

139. Lopez, X.; Bo, C.; Poblet, J. M., Relative Stability in α- and β-Wells-Dawson Heteropolyanions: A DFT Study of $[P_2M_{18}O_{62}]^{n-}$ (M = W and Mo) and $[P_2W_{15}V_3O_{62}]^{n-}$. *Inorg. Chem.* **2003,** 42, 2634-2638.

140. Clemente-Juan, J. M.; Coronado, E., Magnetic clusters from polyoxometalate complexes. *Coord. Chem. Rev.* **1999,** 193-195, 362-394.

141. Kozhevnikov, I., Catalysis by Heteropoly Acids and Multicomponent Polyoxometalates in Liquid-Phase Reactions. *Chem. Rev.* **1998,** 98, 171-198.

142. Adam, W.; Alsters, P. L.; Neumann, R.; Saha-Möller, C. R.; Seebach, D.; Zhang, R., Highly Efficient Catalytic Asymmetric Epoxidation of Allylic Alcohols by an Oxovanadium-Substituted Polyoxometalate with a Regenerative TADDOL-Derived Hydroperoxide. *Org. Lett* **2003,** 5, (5), 725-728.

143. Hill, C.; Prosser-McCartha, C. M., Homogeneous catalysis by transition metal oxygen anion clusters. *Coord. Chem. Rev.* **1995,** 143, 407-455.

144. Neumann, R., Polyoxometalate Complexes in Organic Oxidation Chemistry. *Prog. Inorg. Chem.* **1998,** 47, 317-370.

145. Harmalker, S. P.; Leparulo, M. A.; Pope, M. T., Mixed-Valence Chemistry of Adjacent Vanadium Centers in Heteropolytungstate Anions. 1. Synthesis and Electronic Structures of Mono-, Di-, and Trisubstituted Derivatives of α-$[P_2W_{18}O_{62}]^{6-}$. *J. Am. Chem. Soc.* **1983,** 105, 4286-4292.

146. Finke, R. G.; Rapko, B.; Saxton, R. J.; Domaille, P. J., Trisubstituted Heteropolytungstates as Soluble Metal Oxide Analogues. 3. Synthesis, Characterization, ^{31}P, ^{29}Si, ^{51}V, and 1- and 2-D ^{183}W NMR, Deprotonation, and H^+ Mobility Studies of Organic Solvent Soluble Forms of $H_xSiW_9V_3O_{40}^{x-7}$ and $H_xP_2W_{15}V_3O_{62}^{x-9}$. *J. Am. Chem. Soc.* **1986,** 108, 2947.

147. Hou, Y.; Hill, C. L., Hydrolytically Stable Organic Triester Capped Polyoxometalates with Catalytic Oxygenation Activity of Formula $[RC(CH_2O)_3V_3P_2W_{15}V_3O_{59}]^{6-}$ (R = CH_3, NO_2, CH_2OH). *J. Am. Chem. Soc.* **1993,** 115, 11823-11830.

148. Astruc, D.; Chardac, F., Dendritic Catalysts and Dendrimers in Catalysis. *Chem. Rev.* **2001,** 101, 2991-3023.

149. Twyman, L. J.; King, A. S. H., Catalysis using periphery functionalised dendrimers. *J. Chem. Res. (S)* **2002**, 43-59.

150. van Heerbeek, R.; Kamer, P. C. J.; van Leeuwen, P. W. N. M.; Reek, J. N. H., Dendrimers as Support for Recoverable Catalysts and Reagents. *Chem. Rev.* **2002,** 102, 3717-3756.

151. Martin, I. K.; Twyman, L. J., Acceleration of an aminolysis reaction using a PAMAM dendrimer with 64 terminal amine groups. *Tetrahedron Lett.* **2001,** 42, 1123-1126.

152. Zeng, H.; Newkome, G. R.; Hill, C., Poly(polyoxometalate) Dendrimers: Molecular Prototypes of New Catalytic Materials. *Angew. Chem. Int. Ed.* **2000,** 39, (10), 1772-1774.

153. Chatani, N.; Morimoto, T.; Fukumoto, Y.; Murai, S., $Ru_3(CO)_{12}$ - Catalyzed Cyclocarbonylation of Yne-Aldehydes to Bicyclic α,β-unsaturated γ-Butyrolactones. *J. Am. Chem. Soc.* **1998,** 120, 5335-5336.

154. Alonso, E.; Astruc, D., Introduction of the Cluster Fragment $Ru_3(CO)_{11}$ at the Periphery of Phosphine Dendrimers Catalyzed by the Electron-Reservoir Complex $[Fe^ICp(C_6Me_6)]$. *J. Am. Chem. Soc.* **2000,** 122, 3222-3223.

155. Cheng, L.; Cox, J. A., Preparation of multilayered nanacomposites of polyoxometalates and poly(amidoamine) dendrimers. *Electrochem. Commun.* **2001,** 3, 285-289.

156. Cheng, L.; Pacey, G. E.; Cox, J. A., Preparation and electrocatalytic applications of a multilayer nanocomposite consisting of phosphomolybdate and poly(amidoamine). *Electrochim. Acta* **2001,** 46, 4223-4228.

157. Haimov, A.; Cohen, H.; Neumann, R., Alkylated Polyethyleneimine/Polyoxometalate Synzymes as Catalysts for the Oxidation of Hydrophobic Substrates in Water with Hydrogen Peroxide. *J. Am. Chem. Soc.* **2004,** 126, 11762-11763.

158. Cornils, B., Industrial Aqueous Biphasic Catalysis: Status and Directions. *Org. Process Res. Dev.* **1998,** 2, (2), 121-127.

159. Muller, A.; Peters, F., Polyoxometalates: Very Large Clusters-Nanoscale Magnets. *Chem. Rev.* **1998,** 98, 239-271.

160. Finke, R. G.; Droege, M. W.; Domaille, P. J., Trivacant Heteropolytungstate Derivatives. 3. Rational Syntheses, Characterization, Two-Dimensional $_{183}$W NMR, and Properties of $P_2W_{18}M_4(H_2O)_2O_{68}^{10-}$ and $P_4W_{30}M_4(H_2O)_2O_{112}^{16-}$ (M = Co, Cu, Zn). *Inorg. Chem.* **1987,** 26, 3886-3896.

161. Hornstein, B. J.; Finke, R. G., The Lacunay Polyoxanion Synthon α-$P_2W_{15}O_{56}^{12-}$An Investigation of the Key Variables in Its Synthesis plus Multiple Control Reactions Leading to a Reliable Synthesis. *Inorg. Chem.* **2002,** 41, 2720-2730.

162. Contant, R., Potassium Octadecatungstodiphosphates(V) and Related Lacunary Compounds. *Inorg. Synth.* **1990,** 41, 104-111.

163. Finke, R. G.; Lyon, D. K.; Nomiya, K.; Weakley, T. J. R., Structure of Nonasodium α-Triniobatopentadecawolframatodiphophate-Acetonitrile-Water (1/2/23), $Na_9P_2W_{15}Nb_3O_{62}.2CH_3CN.23H_2O$. *Acta. Cryst.* **1990,** C46, 1592-1596.

164. Nomiya, K.; Kaneko, M.; Kasuga, N. C.; Finke, R. G.; Pohl, M., The Nonasodium Salt of the Triniobium-Substituted Polyoxanion $P_2W_{15}Nb_3O_{62}^{9-}$: A Water-Soluble,

Readily Crystallized Form of This Dawson-Based Soluble Metal-Oxide Organometallics-Support System. *Inorg. Chem.* **1994,** 33, 1469-1472.

165. Morgan, J. R.; Cloninger, M. J., Synthesis of Carbohydrate-Linked Poly(polyoxometalate) Poly(amidoamine) Dendrimers. *J. Polym. Sci. Part A: Polym. Chem.* **2005,** 43, 3059-3066.

166. Jackson, C. L.; Chanzy, H. D.; Booy, F. P.; Drake, B. J.; Tomalia, D. A.; Bauer, B. J.; Amis, E. J., Visualization of Dendrimer Molecules by Transmission Electron Microscopy (TEM): Staining Methods and Cryo-TEM of Vitrified Solutions. *Macromolecules* **1998,** 31, 6259-6265.

167. Gould, M. G.; Griffith, W. P.; Spiro, M., Polyoxometalate catalysis of dye bleaching by hydrogen peroxide. *J. Mol. Catal. A*. **2001,** 175, 289-291.

168. Thompson, K. M.; Griffith, W. P.; Spiro, M., Mechanism of Bleaching by Peroxides. 3. Kinetics of the Bleaching of Phenolphthalein by Transition Metal Salts in high pH peroxide solutions. *J. Chem. Soc., Faraday Trans* **1994,** 90, 1105-1114.

169. Neumann, R.; Levin, M., Aerobic Oxidative Dehydrogenations Catlyzed by the Mixed-Addenda Heteropolyanion $PV_2Mo_{10}O_{40}^{5-}$: A Kinetic and Mechanistic Study. *J. Am. Chem. Soc.* **1992,** 114, 7278-7286.

170. Sloboda-Rozner, D.; Alsters, P. L.; Neumann, R., A Water-Soluble and "Self-Assembled" Polyoxometalate as a Recyclable Catalyst for Oxidation of Alcohols in Water with Hydrogen Peroxide. *J. Am. Chem. Soc.* **2003,** 125, 5280-5281.